**Terms and Conditions of Use of Digitised Theses from Trinity College Library Dublin**

**Copyright statement**

All material supplied by Trinity College Library is protected by copyright (under the Copyright and Related Rights Act, 2000 as amended) and other relevant Intellectual Property Rights. By accessing and using a Digitised Thesis from Trinity College Library you acknowledge that all Intellectual Property Rights in any Works supplied are the sole and exclusive property of the copyright and/or other IPR holder. Specific copyright holders may not be explicitly identified. Use of materials from other sources within a thesis should not be construed as a claim over them.

A non-exclusive, non-transferable licence is hereby granted to those using or reproducing, in whole or in part, the material for valid purposes, providing the copyright owners are acknowledged using the normal conventions. Where specific permission to use material is required, this is identified and such permission must be sought from the copyright holder or agency cited.

**Liability statement**

By using a Digitised Thesis, I accept that Trinity College Dublin bears no legal responsibility for the accuracy, legality or comprehensiveness of materials contained within the thesis, and that Trinity College Dublin accepts no liability for indirect, consequential, or incidental, damages or losses arising from use of the thesis for whatever reason. Information located in a thesis may be subject to specific use constraints, details of which may not be explicitly described. It is the responsibility of potential and actual users to be aware of such constraints and to abide by them. By making use of material from a digitised thesis, you accept these copyright and disclaimer provisions. Where it is brought to the attention of Trinity College Library that there may be a breach of copyright or other restraint, it is the policy to withdraw or take down access to a thesis while the issue is being resolved.

**Access Agreement**

By using a Digitised Thesis from Trinity College Library you are bound by the following Terms & Conditions. Please read them carefully.

I have read and I understand the following statement: All material supplied via a Digitised Thesis from Trinity College Library is protected by copyright and other intellectual property rights, and duplication or sale of all or part of any of a thesis is not permitted, except that material may be duplicated by you for your research use or for educational purposes in electronic or print form providing the copyright owners are acknowledged using the normal conventions. You must obtain permission for any other use. Electronic or print copies may not be offered, whether for sale or otherwise to anyone. This copy has been supplied on the understanding that it is copyright material and that no quotation from the thesis may be published without proper acknowledgement.

# Optimisation of Process Parameters and Tooling during Friction Stir Welding of AA2024-T3

**Daniel Trimble**

SUBMITTED IN FULFILLMENT OF THE REQUIREMENTS FOR THE DEGREE OF DOCTOR OF PHILOSOPHY AT UNIVERSITY OF DUBLIN, TRINITY COLLEGE DUBLIN, IRELAND, SEPTEMBER 2011.

Supervisor: Professor John Monaghan and Dr Garret O'Donnell

The work presented in this thesis was conducted at the department of Mechanical and Manufacturing Engineering, University of Dublin, Trinity College Dublin, Ireland.

# Declaration

I declare that this thesis has not been submitted as an exercise for a degree at this or any University and it is entirely my own work.

I agree to deposit this thesis in the University's open access institutional repository or allow the library to do so on my behalf, subject to Irish Copyright Legislation and Trinity College Library conditions of use and acknowledgements.



Daniel Trimble

Department of Mechanical and Manufacturing Engineering

Trinity College Dublin, September 2011.

# Summary

Friction stir welding (FSW) was invented and experimentally proven at The Welding Institute (TWI) in 1991. The process involves the joining of two metal pieces without melting by joining their molecules together. The tool traverses along the joint causing sufficient frictional heat to soften the material without melting. The rotation of the tool then stirs the molecules together leaving behind a fully consolidated joint. Because it is a solid state process and joining takes place below the melting temperature of the material, a high-quality weld is created with many advantages over fusion welding techniques. However, one of the main advantages of the process is its ability to weld 2xxx series and 7xxx series aluminium alloys which are used extensively within the aerospace industry, but are generally non-weldable using fusion welding techniques. FSW provides a solution to welding these alloys and an alternative to riveting.

The overall aim of the project was to optimise the operational parameters and tooling design, and also to provide a comprehensive understanding of the FSW process during the welding of AA2024-T3 plates. This was achieved through the development of a processing window for various operational parameters; testing of new tooling designs and the comparison of their performance to traditional FSW tooling; characterisation of the forces and temperatures generated and the development of a FE model to simulate the process.

The results achieved indicate that welds produced with translational speeds of 125, 180 and 250 mm/min in conjunction with rotational speeds of 355 and 450 rpm produce welds with optimal tensile strength, greater than 85% of the parent material. The limiting factor associated with maximising the translational speed and hence productivity was found to be the formability of the workpiece due to the occurrence of surface voids and not pin failure due to the occurrence of large welding forces generated at high translational speeds. Hence the development of new tooling designs which can process and stir the workpiece materials more efficiently may enable higher translational speeds.

A tool consisting of an 18mm scrolled shoulder with a triflute or square pin design is recommended in terms of: increased strength and ductility due to increased plastic deformation and mixing of the two workpiece materials; increased material processing; reduction of thermal damage; increased translational speeds due to a reduction in tool lift and increased flexibility during non-linear welding.

All forces and temperatures were found to reach steady state values during translation of the tool along the joint line. Changes to the translational speed had a greater effect on the forces and temperatures than variation of the rotational speed. The largest force encountered was the vertical force and is therefore the limiting factor affecting FSW machine design. Lower forces were recorded using pin designs which promote enhanced material deformation such as the triflute pin. The magnitude of the welding force was significantly lower than the vertical force; however this force can help identify tool designs which process and mix the workpiece material more efficiently.

A 3D model of the FSW process was successfully modelled using the finite element package DEFORM 3D. The model correlated well with experimental results and gave a good representation of the FSW process. The model was capable of successfully predicting material flow, forces, stresses, strains and temperatures generated during the FSW of AA2024-T3.

# Acknowledgements

First of all I would like to sincerely thank Prof. John Monaghan for the opportunity to undertake this PhD and for the great help, guidance and advice over the years. This project would not be possible without him.

I would also like to thank Dr Garret O'Donnell who provided financial support, research instrumentation equipment and organised collaboration with companies such as Kistler, Bombardier Aerospace and The Welding Institute.

Furthermore, I would also like to thank Michael Reilly, Sean Doonan, Gabriel Nicholson, JJ Ryan, Alex Kearns, Daniel Boardman, Peter O'Reilly and Paul Normoyle for their excellent technical support and unlimited patience in assisting me complete my experimental work.

# Table of Contents

# Nomenclature

| Symbol | Unit | Definition |
|---|---|---|
| T | °C | Temperature |
| D | mm | Perpendicular distance from the weldline |
| $C_1$, $C_2$, $C_3$ | - | Constants within thermal flow equation |
| W | watts | Weld Power |
| τ | N.m | Torque |
| Ω | rpm | Spindle rotational speed |
| σ | MPa | Flow stress |
| A | - | Material constant within flow stress equation |
| B | - | Material constant within flow stress equation |
| C | - | Material constant within flow stress equation |
| α | - | Material constant within flow stress equation |
| K | - | Material constant within flow stress equation |
| n | - | Material constant within flow stress equation |
| $\bar{\varepsilon}$ | - | Effective plastic strain |

| | | |
|---|---|---|
| $\dot{\bar{\varepsilon}}$ | - | Effective plastic strain rate |
| $\dot{\bar{\varepsilon}}_0$ | - | Normalizing plastic strain rate |
| ΔH | K J $mol^{-1}$ | Activation energy for deformation |
| G | J $mol^{-1}$ $K^{-1}$ | Universal gas constant |
| $T_{melt}$ | °C | Melting temperature |
| $T_{ref}$ | °C | Reference temperature |
| UTS | MPa | Ultimate tensile stress |
| $F_x$ | kN | Welding force parallel to the direction of tool travel |
| $F_y$ | kN | Side force perpendicular to the direction of tool travel |
| $F_z$ | kN | Vertical force perpendicular to the top surface of the workpiece plates |
| $M_z$ | N.m | Torque acting on the FSW tool |
| FSW | - | Friction Stir Welding |
| TWI | - | The Welding Institute |
| FEM | - | Finite Element Model |
| FEA | - | Finite Element Analysis |
| TMAZ | - | Thermo Mechanically Affected Zone |
| HAZ | - | Heat Affected Zone |

# Chapter 1

# Introduction to Friction Stir Welding

## 1.1 Introduction:

Friction stir welding (FSW) was invented and experimentally proven by The Welding Institute (TWI) in December 1991 [1]. The process is purely mechanical and automated. It involves the joining of two metal pieces without melting them by joining their molecules together. The tool traverses along the joint causing sufficient frictional heat to soften the material without melting. The rotation of the tool then stirs the molecules together leaving behind a fully consolidated joint. An overview of the process is shown in Figure 1. What sets FSW apart from other fusion welding techniques is that it is a solid-state process. The melting temperature of the workpiece is never achieved and remains as a solid throughout the process. Because melting does not occur and joining takes place below the melting temperature of the material, a high-quality weld is created. This characteristic greatly reduces the ill effects of high heat input such as distortion and eliminates solidification defects which are usually associated with fusion welding.

Although the FSW process has many advantages over traditional fusion welding methods due to its solid state nature, it is still in its relative infancy compared with more traditional welding and assembly techniques. In particular, the process has not been implemented within the aerospace industry to the extent that one would have anticipated considering this industry was initially identified by TWI as having the most to gain by the process. This slow uptake of the FSW process will be discussed in further detail in section 1.4

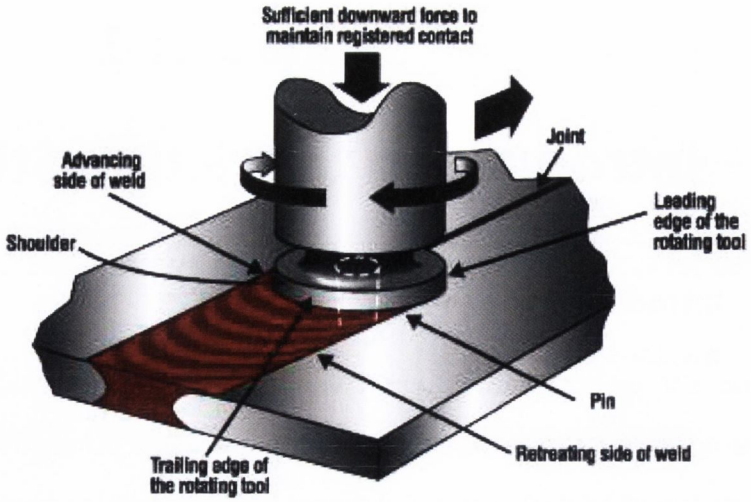


Figure 1: An overview of the Friction Stir Welding Process [2]

## 1.2 The Friction Stir Welding Process:

The friction stir welding process can be described by four stages: Plunge, Dwell, Translation and Extraction Stage. Before the process can begin, the two pieces of sheet or plate material to be welded are clamped rigidly onto a backing plate in a manner that prevents the abutting joint faces from being forced apart due to tool pin penetration. An overview of the different stages can be seen in Figure 2.

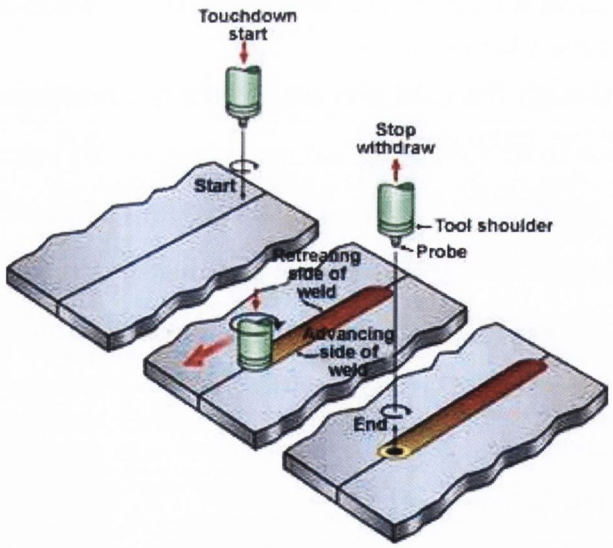


Figure 2: Different stages in FSW [8]

The first stage is the Plunge Stage, where a non-consumable tool rotating at high speeds is slowly plunged into the joint line between the two materials to be welded. The main features of a FSW tool consists of a pin and shoulder, an example of a typical FSW tool can be seen in Figure 3. Contact between the pin and the workpiece creates frictional and deformational heating which softens the workpiece material. The tool is plunged until contact between the tool shoulder and workpiece is accomplished. Shoulder contact further increases workpiece heating, expands the zone of softened material and constrains the deformed material. This ensures that the tool plunge depth is sufficient to establish a consolidated weld throughout the depth of the material but not so deep that the tool strikes the backing plate.

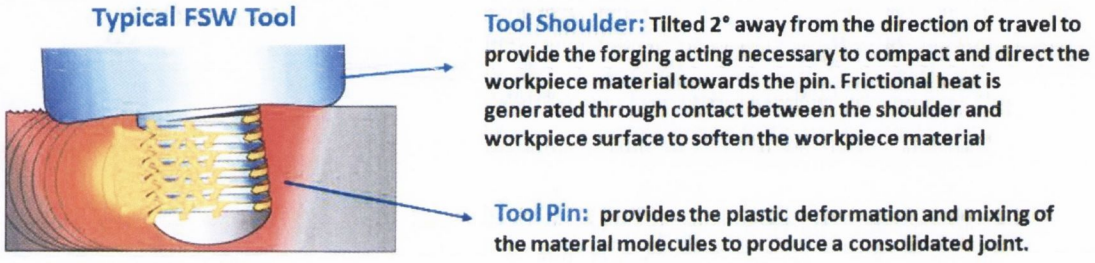


Figure 3: A typical FSW tool [8]

The second stage is the Dwell Stage. During this stage the tool is no longer plunged vertically but is still rotating and sufficient vertical force is supplied to maintain contact between the tool shoulder and the workpiece. The dwell period usually last between 5-20 seconds. During this time, heat is generated within the workpiece by friction between the rotating tool pin and shoulder, and also by severe plastic deformation of the workpiece. Localized heating softens material in the vicinity of the pin and on front of the tool, this is necessary to progress to the next stage.

The third stage is the Translation Stage. During this stage the tool begins to traverse along the joint line between the two plates. This leads to movement of material from the front to the back of the pin, thereby filling the hole in the tool wake as the tool moves forward producing a consolidated joint. During this stage the workpiece material undergoes a forging action underneath the tool shoulder which restricts material flow to a level equivalent to the shoulder position helping to form a continuous joint.

When a sufficient length of weld is produced, the tool is extracted from the welded workpiece and a key hole is left where the tool exits the joint which can be either machined off or filled in. Figure 4 shows two sheets of AA2024-T3 welded together using FSW. A smooth surface is achieved; however some machining may be required to remove any flash produced.

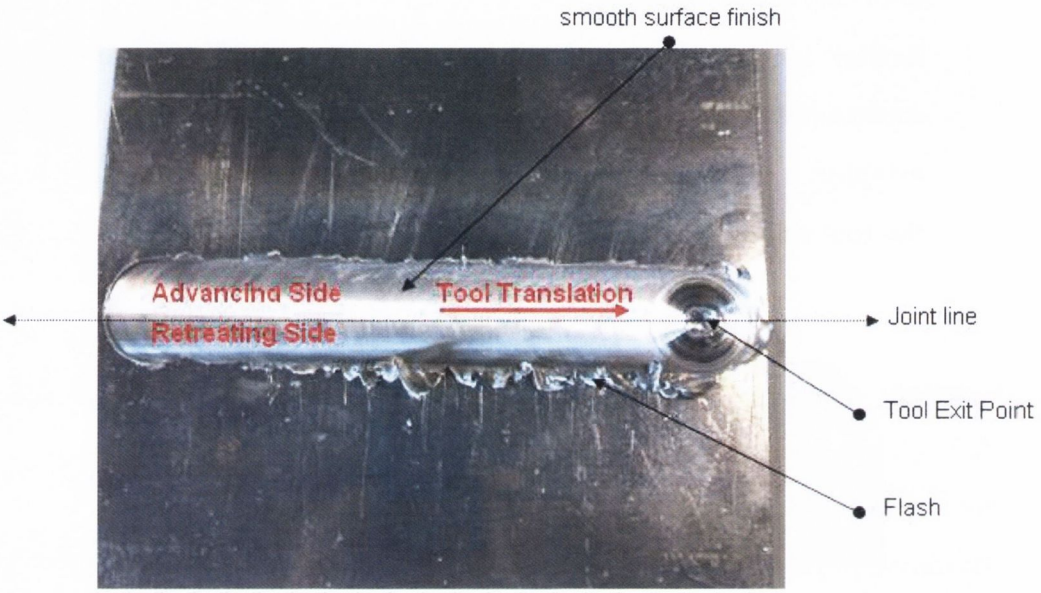


Figure 4: An example of two aluminium plates joined using FSW

## 1.3 Advantages of FSW:

FSW is considered a "green" technology because of its energy efficiency, environmental friendliness and versatility. When compared with conventional welding methods, FSW consumes considerably less energy, no consumables such as a cover gas or flux are used, no harmful emissions are produced during welding and it is relatively quiet thereby making the process environmentally friendly.

In FSW, the melting point of the material is never reached making it a solid state process. Therefore conventional welding defects such as porosity and oxidation which are associated when welding aluminium alloys can be avoided. Furthermore, because FSW does not involve the use of filler material and no melting occurs, any aluminium alloy can be joined without concern for compatibility of composition or solidification cracking which are issues associated with fusion welds. Also, dissimilar aluminium alloys and composites can be joined with equal ease [3-5].

In FSW, the joints are continuous compared with conventional mechanical joints, thereby resulting in improved structural rigidity. On large structures, significant weight saving can be achieved by using FSW. Friction stir welded joints can also improve the fatigue life of a structure as the stress concentrations associated with traditional mechanical fasteners, such as rivets, can be avoided. Additional key benefits of FSW are summarized in Table 1 [6].

| Metallurgical benefits | Environmental benefits | Energy benefits |
|---|---|---|
| Solid phase process | No shielding gas required | Improved materials use (e.g., joining different thickness) allows reduction in weight |
| Low distortion of workpiece | No surface cleaning required | Only 2.5% of the energy needed for a laser weld |
| Good dimensional stability and repeatability | Eliminate grinding wastes | Decreased fuel consumption in light weight aircraft, automotive and ship applications |
| No loss of alloying elements | Eliminate solvents required for degreasing | |
| Excellent metallurgical properties in the joint area | Consumable materials saving, such as rugs, wire or any other gases | |
| Fine microstructure | | |
| Absence of cracking | | |
| Replace multiple parts joined by fasteners | | |

Table 1: Key benefits of friction stir welding [6]

**FSW Aluminium Advantages:**

One of the main advantages associated with the FSW process is its ability to weld any series of aluminium alloys, in particular the 2xxx series and 7xxx series alloys. These alloys are used extensively within the aerospace industry due to their high strength to weight ratio. However, these alloys are mostly non-weldable using fusion welding methods due to problems with oxidization, solidification, shrinkage, sensitivity to cracking, hydrogen solubility and the resultant porosity problem [7]. Therefore, the majority of aircraft structural parts all tend to be mechanically joined using rivets.

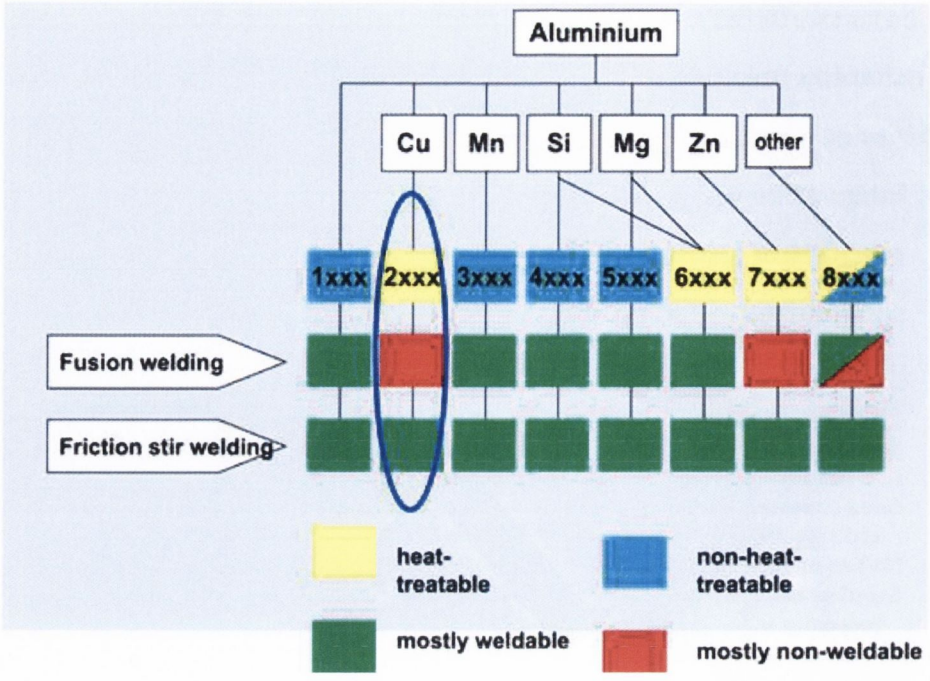


Figure 5: Weldability of Aluminium Alloys [19]

Frictions stir welding has many advantages over riveting:

- FSW provides greater fatigue strength, this is important when considering the life cycle of an aircraft especially during take-off and landing
- Using riveting, the two components remain as separate entities. FSW consolidates the two components into one therefore providing more structural rigidity.
- Unlike FSW, riveting cannot join two components in a butt-joint configuration without the presence of a cover plate. This means more material which adds to the weight of the structure.
- The shape of rivets increases the surface area of aerospace structures which can increase wind friction and hence increase drag which is undesirable. This is not an issue with FSW as it produces a smooth surface finish.
- Many thousands of rivets are required when assembling an aerospace structure which increases the aircrafts overall weight, fuel consumption and hence energy requirements. FSW is a non-consumable process therefore no weight is added.

## 1.4 Disadvantages/limitations of FSW:

As mentioned previously, FSW is still in its relative infancy compared to more traditional welding and joining methods. Although FSW has many advantages over riveting and mechanical fasteners, the process has not been implemented within the aerospace industry to the extent that one would have anticipated for a number of reasons some of which include:

The aerospace industry tends to be more conservative than most other industries due to the nature and operating environments of their products. Specifications or standards are the backbone of consistency. Currently, a few professional societies have technical committees entrusted with developing FSW process specifications. In addition some large aerospace organisations (NASA and Boeing) have developed their own welding specifications. These companies have adopted the FSW process as it provides solutions to critical problems rather than using FSW as an alternative to an existing technology. For example, Boeing used FSW to repair faulty MIG welds on aerospace fuel tanks which would have been scrapped otherwise. However, specifications have not yet emerged for general use. Lack of process specifications is a considerable barrier for industry-wide technological implementation. Most companies operate in a follower mode. That is, they wait until a significant number of technology adoption cases emerge to lower the risk of uncertainty. A broader acceptance of FSW will be feasible only after common specifications are readily available. The research community can help the FSW process by building demonstrative prototypes, establishing design guidelines and specifications, identifying new applications and presenting this information to new audiences. At this moment there is simply an insufficient amount of quantitative data available for many aerospace companies to become more comfortable with the FSW process. One of the objectives of this project was to help develop FSW process specifications for the FSW of aluminium 2024-T3 plates.

FSW of sensitive components can be restricted due to the large downward forces and heavy duty clamping required to fix the workpiece into position. This is especially the case in the aerospace industries as rigidly clamping structural components can sometimes be geometrically difficult. This is not a problem with riveting which is much more flexible than FSW. In FSW it is also necessary to have a backing plate underneath the workpiece

to support the high vertical forces, again highlighting the low flexibility of the process. Due to the large forces generated, equipment can be expensive as most commercially made equipment is individually designed for a given application and hence is more expensive than mass produced machines. This high equipment cost can be tolerated in high volume or high added value applications. Apart from the cost of equipment, which must be suitable for the intended joints, the FSW process has some tooling and setup costs that must be taken into account when calculating the cost per weld. Tight concentricity requirements, when needed, may be difficult to achieve. Also finishing operations may be required which adds to the total cost. Therefore, for short runs the process may not be economical. The cost and design of these machines will dictate the affordability of this technology. For widespread use of FSW across all industries, it is imperative to develop low cost machines. A better understanding of the forces occurring during the FSW process can help aid with the design of more efficient, cheaper and flexible machinery and the development of improved tooling designs. Characterizing the forces generated during the FSW of aluminium 2024-T3 was another objective during project.

The large number of variables that must be considered when implementing the process may also discourage the implementation of the process in some cases. Some of the variables to be considered are shown in Figure 6.

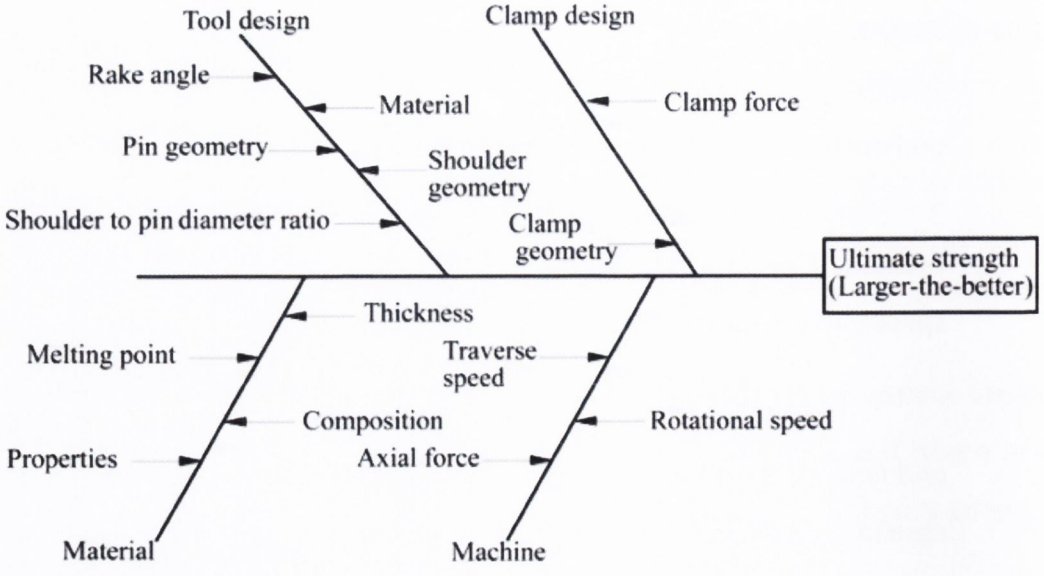


Figure 6: Variables to be considered when employing the FSW process [19]

## 1.5 Applications of FSW:

Friction Stir welding has many potential applications in numerous industries due to its many advantages over traditional fusion welding and joining techniques. Although there has been a relatively slow uptake of the process due to a number of reasons highlighted in the previous section, some companies have adopted the FSW for different applications as the process provided solutions to well recognised problems, shortcomings or achieved significant cost savings. Some of these applications are shown in Table 2.

| Company | Application | Reference |
|---|---|---|
| Boeing, US | Delta II Rockets | 9 |
| Eclipse, US | Aircraft Structure | 10 |
| Hydro Aluminium | Ship Deck Panels | 11 |
| U.S. Military Navy | Freedom Warship | 12 |
| Mazda RX-8, Japan | Aluminium Body Assemblies | 13 |
| Fontaine Trailers, US | Aluminium Trailers | 14 |
| Hitachi, Japan | Train Bodies | 15 |
| RIFTEC, Germany | Food Trays | 16 |
| SKB, Sweden | Copper Nuclear waste Canisters | 17 |

Table 2: Examples of some FSW applications

**Aerospace Industry:**

As mentioned in previously, alloys such as the 2XXX and the 7XXX series are widely used for aerospace structures such as fuselage, fins, wings, etc. Unfortunately, such high-strength aluminium alloys are difficult to join by conventional fusion welding. Therefore, traditionally, a large amount of aerospace structures are joined by means of riveting. The emergence of friction stir welding provides an opportunity to alter the traditional approach for producing lightweight assemblies with cost savings at the system level. TWI recommends that FSW can be used in the following potential aerospace applications:

- Wings, fuselages, empennages
- Cryogenic fuel tanks for space vehicles
- Aviation fuel tanks
- External throw away tanks for military aircraft
- Military and scientific rockets
- Repair of faulty MIG welds
- Various primary and secondary structural components

Although FSW has the ability to weld 2xxx and 7xxx series aluminium alloys and has many advantages compared to riveting, the process has not been implemented within the aerospace industry to the extent that one would have anticipated due to a number of reasons outlined in section 1.4. At present, most aerospace FSW applications have been technology driven where FSW provides solutions to major problems rather than providing an alternative. These applications have been limited to space shuttle division of large US companies such as Lockheed Martin, Boeing and NASA. The majority of commercial aircraft manufacturers have at present not adopted the FSW process. However, companies such as Airbus and Bombardier are currently researching the possibilities of adopting the FSW process for future generation of aircraft.

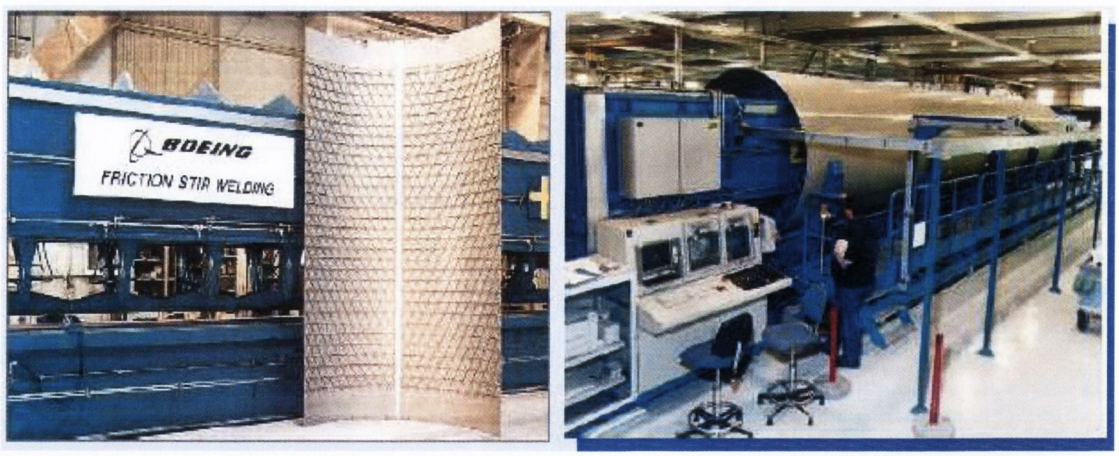


Figure 7: FSW of Boeing Delta II Rocket Tanks [18]

Eclipse Aviation is the only aircraft manufacturer at present that has adopted FSW for joining skins components and structures in the Eclipse 500 aircraft which was first delivered in 2006 [10] and is shown in Figure 8. The welded portions of the Eclipse 500 are shown in Figure 9. They include cabin skins, aft fuselages skins, upper and lower wing skins, side cockpit skins and the engine beam [10].

Figure 8: Eclipse 500 aircraft [10]

Figure 9: Eclipse 500 FSW Assemblies [10]

## 1.6 Research Objectives:

The slow or lack of uptake of the FSW process within the aerospace industry is attributed to a lack of process specifications, lack of design guidelines, the generation of large forces requiring high cost machinery and the large number of variables that must be considered before adopting the FSW process. All of the above presents a serious barrier for industry-wide technological implementation. Also, at present most commercial airliners are completely designed, modelled and tested using computer aided and engineering software before manufacture. Therefore, the development of a finite element model to simulate the process is also necessary to increase the uptake of the process within the aerospace industry.

The workpiece material chosen for this project was the aerospace aluminium alloy 2024-T3 of thickness 4.82mm. The overall aim of the project was to optimise the operational parameters and tooling design, and also to provide an extensive understanding of the FSW process during the welding of this material. The purpose is to provide reliable experimental and FE data to help address process issues and thereby

contribute to a greater uptake of the FSW process within the aerospace industry. Also, as the only University in Ireland (at present) researching this remarkable process, it is hoped this project will introduce the capabilities of FSW to new audiences. The primary objectives of this project were as follows:

1. Development of a FSW rig that can accommodate a range of different research instrumentation to monitor the FSW process.

2. Develop specific guidelines on how the FSW process should be implemented with respect to the chosen workpiece material.

3. Design, manufacture and test a number of complex tooling designs to determine which tooling arrangement produces optimal results.

4. Monitor the temperatures occurring during the process to get a better understanding of heat generation and thermal flow.

5. Characterize the force occurring during the process to get a better understanding on tooling/machine design and requirements.

6. Develop a processing window for a range of different operational parameters to determine their effect on the resultant welded joint.

7. Develop a fully thermo mechanical FE model capable of modelling the FSW process.

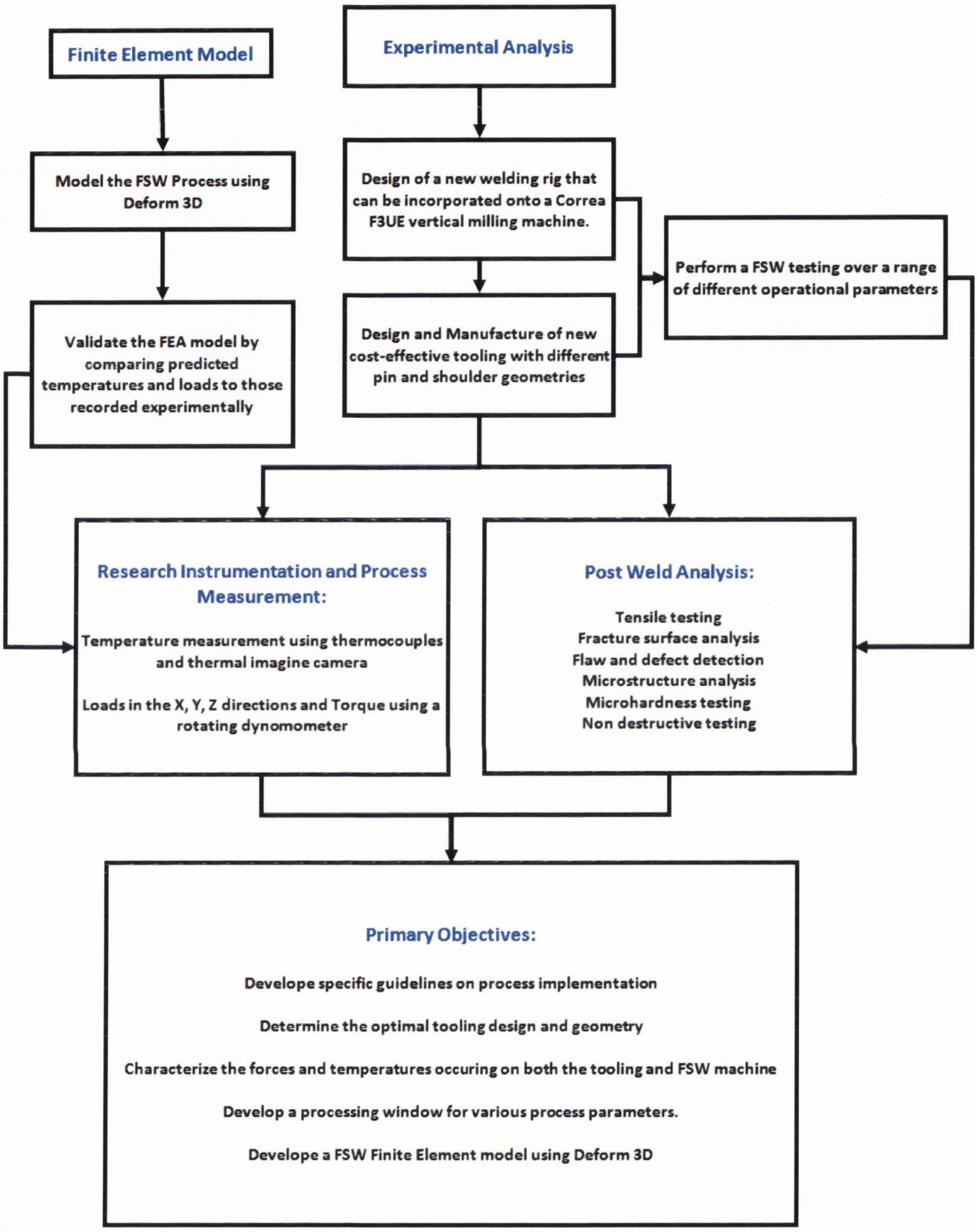


Figure 10: Project Overview / methodology

# Chapter 2

# Literature Review

There are a large number of variables to consider when implementing the FSW process and they have various causes and effects. As a result there are many research papers available focusing on different aspects of the FSW process. Throughout this chapter the main emphasis is on previous research that involved FSW of a similar 2xxx series aluminium alloy to that used throughout this project (AA2024-T3) and also similar tooling, workpiece thickness, tooling design and operational parameters. However, in some cases a more general overview of particular aspects is presented.

## 2.1 Friction Stir Welding Tooling:

The tool serves three primary functions during the FSW process. That is, heating of the workpiece, movement of the material to produce the joint and containment of the hot metal beneath the tool shoulder. Heating is created within the workpiece both by friction between the rotating tool pin and the shoulder with the workpiece and by severe plastic deformation of the workpiece. The localized heating softens the material around the vicinity of the pin. This combined with the tool translation and rotation leads to movement of material from the front to the back of the pin, therefore filling the hole left behind from the tool wake as it transverses forward along the weld line. The vertical force applied by the tool shoulder on to the workpiece surface prevents material flow above the initial workpiece top surface.

Friction Stir Welding is not possible without the non consumable tool. Therefore, tool design is critical to ensure optimum weld performance. There are four factors to decide upon when designing a FSW tool:

- Tool material
- Shoulder design
- Pin design
- Tool dimensions

When choosing these factors it is also necessary to consider the following variables for a particular FSW application:

- Workpiece materials
- Joint configuration (Lap, but joint etc..)
- Process parameters ( rotational speed, translational speed, tilt angle)
- Particular application

### 2.1.1 Tool Materials:

Knowledge of the tool material properties is important when selecting the correct tool material. Some of the characteristics to consider are:

- **Cost and Availability:** a tool material is not useful if a steady supply is not available at a reasonable cost.

- **Machinability:** some tools are designed with complex features on both the shoulder and the pin. Any material that cannot be machined relatively easily to the correct dimensions should not be considered

- **Ambient and Elevated Temperature Strength:** tool material must be able to withstand the compressive and shear loads both as the tool enters the workpiece at ambient temperature and as it traverses along the joint line at elevated temperatures. Prevention of tool fracture or distortion is essential.

- **Wear Resistance:** excessive wear can alter the tool shape, therefore increasing the probability of defects and reducing tool life.

- **Fracture Toughness:** Local stresses and strains produced when the tool first touches the workpiece are sufficient to break the tool. Lienert and Stellwag [20] reported that tool damage was most significant during the initial plunge and dwell phases during FSW.

- **Tool Reactivity:** Tool materials must not react with the environment or the workpiece as this could alter surface properties of the tool.

There are many published reports available for a range of different tool materials and potential FSW applications. Table 3 shows a summary of the current tool materials used in FSW in relation to workpiece material and thickness [19]. Table 4 displays the properties of the different tool materials [19]. Throughout this project AISI H13 tool steel was used to manufacture the FSW tooling. The advantages of using this tool steel are that it is abundant, easily machined, has a low cost and has well established characteristics. AISI H13 is a chromium-molybdenum hot-worked air hardened steel. It is known for its good elevated temperature strength, thermal fatigue resistance and wear resistance [21]. In addition to FSW of aluminium alloys, H13 tools have also been used to friction stir weld copper. For example, Anderson and Andrews successfully friction stir welded 3mm thick copper plates using H13 as the tool material [17].

| Alloy | Thickness mm | Tool Material | Status |
|---|---|---|---|
| All common Al alloys, Mg alloys | <12 | AISI-H13, -M42, other tool steels | Commercial use or development |
| Al alloys except 7xxx | 12 < t < 75 | AISI-H13, -M42, other tool steels | Commercial use, + development |
| Al 7xxx alloys | 12 < t < 50 | Densimet D176, Cobalt MP159 | Development |
| Copper + alloys | <50 | Densimet D176 Cobalt MP159 Nickel alloys | Development + commercial use |
| Titanium + alloys | <10 | W-25Re | development |
| C-Mn steels Stainless steels Ni alloys | <15 | W-25Re, PCBN, W alloys, ceramics | development |

Table 3: Current tool material used for FSW [19]

| Material | $T_{max}$ °C | Available ? | Machinable ? | Reacts with ? | Thermal Stability |
|---|---|---|---|---|---|
| Tool Steels | 500 | Excellent | Good | Ti | Good |
| WC-Co | 800 | Excellent | Very Poor | Ti | Good |
| W Composites | 800 | Excellent | Good | OK | Good |
| Refractory Metals | 1000+ | Good | Poor | OK | Some may oxidise |
| Ni alloys | 800 | Poor | Poor | Ti | Good |
| Co alloys | 800 | Good | Poor | Ti | Good |
| Stainless steels | 800 | Excellent | Good | Ti | Good |
| Intermetallics | 800+ | Very poor | Very Poor | Some with Ti | Mostly Good |
| Ceramics | 1000+ | Variable | Very Poor | Some with Ti | Excellent |

Table 4: FSW Tool Material Properties [19]

### 2.1.2 Design of the Tool Shoulder:

The function of the shoulder is to provide frictional heating and also to provide the downward forging action necessary for weld consolidation. The first shoulder design successfully used for FSW had a concave geometry [1] as illustrated in Figure 11 and is still the most common shoulder design used in FSW. The shoulder concavity is produced by a small angle between the edge of the shoulder and the pin, between 6-10°. During the tool plunge, material displaced by the pin is fed into the shoulder cavity which acts as a reservoir for the material back extruded by the deformational plunging of the pin and hence the forging action of the shoulder. Translation of the tool along the weld line forces new material into the shoulder cavity, thereby pushing the existing material into the flow of the pin. Utilisation of this concave shoulder requires a tool tilt angle of 2-4°, Figure 12 illustrates the tool tilt angle. This tilt angle is critical in maintaining the material reservoir and enabling the trailing edge of the shoulder to impart a compressive forging force on the workpiece to ensure a consolidated weld.

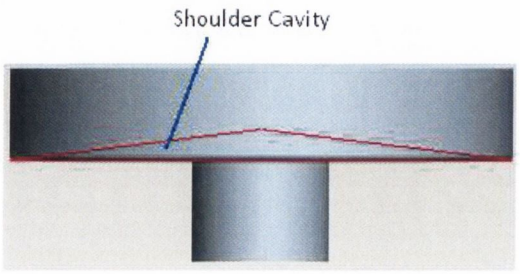


Figure 11: Shoulder cavity on a concave shoulder

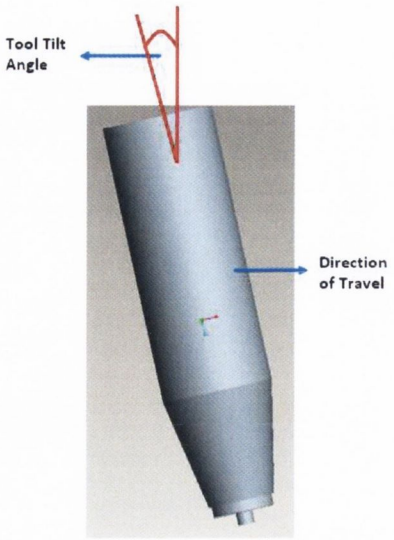


Figure 12: Tool Tilt Angle

The majority of research (past and present) conducted on the FSW of aluminium 2024 and other 2xxx series alloys used a concave shoulder design [some examples: 42, 43 47, 49, 50, 91, 92, 93]. Another example is Elangovan and Balasubramanian who examined the influences of concave tool shoulder diameter (15, 18 and 21mm) on the FSW of 6mm thick AA6061 plates [24]. These authors reported that of the three shoulder diameters used to fabricate the joints, a tool with an 18 mm shoulder diameter produced a defect free weld with the greatest joint efficiency and microhardness values irrespective of tool pin profiles. An example of these authors results are shown in Figure 13 . They attributed this to the relationship between the shoulder diameter and the heat generation due to friction. These authors reported that a large shoulder diameter of 21mm will generate more heat due to the larger contact area and greater peripheral velocity. Which resulted in a wider TMAZ and HAZ region and hence the tensile properties and weld quality of the joints deteriorated. They reported that smaller tool shoulder diameter of 15mm generates less heat due to its smaller contact area and lower peripheral velocity. This resulted with insufficient weld consolidation.

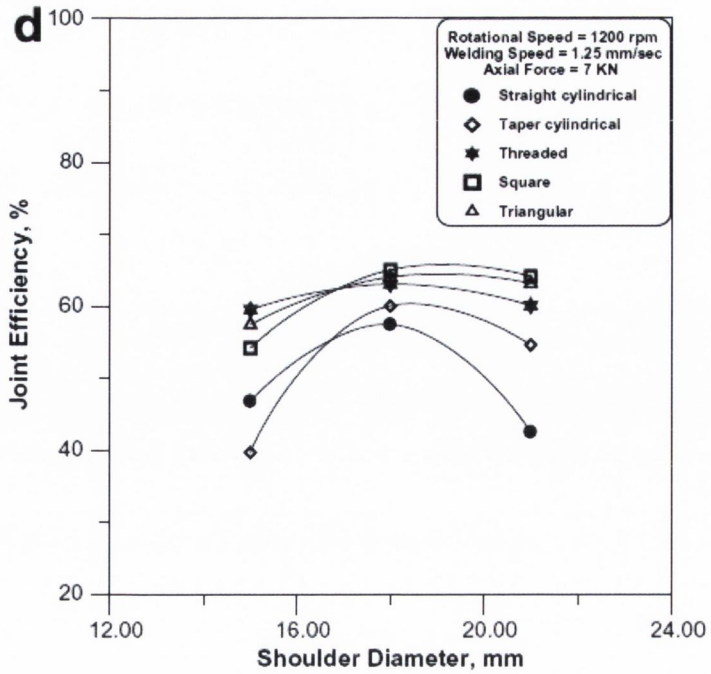


Figure 13: Effect of Shoulder Diameter on Joint Efficiency, Elangovan and Balasubramanian [24]

A more recent tool development by TWI is a shoulder having a scrolled design machined onto it and is shown in Figure 14. Some of the advantages claimed by TWI regarding the scrolled shoulder are as follows:

- The channels direct deformed material from the edge of the shoulder towards the pin, therefore eliminating the need for a tilt angle
- Eliminating the tilt angle enables higher welding speeds, the ability to produce non-linear welds and also reduces tool lift.
- Material within the spiral channel is continuously sheared from the plate surface and provides an enhanced shoulder friction heating surface. This enables the use of a smaller diameter tool shoulder.
- Elimination of weld surface undercut which results in a reduction in flash and an improved surface finish. Therefore the need for post weld removal of flash for aesthetic, corrosion or fatigue prevention reasons is eliminated.

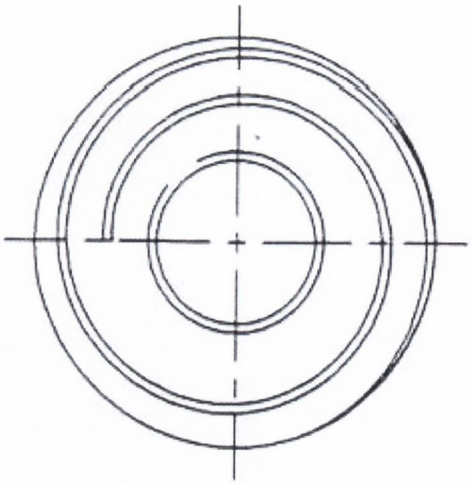

Figure 14: Scroll shoulder Design [23]

Only a small number of authors have implemented the scrolled shoulder design during FSW. The TWI tends to keep their most recent/advanced tooling designs and results confidential for companies who hold a FSW licence from TWI. Therefore information of the scroll design (number of revolutions, pitch length, scroll height, land width, shoulder diameter) and process specification (optimal shoulder plunge depth) is not readily available. This may explain the lack of research conducted using the scrolled shoulder design. To date no authors have publically published papers reporting successful Friction Stir Welding of the workpiece material chosen for this project (AA2024-T3) using a scrolled shoulder design.

Scialpi and Filippis examined the effects of shoulder geometry on microstructure and mechanical properties of friction stir welded aluminium 6082 butt joint of thickness 1.5 mm [27]. They examined the effects of three different shoulder designs which are shown in Figure 15. These authors reported that for tensile tests, the three joints showed good strength and very little differences between the 3 designs. (see Table 5). Similar results were concluded for micro hardness tests.

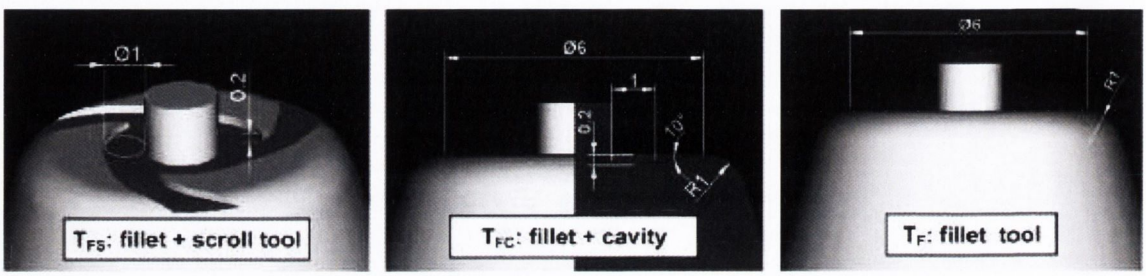

Figure 15: Three Different Shoulder Designs used by Scialpi and Filippis [27]

UTS for transverse tensile test at room temperature

| | UTS (MPa) | $UTS_W/UTS_{BM}$ (%) |
|---|---|---|
| Base metal | 331 | 100 |
| $T_{FS}$ | 252 | 76 |
| $T_{FC}$ | 254 | 77 |
| $T_F$ | 252 | 76 |

Table 5: Tensile tests Performed by Scialpi and Filippis [27]

Leal and Leitao produced friction stir welded butt joints in 1mm thick plates of AA5182 and AA6016-T4 aluminium alloys [28]. These authors used two different shoulder designs, a concave shoulder and a scrolled shoulder which are illustrated in Figure 1. These authors reported a reduction in weld thickness for the concave shoulder but reported no reduction in weld thickness with the scrolled shoulder. They also reported that the concave shoulder produced a smoother surface finish compared to the scrolled shoulder as shown in Figure 17.

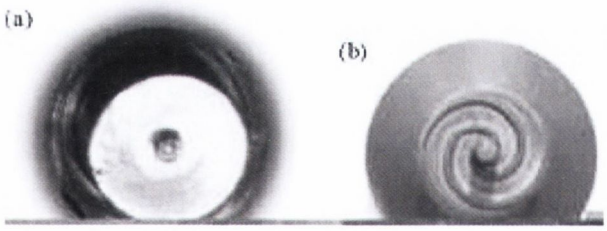


Figure 16: (a) Concave Shoulder, (b) Scrolled Shoulder used by Leal and Leitao [28]

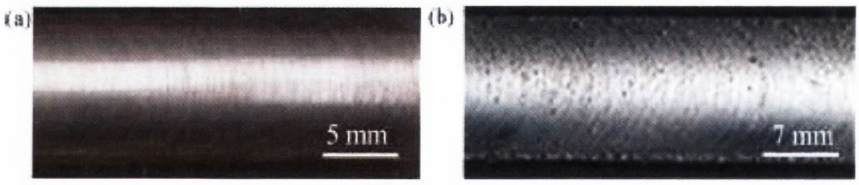


Figure 17: Surface Finish (a) Concave Shoulder and (b) Scroll Shoulder [28]

### 2.1.3 FSW Pin Design:

The function of the tool pin in FSW is to produce deformational and frictional heating of the workpiece materials. It is designed to merge the two workpiece materials together by shearing the material in front of the tool and then moving it behind the tool. The depth of deformation throughout the workpiece thickness is directly proportional to the length of the tool pin. Additionally, it is also important to consider the tool pin design when choosing a translational speed. High translational speeds induce large forces upon the tool pin which must be able to withstand these forces otherwise pin fracture can occur.

There is a wide range of different tool pin designs available and discussed in published literature. Tool pins come in many different shapes, sizes and some have features machined onto them. The first FSW pin cited in the original FSW patent [1] consists of a cylindrical threaded pin and an example of this type of design is shown in Figure 18. The intended function of the threads on the pin is to transport the workpiece material from the shoulder down to the bottom of the pin. Therefore a tool rotating in a clockwise direction will require left handed threads.

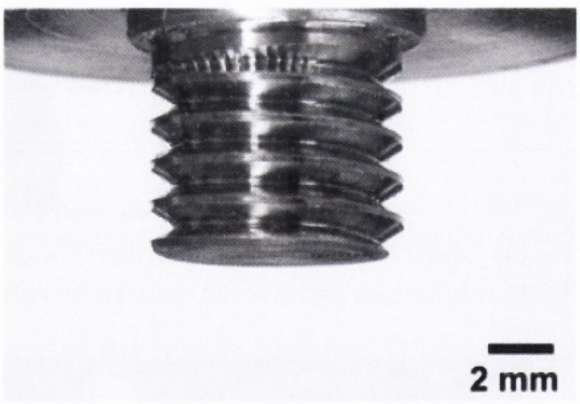


Figure 18: Threaded Cylindrical Pin [1]

In some FSW applications, threaded features on the pin cannot survive without fracture or severe wear. These applications require the tool pin to operate under aggressive environments, for example high temperature or highly abrasive composite alloys. The pins cannot retain their threaded features without excessive pin wear or fracture. In such cases a unthread pin is used due to their robust but yet simple design, Figure 19. An unthreaded tool is also used when welding thin sheets. Pin designs for thin sheets are small with little surface area for features. Machining threads onto the pin

would significantly weaken it and cause premature pin failure. For example, Scialpi et al [27] used an unthreaded tool during the FSW of AA6082 with a thickness of 1.5mm and report weld strength efficiencies between 76 – 77% of the parent material. Shanmuga and Murugan [26] also used an unthreaded cylindrical pin design during the FSW of dissimilar aluminium alloys, aa2024 and AA5083.

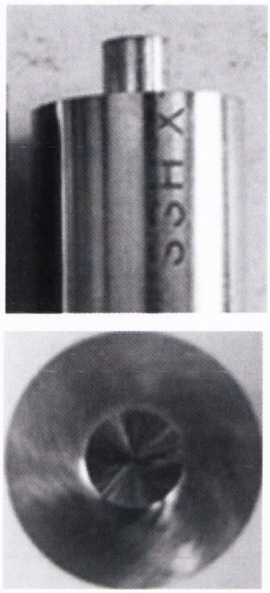

Figure 19: Unthreaded Cylindrical Pin [26]

One adaptation of a cylindrical or straight (threaded or unthreaded) FSW tool pin is to place a taper onto it as shown in Figure 20. As the tool traverses along the weld line, the largest moment load acting on the tool occurs at the base of the pin. The base of a tapered pin will be stronger than that of a cylindrical pin due to its greater thickness. This enables faster welding speeds and also the ability to weld thicker plates. For example Fonda and Bingert [30] used a FSW pin with a taper to FSW 25mm thick aluminium-lithium alloy 2195 plates.

Figure 20: Tapered Threaded FSW Tool Pin [30]

Another feature that has been machined onto the FWS pin is a number of flats; Figure 21 shows an example of a tool with flats. Thomas et al [25] stated that the addition of flat regions to the tool pin increased the deformation of the plasticised workpiece material by acting as paddles and producing local turbulent flow which increases mixing of the materials. During FSW testing of 25.5mm thick 5083-H131 plates, Colligan, Xu and Pickens reported that a reduction in transverse forces and tool torque was directly proportional to the number of flats placed on a truncated cone [32].

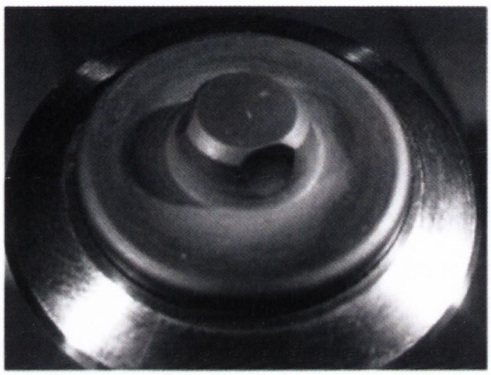

Figure 21: Unthreaded Tool Pin with 3 Flats [31]

A more recent (2010) paper on tool pin design was published by Shanmuga and Murugan [26]. These authors tested 5 different pin designs (tapered Cylindrical with Groves (CG), Tapered Square (TS), Tapered Hexagon (TH), Paddle Shape (PS) and Straight Cylindrical (SC)) during the FSW of AA2024 and AA5083 of 5mm thickness. The different tooling designs tested by these authors can be seen in Figure 22. Results indicated that the TH tool pin closely followed by the TS tool pin produced the highest tensile strength and elongation over a range of different rotational speeds (800 – 1600 rpm) and translational speeds (40 – 80 mm/min). This was attributed to the flat faces associated with these pin increasing the amount of plastic deformation and mixing of the workpiece materials.

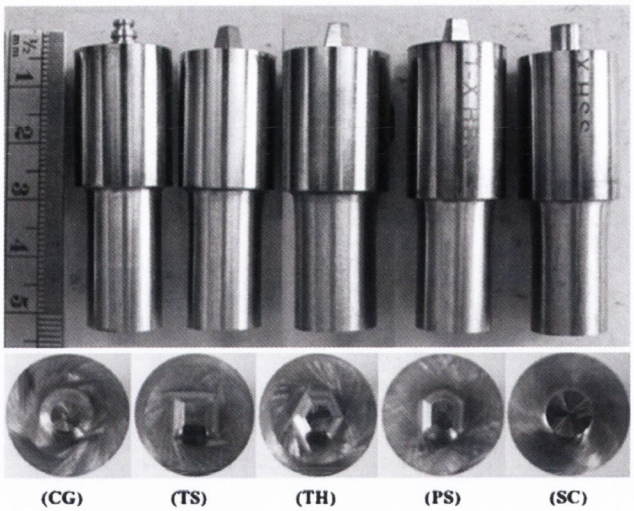


Figure 22: Different pin shapes, Shanmuga and Murugan [26]

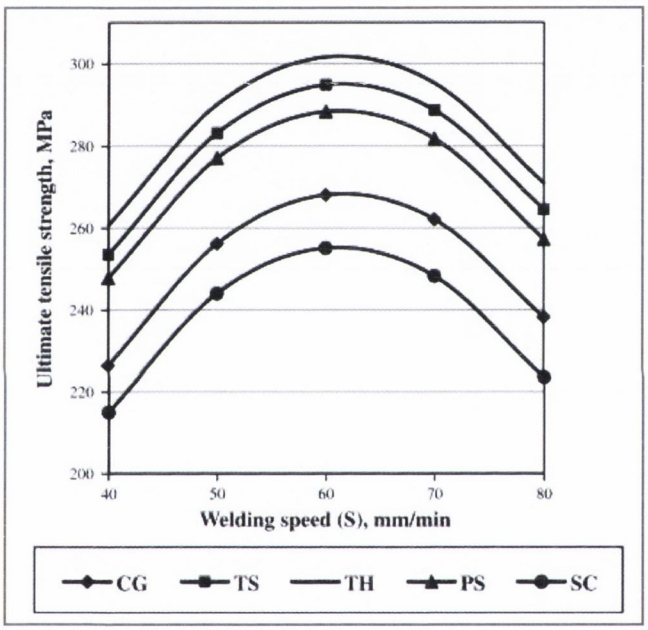


Figure 23: UTS for different pin design, Shanmuga and Murugan [26]

K. Elangovan and V. Balasubramanian also examined the effects of tool pin design on the FSW of AA2219 plates of 6mm thickness [34,35]. The five different pin designs shown in Figure 24 were used and welds were produced using three different rotational speeds (1500, 1600, 1700 rpm) and three different translational speeds (0.37, 0.76, 1.25 mm/s). The results shown in Figure 25 indicated that welding using the square pin design always produced defect free welds irrespective of rotational and translational speeds, joints fabricated using the square tool profile exhibited superior tensile properties compared to the other joints. Again this was attributed to the flat faces of the

square pin producing a pulsating action which encouraged increased plastic deformation and mixing of the workpiece materials.

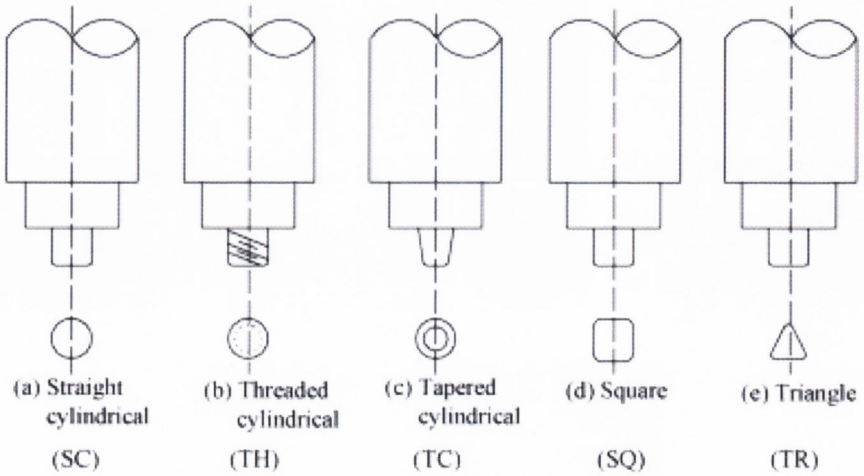


Figure 24: Elangovan and Balasubramanian, tool pin profiles [34]

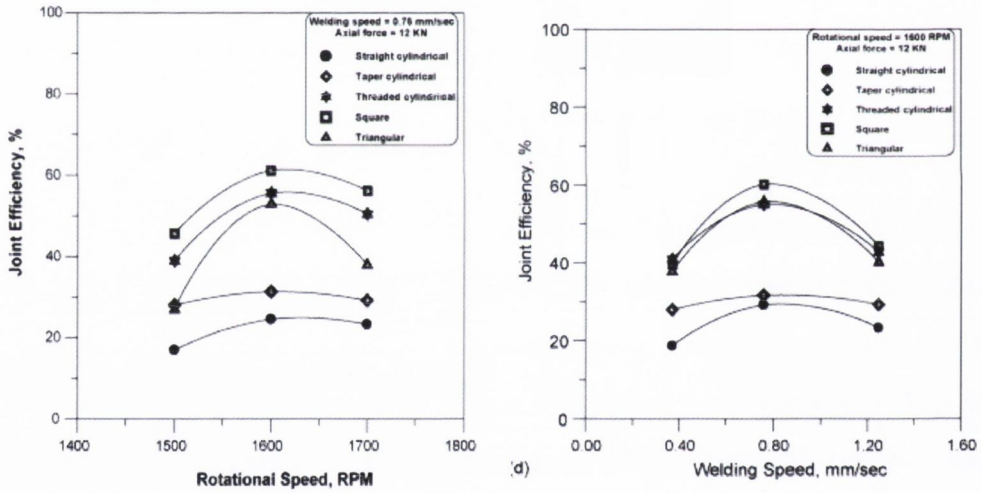


Figure 25: Elangovan and Balasubramanian, effect of pin profile on joint efficiency [34]

The MX Triflute pin is the latest tool pin designed by TWI for FSW of both aluminium alloys and copper alloys [36, 37]. It consists of a three flute tapered design cut into a helical ridge. Some of the advantages claimed by TWI regarding the MX Triflute tool pin are as follows [29]:

- Triflute pin displaces 70% less material during welding than a cylindrical pin and hence reduces the stress acting on the tool during welding.

- Helical flutes and threaded features produce a more efficient material flow path, the break up and dispersal of surface oxides, and an increase the interface between the pin and the plasticised material.
- The major factor determining the high performance and the superiority of the MX Triflute probe over a conventional cylindrical pin is the ratio of the volume of the pin swept during rotation to the volume of the probe itself. The ratio between dynamic volume as opposed to the static volume for the Triflute pin is 2.6:1 where as it is 1.1:1 for a cylindrical pin. This indicates the increased plastic deformation and mixing of the workpiece material associated with the Triflute pin design.

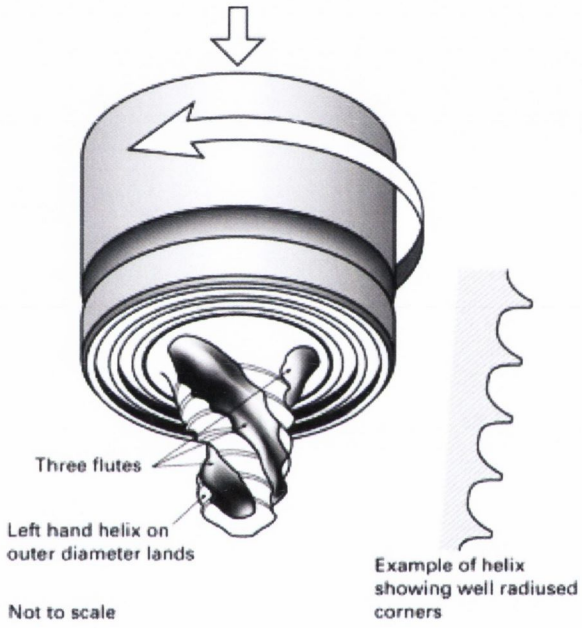


Figure 26: MX Triflute Tool Pin [36]

Similar to the scrolled shoulder design, only a limited number of authors have implemented the MX Triflute design during FSW. This is because as mentioned earlier the TWI tend to keep their most recent/advanced tooling designs and results confidential to companies holding one of their FSW licences. However papers that do report the use of the MX Triflute pin don't give any great detail of the design, operational parameters, results and process specifications. For example, Strangwood and Davis report the production of successful FSW butt joints of AA5251 using an MX Triflute tool [38]. SKB a Swedish nuclear waste management company, who are currently manufacturing 50mm thick copper canisters using FSW to store nuclear waste, reported that changing to an MX

Triflute pin design increased the tool travel speed by 2.5 compared to their previous threaded pin design without sacrificing weld strength [39].

### 2.1.4 FSW Tool Dimensions

The workpiece thickness determines the pin length to achieve a consolidated weld throughout the thickness. Pin diameters need to be small enough to allow consolidation of the workpiece material behind the tool but also must be large enough to support the traverse load and not fracture. The ratio of shoulder diameter to pin diameter is dependent on the material thickness and the heat input required. Researchers have preformed successful welds using a range of different shoulder-to-pin ratios for different materials and thicknesses. Some of these are listed in Table 6. TWI reported a number of different tool dimensions to give optimum performance for various aluminium alloy of different thickness [40] and these recommendations are shown in Figure 27.

| shoulder Diameter (mm) | Pin Diameter (mm) | Shoulder-to-pin ratio | Workpiece material | Thickness (mm) | Ref |
|---|---|---|---|---|---|
| 13 | 5 | 2.6:1 | Al 6061-T6 | 3 | 41 |
| 20-30 | 8-12 | 2.5:1, 1.6:1 | Al 7050, 2195, 5083, 2024, 7075 | 6.35 | 42 |
| 23 | 8.2 | 2.8:1 | Al 2024-T351 | 6.4 | 43 |
| 20, 16 | 6 | 3.3:1, 2.7:1 | Al 5083 and 6061 | 5.5 | 44 |
| 12 | 4 | 3:1 | Al 1050 and oxygen free copper | 1.8 | 45 |
| 25.4 | 7.87 | 3.22:1 | Al 7075-T7351 | 9.53 | 46 |
| 23 | 8.4 | 2.7:1 | Al 2524-T351 | 6.4 | 47 |
| 20 | 4 | 5:1 | Al 6064 to Carbon Steel | 4.5 | 48 |
| 23 | 8.2 | 2.8:1 | Al 2024-T351 | 7 | 49 |
| 10 | 3.8 | 2.6:1 | Al 2095 | 1.63 | 50 |
| 25 | 9 | 2.8:1 | Al 5251 | 5 | 51 |

Table 6: Summary of tool dimensions used by different researchers

| Aluminium Alloy | Material Thickness mm | FSW Tool Dimensions | | | | | | | | | | |
|---|---|---|---|---|---|---|---|---|---|---|---|---|
| | | A† | B | C* | D | E | F | G | H | I | J | K |
| 2014 | 3.2 | M5 x 0.7 | 3.75 | 3.0 | 15 | 10° | 0.7 | 6 | 26 | 11 | 2 | 2 |
| 2219 | 6.4 | M8 x 1 | 6 | 6.2 | 25 | 7° | 1 | 10 | 35 | 19 | 2 | 2 |
| 5083 | 12.7 | M11 x 1.25 | 8.25 | 12.5 | 33 | 7° | 1 | 10 | 35 | 28 | 2 | 2 |
| 5754 | 1.6 | M3 x 0.5 | 2.5 | 1.4 | 10 | 7° | 0.5 | - | 15 | - | - | - |
| 6082 | 1.6 | M3 x 0.5 | 2.5 | 1.4 | 7.5 | 10° | 0.5 | - | 15 | - | - | - |
| | 3.2 | M5 x 0.7 | 3.75 | 3.0 | 12.5 | 10° | 1 | 6 | 26 | 9 | 2 | 2 |
| | 6.4 | M8 x 1 | 6 | 6.2 | 20 | 8° | 1 | 10 | 35 | 15 | 2 | 2 |
| | 12.7 | M11 x 1.25 | 8.5 | 12.5 | 25 | 10° | 1 | 10 | 35 | 19 | 2 | 2 |
| 7075 | 3.2 | M6 x 0.75 | 4.5 | 3.0 | 15 | 10° | 0.7 | 6 | 26 | 11 | 2 | 2 |
| | 6.4 | M10 x 1.25 | 7.5 | 6.2 | 25 | 8° | 1 | 10 | 35 | 19 | 2 | 2 |
| | 12.7 | M12 x 1.5 | 9 | 12.5 | 30 | 7° | 1 | 10 | 35 | 19 | 2 | 2 |

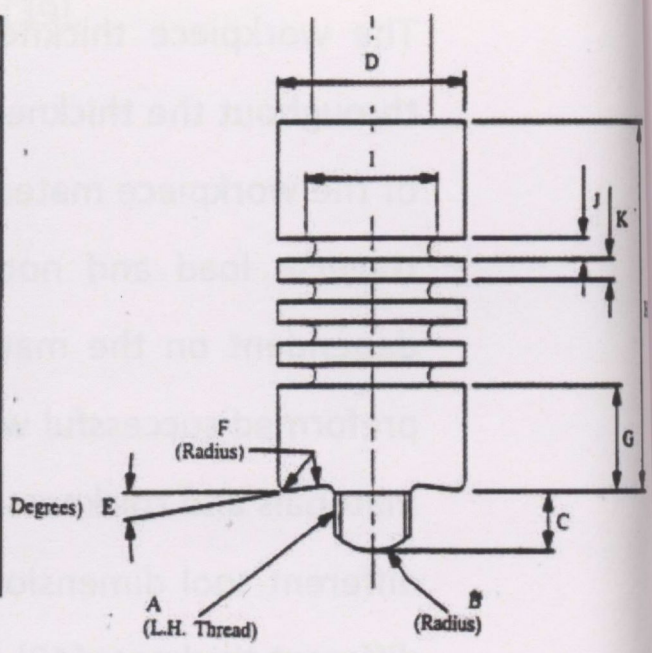


Figure 27: TWI recommended tool dimensions [40]

## 2.2 Friction Stir Welding Operational Parameters:

The operational parameters controlled through the FSW machine are listed below:

- Rotational speed
- Translational speed (welding/traverse speed)
- Tool tilt angle
- Plunge Speed
- Tool plunge depth (position controlled machinery)
- Tool vertical force (force controlled machinery)

All of these parameters are inputs into the process and vary in relation to the material to be welded, the weld depth required and the FSW tool designed used. The choice of parameters to be used is determined by the quality and performance requirement of the welded component or application. For example strength, ductility, formability, corrosion performance, dissimilar welds etc. Although there are many different performance requirements to decide upon in FSW, the primary goal is to produce a defect free weld with optimum weld strength efficiency or a weld strength efficiency above an acceptable standard. With those two goals in mind, the most influential operational parameters are tool rotational speed and translational speed. Lakshminarayanan and Balasubramanian carried out a Taguchi analysis on the FSW of aluminium alloys and reported that rotational speed and translational speed were the most significant operational parameters contributing to tensile strength of FSW joints. An example of their results is shown in Figure 28 [52].

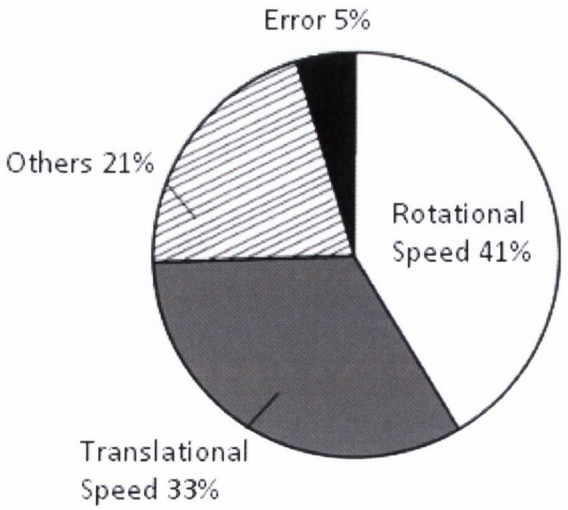


Figure 28: Percentage significance of operational parameters for FSW [52]

A large range of rotational speeds and translational speeds have been reported by different authors. This is attributed to the large number of factors affecting these chosen parameters which include; machine limitations, tool shoulder and pin geometry, tool material, workpiece material and workpiece thickness. Even when considering a single material, AA2024, with a thickness range between 3 – 6 mm, there is a large range of operational parameters reported by authors as indicated in Table 7. Also, it can be seen that many authors fail to specify the exact operational parameters, tooling designs and dimensions chosen during their research, which prevents the emergence of general process specifications associated with this particular material and thickness.

| Workpiece | Workpiece Thickness (mm) | Tool Pin | Tool Shoulder | Tilt Angle | Rotational Speed (rpm) | Translational Speed (mm/min) | Date | Reference |
|---|---|---|---|---|---|---|---|---|
| 2024-T3 | 4 | N/A | N/A | N/A | 800-2400 | 80-240 | 1999 | 72 |
| 2024(T351 and T6) | 6 | screw head pin, no diameter given | concave shoulder, 16mm diameter | 1-2 degrees | 850 | 120 | 2005 | 91 |
| 2024-T3 | 6 | N/A | N/A | N/A | 340 - 531 | 272 - 476 | 2004 | 56 |
| 2024-T3 and 6065-T4 | 4 | 5mm diameter cylindrical threaded pin | concave shoulder, 15mm diameter | N/A | 500 - 1200 | 150 - 400 | 2007 | 92 |
| 2024-T3 | 5 | threaded, 6mm diameter, height 5.5mm | 16mm diameter | N/A | 850 | 120 | 2005 | 95 |
| 2024-T3 | 6 | N/A | N/A | N/A | N/A | N/A | 2011 | 94 |
| AA2024-T6 and AA5083-H321 | 5 | Numerous pin shapes (cyl, sq, hex,paddle, groves) | N/A | N/A | 800 - 1600 | 40 - 80 | 2010 | 26 |
| 2024-T351 | 3 | screw taper, 5mm base, 4mm tip, 2.9mm length | 17mm diameter | 2-3 | 2140 | 40 | 2009 | 93 |
| 2024-T351 | 6.35 | M8 threaded tool | N/A | N/A | 215 - 468 | 75 - 154 | 2007 | 57 |

Table 7: Operational parameters during FSW of 2xxx series aluminium alloys

TWI claims that the flexibility of the FSW process is attributed to the range of operational parameters. However changing these operational parameters can have a significant effect on the mechanical properties of the welded joint, desired application, and the forces acting on the tooling and machinery. Therefore specific process guidelines need to be established with a clear understanding of the resulting outcome if FSW is to be implemented to a greater extent within the manufacturing industry.

### 2.2.1 Effect of Rotational Speed:

FSW can be conducted over a wide range of rotational speeds. However, in general too low a rotational speed will reduce the amount of heat generated through friction and plastic deformation by the tool shoulder and pin on the workpiece. Insufficient heat generation will not soften the workpiece material sufficiently and therefore will increase the stresses acting on the tool as it traverses through the workpiece and increase the risk of tool fracture. Too low a rotational speed can also result in a lack of stirring of the material to be welded which leads to a poor weld consolidation, the formation of defects and poor weld strength. On the other hand too high a rotational speed can also cause problems due to overheating. For FSW to maintain its claim as a steady state process, the maximum temperature must not exceed 80% of the melting point temperature of the material to be welded. Restricting elevated temperatures and melting also ensures FSW avoids conventional welding defects. In heat treated alloys, excessive heating can reverse the heat treatment and reduce the strength of the alloy. Also, the majority of heat generation occurs at the top surface due to contact between the shoulder and workpiece. Therefore excessive heating can cause uneven heat dispersion through the thickness of the workpiece material and may cause distortion of the workpiece.

Moataz and Hanadi [53] have stated that at very high rotational speeds, second phase (strengthening) particles would suffer more fragmentation and this would lead to segregation of particles in other parts of the TMAZ. These authors report that as the rotational speed is decreased, the temperature within the nugget decreases and the volume fraction of coarse second phase particles increases. Hence, the tool rotation speed must be optimized to obtain a nugget region having fine particles uniformly distributed throughout the matrix.

Many authors have reported different optimum rotational speeds for different materials and for different alloying grades. For example V. Balasubramanian friction stir welded a range of aluminium alloys (AA1050, AA6061, AA2024, AA7039 and AA7075) at various rotational speeds. This author reported defect free welds at different rotational speed depending on the particular alloy. For example, AA2024 plates were friction stir welded at 1000, 1100, 1200, 1300 and 1400 rpm. Defect free welds were only reported at rotational speeds of 1200 rpm. This author also suggests that the optimal rotational

speed is directly proportional to the yield strength of the aluminium alloy. The lower the yield strength of the aluminium alloy, the lower the tool rotational speed required to produce a defect free weld.

M.A. Sutton et al investigated the relationship between ultimate tensile strength and total elongation for various rotational speeds (100 to 800 rpm) at a fixed translational speed of 2.11 mm/s on the FSW of AA2024 [55]. The effect of rotational speed on the ultimate tensile strength (UTS) and total elongation of a test piece is shown in Figure 29. Initially, the value of UTS increases significantly as the rotational speed is increased until an optimal value of UTS is reached at 480 rpm. Further increases of rotational speed resulted in welds with lower UTS values. This is also mirrored by the total elongation of the weld specimens, as the elongation declines sharply between 480 and 600 rpm. It was argued by the author that this was due to overheating which caused grain boundary melting and the formation of brittle structures within the weld. If there are low melting regions embedded in the bulk higher-melting material, then local melting may occur and this may be detrimental to the final properties of the weld resulting in defects.

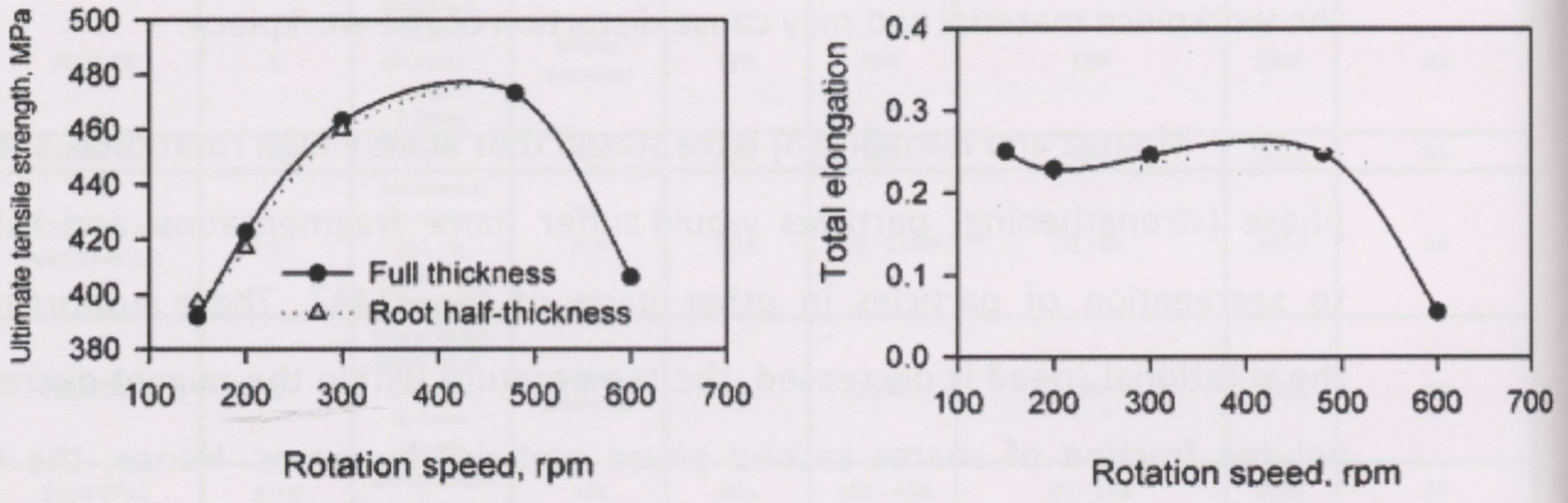


Figure 29: M.A. Sutton, effect of rotational speed on (a) UTS and (b) elongation [55]

K. Elangovan et al examined the influence of rotational speed (1500, 1600 and 1700 rpm) on the FSW of 6mm thick AA2219 plates [34]. For a fixed translational speed of 0.76 mm/s, these authors report that joints fabricated at a rotational speed of 1600 rpm showed superior tensile properties and microhardness values compared to the other joints, irrespective of tool profiles used. An example of these authors results can be seen in Figure 30. These authors state that rotational speeds above 1600 rpm caused excessive release of stirred materials to the upper surface, which resulted in voids within the nugget zone. Also, rotational speeds below 1600 rpm resulted in lack of stirring. These

authors also report an increase in test piece elongation with increasing rotational speed and attributed this to the increased heat input for higher rotational speeds.

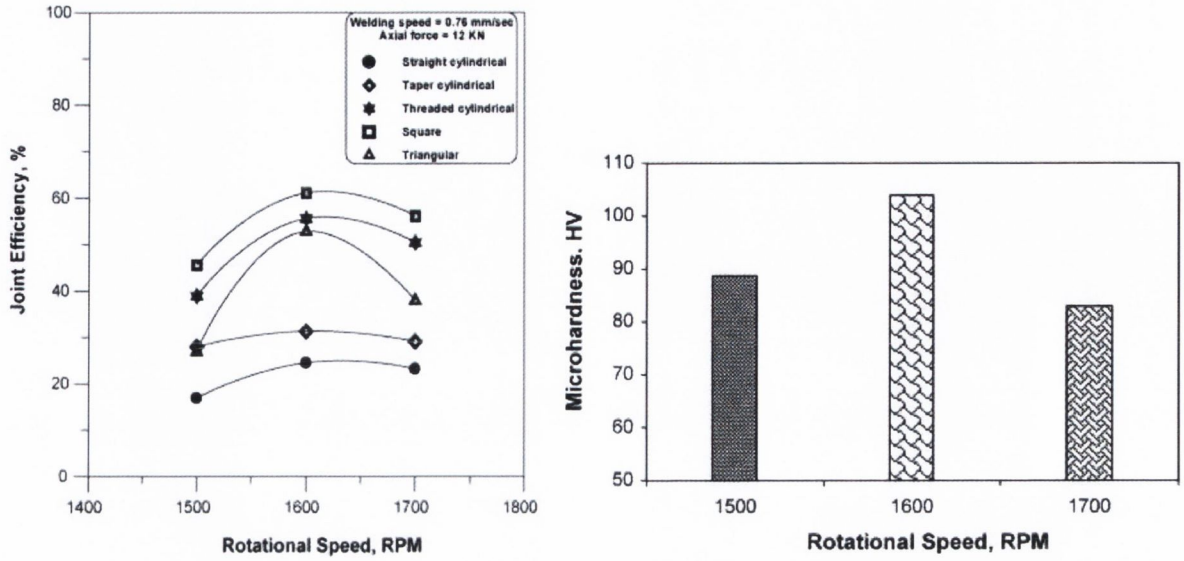


Figure 30: Elangovan, effect of rotational speed on joint efficiency and hardness in the nugget zone [34]

### 2.2.2 Effect of Translational Speed:

The translation speed of the tool is the constant speed at which the tool is feed along the joint line of the workpiece plates and is also referred to as the welding speed. The translational speed has a direct relationship with the rotational speed. A lower translational speed will permit more time for rotary action which will include increased heat input and enhanced stirring of the workpiece. A higher translation speed on the other hand will have the opposite effect. Also, higher translational speeds increase the force acting on the front of the tool as it traverses through the workpiece and can cause tool fracture. One of the main advantages of FSW over conventional welding techniques and mechanical joining is its speed and efficiency in producing a consolidated weld in one pass. Therefore there is a constant drive to increase tool translational speeds for industrial applications to increase productivity without sacrificing weld strength and increasing the risk of tool fracture. Therefore, finding the correct combination of tool rotational speed and translational speed is essential.

Similar to the rotational speed, many authors have reported the production of consolidated friction stir welds at various translational speeds for various materials and also different alloying grades. For example V. Balasubramanian friction stir welded a

range of aluminium alloys (AA1050, AA6061, AA2024, AA7039 and AA7075) at various translational speeds [54]. This author reported defect free welds at different translational speeds depending on the particular alloy, examples are shown Figure 31. For example, AA2024 plates were friction stir welded at a fixed rotational speed of 1200 rpm with varying translational speeds (22, 45, 75, 100 and 135 mm/min). Optimum defect free welds were reported at a translational speed of 75 mm/min. This author also suggests that the welding speed has an inverse relationship with the yield strength of the aluminium alloys.

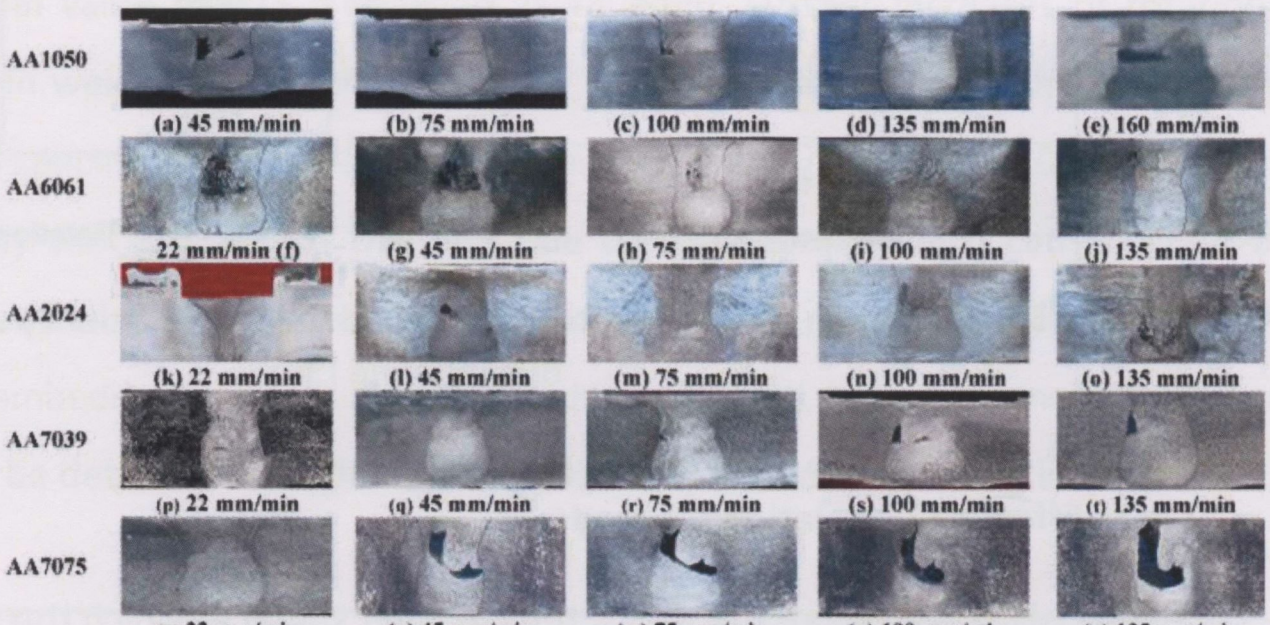


Figure 31: V. Balasubramanian, effect of translational speed on macrostructure of aluminium alloys [54]

K. Elangovan et al investigated the influence of translational speed on the formation of the friction stir processing zone in AA2219 [35]. Using various tool profiles, these authors performed a range of friction stir welds at a fixed rotational speed of 1600 rpm and various welding speeds ( 0.37, 0.76 and 1.25 mm/s). Results indicated that joints fabricated at a welding speed of 0.76 mm/s demonstrated superior tensile and elongation properties regardless of the tool geometry, Figure 32. These authors attributed this to optimum thermal input at this translational speed. Higher translational speeds resulted in a lower heat input per unit length of the weld and lack of stirring in the friction stir processing zone which resulted in poor tensile and elongation properties. A lower welding speed encouraged higher temperatures with a slower cooling rate which caused grain growth and severe clustering of CuAl precipitates which again resulted in poor tensile and elongation properties.

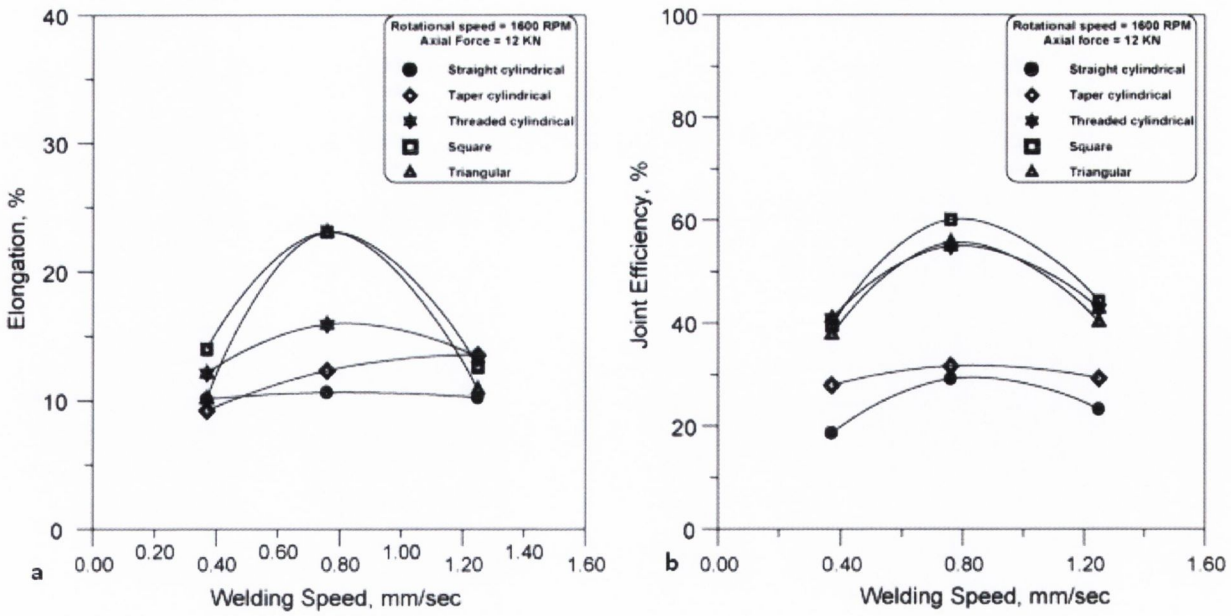


Figure 32: K. Elangovan, effect of welding speed on (a) Elongation and (b) Joint efficiency% [35]

J.K. Kristensen et al investigated tensile strength as a function of translation speed when friction stir welding 6mm thick AA2024-351 [56]. For fixed rotational speeds, a decrease in ultimate tensile strength was found with increasing translational speeds between 270 to 560 mm/min.

During the FSW of AA2024-T351 6.35mm thick plates, Jariyaboon reported on the variation of hardness across the weld line as a function of translational speed [57]. For a fixed rotational speed of 468 rpm, increasing the translational speed from 75 to 154 mm/min resulted in increased hardness across all weld zones. Similar results were also found by Reynolds and Pohlman when translation speeds where increased from 51 to 204 mm/s [58].

### 2.2.3 Effect of Tool Tilt Angle:

The tool tilt angle is the inclination angle of the tool opposite to the tool travel direction. As mentioned in section 2.1.2 the function of the tilt angle is to maintain the material reservoir and thereby enable the trailing edge of the shoulder to impart a compressive forging force on the workpiece to ensure a consolidated weld. Generally a tilt angle of between 2-4° is sufficient to produce a consolidated weld. TWI report an optimum tool tilt angle of 3° for friction stir welding of aluminium butt joints [40]. Chen

and Yan [59] preformed friction stir butt welds on 4mm thick AA5456 at various tool tilt angles (1.5˚ to 4.5˚). For a fixed rotational and translational speed of 1000 rpm and 180 mm/min respectively, these authors report optimal tensile strength was achieved for a tool tilt angle of 3.5˚ as shown in Figure 34.

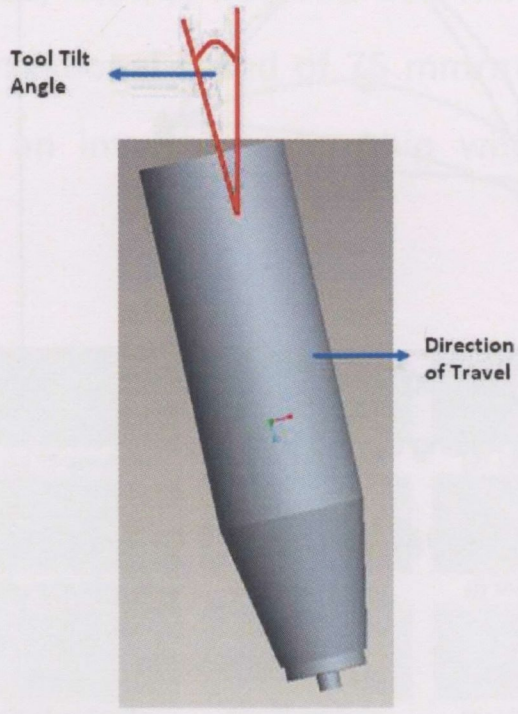


Figure 33: Tool Tilt Angle

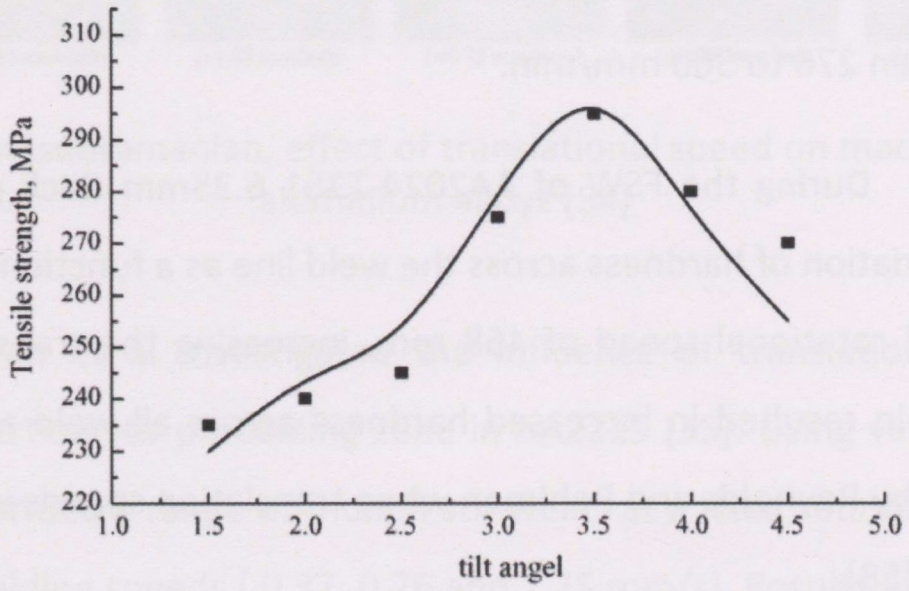


Figure 34: H. Chen, effect of tool tilt angle on tensile strength [59]

## 2.3 Weld Zones in Friction Stir Welding:

Figure 35 is a graphical representation of the four distinctive zones which can be found in a friction stir weld:

- **A: Parent Material (PM)**. This area is unaffected by heat or deformation
- **B: Heat Affected Zone (HAZ)**. Area affected by heat but not plastically deformed
- **C&D: Thermo-Mechanically Affected Zone (TMAZ)**. Area affected by heat and deformation. In most materials, all of the TMAZ will recrystallized. In aluminium, only the hottest part will recrystallized to form the nugget.
- The **Nugget** is still classified as part of the TMAZ. Aluminium alloys show both recrystallized (D) and non-recrystallized (C) TMAZ areas.

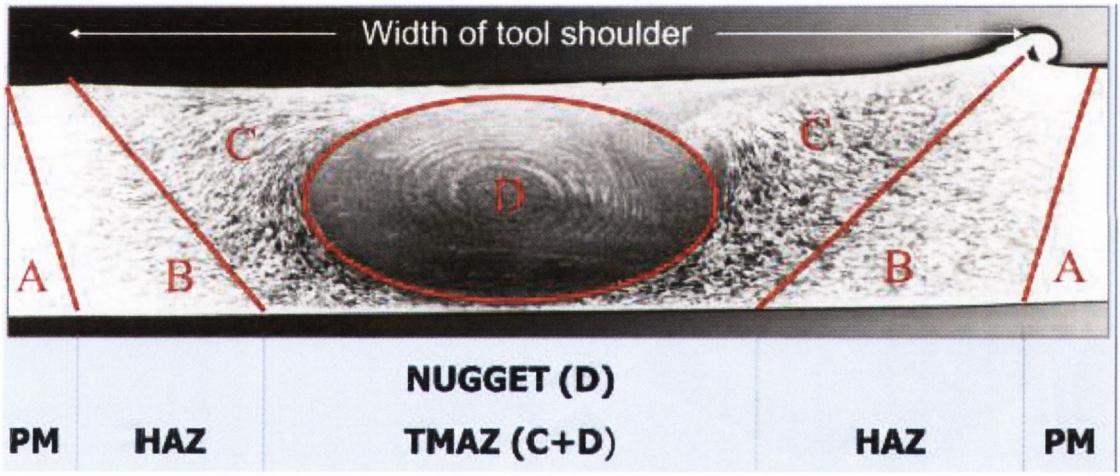


Figure 35: Weld Zones in the FSW of aluminium [40]

### 2.3.1 Nugget Zone:

During the FSW process, as the tool translates along the weld, material must flow around the pin thereby undergoing intense plastic deformation at elevated temperatures. This region around the pin is known as the nugget zone and the microstructure it exhibits is completely unrecognisable from that of the base material. The grains within the nugget are completely demolished by the tool pin and are replaced with fine, equiaxed grains. This is a result of the continuous dynamic recrystallization occurring in this zone due to severe plastic deformation at an elevated temperature. A wide range of nugget grain sizes can be achieved by manipulation of the welding process parameters. For example,

Jariyaboon et al showed that welding parameters, especially rotational speed, has an effect on grain size in the nugget [57]. At a fixed translational speed, increasing the rotational speed resulted in larger grains within the nugget zone due to an increase in heat input. Depending on the operational parameters, some authors have reported grains sizes within the nugget on the order of 10s of micrometers to less than 1μm [60, 24].

### 2.3.2 Thermo-mechanically affected zone (TMAZ)

Thermo-mechanically affected zone is found at either side of the nugget zone. Although this zone has not been directly subjected to pin or shoulder action, due to internal shear stresses, it has experienced severe thermo-mechanical alteration. However, no dynamic recrystallization occurs in this region [61]. Consequently the microstructure of the TMAZ is recognisably that of the base material, but severely deformed. The temperatures in this zone although not great enough to cause dynamic recrystallization, will cause a slight tempering effect of the material. Therefore the material properties in this region tend to be lower than those found in the base material.

### 2.3.3 Heat affected zone (HAZ)

The HAZ is located on either side of the TMAZ. It is defined as the part of the weld zone that is not mechanically affected but does undergo a considerable thermal cycle. The size of the HAZ will be dependent on peak temperatures achieved around the tool and the thermal conductivity of the material being welded. The size of the HAZ can be assessed by conducting hardness tests and or observing the microstructure of the material. The hardness will transition towards the same value as the parent metal with increasing distance from the weld centerline. Ideally the HAZ should be kept as small as possible and can be controlled by altering weld parameters. Nevertheless the HAZ developed during FSW is significantly smaller than that of traditional fusion welding due to the lower temperatures required. Degradation of the base metal properties can be expected in the HAZ, this degradation is caused by micro structural modifications associated with the elevated temperatures experienced in this zone [62].

## 2.4 Imperfections Found in Friction Stir Welding:

A flaw is an unintentional imperfection in a welded structure which may or may not compromise the integrity of the structure. After a critical assessment, it could be regarded as a defect or accepted as a tolerable flaw. A defect is an imperfection in a weld whose presence cannot be tolerated. It must be removed or other remedial action must be taken. Many types of welding imperfections exist. Solidification related flaws such as hot cracking, gas evolution flaws such as porosity and metallurgical flaws such as cold hydrogen cracking, reheat cracking etc are the traditional imperfections produced in fusion welds. There are also a number of procedure induced flaws such as lack of fusion, slag entrapment, undercut, burn-through etc. However it must be noted that none of these flaws occur during friction stir welding. Imperfections in friction stir welding do exist and are primary based on the following types:

- Root Flaws
- Inadequate Plastic Flow
- Oxide Entrapment / Joint Line Remnants

### 2.4.1 Root Flaws:

These are potentially the most serious flaws. They are areas of no bond or weak bond close to the root, located on the deformed original joint line. They are normally caused by the root being too cool or the pin being too short. Root flaws can be quite long and are difficult to detect by non-destructive methods such as radiography, dye penetrant inspection and visual examination. The only definitive method currently available is a destructive bend test or tensile test. Figure 36 shows a root flaw caused by the tool pin being too short. This results in a workpiece that is not welded throughout its thickness. Root flaws like this cause a reduction in tensile properties and fatigue strength [67].

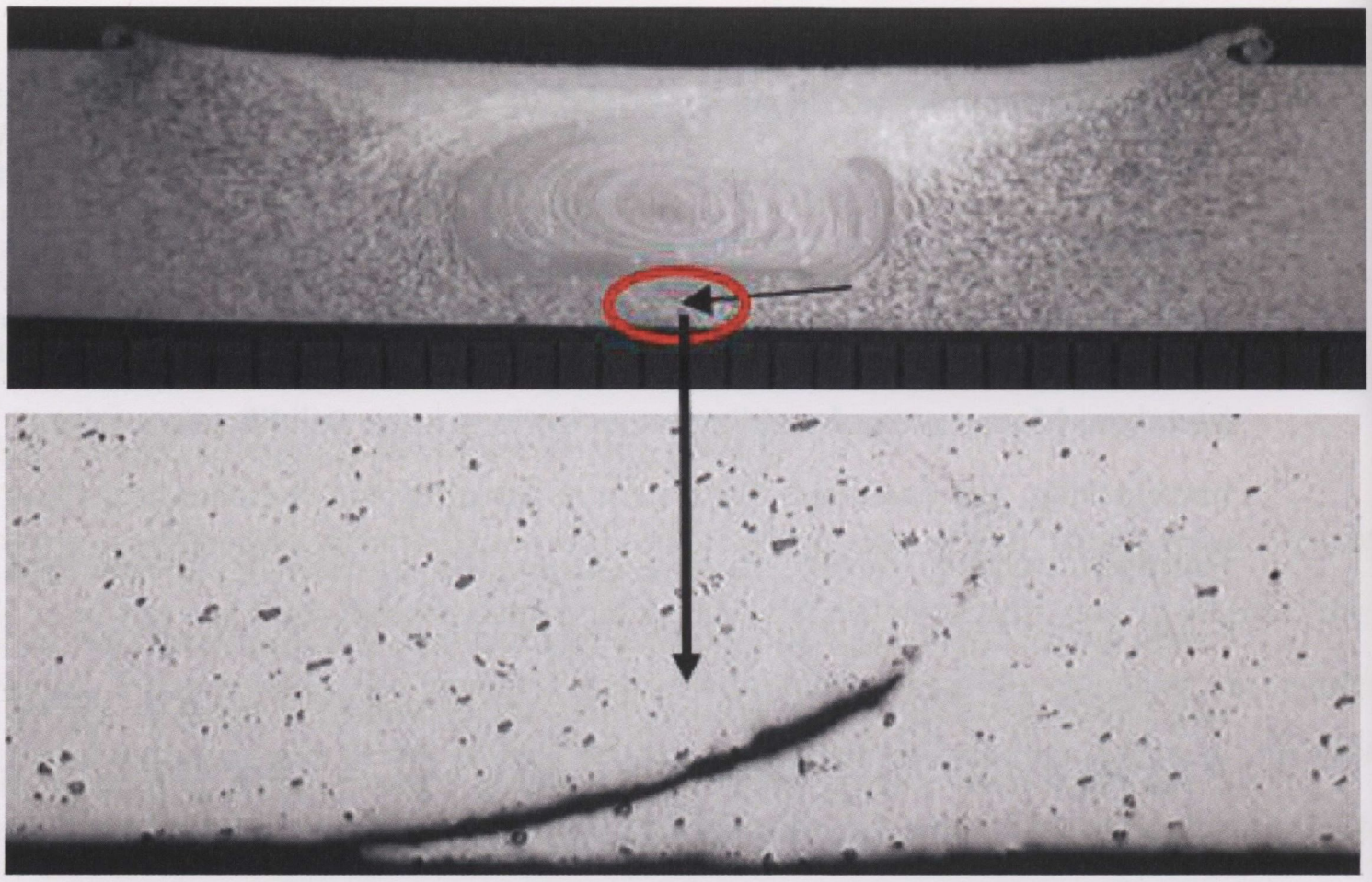

Figure 36: An example of a root flaw which occurred during FSW [67]

### 2.4.2 Inadequate Plastic Flow:

A good level of plastic flow is needed to make a friction stir weld. If the material cannot flow, it will fracture under severe forces, leaving voids (sometimes incorrectly called porosity) which maybe large or small and either buried or surface breaking. Sometimes a void can occur right throughout the length of the weld; this is sometimes called a tunnel flaw. Voids can be found in any part of the weld. However, they are often found in the transition between the shoulder dominated and pin dominated regions where material flow is more likely to be chaotic. An example of a void caused by inadequate plastic flow of the workpiece material can be seen in Figure 37.

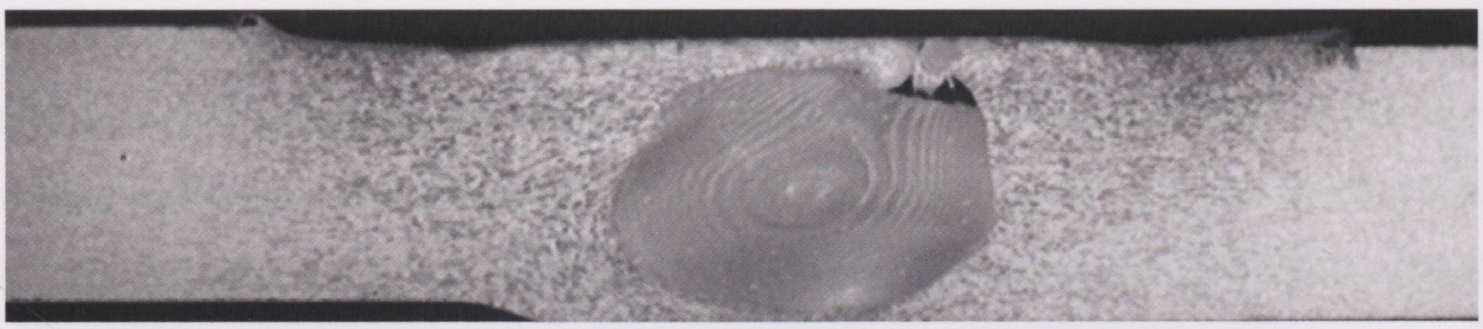

Figure 37: Occurrence of a void due to inadequate plastic flow during FSW [76]

### 2.4.3 Oxide Entrapment / Joint Line Remnants:

In any friction stir weld, it is possible to trace the original, highly deformed joint line. This called the joint line remnant. The faying surfaces are always covered by an oxide layer. Due to the high strains, the faying surfaces will be distorted and stretched during the welding operation and consequently the oxides on the surface will be broken up and redistributed. If large oxide particles are present, this will make the original joint line more visible. Although the joint line remnant is occasionally associated as an area of weakness, it is not an imperfection as it is always there. However, if there is a high density of oxides, this can compromise the integrity of the weld. Figure 38 shows a joint line remnant on the cross sectional area of an un-etched friction stir weld.

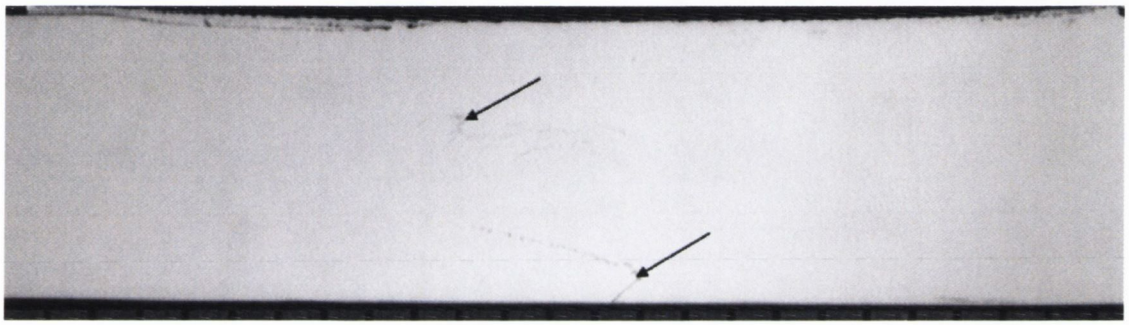

Figure 38: Joint Line Remnant [76]

## 2.5 FSW Machinery:

The choice of a particular type of machine for a given application should be based on both economic and technical factors. Economic factors include cost and productivity. Technical factors include force, stiffness, sensing and flexibility (number of axis) etc. There are three basic equipment solutions that can be considered when deciding on a machine for friction stir welding:

- Custom Built Machines
- Robots
- Modifying Existing Machines

### 2.5.1 Custom Built FSW Machines:

Custom built machines are available in many sizes and shapes and can have a large range of technical capabilities. As the name implies, they tend to be built to the exact requirements for a specific application. As a consequence, their cost has a large range, from under €10,000 to millions of euro. There are several suppliers of this type of equipment:

- ESAB (Sweden)
- General Tool (USA)
- MTS (USA)
- Hitachi (Japan)

An example of a custom built machine is one that is used by Marine Aluminium in Norway for the welding of long extrusions required to fabricate panels for shipbuilding and is shown in Figure 39. Using this machine, multiple extrusions are welded together to create a large panel. Another example is the 4-axis gantry machine used for FSW research in TWI Sheffield UK which is shown in Figure 40.

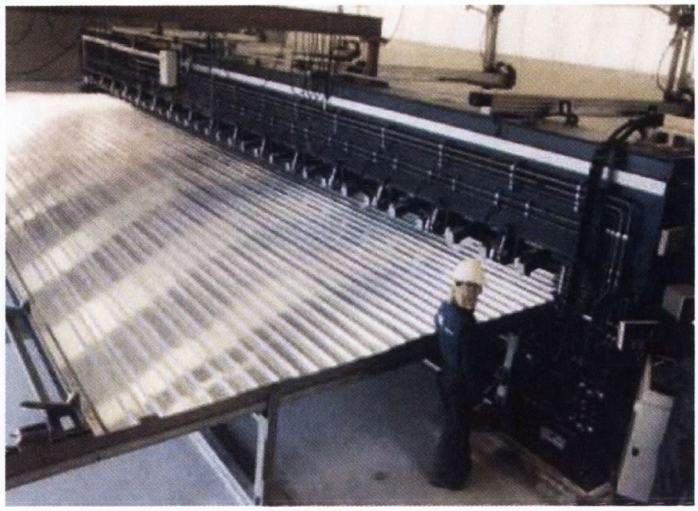

Figure 39: Custom built FSW machine for welding long extrusions used by Marine Aluminium [11]


Figure 40: TWI custom built gantry machine [19]

### 2.5.2 Robotic FSW Machines:

Robots have two main advantages that will eventually make them the preferred solution for many FSW applications. The first is cost, because they are produced in moderate production volumes, their cost is significantly lower than custom built machines. The second is increased flexibility which allows for significant production improvements. For example, consider a part which requires welds on multiple sides at different locations. A robot can produce welds on multiple sides of a part in a single setup. This reduces non-value-added material handling applications and can increase production efficiency which will reduce the net welding costs. However, some robots cannot deliver and support the large forces and the required stiffness associated with FSW. While some robots that can

deliver a thrust force of approximately 4.5 kN, this limits their FSW capabilities to materials of low thicknesses. It is thought that in the next couple of years, robots will be capable of FSW materials of increased thickness with continual development. Figure 41 shows two different robots used for FSW of thin materials at TWI Sheffield.

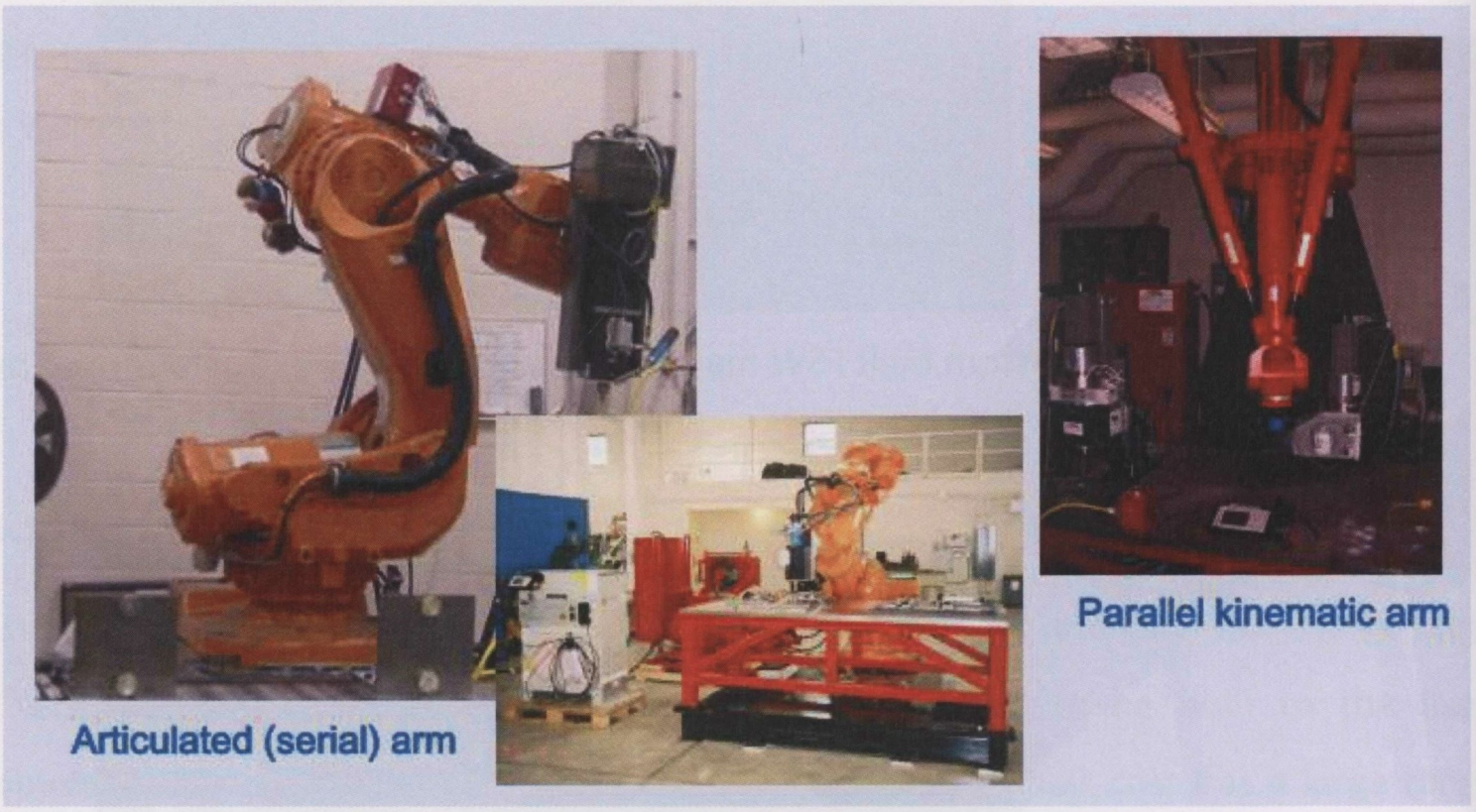


Figure 41: FSW Robots at TWI Sheffield [19]

### 2.5.3 Modified FSW Machines:

An Alternative to the custom built machines is to modify existing machinery. Friction stir welding is similar in nature to machining. Therefore a lot of milling machines can be modified to accommodate friction stir welding. However, FSW requires more force and produces more heat than a typical machining operation and consequently this must be considered before modification. Older milling machines tend to be larger and more robust than newer ones, thereby making them more suitable for FSW. Although large scale production using FSW is not possible using a modified milling machine, they are nevertheless extremely efficient for both research work and training. For example, Leal and Leitao [28] used a modified milling machine to investigate the effects of shoulder geometry on the FSW of AA5182 and AA6016 sheets. G. Biallas et al [72] also used a modified milling to investigate the mechanical properties and corrosion behaviour on friction stir welded aluminium 2024-T3 joints. The Machine used in this research project is also a modified milling machine, details are given in Section 3.1.

## 2.6 Aluminium 2024-T3:

Aluminium 2024 is one of the best known high strength aluminium alloys and it also has excellent fatigue resistance. Due to its high strength to weight ratio, aluminium 2024 has many applications within the aerospace industries where weight saving is essential without compromising strength. In plate form, products are used for fuselage structures, wing tension members, shear webs and ribs. Sheet products, usually alclad, are used extensively in commercial and military aircraft for fuselage skins, wing skins and engine areas where elevated temperatures to 121°C are often encountered. It also has applications in the following components: Aircraft fittings, gears and shafts, bolts, clock parts, computer parts, couplings, fuse parts, hydraulic valve bodies, missile parts, munitions, nuts, pistons, rectifier parts, worm gears, fastening devices, veterinary and orthopaedic equipment [73].

To strengthen AA2024, it initially undergoes a T3 solution heat treatment, to put the alloy into a single phase solid solution condition. It may be difficult to reach an entirely single phase solution, but as much as possible of the alloying element is taken into solution without melting the mixture. This solution is then quenched to room temperature. At this point some cold working is applied to the material resulting in approximately 1.5 – 3 % strain. This cold working increase the dislocations density and these dislocations provide nucleation points for heterogeneous nucleation of the precipitates, after which natural ageing is allowed to occur. This allows the mixture to decompose into a two phases, a solid matrix solution and the precipitate strengthening phase. Since the corrosion resistance of Aluminium 2024 is quite low, it usually comes in Alclad form where a thin surface layer of pure aluminium is applied to prevent corrosion.

## 2.7 Finite Element Analysis (FEA):

The first developments of Finite Element Analysis (FEA) can be traced back to the work by Alexander Hrennikoff (1941) and Richard Courant (1942). It originated from the need to solve complex elasticity and structural analysis problems in civil and aeronautical engineering. It is a numerical technique for finding approximate solutions of partial differential equations (PDE) as well as integral equations. The solution approach is based either on eliminating the differential equation completely (steady state problems), or rendering the PDE into an approximating system of ordinary differential equations, which are then numerically integrated using standard techniques such as Euler's method, Runge-Kutta etc.

FEA uses a complex system of points called nodes which make a grid called a mesh. An example of a meshed car is shown in Figure 42. The mesh is programmed to contain the material and structural properties which define how the structure will react to certain loading conditions. Nodes are assigned at a certain density throughout the material depending on the anticipated stress levels of a particular area. Regions which will sustain large amounts of stress usually have a higher mesh density than those which experience little or no stress. Points of interest may consist of: fracture point of previously tested material, fillets, corners, complex detail, and high stress areas. The mesh acts like a spider web in that from each node, there extends a mesh element to each of the adjacent nodes. This web of vectors is what carries the material properties to the object, creating many elements.

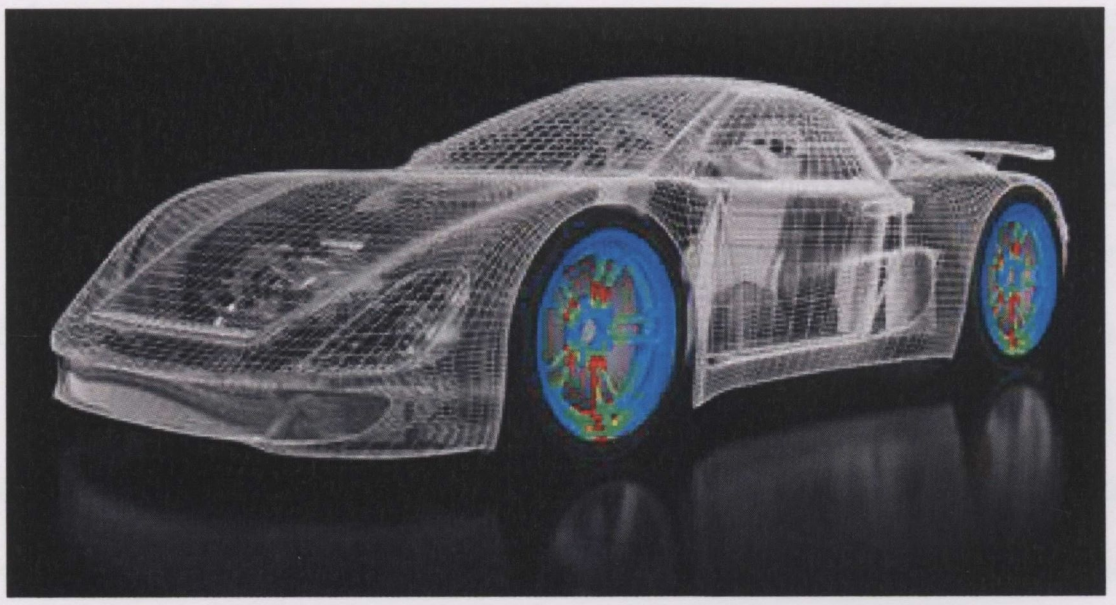

Figure 42: An example of a meshed car using FEA [79]

The advantages of FEA are numerous and important. A new design concept may be modeled to determine its real world behavior under various load environments, and may therefore be refined prior to the creation of drawings while changes are inexpensive. Once a detailed CAD model has been developed, FEA can analyze the design in detail, saving time and money by reducing the number of prototypes required. An existing product which is experiencing a field problem, or is simply being improved, can be analyzed quickly with reduced cost. In addition, FEA can be performed on increasingly affordable computer workstations and personal computers, and professional assistance is available. It is also important to recognize the limitations of FEA. Commercial software packages and the required hardware, which have seen substantial price reductions, still require a significant investment. The method can reduce product testing, but cannot totally replace it. Probably most important, an inexperienced user can deliver incorrect answers, upon which expensive decisions will be based. FEA is a demanding tool, in that the analyst must be proficient not only in structural mechanics, but also in mathematics, computer science, and especially the finite element method itself.

### 2.7.1 DEFORM 3D:

DEFORM is an engineering software package produced by the Scientific Forming Technologies Corporation. DEFORM 2D and 3D are both elasto plastic modeling packages capable of full thermo mechanical modeling. Both packages operate via a graphic user interface. DEFORM is based on the finite element method and has been in use in industry for two decades. The software package is well suited to modeling the FSW process as it is capable of predicting large deformation material flow and thermal behavior with precision. The DEFORM system consists of three modules.

(1) **Pre Processor:** This module is used to define the problem. The general approach is to use the pre processor to define the geometry, material properties and boundary conditions of the work piece and tooling. Then sequentially simulate each process which the workpiece has to undergo. DEFORM simulations can be run either as two dimensional (2D) or three dimensional (3D) models. In general, 2D models are smaller, easier to set up, and run more quickly than 3D models. 2D simulations can usually provide a large percentage of the data a 3D program can with a massive saving

in set up and run times. However in the case of FSW it was felt a full 3D analysis was required.

(2) **Simulation Process:** All models used in this thesis employed a rigid-viscoplastic material model. The formulation used in DEFORM assumes that the material stress increases linearly with strain and strain rate until a threshold strain rate is reached, referred to as the limiting strain rate. The material deforms plastically beyond the limiting strain rate. The plastic material behaviour of the object is specified with a material flow stress function or flow stress data. The basic equations of equilibrium, constitutive relations and boundary conditions are converted to nonlinear algebraic equations by utilizing the FEM discretisation procedure. The user selects one of two solution techniques within DEFORM. All simulations presented in this thesis use direct iteration as opposed to the newton raphson method. The Deform manual recommends direct iteration for applications that involves large amounts of workpiece plastic deformation as it is more likely to converge than the newton raphson method. However, direct iteration is more likely to require more iterations. Simulations time varies depending on the complexity of the problem, for example the loading condition and also the size of the mesh. Although an object with finer mesh elements will yield a greater quantity of solution data, it will also increase the simulation time significantly.

(3) **Post Processor:** Once the simulation process has been completed, the results can be analysed. The post-processor is used for reading the database file from the simulation engine and displaying the results graphically, and for extracting numerical data. A wide range of options are available to analyze the results in the form of state variables which are shown in Figure 43.

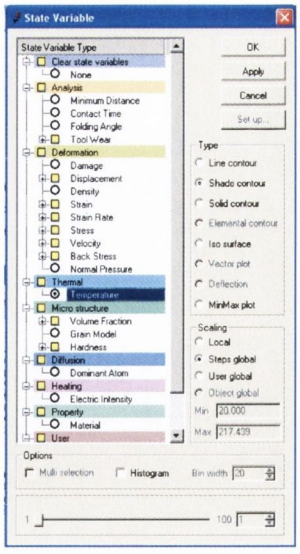


Figure 43: DEFORM 3D state variables in the post processor

### 2.7.2 Finite Element Modelling of FSW:

In the recent past, numerous attempts have been made to successfully produce a 3 dimensional model of the friction stir welding process using a range of different commercial software. For example, Xu and Deng [81] developed a 3D finite element to simulate the FSW process with a focus on velocity field, material flow characteristics and the equivalent plastic strain distribution. These authors used the commercial FEM code ABAQUS and compared their predicted results to experimental data available. They observed reasonable correlation between the equivalent plastic strain distribution and the distribution of the microstructure zones in the weld.

Ulysse [90] presented a 3D FEM visco-plastic model for FSW of thick aluminium plates using the commercial FEM code FIDAP. Ulysse investigated the effect of tool speeds on the process parameters. It was found that the higher translational speed leads to higher welding force, while increasing the rotational speed has the opposite effect, that of force reduction. Reasonable agreement between the predicted and the measured temperature was obtained and the discrepancies were explained as an inadequate representation of the constitutive behaviour of the material for the wide ranges of strain-rate, temperatures and strains typically found during FSW. A comparison of the experimental and predicted temperatures recorded by Ulysse is shown in Figure 44.

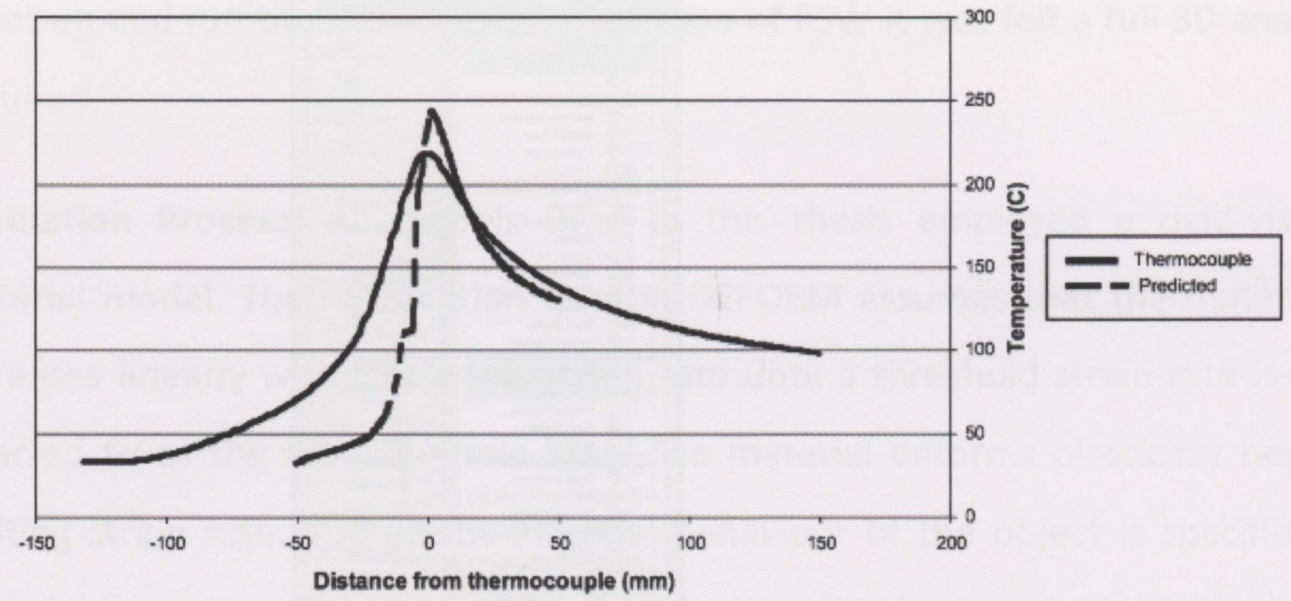


Figure 44: Predicted FSW temperature compared to experimental temperature, Ulysse [90]

Chen and Kovacevic [82] developed a 3D FEM model to study the thermal history and thermo-mechanical phenomena in the butt-welding of aluminium alloy 6061-T6 using the commercial FEM code ANSYS. Their model incorporated the mechanical reaction between the tool and the weld material. Experiments were conducted and an X-ray diffraction technique was used to measure the residual stress in the welded plate. The welding tool (i.e. the shoulder and pin) in the FEM model was modelled as the heat source, with the nodes moved forward at each computational time step. The predicted temperature 10mm from the weldline agreed closely with experimental measured temperatures and is shown in Figure 45.

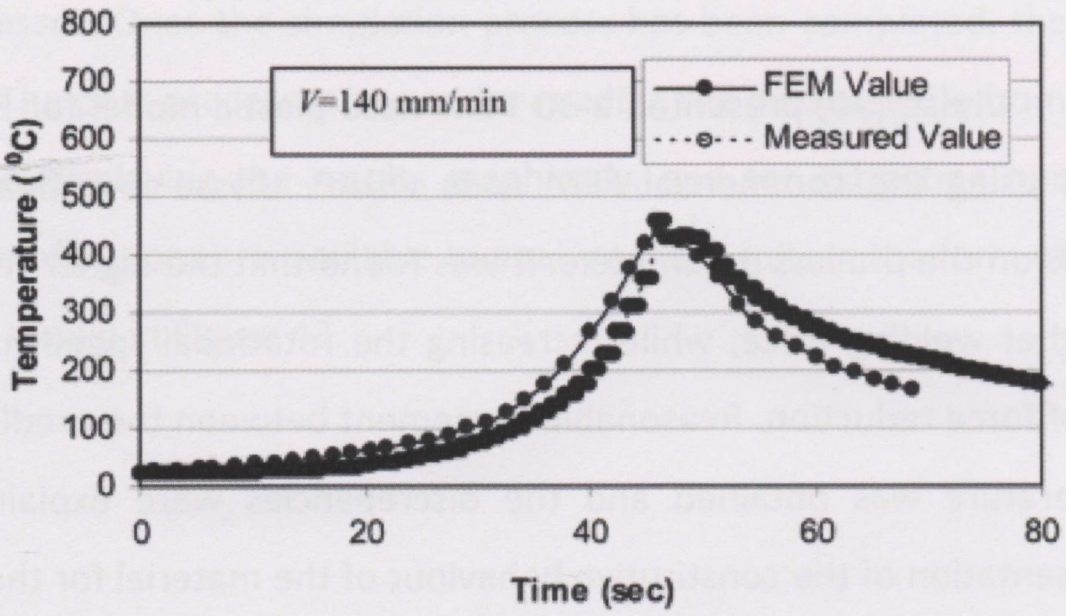


Figure 45: Predicted FSW temperature compared to experimental temperature, Chen and Kovacevic [82]

Colegrove and Shercliff used the Computational Fluid Dynamics commercial software FLUENT for a 2D and 3D numerical investigation on the influence of pin

geometry during FSW [83,84]. These authors compared different pin designs in terms of material flow and welding forces on the basis of both a stick and a slip boundary condition at the tool–workpiece interface. In spite of the good obtained results, the accuracy of the analysis was limited by the assumption of isothermal conditions.

One of the few authors reporting successful modelling of the FSW process using DEFORM 3D is G.Buffa et al [85, 86] who developed a continuum based FEM model based on the FSW of AA6082-T6 plates with a thickness of 3mm. These authors validated the model by comparing FE results with experimental results of temperature distribution. Figure 46 shows a comparison of the temperature predicted by the model and those recorded from experiments at 8mm from the weld line. Figure 47 shows the flow stress model employed and material constants determined by a numerical regression based on the experimental data. This model was used to investigate the distribution of temperature and strain in the heat affected zone and the weld nugget. The model employed a rigid-viscoplastic temperature and strain rate dependent material model. This proposed model was capable of predicting the effect of process parameters on process thermo-mechanics, such as the temperature, strain, strain rate as well as material flow and forces.

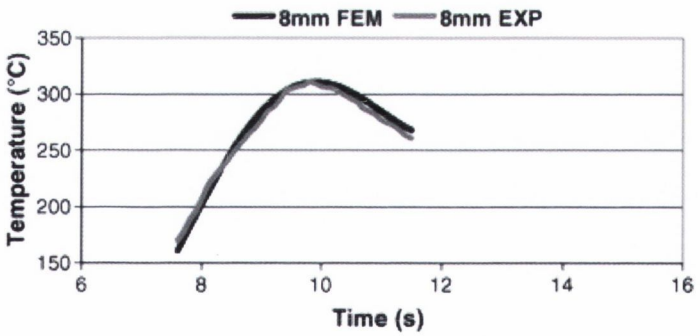


Figure 46: G. FSW temperature predictions compared to experimental, G.Buffa [85, 86]

$$\sigma = KT^{A}\left(\frac{\dot{\varepsilon}}{\varepsilon}\right)^{B}\left(\varepsilon\right)^{C}$$

Where

K = 2.69E10
A = -3.3155
B = 0.1324
C = 0.0192

Figure 47: Flow stress equation used by G. Buffa

## Summary of Literature Review:

There are a large number of variables that must be considering when implementing the FSW process. To date no process specifications or general designs guidelines are available on which tooling geometry and operational parameters should be employed for specific workpiece materials and thicknesses. Therefore as a result, even when considering a single material, AA2024, with a thickness range between 3 – 6mm there is a large range of different tooling designs and operational parameters reported in research papers. Another issue with previously published research papers on AA2024 is the lack of information provided on tooling design/geometry, operational parameters and process implementation. Only a small number of papers have been published on the more recent TWI tooling designs such as the Mx Triflute pin and the Scrolled shoulder designs. This is because TWI tends to keep their most recent/advanced tooling designs and results confidential to companies who hold a FSW licence from TWI.

Flaws associated with fusion welds such as hot and reheat cracking, porosity, lack of fusion, slag entrapment, undercut, burn-through etc do not occur in FSW. The main imperfections associated with FSW are root flaws, inadequate plastic flow and oxide entrapment.

The majority of FSW industrial applications are performed on expensive custom build machinery. Robots are the preferred choice; however their lack of stiffness and power limits their FSW capabilities to materials of low thickness. A better understanding of the forces may help minimise the power and stiffness requirements and along with robotic machine improvements may increase the number of possible FSW applications using robots.

In the recent past, numerous attempts have been made to successfully produce a 3D model of the FSW process. A number of different software packages have been used (ABAQUS, FIDAP, ANSYS, FLUENT and DEFORM) to investigate a number of different aspects such as velocity field, material flow, stress and strain distributions, thermal flow, operational parameters, tooling designs, forces etc. However, the majority of authors focus on validating their model by comparing experimental temperatures to those predicted by the model alone. A more consistent model would be one that is validated by comparing both experimental temperatures and forces generated to those predicted by the FE model.

# Chapter 3

# Research Programme

## 3.1 FSW Machine:

A Correa F3UE vertical milling machine was modified for use as a FSW rig during this project and is shown in Figure 48. Leal [28] and Biallas [72] also used a modified milling machine to successfully conduct Friction Stir Welding research. The main Spindle is made from a nickel chrome steel, hardened inside and out and mounted in taper roller bearings. All gear box components and shafts are manufactured from molybdenum-chrome steel. The gears were hardened, ground and oversized to transmit full motor power. The Feed Box is driven by a separate motor and the driven gears and shafts are also made of molybdenum-chrome steel. Twin electromagnetic clutches allow easy feed change from slow to rapid traverse.

Figure 48: Modified milling machined converted to perform FSW at Trinity College Dublin

Figure 49 and Figure 50 illustrate the different levers used to control and adjust the operating parameters. The tool plunge speed could either be controlled manually or automatically. An analogue plunge depth indicator was used to control the depth of tool penetration into the workpiece. Automatic plunge rates ranged from 4-250 mm/min. However, plunge rates higher than 16 mm/min could not be used during testing due to accuracy issues using the analogue plunge depth indicator. Tool plunge depth during FSW is crucial to complete a successful weld, an accuracy of at least 0.1 mm is required. Because the plunge depth indicator is an analogue one, when using automated plunge speeds the table movement must be stopped manually at the correct position using the scaled indicator. Stopping the vertical feed at the correct depth was challenging at high plunge speeds due to accuracy issues. However, it was possible to achieve faster plunge speeds by manually controlling the vertical movement of the table using a lever whilst still achieving an acceptable degree of accuracy. The translational speed was controlled through an automatic feed table. During testing, the tool remains in a fixed position while the table moves the workpiece. Translational speed ranging from 11.2-710 mm/min could be chosen. The rotational speed of the tool was controlled through a reduction gear box at the side off the spindle head. Rotational speeds ranging from 28-1400 rpm could be selected. The head of the milling machine could also be adjusted and set for different tool tilt angles.

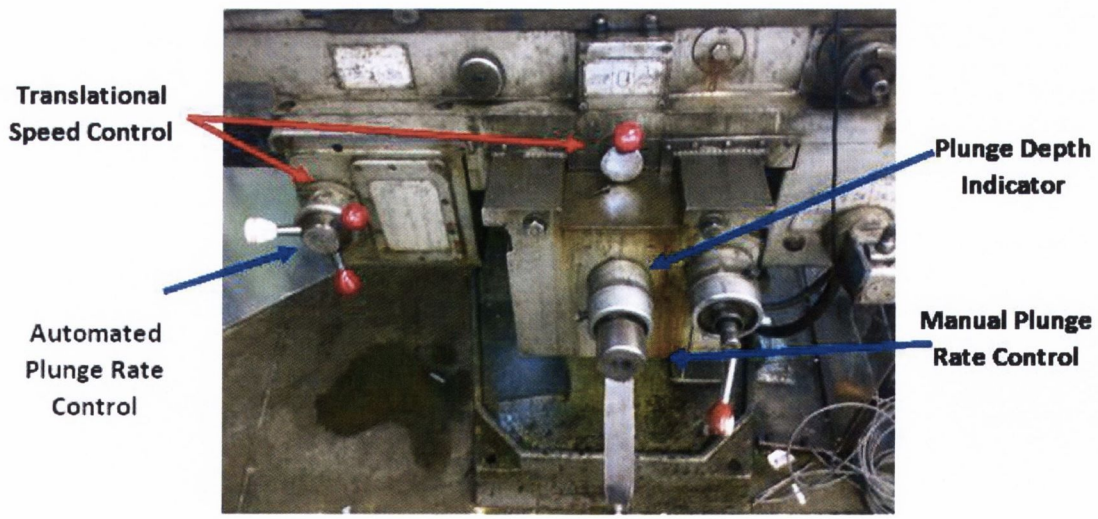


Figure 49: Plunge Rate and Translation Speed Control


Figure 50: Rotational speed and tool tilt angle adjustment

## 3.2 FSW Rig:

FSW is a process that generates high forces. Therefore it is necessary to ensure that the workpiece plates are rigidly restrained with an appropriate rig prior to welding. The forces acting on the workpiece are shown in green in Figure 51. The workpiece must be fixed appropriately to prevent movement during welding. A large base plate was attached to the milling machine table to secure all clamping and the base plate. Figure 52 illustrates the clamping necessary to secure the workpiece. End stops are used to prevent movement due to the welding force. During the plunge stage, the tool pin will try and separate the joint configuration leaving a gap between the two workpiece plates. The presence of a gap due to separation of the workpiece plates is a common problem. Gaps may form due to improper clamping or due to imprecision when cutting the plates to the appropriate size. The presence of a gap may result in a tunnel defect and reduce the mechanical properties of the finished weld. The side clamps prevent this gap occurring and also prevent rotation of the workpiece plates due to torque. A backing plate is placed beneath the workpiece to prevent the workpiece from moving vertical downwards due to the vertical force generated and damaging the base plate. The shoulder is the primary source of heat generation (refer to section 4.3.3 pg 95 for further information) but its affect decreases along the thickness of the workpiece. This may result in higher thermal stresses on the top surface of the weld compared to the weld root and may cause (along with the high vertical forces, refer to section 4.4.1 for further information) distortion of

the workpiece with the outer edges rising to form a V-shape during welding. To prevent this distortion of the workpiece, vertical clamps with M10 bolts were used to prevent movement of the workpiece in the vertical direction. Detail drawings of all the FSW rig components are shown in section 7.1 pg 201.

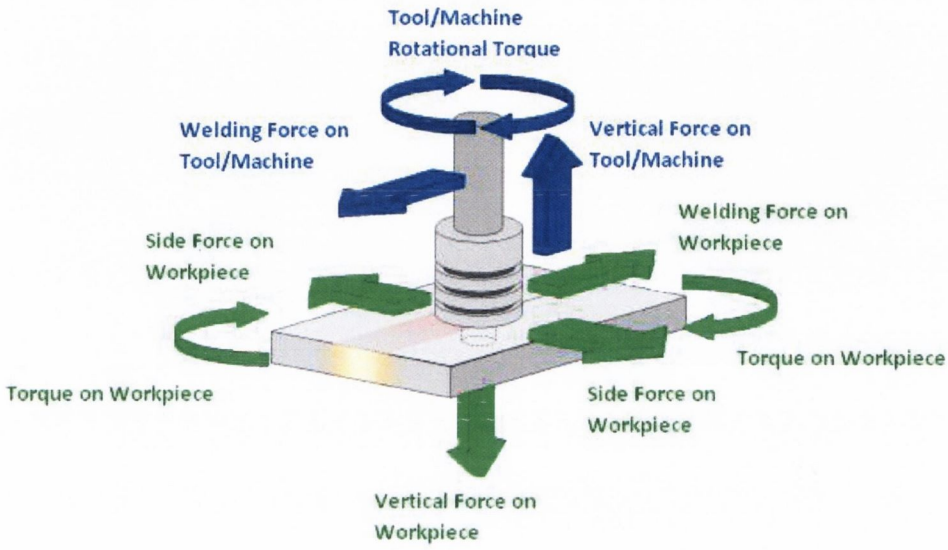


Figure 51: Forces generated during the FSW process

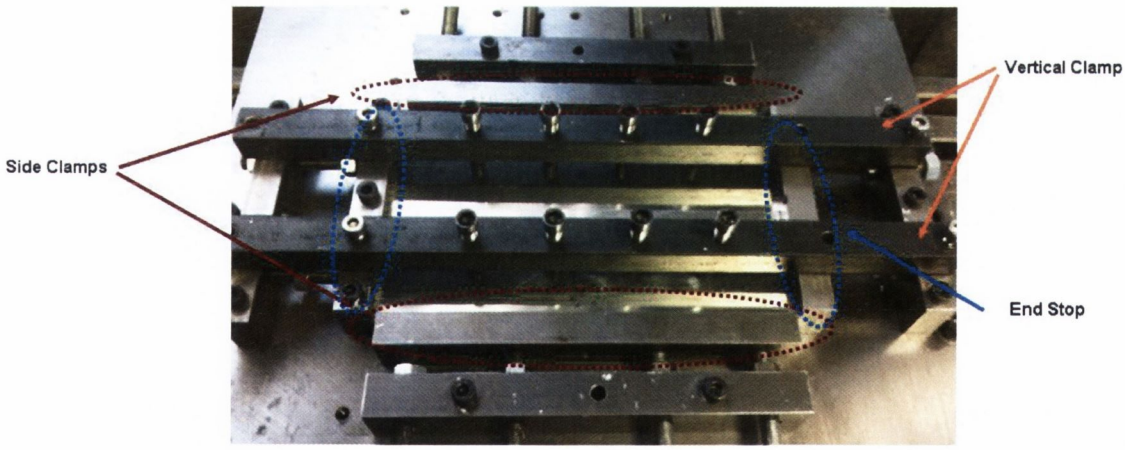


Figure 52: Workpiece and clamping set up

## 3.3 FSW Tooling:

Throughout this research all tools were fabricated from AISI H13 steel. The advantages of using H13 tool steel are that it is abundant, easily machined, has a low cost and has established characteristics. AISI H13 is a chromium-molybdenum hot-worked air hardened steel. It is known for good elevated temperature strength, thermal fatigue resistance and wear resistance [21]. The chemical composition of H13 is outlined in Table 8. In addition, once the FSW tool parts where manufactured, the tool parts underwent a heat treatment process to improve their strength at elevated temperatures.

Heat treatment involved the following stages:

- Vacuum Furnace, 15 minute cycle to 750˚C, hold for 20 minutes
- Vacuum Furnace, 15 minute cycle to 950˚C, hold for 20 minutes
- Vacuum Furnace, 15 minute cycle to 1030˚C, hold for 40 minutes
- Quench with nitrogen gas at 4 bar
- Two tempers at 580˚C for 120 minutes
- Air cool to room temperature after each temper
- Final hardness of 50 Rockwell

| Element | Weight % |
|---|---|
| Iron (Fe) | 88.79 – 91.42 |
| Carbon (C) | 0.32-0.45 |
| Manganese (Mn) | 0.20-0.50 |
| Silicon (Si) | 0.80-1.20 |
| Chromium (Cr) | 4.75-5.50 |
| Nitrogen (Ni) | 0.3 |
| Molybdenum (Mo) | 1.10-1.75 |
| Vanadium (V) | 0.80-1.20 |
| Copper (Cu) | 0.25 |
| Phosphorous (P) | 0.03 |
| Sulphur (S) | 0.03 |

Table 8: Composition of H13 Tool Steels [21]

### 3.3.1 Traditional FSW Tooling:

Traditional FSW tooling consists of a long one piece structure machined from round bar stock. A long tool shaft is required to fix the tool into the chuck of the machine and to provide stability during welding. However, the critical features of the tool (shoulder and pin) are located at the bottom of the tool and represent a small proportion of the overall structure as illustrated in Figure 53. Although H13 is relatively cheap, there are still significant costs with manufacturing and subsequent heat treatment. Heat treatment is required when using H13 for FSW purposes; the cost is calculated through the weight of volume of the material and therefore adds significantly to the cost. At present there are no suppliers within Ireland and therefore all tools must be order through UK companies or machined in house.

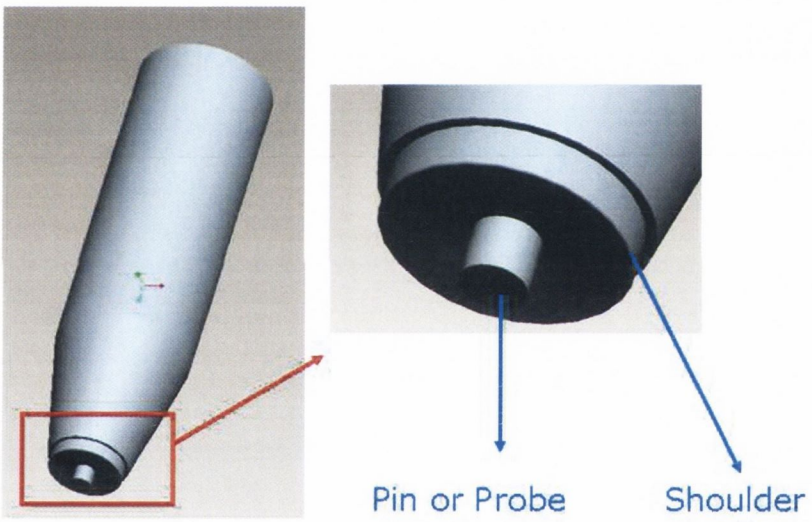


Figure 53: Traditional FSW Tool

### 3.3.2 Design of New Cost Effective Tools:

One of the objectives of the project was to evaluate the effect of different pin and shoulder geometry designs on the FSW process. To keep costs to a minimum, a new three-piece tool was designed, manufactured and tested within the university. The tool components are shown in Figure 54. This design consisted of a tool holder shaft, fabricated from low cost mild steel which is inserted into the spindle of the milling machine. The project focused mainly on two different shoulder designs both 18mm diameter: a concave shoulder and a scrolled shoulder were developed and these are

shown in Figure 55. However other shoulder designs were developed during preliminary testing to optimise the scrolled design and also investigate the effect of shoulder diameter. A number of different pin designs were also tested; these are shown in Figure 56 (Triflute, Square, Cylindrical and Tapered Cylindrical). Each pin had a diameter of 7mm and was manufactured from H13 tool steel. All tools were manufactured from H13 tool steel and finally heat treated to a hardness of 50 Hrc. All tool parts were designed and manufactured within the department except the complex triflute design which was purchased from The Welding Institute UK. The project focused on more recent tooling developments such as the scrolled shoulder and triflute pin due to the lack of published research papers on these particular tooling designs. The performance of this tooling arrangement was also compared to more traditional tooling designs such as the concave shoulder and basic tool pin shapes. Detailed drawing of all tool parts can be seen in section 7.2 pg 203.


Figure 54: 3-Piece Tool Design


Figure 55: Concave and scrolled shoulder design

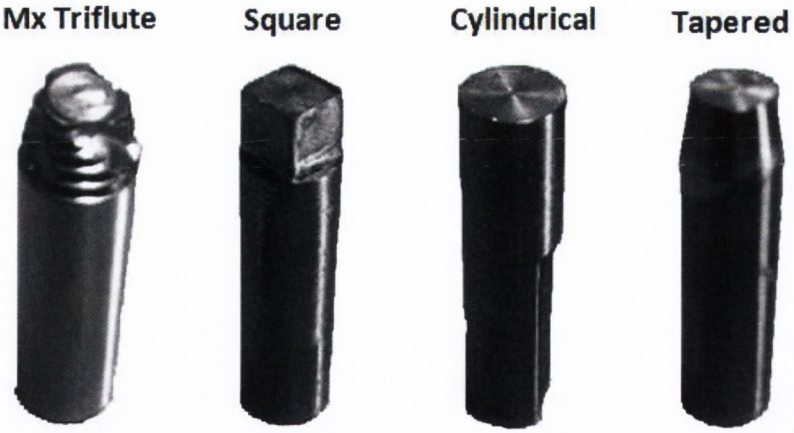


Figure 56: Pin Designs

The 3-piece tool design has significant advantages over traditional FSW tools:

- Traditional tools consist of a shoulder and pin machined as one large single unit. If either the shoulder or pin fails due to fracture or wear, the entire tool must be scraped and replaced. Consequently using a 3 piece designs enables parts of the tool to be interchanged easily.
- Using the traditional method of manufacturing tools for this research (2 shoulder designs and 4 pin designs), a minimum of 8 tools would have had to be machined and heat treated. Using a 3-piece design, only 2 shoulders and 4 pins were required. This reduced costs of material, machining and heat treatment.
- Using this new design it was possible to manufacture the shoulder and pin from different materials thereby enabling a hybrid tooling design if required.
- The shoulder insert contains a control rod (Figure 57) along its centre to adjust the height of the tool pin to allow the welding of different material thicknesses.

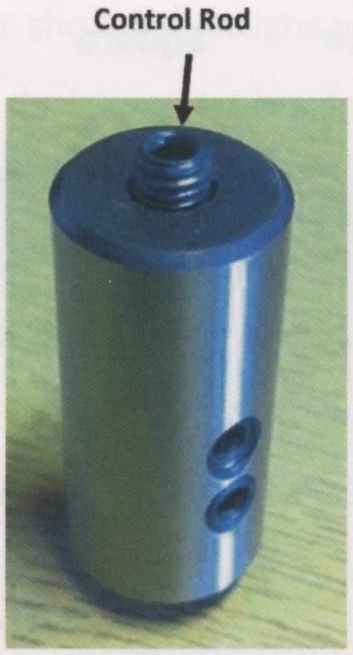


Figure 57: Control Rod

### 3.3.3 Scrolled Should Design:

Initially two types of scrolled shoulder designs were tested and these are shown Figure 58. The depressed scroll design had the scrolled feature machined into the shoulder to a depth of 1mm and the raised shoulder had the area around the shoulder machined away so the scrolled feature stepped down 1mm in height from the shoulder base. Both designs were tested to see if welding with a zero tilt angle was possible. The raised scroll design was capable of producing a consolidated well with a zero tilt angle. However the depressed scroll produced a surface tunnel void during welding. The purpose of the scrolled shoulder is to continuously transport and direct deformed material from the outer edge of the shoulder towards the pin. The depressed scroll shoulder did not transport sufficient deformed material during welding and hence a tunnel surface void occurred. This was also the case when a double depressed scroll was used to increase the amount of material flow as shown in Figure 58. Using a 2˚ tool tilt angle, a consolidated weld was produced using the depressed scroll design. However, unlike a concave shoulder this design did not have a cavity which acts as a reservoir for the deformed workpiece material when welding with a tilt angle and hence welding produced a surface finish with poor quality.

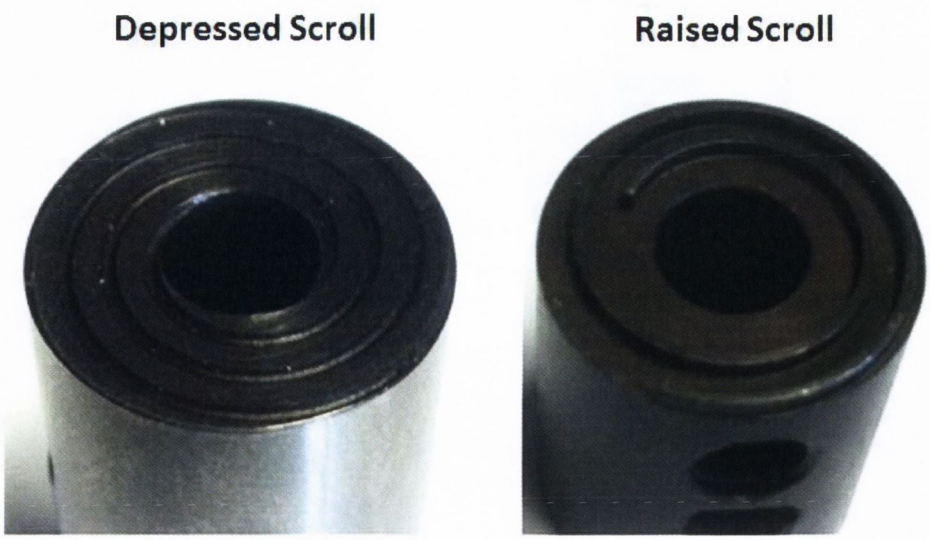


Figure 58: Different scrolled shoulder designs

Figure 59: Bad surface finish from scrolled design A with 2° tilt angle

## 3.4 Workpiece Material:

The workpiece material chosen for this project was rolled Aluminium 2024-T3 with a thickness of 4.82mm. The plates were cut to the required size using a band saw and the dimensions of each workpiece plate can be seen in Figure 60. The composition of the materials is outlined in Table 9 and some of the relevant mechanical and physical properties the workpiece material is presented in Table 10.

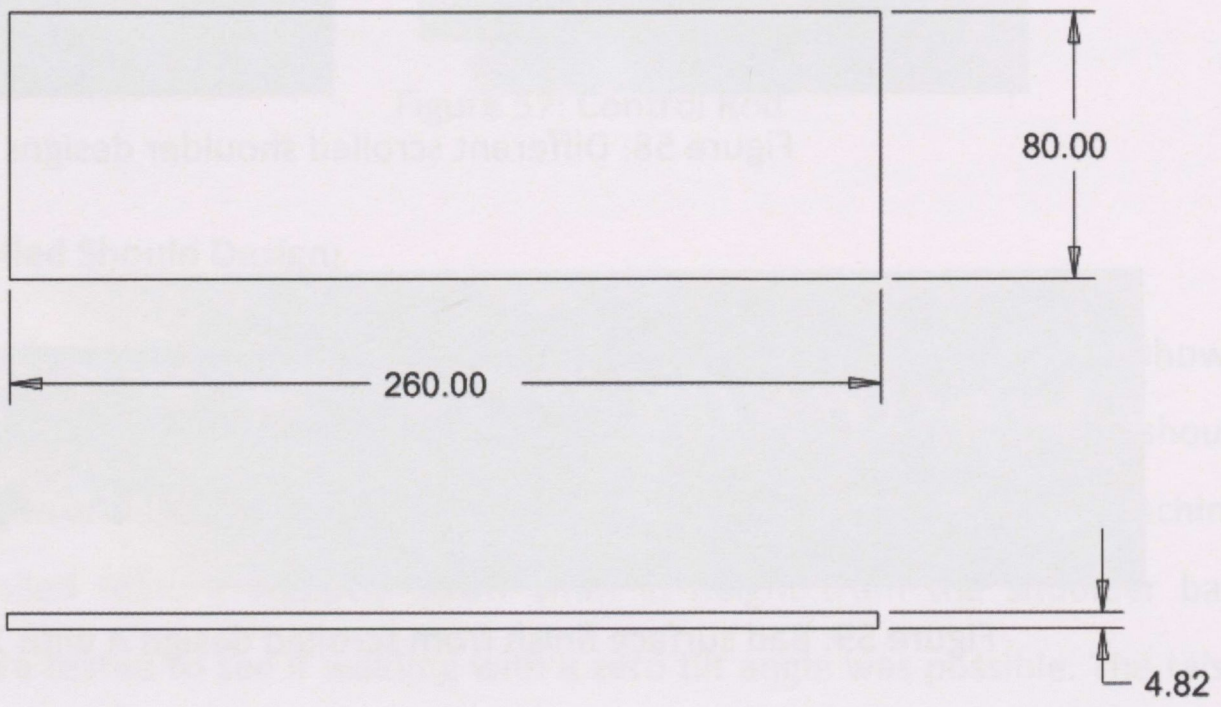


Figure 60: Aluminium 2024-T3 workpiece plate dimensions

| Element | % by Weight |
|---|---|
| Aluminium (Al) | 90.7 - 94.7 |
| Chromium (Cr) | Max 0.1 |
| Copper (Cu) | 3.8 - 4.9 |
| Iron (Fe) | Max 0.5 |
| Magnesium (Mg) | 1.2 – 1.8 |
| Silicon (Si) | Max 0.5 |
| Titanium (Ti) | Max 0.15 |
| Zinc (Zn) | Max 0.25 |
| Other total | Max 0.15 |

Table 9: Composition of Aluminium 2024-T3 [77]

| Properties | Units | Aluminium 2024-T3 |
|---|---|---|
| Tensile Strength | MPa | 427 |
| Elongation | % | 10-15 |
| Vickers Hardness | VHN | 130 |
| Density | kg/m3 | 2770 |
| melting Point | °C | 502-638 |
| Electrical Resistivity | Ω.m | 5.82E-06 |
| Thermal Conductivity | w/m.K | 121 |
| Young's Modulus | MPa | 73 |

Table 10: Mechanical and Physical Material Properties [76]

## 3.5 Research Instrumentation and Process Measurement :

### 3.5.1 Force Monitoring:

A rotating 4-component dynamometer RCD manufactured by Kistler was incorporated onto the welding rid to record the forces acting on both the FSW tool and Machine. The dynamometer connected directly into the spindle of the milling machine and contained a holder for the FSW tool. The dynamometer was capable of measuring the torque and forces in the X, Y, and Z directions. The ranges for the threshold forces are illustrated in

| | |
|---|---|
| $F_x$ | -15 kN – 15 kN |
| $F_y$ | -15 kN – 15 kN |
| $F_z$ | -30 kN – 30 kN |
| $M_z$ | -1100 N.m – 1100 N.m |

Table 11. The forces were measured suing piezo-electric crystals, the signals from which are continuously sampled at a rate of 7.8 kHz for each channel, and are processed through the Kistler 9124B multi-channel signal conditioner. The signal conditioner was connected to a PC and the output was recorded on a Microsoft Excel sheet through a LabView interface at a rate of 10Hz in order to reduce the amount of data collected.

| | |
|---|---|
| Fx | -15 kN – 15 kN |
| Fy | -15 kN – 15 kN |
| Fz | -30 kN – 30 kN |
| Mz | -1100 N.m – 1100 N.m |

Table 11: Dynamometer force monitoring capability

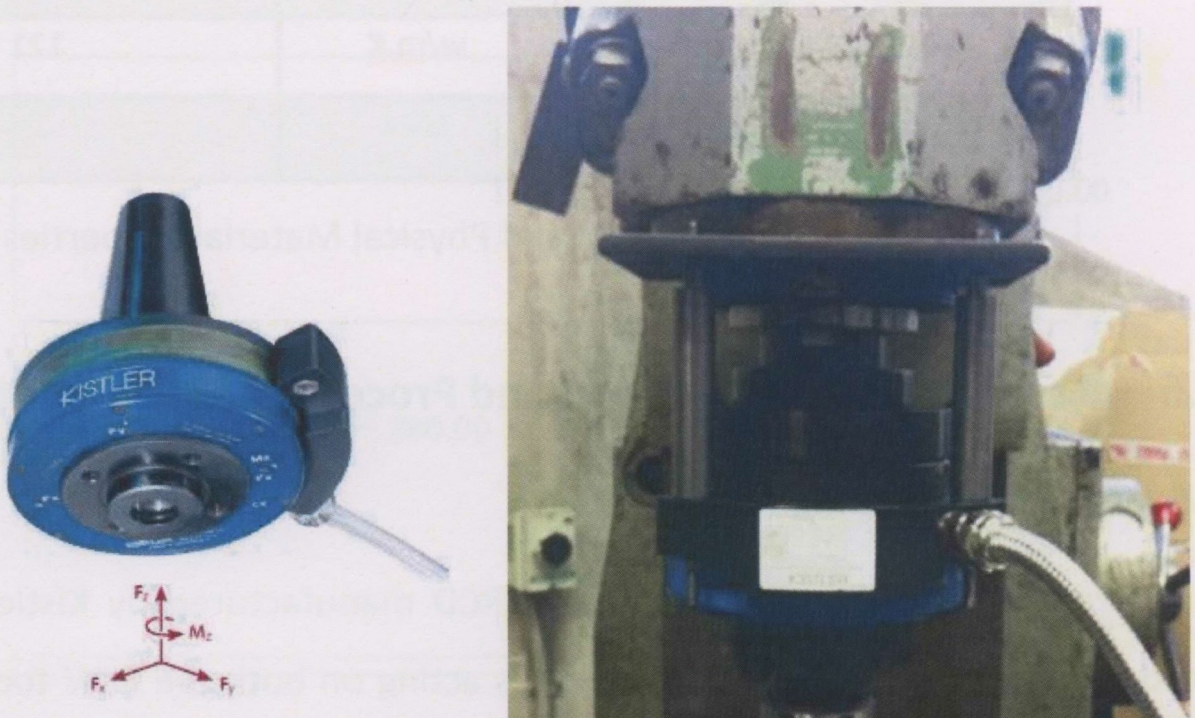


Figure 61: Kistler Dynamometer

### 3.5.2 Temperature Monitoring:

Type K insulated thermocouples with 310 stainless sheet probes of length 150mm and 1.5mm diameter were used to record the temperature at specific locations during the FSW process. These thermocouple were chosen due to their high operating temperature range from 0°C to +1260°c and accuracy. The thermocouples were also very rugged, flexible and particularly suitable for high vibration and pressure applications. High conductive thermal glue was also used to ensure the ends of the thermocouple remained in contact with the workpiece. Holes 1.6mm in diameter were drilled to a depth of 4mm from the surface of each plate to accommodate the thermocouples. It was important to ensure that the thermocouples were at a sufficient distance from the tool pin to prevent the thermocouple being damaged during the welding process. Therefore, each hole was

machined 15mm from the weld centre line. Figure 62 shows the location of the thermocouple holes.

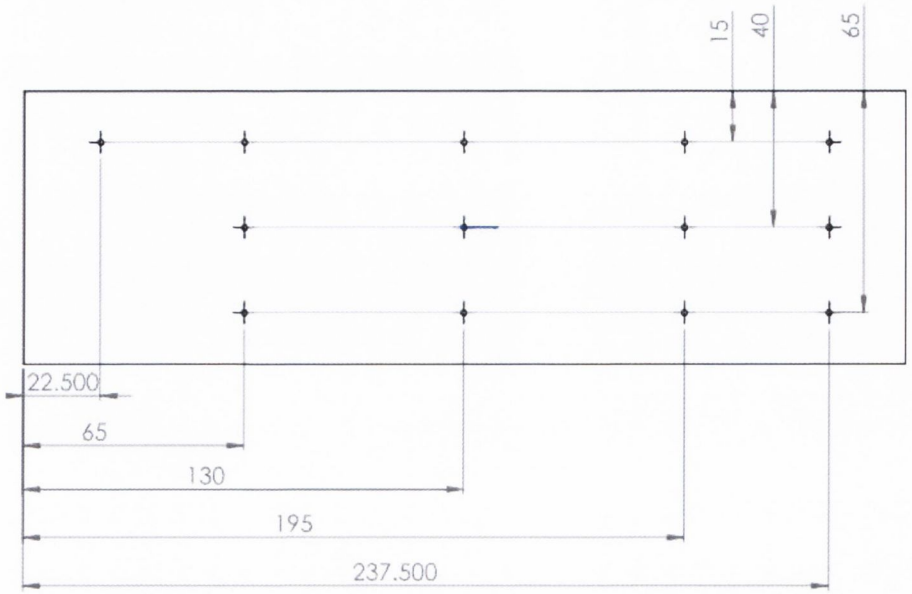


Figure 62: Workpiece plate with 13 thermocouple holes

An infrared camera FLIR P20 shown in Figure 63 was also used to monitor the temperature during FSW testing and the product specifications are shown in Table 12. Exact temperature measurement using this equipment was difficult due to emissivity values associated with the aluminium workpiece. The workpiece plates were highly polished and hence heat from the surroundings was reflected from the surface and picked up on the camera. Another issue was determining the emissivity values and differences between the polished surface of the workpiece and the roughed surface left behind due to welding. Also, during welding the vertical clamps were not used to achieve a better overview of thermal flow, this resulted in slight distortion of the workpiece. However, the camera was possible of predicting approximate temperature and relative thermal flow through the workpiece plates, tooling and rig.

Figure 63: Infrared camera

| Product Specifications | |
|---|---|
| System Type | **Focal Plain Array** |
| Spectral Range | **Long Wave** |
| Detector | **320 X240** |
| Detector Material | **Microbolometer** |
| Measurement Accuracy | **+/- 2 Degrees C** |
| Measurement Range | **-40 to 500 C** |
| With Filter | **500 C** |
| Field View | **24 X 18 Degrees** |
| Cooling | **Uncooled** |
| Spatial Resolution | **Lens Dependent** |
| Thermal Sensitivity | **<0.10 at 30 Degrees C** |
| Detector Refresh Rate | **60 Hz** |
| Dynamic Range | **14 Bit** |
| Emmissivity Adjustment | **.01-1.00** |
| Palettes | **Multiple** |
| Display Type | **LCD and Eye Piece** |
| Image Storage Capacity | **1000+ Images Per Card** |
| Storage Medium | **PCMCIA** |
| Operating Temperature | **-20 to 55C** |
| Camera Weight | **< 5.0 Lbs** |
| Camera Size | **8 X 6 X 4** |
| Focus Distance | **12 Inches to Infinity** |
| Video Output | **60 Hz NTSC** |
| Power Supply | **Battery or AC** |
| Voice Annotation | **Yes** |
| Available Accessories | **Lenses, PCMCIA Cards, Software, Batteries** |

Table 12: Infrared camera FLIR P20 product specifications [80]

## 3.6 Post Weld Analysis:

Post weld analysis consisted of three different procedures: tensile testing, Vickers microhardness testing and macro/microstructure analysis. After welding, each plate was sectioned to provide sufficient samples for the three different procedures.

### 3.6.1 Tensile Testing:

The tensile test pieces cut from the welded plates were initially examined for the presence of flaws and then tested using an Instron 8801. Four tensile test pieces were cut from each weld to British Standard (BSEN 10002-1:2001) as illustrated in Figure 64. Each of the test pieces was mounted in the Instron and loaded at a strain rate of 1 mm/min. Once each specimen fractured, the test data was plotted as a stress-strain graph and the ultimate tensile strength and fracture stress of the specimen was calculated.

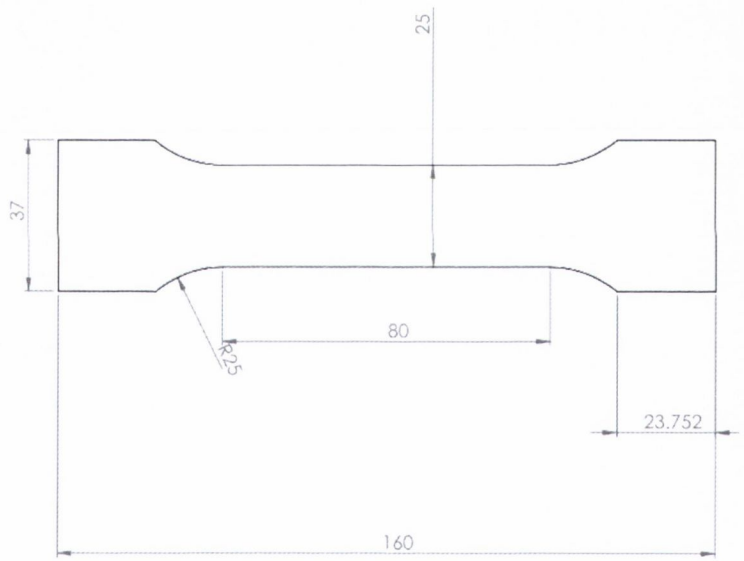


Figure 64: Dimensions of tensile test specimen according to British Standards

Figure 65: Instron 8801 used for tensile testing

### 3.6.2 Vickers Micro Hardness Testing:

One cross sectional sample perpendicular to the weld direction was cut from each weld for microhardness testing. This sample was polished so that the indentation left by the indenter could be easily viewed under a microscope. Once the samples had been polished they underwent a Vickers microhardness test using a Mitutoyo MVK-H1 microhardness machine. Hardness tests were performed 1 mm apart, starting at the weld centre and moving either side until the unaffected base material was reached. This method was employed as it provided an accurate picture of the hardness variation across each of the zones within the weld (TMAZ, HAZ and Base material).


Figure 66: Mitutoyo micro hardness testing equipment

### 3.6.3 Macrostructure and Microstructure Analysis:

One cross sectional sample perpendicular to the weld direction was cut from each weld for macro/micro-structural analysis. The samples were prepared for metallographic analysis using standard metallographic procedures. To remove all the tool marks left by the machining process the sample was first mounted in resin using a Metaserv mounting rig as shown in Figure 67 and then progressively polished with finer abrasives (10μ -1μ) until all tooling marks and scratches were removed.

Figure 67: Metaserv mounting press

To reveal the different weld zones, samples were etched using Keller's reagent. The solution was made up from 150 ml of water, 3 ml of nitric acid, 6 ml hydrochloric acid and 6 ml of hydrofluoric acid. Once all the samples had been successfully etched, their microstructure was viewed with a Leica S6D optical microscope which had an optical zoom up to 1000x magnification.

## 3.7 Finite Element Model:

The finite element package DEFORM 3D V5.1 was used to produce a finite element model of the friction stir welding process. To validate the model, temperatures and forces predicted by the model where compared to experimental results. The FEA simulations were divided into two stages, tool plunge and tool translation. One of the unique features of this model was the representation of the two abutting aluminium sheets as one continuous block rather than as two separate objects. This method avoided numerical contact instabilities that resulted from the discontinuities present at the edge of the two sheets and caused the simulations to fail. The rotating tool moves forward and welds a crack left behind the pin as it advances along the welding line. This model prevented numerical instabilities which resulted in voids, mesh distortion and subsequent program stoppage.

### 3.7.1 Workpiece Material:

The Aluminium 2024 workpiece was modelled as a viscoplastic object. An absolute mesh density was chosen with tetrahedral elements approximately 5mm in length to mesh the workpiece. However, mesh windows with elements 1mm in length were used to concentrate mesh density around the vicinity of tool pin and shoulder contact. These are locations where high stress and strains are expected and therefore a finer mesh was employed in these regions as shown in Figure 68. Mesh windows were set to follow the tool path during tool translation thereby ensuring they remain active throughout the welding process. Weighting factors were used to aid correct remeshing of the workpiece which was set to every 5 steps to maintain mesh integrity. However, frequent remeshing increased computational time significantly. The length and width of the workpiece was reduced in size (160 x 80 mm) to that of experimentally welded plate to help reduce computational and remeshing times. Mechanical properties of AA2024-T3 alclad shown in Table 10 pg67 were inserted into the model. Contact conditions were added to the model using the inter object tool in the pre processor. A shear friction factor of 0.61 is recommended between aluminium and steel [22] and was implemented into the model. Also an interface heat transfer coefficient of 11 N/s/mm/C was used during all simulations [87].

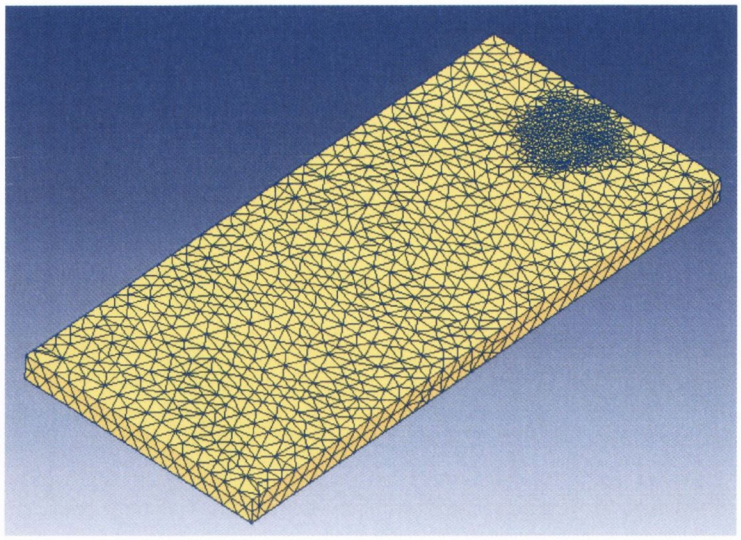

Figure 68: Meshed aluminium 2024-T3 workpiece

One of the major issues associated with the model was describing the flow stress of the workpiece material. This was critical as the temperatures and stresses resulting from the FSW process are determined from the chosen flow stress equation. Initially three different flow stress equation were investigated and are shown in Figure 69. These include the Sellers-Tegart law [98], Johnson Cook material law [99] and an empirical equation adopted by Fratini [87]. The equation developed by the Johnson Cook law gave the best representation of the FSW process, where $\sigma_y$ is the yield stress, $\bar{\varepsilon}$ the effective plastic strain, $\dot{\bar{\varepsilon}}$ the effective plastic strain rate, $\dot{\bar{\varepsilon}}_0$ the normalizing strain rate (typically 1.0 $s^{-1}$) and A, B, C, n, $T_{melt}$, $T_{ref}$ and m are material/test constants. The resulting flow stress curves are illustrated in Figure 70. An important feature of the flow stress model is the reduction of stress with increasing temperature.

Sellars-Tegart Law

$$\dot{\bar{\varepsilon}} = A\left[\sinh\left(\alpha\bar{\sigma}\right)\right]^n \exp\left[\frac{-\Delta H}{RT_{abs}}\right]$$

$A = 0.016$

$\alpha = 0.085$

$\Delta H = 148880$

$n = 4.27$

$R = 8.314$

Johnson Cook Material Law

$$\sigma_y = \left(A + B\left[\bar{\varepsilon}\right]^n\right)\left(1 + \ln\frac{\dot{\bar{\varepsilon}}}{\dot{\bar{\varepsilon}}_0}\right)\left(1 - \left(\frac{T - T_{ref}}{T_{melt} - T_{ref}}\right)^m\right)$$

$A = 369$

$B = 684$

$n = 0.73$

$C = 0.0083$

$m = 1.7$

$T_{melt} = 502$

$T_{ref} = 25$

Fratini

$$\sigma = KT^A\left(\dot{\bar{\varepsilon}}\right)^B\left(\bar{\varepsilon}\right)^C$$

$K = 2.69E10$

$A = -3.3155$

$B = 0.1324$

$C = 0.0192$

Figure 69: Different flow stress equations

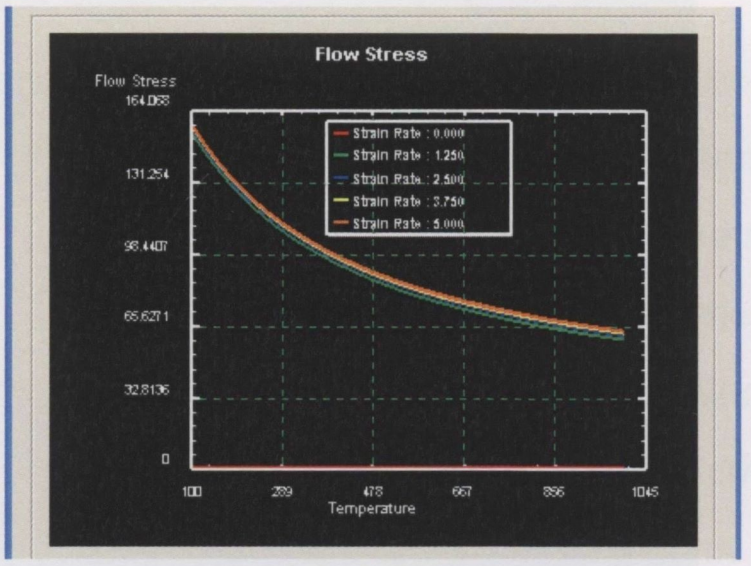


Figure 70: Johnson Cook Flow stress curves

### 3.7.2 Tooling and Clamping:

No boundary conditions or constrains were placed on the nodes of the workpiece so as not to impede any material flow. Therefore a box die was used shown in Figure 71 to house the workpiece and simulate the experimental clamps. In most operations the box was assigned the material properties of mild steel (AISI 1015), meshed with tetrahedral elements 5mm in length and given the same thickness as the backing plate and clamps in order to model thermal flow throughout the clamping arrangement. However, this increased the computational time significantly and hence in some instances, the box was modelled as a rigid object with no mesh.

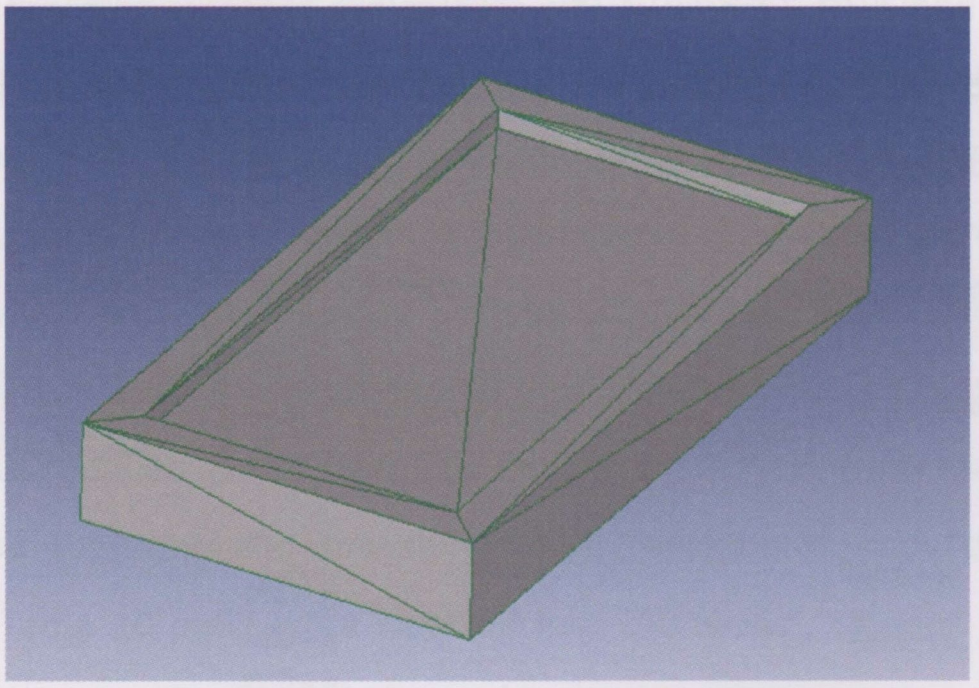

Figure 71: Box used to clamp the workpiece

The assumption of the box as a solid rigid object assumes that there is no deflection of the mild steel side and end stop clamps (Figure 52). S-beam load cells were

used to measure the forces acting on the clamps during experimental testing as illustrated in Figure 72. The largest force (4-5 kN) was found to act on the side clamps. Figure 73 illustrates a schematic of the forces acting on the side clamps. The stress acting on the clamp can be calculated theoretically to be 4.14 MPa hence the associated strain can be calculated to be approximately to be 0.00198 %. This corresponds to a deflection of 0.000396mm along the width direction. Hence the assumption of the FEM box as a solid rigid object is reasonable as there is no significant deflection of the clamps during experimental testing.

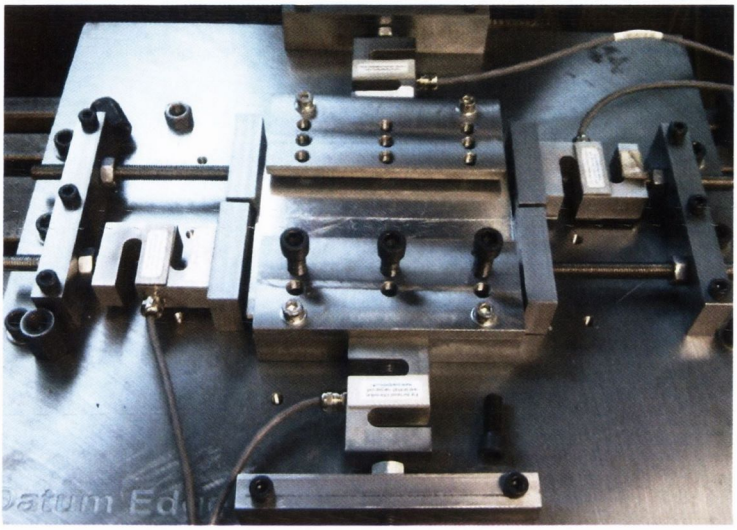

Figure 72: S-beam loads cells used to record the clamping forces

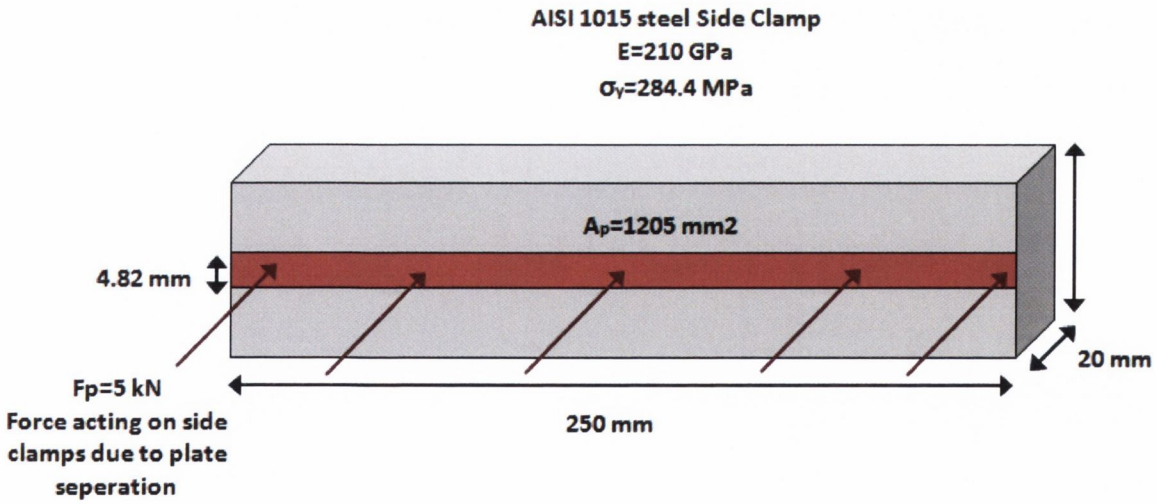


Figure 73: Schematic of the force acting on the side clamps

The tool designs discussed in section 3.3 where modelled using SolidWorks 2010 and imported into DEFORM 3D as STL files. Samples of some of the tools modelled are

illustrated in Figure 74. Detailed drawing of the triflute pin was not available as it was purchased commercially from TWI. Therefore a threaded pin was used to represent the triflute pin. In some operations the tool was modelled as a rigid object, this assumption is reasonable as the yield strength of aluminium is significantly lower than the yield strength of H13 tool steel. Only the tool pin and shoulder geometries and not the parent holder were incorporated into the model to help reduce computational and remeshing time. In most operations the tool was assigned the material properties of AISI H13 tool steel, meshed with tetrahedral elements 0.4mm in length in order to model the thermal flow, stresses and strains occurring. Again, this increased the computational time significantly and hence in some instances, the tool was modelled as a rigid object with no mesh or material properties.

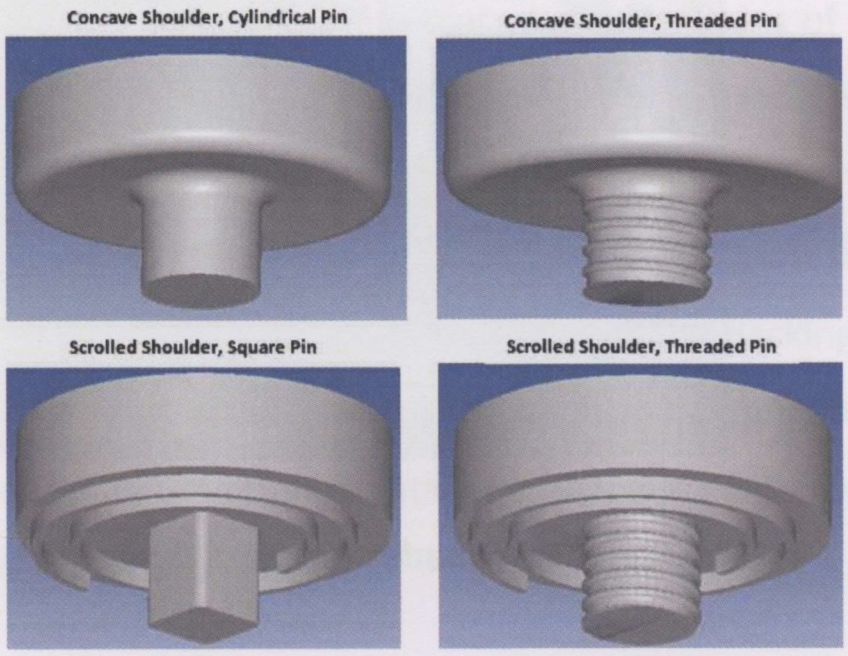


Figure 74: Cylindrical tool FE model

Note that Deform does not allow modeling of the tool as anything other than a homogenous single material entity. However, during experimental testing a three piece tooling system was used. The assumption of the tool as a single entity is reasonable as there is minimal insignificant deflection at the two extra interfaces. This is due to two reasons: firstly, a small sliding fit tolerance of 0.05mm was used for both interfaces and secondly, only a small percentage of shoulder (25%) and pin (17%) were exposed outside the parent tool holder and shoulder respectively. Figure 75 illustrates a schematic of the maximum deflection possible at both interfaces. Using simple trigonometry, $\alpha$ can be calculated as .095° and the deflection of the shoulder ($D_s$) to be 0.066mm. Similar for the pin, $\theta$ can be calculated as 0.13° and deflection of the pin ($D_p$) to be 0.06 mm. Hence the

deflection at both interfaces is extremely small and insignificant. However, using a dial gauge and applying a force of 5 kN (average welding force recorded) to the tool, the deflection was measured experimentally and found to be lower than the theoretical value and equal to approximately 0.03 – 0.04 mm combined over both interfaces.

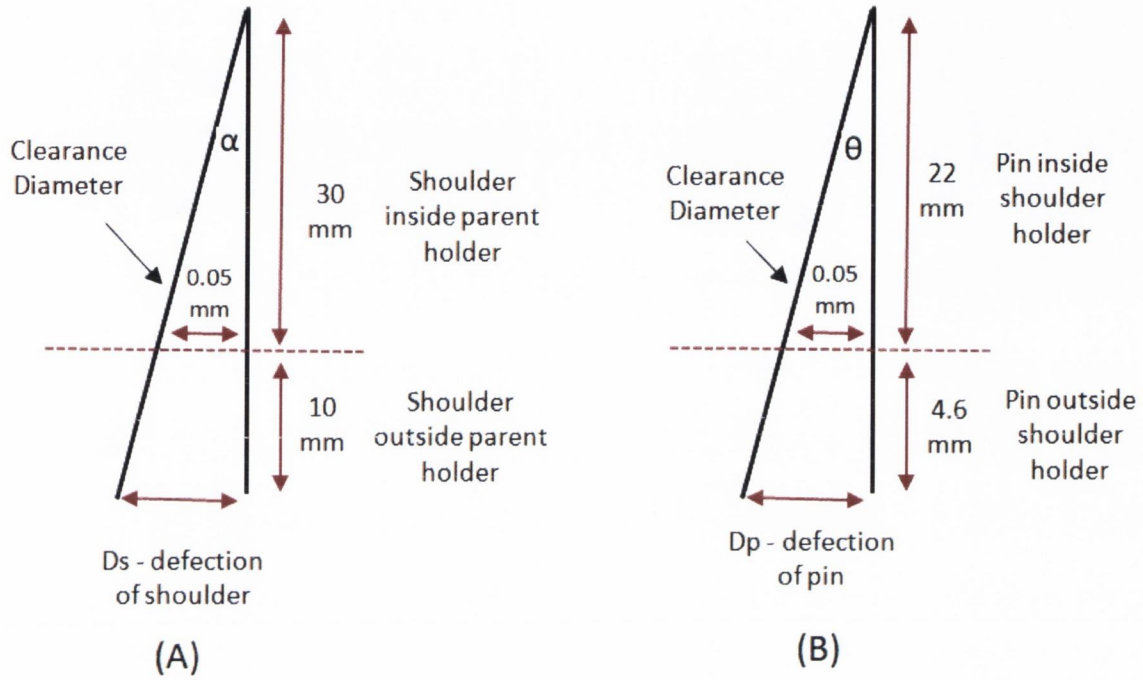


Figure 75: Deflection of the tool at interface between (A) parent holder and shoulder and (B) shoulder and pin

# Chapter 4

# Results and Discussion

## 4.1 Process Specifications on Plunge Depth and Pin Length:

Once all FSW tooling was manufactured and the necessary heat treatment applied, the next stage was to develop process specification on the optimal shoulder plunge depth and optimal pin length. The aim was to achieve a fully consolidated weld throughout the thickness of the material, achieve a smooth surface finish and avoid any visual defects; a weld exhibiting these properties can be seen in Figure 76.

Figure 76: Smooth surface finish with no surface defects

### 4.1.1 Plunge Depth:

The plunge depth refers to the depth that the shoulder is immersed into the workpiece surface during welding. When using a 1mm scrolled shoulder an optimal plunge depth was reached when the shoulder was plunged 0.3 – 0.5mm into the workpiece surface. When using a concave shoulder an optimal plunge depth was reached when 70 – 80% of the shoulder is in contact with the workpiece surface, a schematic is shown in Figure 77.

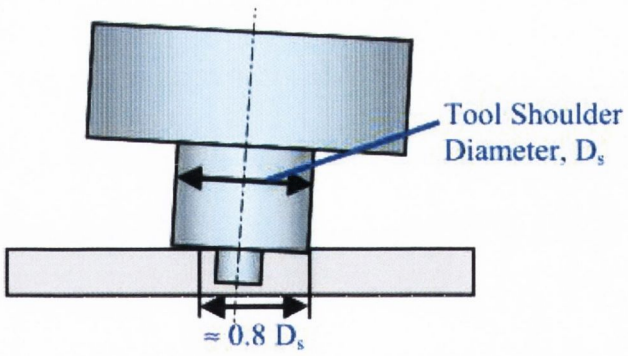


Figure 77: Plunge depth for a concave shoulder with 80% of the shoulder contact with the workpiece

Insufficient plunge depths produced welds with visible cracking and/or surface voids along the top surface, an example is shown in Figure 78. This occurs due to low contact pressure between the tool shoulder and workpiece surface. This shoulder contact is necessary for the forging action of the shoulder to compact and direct the workpiece material towards the tool pin to produce a consolidated weld. The lower contact pressure also results in insufficient frictional forces between the tool and work piece and as a consequence, weld temperatures fail to reach sufficiently high levels to soften the workpiece material which is necessary to produce a consolidated weld. The tool shoulder, as well as producing frictional heating, is also used for bulk transport of material forwards during the weld process. Consequently sufficient contact pressure must be maintained between the tool shoulder and the workpiece surface to drive any material displaced by the tool pin back into the weld cavity ensuring a consolidated weld.

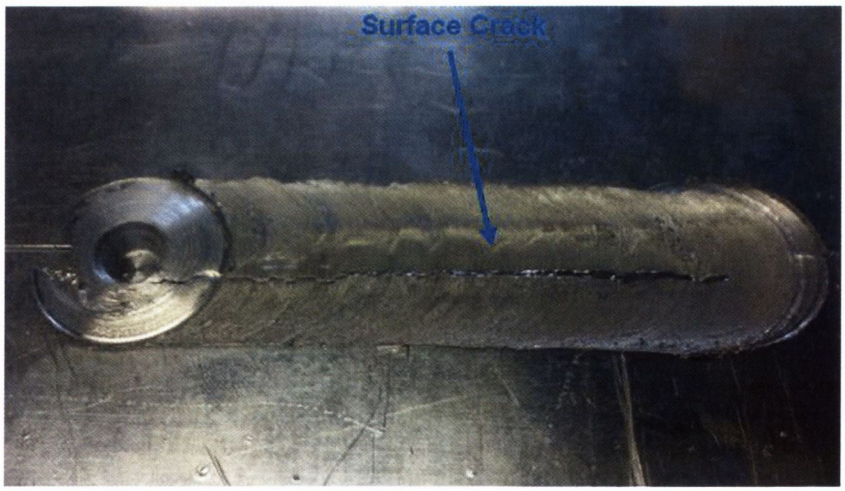


Figure 78: Surface defect due to an insufficient plunge depth

Excessive plunge depths were found to produce excess flash and higher tool/machine forces. This was attributed to the large contact pressure resulting in the tool shoulder acting like a milling tool, removing material from the top surface of the joint and applying more pressure on the workpiece surface. A weld made using an excessive plunge depth is shown in Figure 79. Excessive contact pressure also results in increased frictional forces between the shoulder and the workpiece, which results in high temperatures in the weld region, with the risk of localized melting. High stresses were also induced in the surrounding structure due to higher tool loading. The surface of the welded joint is left very rough with flaking due to localized melting on the top surface of the joint.

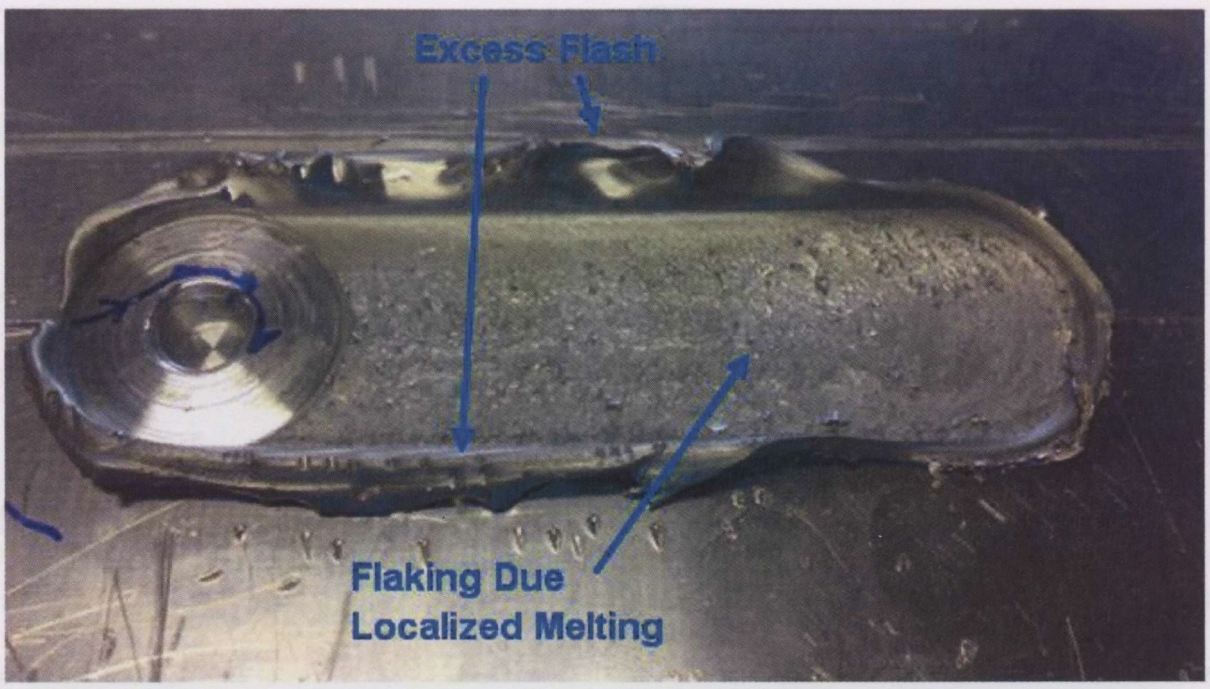


Figure 79: Excess flash generation and flaking due to an excessive plunge depth

### 4.1.2 Pin Length:

An optimal pin length was found when a clearance distance of between 0.1 – 0.2 mm was maintained between the tip of the pin and the root of the weld during FSW. Pin lengths with a clearance distance greater than 0.2mm resulted in the formation of unconsolidated welds throughout the thickness of the workpiece (root flaw) which can be detrimental to the weld quality. The strength of the weld was found to decrease significantly with increasing clearance distances due to the occurrence of these root flaws. Also the bottom surface of the weld is more vulnerable to corrosion as the joint line is still visible. Further details on root flaws are provided in Section 2.4.1. Pin lengths with a clearance distance less than 0.1mm increased the risk of the tip of the tool pin striking the backing plate beneath the workpiece material. This can cause serious damage

to the tool resulting in tool fracture and may also cause the workpiece plates to weld onto the backing plate.

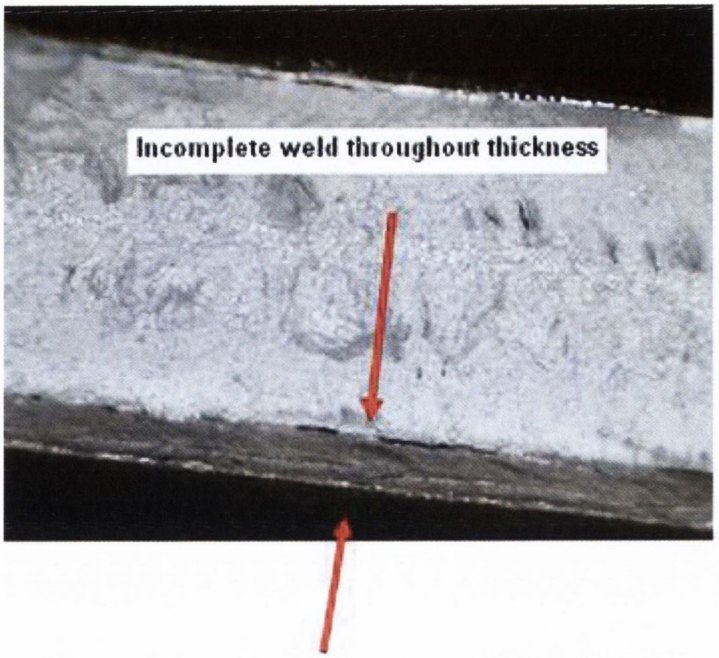


Figure 80: Example of a root flaw due to insufficient pin length

## 4.2 Range of Operational Parameters and Tooling Designs:

A test matrix was developed to vary the operational parameters of both rotational speed and translational speed and is shown in Table 13. The choice of these values was based on a combination of random trials conducted using various settings, on FSW process parameters recommendations from the work of previous authors, and on the limitations of the convert FSW milling machine. To determine the optimal operating parameters, 42 welds were fabricated using the most recent tooling developments which consisted of a scrolled shoulder with a triflute pin. This tooling arrangement was chosen due to the lack of published research papers on these particular tooling designs (see section 2.1 for further details). Temperatures and forces generated during welding were recorded and each weld was sectioned for post weld analysis. During testing, the following parameters were kept constant:

- Plunge rate at 16mm/min
- Dwell time of 8 seconds
- Plunge shoulder depth of 0.5mm
- Pin length from the top surface of the scrolled feature was 4.1mm to maintain a 0.2mm clearance distance between the tip of the pin and the root of the weld.
- Because a scrolled shoulder was chosen, it was possible to weld with a zero degree tool tilt angle.

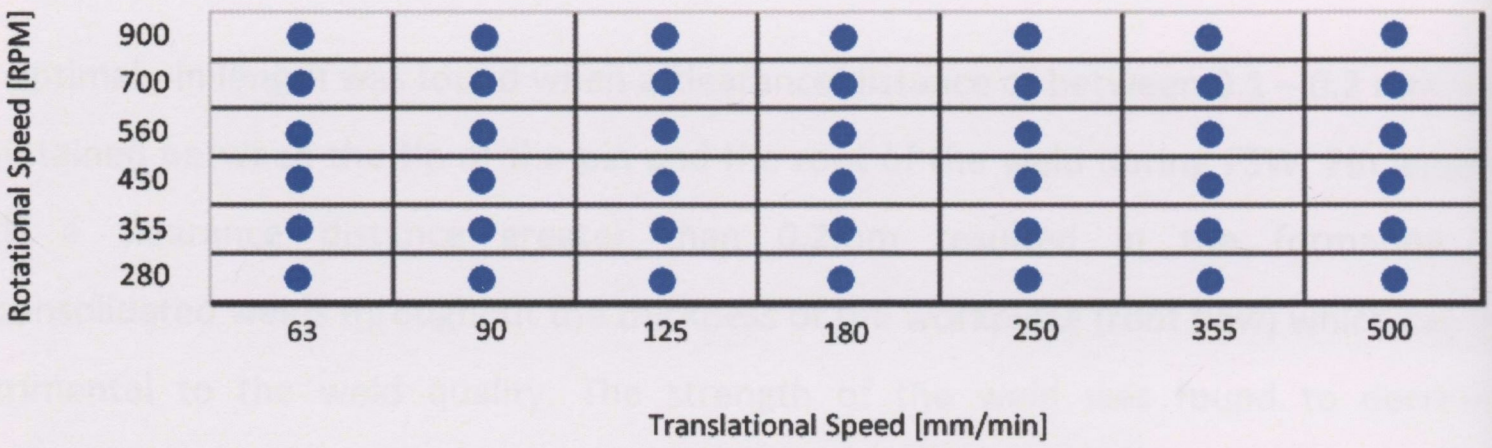


Table 13: Matrix of Operating Parameters to determine the effect of rotational and translational speed

The next stage consisted of optimising tooling design by investigating the effects of tool shoulder and pin designs on the FSW process. This was achieved by fabricating welds using a combination of either a scrolled shoulder or concave shoulder with the 4 different pin designs at two sets of constant operational parameters. These operational parameters were chosen based on the high weld strength achieved during testing of the 1st matrix of operational parameters. As before, temperatures and forces generated during welding were recorded and each weld was sectioned for post weld analysis. During testing with the concave shoulder, the following parameters were kept constant:

- Plunge rate at 16mm/min
- Dwell time 8 second
- When using the concave shoulder, the shoulder was plunged until 80% of its diameter remained in contact with the workpiece surface.
- Pin height from shoulder base was 4.35 to maintain a 0.2mm clearance distance between the tip of the pin and the root of the weld.
- Tool tilt angle of 2°

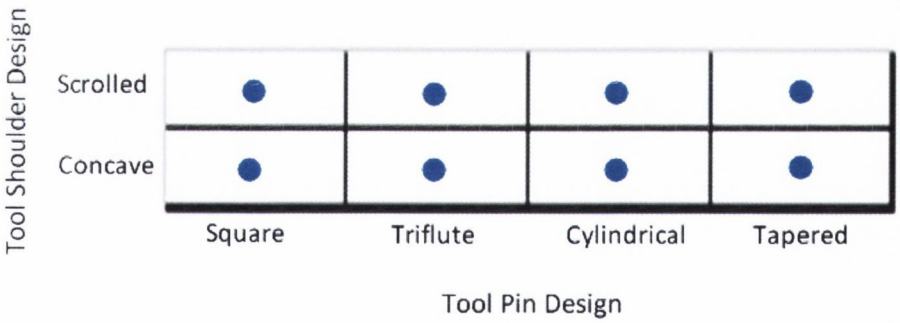


Table 14: Matrix to evaluate the effect of tooling design

## 4.3 Heat Generation & Temperature Measurement:

Heat generation in FSW is necessary to soften the workpiece material for the subsequent stirring and extrusion/forging process to achieve a consolidated weld. The amount of heat conducted into the workpiece determines the quality of the weld, residual stress and distortion of the workpiece. This softening of the workpiece also reduces the loads acting on the tool and the welding machinery. Depending on the choice of tool material, the amount of heat that flows to the tool can also dictate the life of the tool and the capability of the tool for the FSW process. Heat is generated through a combination of friction and plastic flow during deformation of the workpiece material. The magnitude of heat generation is influenced by the operational parameters, thermal conductivity of the workpiece; material thickness; tool geometry and the backing plate. Figure 81 shows a schematic of the heat generation and flow during the FSW process.

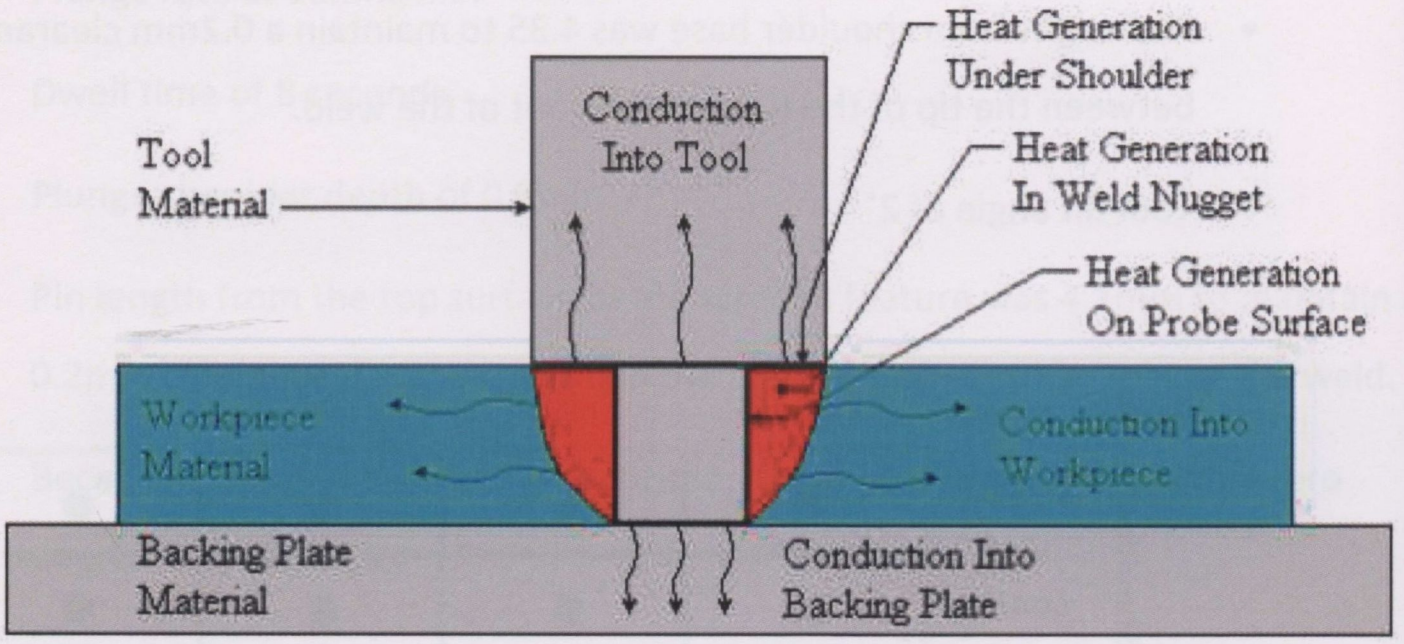


Figure 81: Heat generation and flow during FSW

As mentioned in section 3.5.2, type K thermocouples were inserted and glued into the aluminium plates to measure temperatures generated during the process. The layout and labelling of thermocouple holes on each plate can be seen in Figure 82. One error associated with temperature measurement was the location of the tool on the weld line. If the tool is not exactly positioned on the joint centre line, more of the tool shoulder (which generates the majority of the heat, see section 4.3.3) will act on one side of the joint line than another and therefore more heat generation will appear to occur more prominently on one side (*advancing or *retreating) than the other. A similar issue arises

if the edges of the plates are not perfectly square; the tool will traverse slightly more to one side of the joint. To prevent such errors, the average temperature for corresponding thermocouples on both the advancing and retreating sides were taken.

*Advancing Side: Plate or side of the weld where the tool rotation direction is the same as the tool travel direction

*Retreating Side: Plate or side of the weld where the tool rotation direction is opposite to the tool travel direction

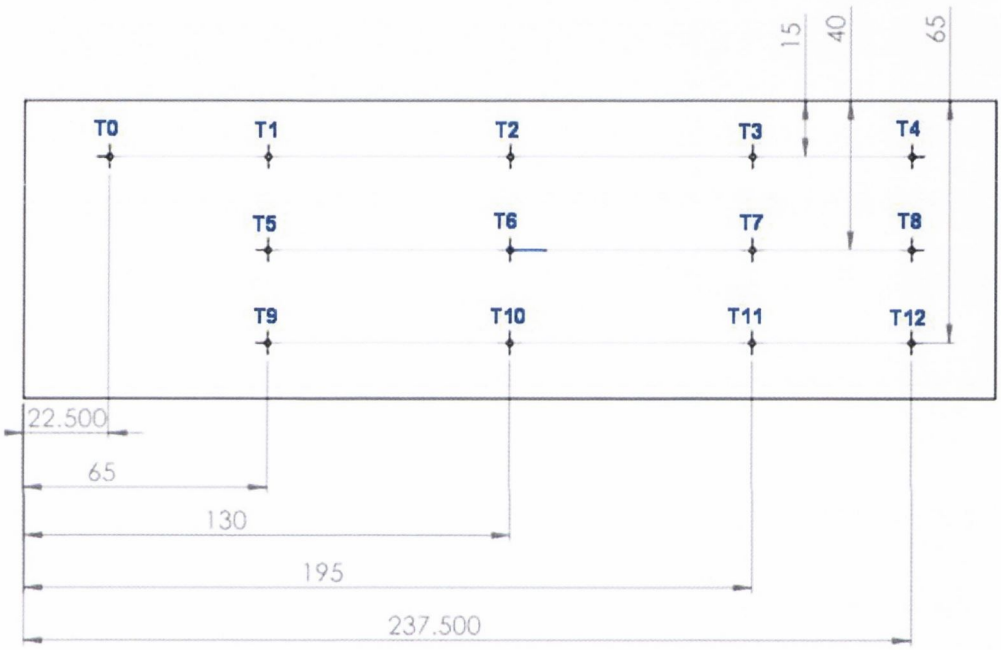


Figure 82: Thermocouple position, layout and labelling

Typical temperature measurements recorded at locations close to the joint line (T0 – T4) are illustrated in Figure 83. Peak temperatures from each thermocouple were recorded when the tool traverses across its location. Thermocouples T1, T2 and T3 recorded similar steady state temperatures of approximately 225˚C for these particular parameters. Jariyaboon et al [57] recorded a similar temperature of approximately 250˚C at a similar distance from the weldline during the FSW of AA2024-T351. These authors implemented a lower welding speed of 154 mm/min which may explain the higher temperatures recorded (see section 4.3.1.1 for further details).

Thermocouples T0 and T4 recorded significantly higher temperatures (approximately 275˚C) than T1, T2 and T3. T0 is located at the tool entry site. As mentioned in section 4.1, the tool was plunged into the workpiece at a speed of 16mm/min to a shoulder plunge depth of 0.5mm. This plunge process takes 17.5s to complete plus an additional 8s during the dwell stage. During both these stages, the tool remains at close proximity to T0 which explains the large increases in temperature measurements. Evidence for this can be seen by noting the large increase in temperature, approximately 100˚C during the dwell phase. The excess heat generated during the dwell stage is necessary to soften the workpiece material before the tool begins to traverse, thereby reducing the risk of tool fracture. A similar explanation can explain the increase in temperature at T4. The tool extraction point is located at T4 and the modified milling machine requires the tool to be extracted manually using the manual plunge rate control (see Figure 49 pg57). The time taken to stop the tool from traversing and to fully extract the tool from the workpiece accounts for this extra increase in temperature recorded at T4. Thermocouples T1, T2 and T3 provide a better representation of the temperature occurring during the actual welding of the plates.

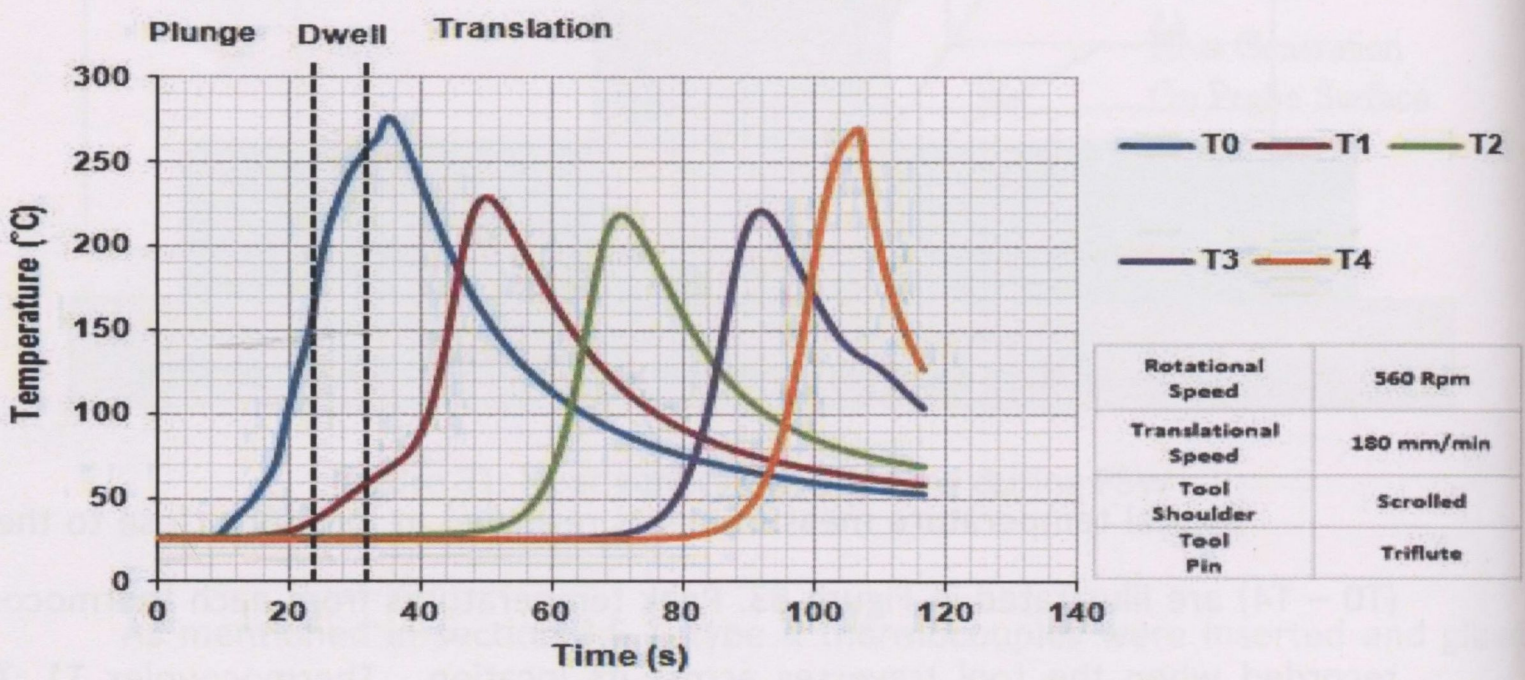


Figure 83: Temperature measurement T0 – T4

### 4.3.1 Effect of Operational Parameters:

#### 4.3.1.1 Translational Speed Effect:

A sample of the temperature results recorded for the various translational speeds employed during testing is presented in Figure 84. The effect of increasing translational speeds on heat generation for a fixed rotational speed of 355 Rpm is illustrated. The average temperature recorded across T1, T2 and T3 were taken. For all experimental tests it was concluded that regardless of the rotational speed, increasing the translational speed was accompanied with a decrease in the temperature recorded. For example, increasing the translational speed from 90mm/min to 500 mm/min resulted in a temperature decrease of approximately 112˚C. As mentioned previously, heat is generated through a combination of friction and plastic deformation of the workpiece material. Increasing the translational speed will reduce the amount of time available for the heat generation process to occur and hence lower temperatures were recorded. Similar results were recorded by J. Chao [74] during the FSW of 8.1mm thick AA2195 plates and M. Jariyaboon [57] during the FSW of 6.35mm thick AA2024-T351 plates.

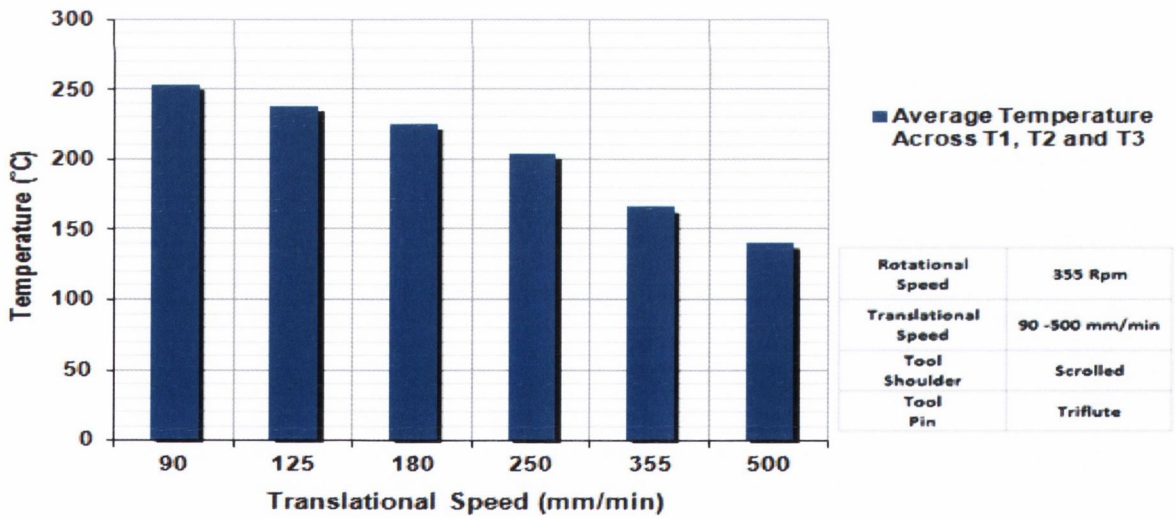


Figure 84: Average temperature measurements across T1, T2 and T3 with increasing translational speed

#### 4.3.1.2 Effect of Rotational Speed:

A sample of the temperature results recorded for various rotational speeds during testing is shown in Figure 85. The effect of increasing rotational speed on heat generation for a fixed translational speed of 90 mm/min is illustrated. The average temperatures recorded across thermocouples T1, T2 and T3 were taken. For all experimental tests it was concluded that regardless of the translational speed, increasing the rotational speed was accompanied by an increase in the temperature. For example, increasing the rotational speed from 280 rpm to 450 rpm resulted with an increase in temperature of approximately 17°C. This increase in temperature with increasing rotational speeds was expected; increasing the rotational speed increases the amount of frictional heating occurring between the tool shoulder and the workpiece surface and hence a higher temperature is generated. Both Jariyaboon [57] and Tang [63] reported similar increases in temperature with increasing rotational speeds during the FSW of 6.35mm thick AA2024-T351 plates and 6.35mm thick AA6061-T6 plates respectively. However, it was noted that the translational speed had more of an influence on the temperatures recorded than the rotational speed for the range of operational parameters tested. This was attributed to the relatively small size of the shoulder (18mm diameter) which reduced the amount of heat generation due to reduced surface area contact with the workpiece and lower peripheral velocities. Preliminary tests on a larger shoulder (22mm diameter) showed an increase in temperature compared to the 18mm shoulder due to an increase in the surface area contact and higher peripheral velocities.

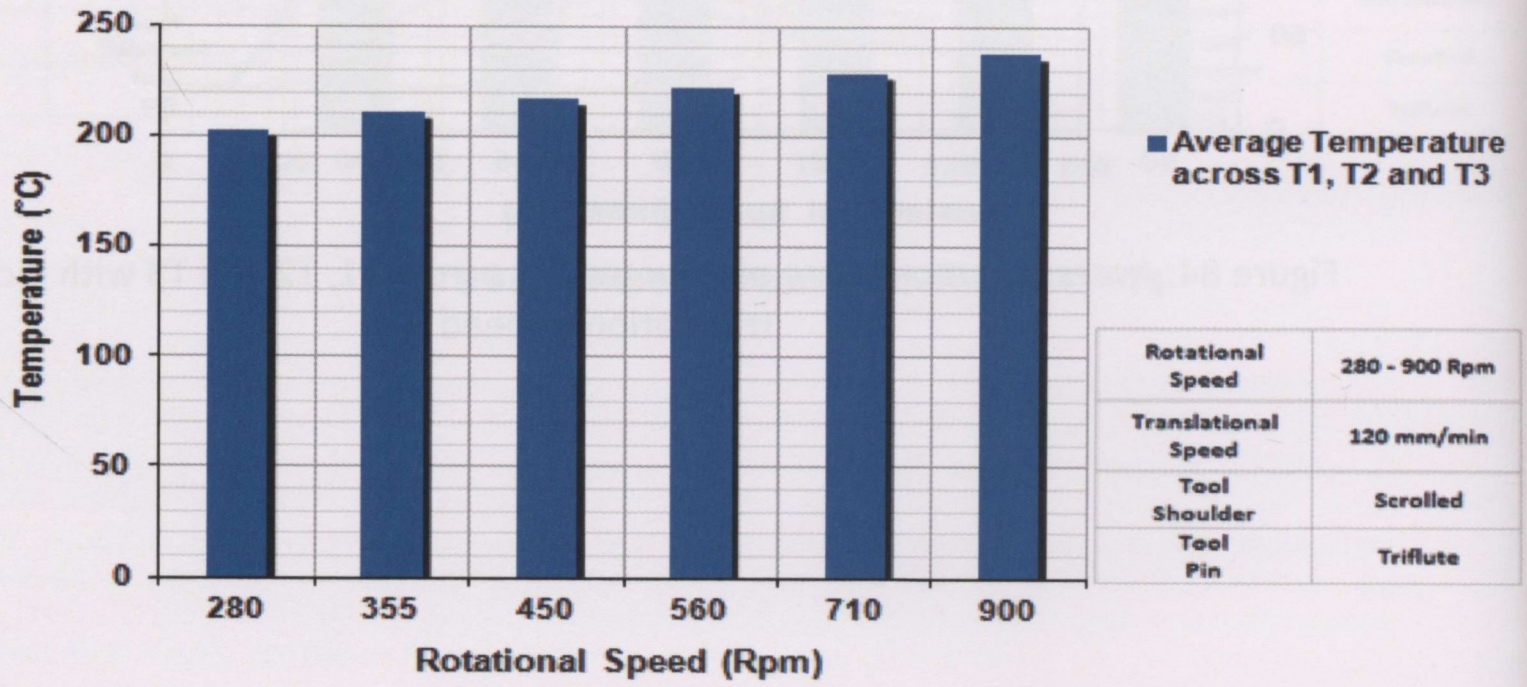


Figure 85: Average temperature measurements across T1, T2 and T3 with increasing rotational speed

#### 4.3.1.3 Interaction between operational parameters:

Variation of either the rotational speed or the translational speed has a significant effect on the heat generated during the FSW process. However, a dependant relationship exists between both the rotational speed and translational speed. This relationship affects all aspects of the FSW process (temperature, forces and weld mechanical properties). The rotational speed regulates the magnitude of material deformation and friction occurring. For example higher temperatures were recorded when the rotational speed was increased. The translational speed regulates the time allocated for the rotational effect. For example, a slow translational speed permits more revolutions of the tool per millimetre than a higher translational speed.

This interaction between rotational speed and translational speed can be seen in Figure 86. Two observations can be made from this graph. Firstly, a greater increase in temperature is recorded when the translational speed is increased whilst implementing a higher rotational speed rather than a lower rotational speed. For example, increasing the translational speed from 90 to 355 mm/min, a temperature difference of 75 °C is recorded when a rotational speed of 560 Rpm is implemented. Whereas, a lower temperature difference of 59°C is recorded if a rotational speed of 280 Rpm is implemented. Similarly, a greater temperature difference is recorded when the rotational speed is increased whilst implementing a lower translational speed rather than a higher one.

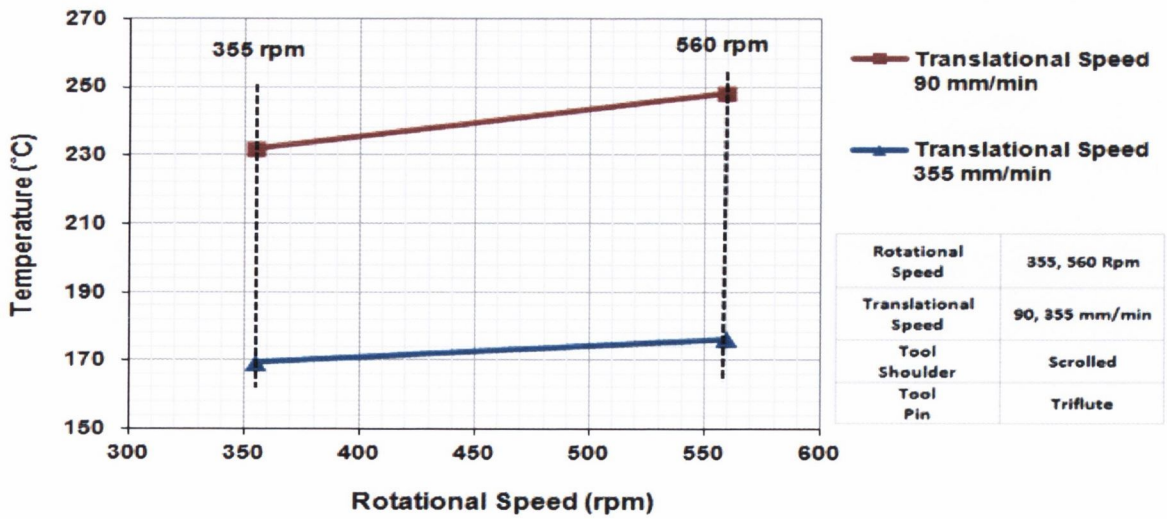


Figure 86: Average temperature measurement across T1, T2 and T3; interaction between operational parameters

The relationship between the translational and rotational speed can be explained by characterising the operational parameters in terms of revolutions of the tool per millimetre travelled along the joint line (rev/mm). Figure 87 illustrates the results shown in Figure 86 with the operational parameters characterised in the format rev/mm. As expected, the temperature increases with increasing rev/mm. The greater number of tool revolutions per millimetre increases the amount of material deformation and friction occurring between the tool and the workpiece. Hence, more heat is generated.

Many authors tend to use the method of (rev/mm or mm/rev) to characterise the two operational parameters together when analysing results [33, 56 and 54]. However, this method does not give a true representation of the results in some cases. For example, consider the two sets of parameters:

1) Rotational speed = 450 Rpm, Translational speed = 180 mm/min
2) Rotational speed = 900 Rpm, Translational speed = 355 mm/min

The FSW tool rotates 2.5 times for every millimetre travelled (2.5 rev/mm) along the joint line for both sets of parameters. This would seem to suggest that the heat generated by the two sets of parameters during welding should be approximately the same. However, this is not the case; the 1st set of parameters recorded an average temperature of 229.15 ˚C whereas the 2nd set of parameters recorded an average temperature of 191.49 ˚C. The reason for this difference is the elimination of the time factor using this method. For example, if two plates of identical length were welded together using both sets of parameters. Welding would take longer using the 1st set of parameters (nearly 50% longer), this permits extra time for friction and hence heat generation to occur which explains the higher temperature recorded.

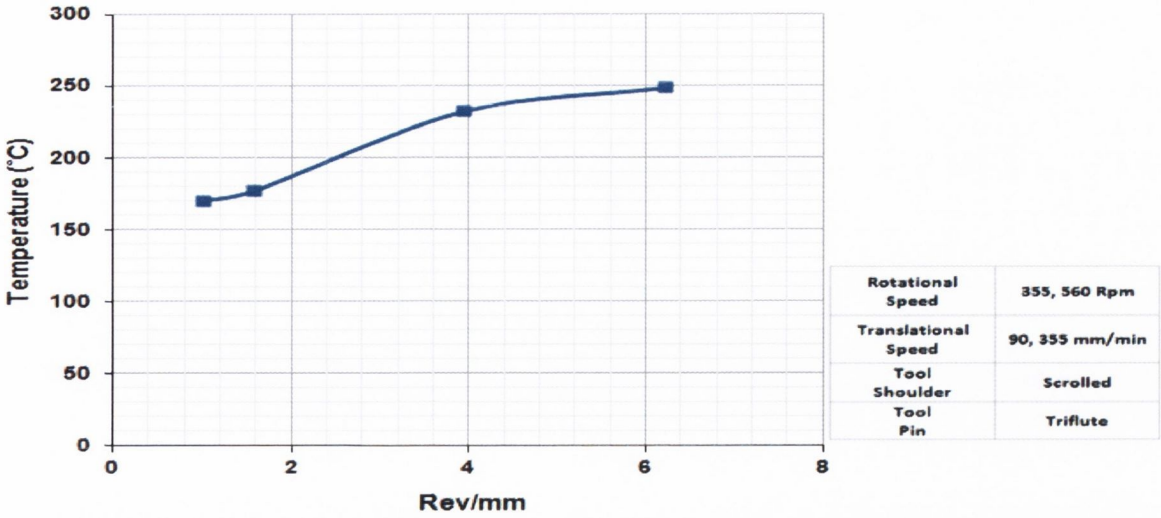


Figure 87: Average temperature measurement across T1, T2 and T3; interaction between operational parameters in terms of rev/mm

### 4.3.2 Effect of Different Pin Geometries:

Four different pin geometries (Square, Triflute, Cylindrical and Tapered) were used to examine the effect of varying the pin geometry on the temperature measured. Figure 88 shows the temperature recorded at T2 for the four different pin geometries at a rotational speed of 450 Rpm and a translational speed of 180 mm/min using a scrolled shoulder. Figure 89 shows the average temperature across T1, T2 and T3 during the same test. It is clearly evident that variation in pin geometry did not have a significant effect on heat generation. These results suggest that the shoulder is the primary source of heat generation. Further tests were conducted to clarify this (see section 4.3.3). Similar results were recorded by Hidetoshi Fujii who measured the temperature generated during the FSW of various aluminium alloys. This author used three different pin designs (Cylindrical, Cylindrical with threads and triangular prism) and reported no significant variation in temperature for the different pin designs. This author attributed this to the tool shoulder being the primary source of heat generation and hence changing the pin design did not have a significant effect.

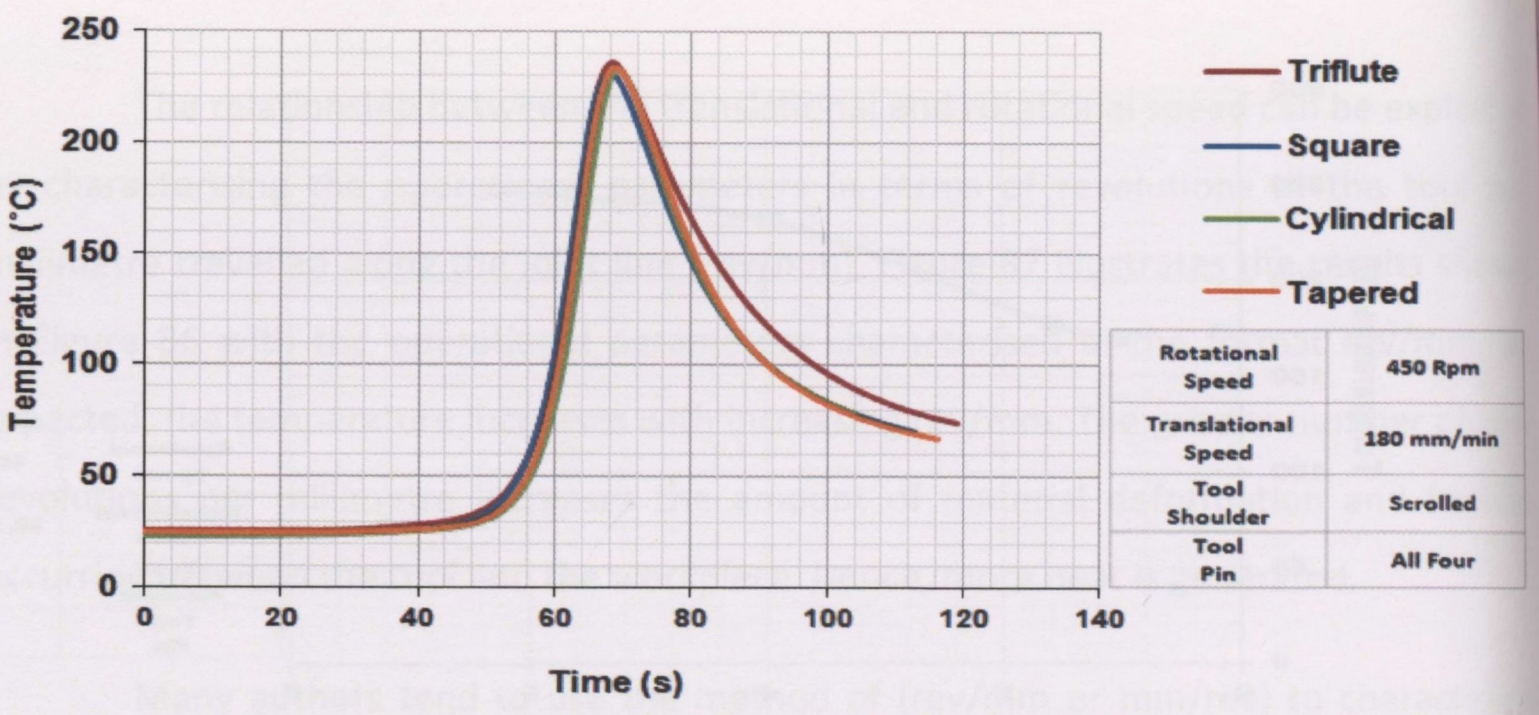


Figure 88: Temperature measurement at T2 for different pin geometries

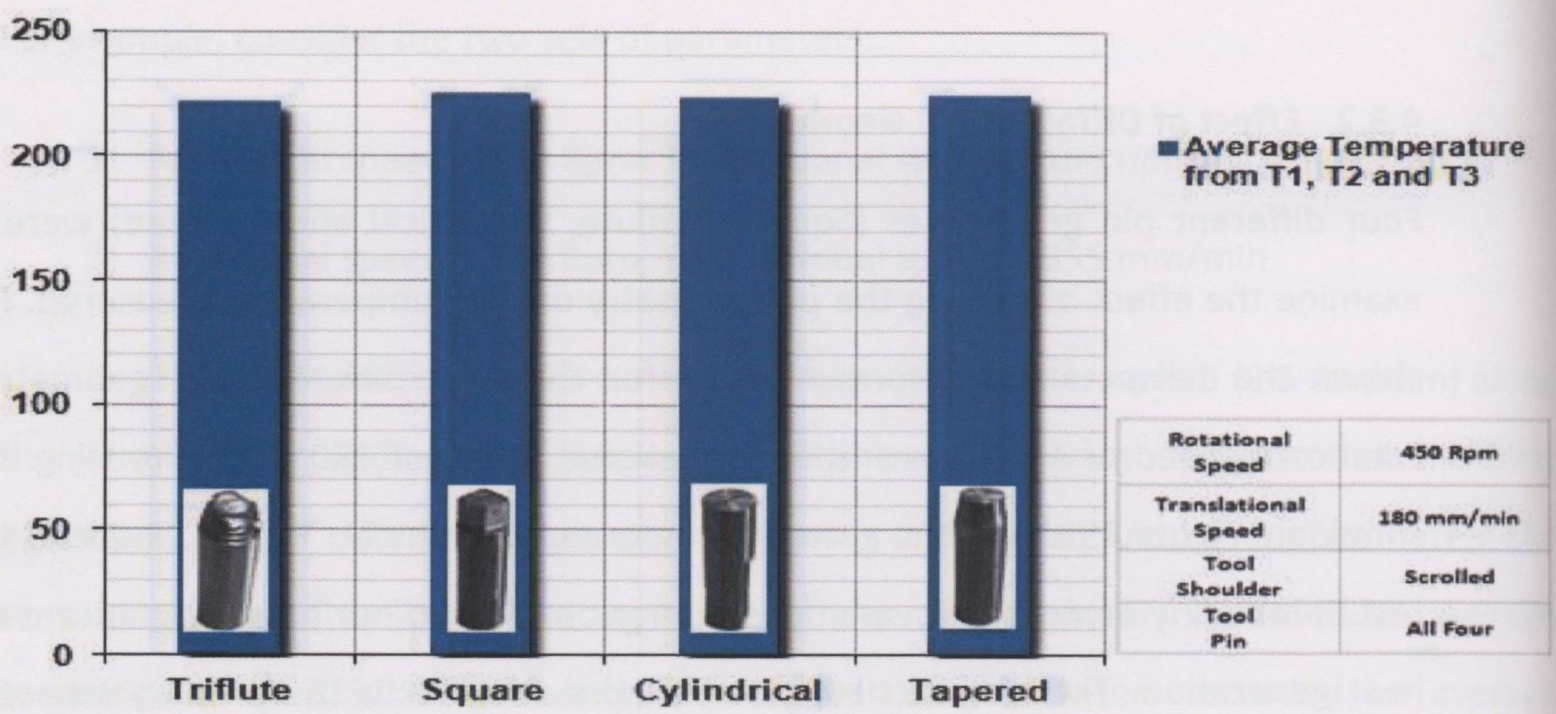


Figure 89: Average temperatures across T1, T2 and T3 for different pin geometries at 450 Rpm and 180 mm/min

### 4.3.3 Tool Pin and Shoulder Thermal Contribution:

Results from section 4.3.2 seem to indicate that the majority of heat generation is contributed by the tool shoulder. Similar results have been reported by different authors suggesting that the amount of heat input from deformational heating around the pin tool has been estimated to range from 2% to 20% [63, 65, 66]. To examine this further, temperature measurements were recorded during welding with no tool pin present. This gave a clear indication of the heat generated by the tool shoulder alone. By comparing the results to an identical weld (same operational parameters) with both the tool shoulder and pin in place, it was possible to calculate the heat generated by the tool pin. The results are shown in Figure 90 and give a clear indication of the heat generated by the tool shoulder and pin across thermocouples T1, T2 and T3. As expected, the results confirm that the tool shoulder is the primary source of heat generation and accounts for approximately 93 % of the total heat generated. Whereas the heat generated by the tool pin accounts for approximately 7% of the total heat generated.

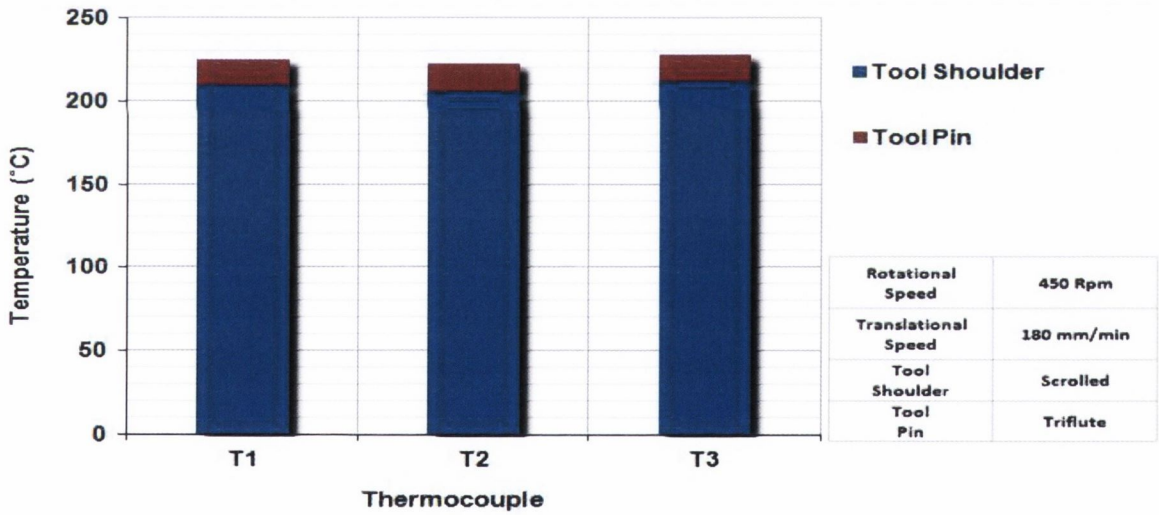


Figure 90: Heat Generated by the tool shoulder and pin

### 4.3.4 Thermal Flow Throughout the Workpiece:

The thermal flow across the width of the workpiece is illustrated in Figure 91. Thermocouples T2, T6 and T10, are all located 130mm along the length of the workpiece at distances 15, 40 and 65mm respectively from the joint line (see Figure 82). As expected, the temperature decreases with increasing distance from the weld line. M. Hwang et al [64] reported similar results during FSW of 3.1mm thick aluminium 6061-T6 plates. It is evident that there is a large drop in temperature, of approximately 150 ˚C, between T2 and T6 over a small distance of 25mm. This indicates that a large quantity of heat is being conducted through the backing plate underneath the workpiece and also through the tool.

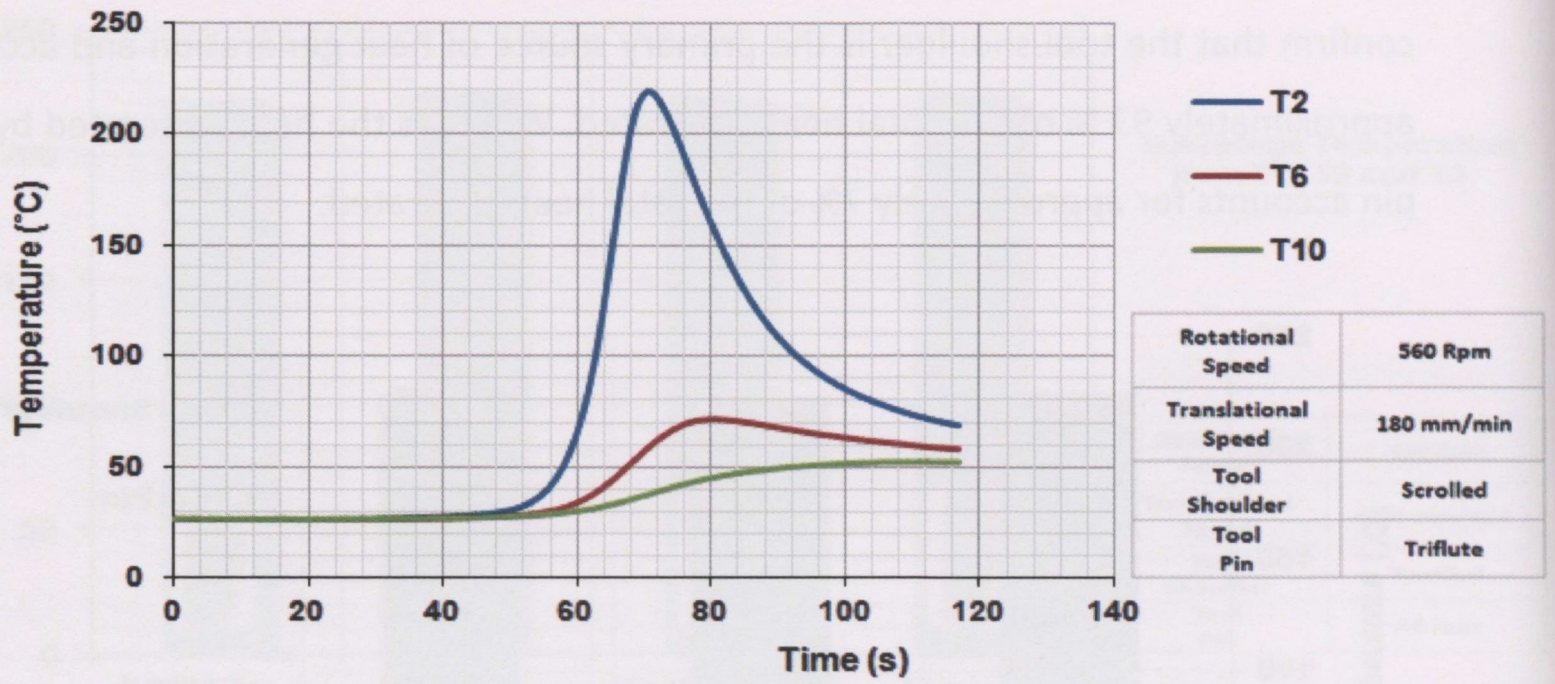


Figure 91: Thermal flow along the width of the workpiece

To investigate if the temperature reaches a steady state during the FSW process, 10 thermocouples (5 on the advancing side and 5 on the retreating side) were placed parallel to the weld direction. Thermocouples were placed at significant distances away from both the tool insertion point and tool exit point. This arrangement reduced the interference of the high temperatures which were recorded during the plunge, dwell and extraction stages (see Figure 83) and therefore provided a better understanding of the heat generated during the actually welding process. The thermocouple layout is illustrated in Figure 92. M. Hwang et al [64] reported steady state temperature measurements during the FSW of 3.1mm thick aluminium 6061-T6 plates. However, the length of plates used by these authors was only 60mm in length. Also, these authors only examined one particular set of parameters (rotational speed of 920 Rpm and translational

speed of 20 mm/min). Both of these factors suggest insufficient evidence as to whether the heat generation reaches a steady state for longer weld runs and also different combinations of operational parameters. During this project, plates 260 mm (Figure 60) in length were used with a range of different operational parameters (Table 13) to determine if temperature measurement reached a steady state during FSW.

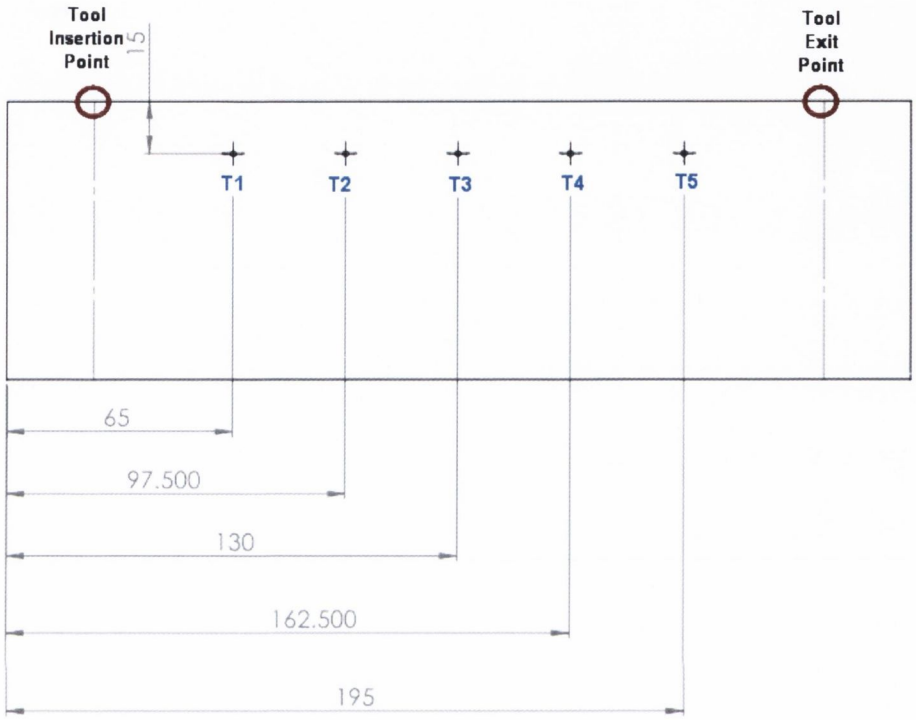


Figure 92: Thermocouple position, layout and labelling 2

A sample of the temperature measurements parallel to the weld line is shown in Figure 93. Results indicated that regardless of the operating parameters, distribution parallel to the welding direction reached steady state values during the FSW process. For example Figure 93 shows this steady state heat generation for a range of different translational speeds. A standard deviation of less than 10°C was recorded between adjacent thermocouples. Similar steady state temperature distribution results were recorded with variation in the rotational speed. Figure 93 also illustrates the reduction in temperature (heat generation) with increasing translational speeds (see section 4.3.1 for further details).

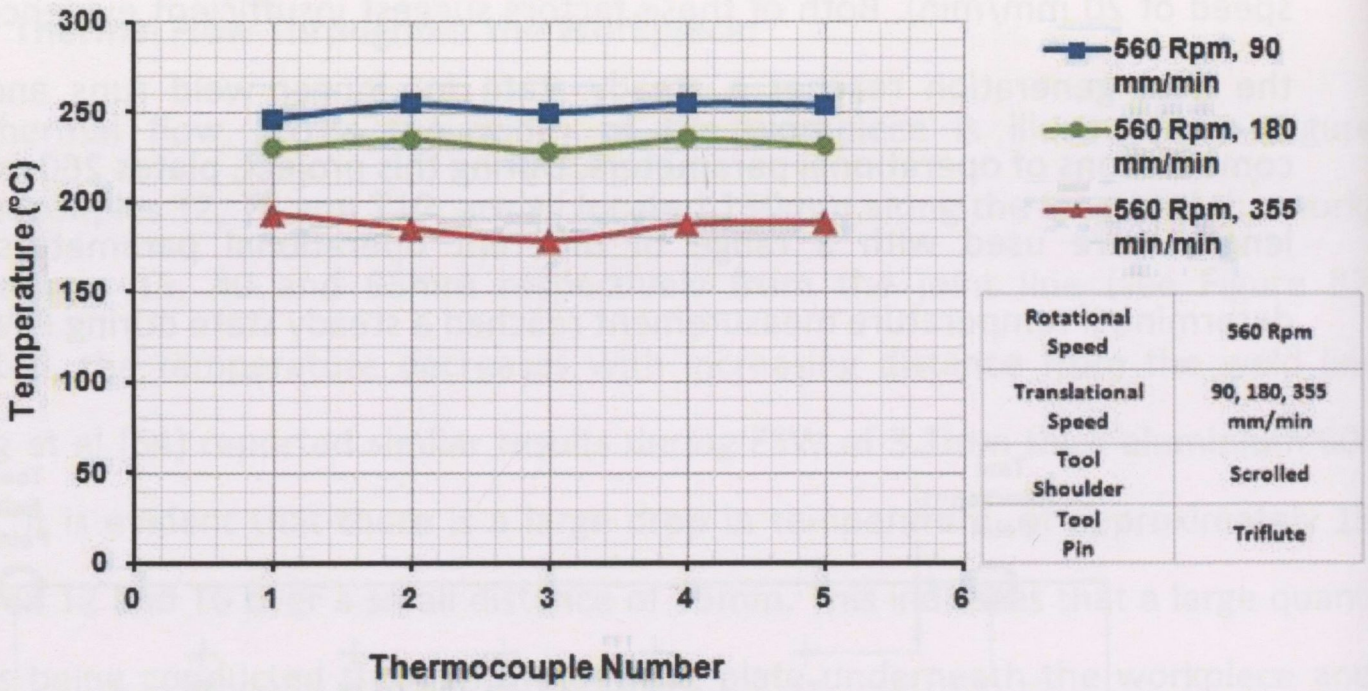


Figure 93: Temperature measurement parallel to the weld line

Results on the thermal flow indicate that the tool acts as a local heat source generating little thermal flow throughout the workpiece outside the vicinity of the tool. For example Figure 91 illustrated the lack of thermal flow throughout the workpiece perpendicular to the direction of tool travel. Table 15 shows the thermal flow across 5 thermocouples as the tool traverses across their location points. As illustrated in Figure 92 all thermocouples are 32.5mm adjacent to the next. The table indicates the lack of thermal flow ahead of the tool. For example, the column representing T5 shows the slow increase in temperature until the tool is at least 32.5mm from its location (distance of 162.5mm) where the temperature increases from 34.4 ˚C to 96˚C and then jumps to a maximum of 261.07 ˚C when the tool passes the T5 location (195mm). Further evidence verifying that the tool acts as a local heat source can be seen in Figure 94 which shows the thermal flow throughout the workpiece using thermal imaging analysis and highlights that high temperatures are only recorded near the FSW tool.

| Tool Location | T1 | T2 | T3 | T4 | T5 |
|---|---|---|---|---|---|
| 65mm | 257.8204 | 100.1154 | 37.40244 | 26.4448 | 24.70429 |
| 97.5mm | 167.9756 | 267.5821 | 95.79059 | 35.47467 | 26.02019 |
| 130mm | 108.6857 | 171.2834 | 263.54 | 88.93748 | 34.4032 |
| 162.5mm | 81.13882 | 108.0769 | 166.5766 | 267.2046 | 96.15344 |
| 195mm | 67.78147 | 81.24291 | 106.1929 | 163.1656 | 261.0757 |

Table 15: Thermal flow parallel to the direction of tool travel

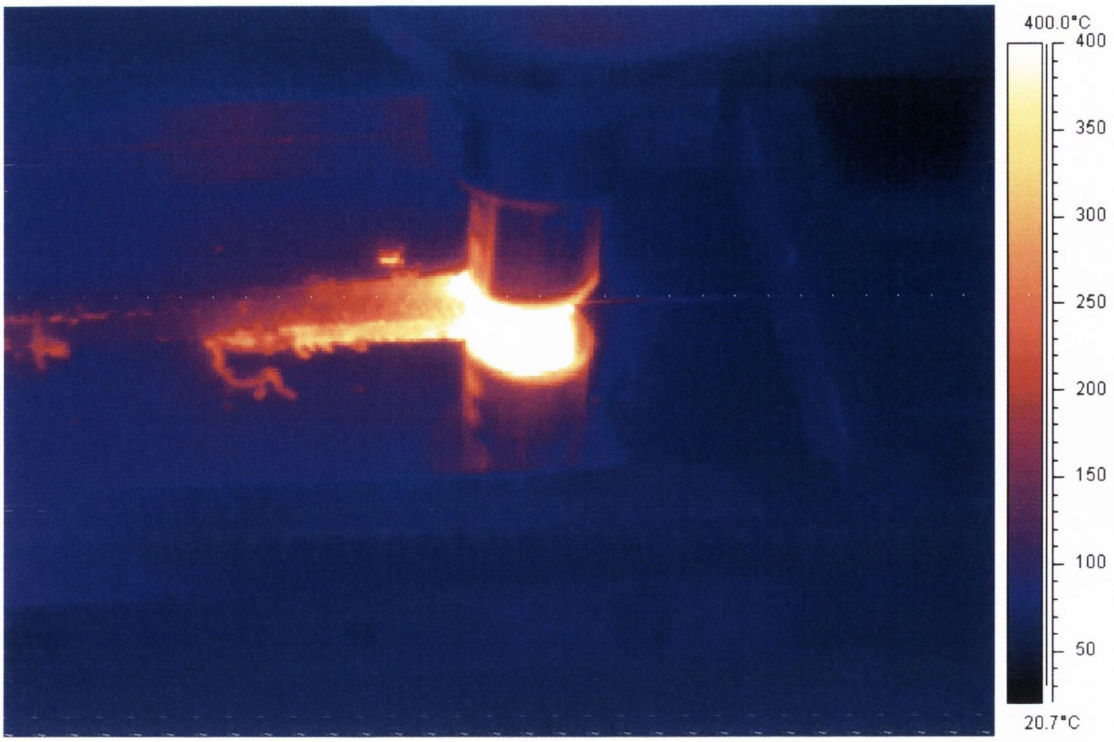


Figure 94: Thermal imaging

### 4.3.5 Numerical Prediction of Temperature at the Joint Line:

A regression analysis was used to predict the temperature distribution close to the joint line. Thermocouple measurements were taken closer to the joint line compared to previous measurements. To achieve this, holes were machined along the thickness of the workpiece plates and the thermocouples were inserted in a horizontal direction rather than a vertical direction as used previously. This enabled temperature measurements closer to the joint line as damage to the thermocouples from the rotating shoulder was avoided. This technique was not used throughout experimental measurements as a lot of preparation was required and weld sample test pieces for tensile, microhardness and microstructural analysis were not possible. The thermocouple layout can be seen in Figure 95 and a sample of results can be seen in Figure 96. As expected, temperatures increase with increasing distances towards the weld line with thermocouple T3 recording the highest temperature of 346 °C.

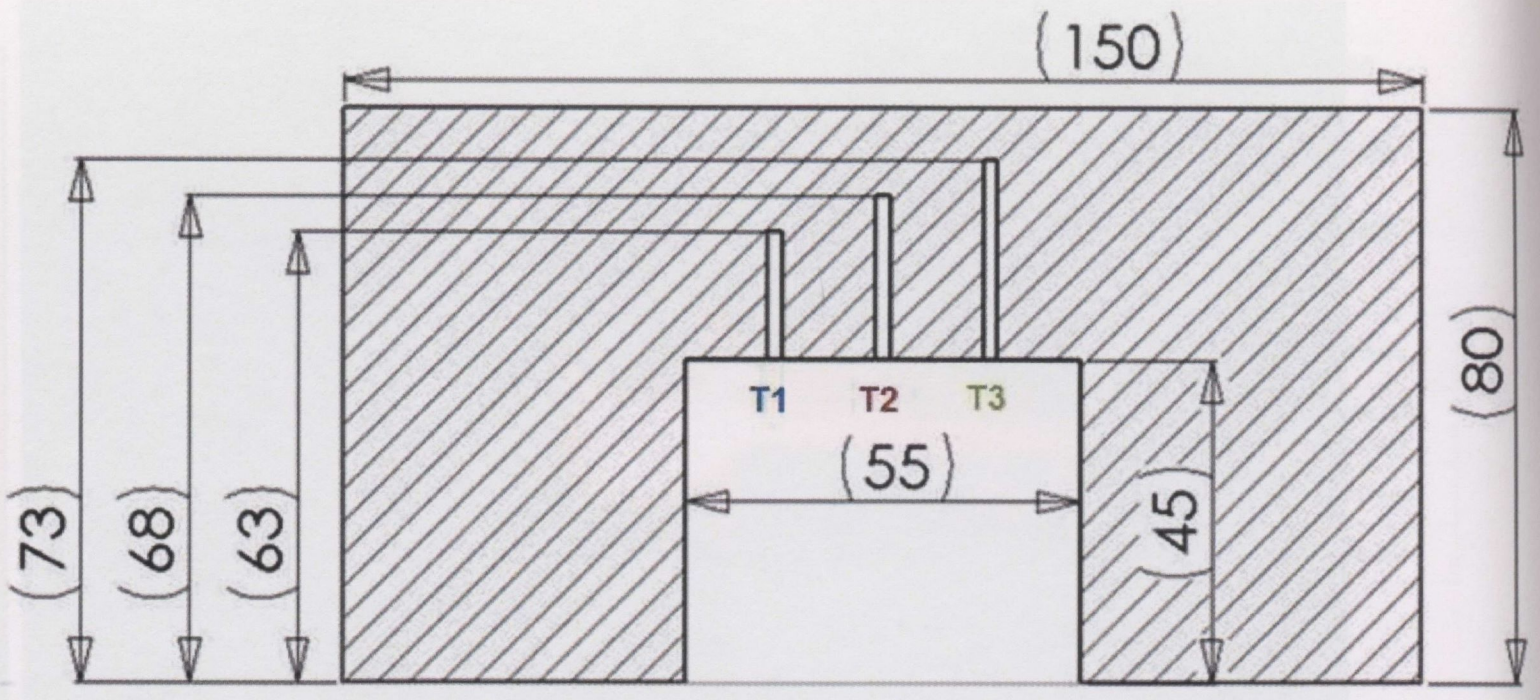


Figure 95: Thermocouple position, layout and labelling 3

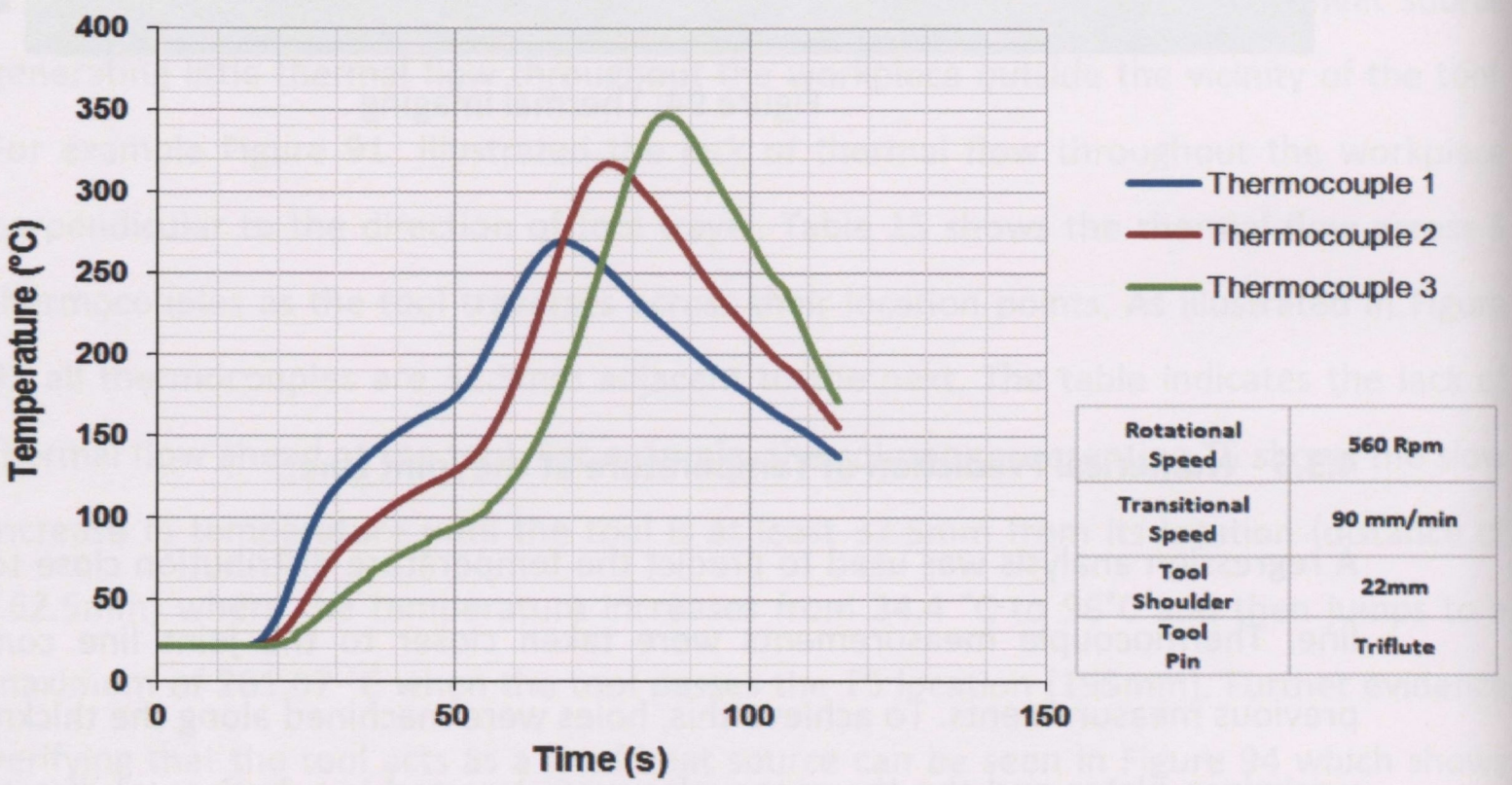


Figure 96: Temperature measurement close to the joint line

One linear and two second-order models were used to describe the temperature distribution in the width direction close to the joint line and these are shown in Equations 1. T is the temperature at a point with a distance d from the joint line and the parameters $a_1$-$a_7$ are determined by the least square method [100]. The square error E used in the least squares method is shown in Equation 2, where $\Delta T_i$ is the difference between the regression values and the experimental data. Three temperature values from the thermocouples in the width direction were used, hence i=3.

$$T = a_1 + a_2 d \quad (1)$$

$$T = a_3 + a_4 d^2 \quad (2)$$

$$T = a_5 + a_6 d + a_7 d^2 \quad (3)$$

Equations 1: Thermal flow equations

$$E = \sqrt{\sum_{i=1}^{3} (\Delta T_i)^2 / 4}$$

Equation 2: Square error using least squares method

The experimental data, regression values and the square errors of the temperatures for each of the three model equations are shown in Table 16. The regression curves for temperature distributions in the width direction are shown in Figure 97. For the three models, the second order model with three terms produced the lowest square error (E=0.37 °C) and predicted a temperature of 355.648 °C at the joint line. However, all three models predicted maximum temperatures at the joint line to be significantly lower than the solidus temperature of aluminium 2024-T3 which is approximately 502 - 638 °C [73]. M. Hwang et al [64] performed a similar regression analysis to predicted the temperature on the joint line during the FSW of 3.1mm thick aluminium 6061-T6 plates. These authors used similar equations and reported a joint line temperature of approximately 380°C. However, this increase in temperature can be attributed to the higher rotation speed (80 rpm) and the lower translational speed (60 mm/min) used by these authors.

| Measured Temperature | | $T_1$ | $T_2$ | $T_3$ | Square error (E) | Predicted Joint Line Temp |
|---|---|---|---|---|---|---|
| | | 269.1 | 317.47 | 346.63 | °C | °C |
| $T = 404.19 - 7.76d$ | Regression Value | 272.27 | 311.07 | 349.87 | 3.921 | 404.19 |
| | Error ($\Delta t_i$) | -3.17 | 6.4 | -3.24 | | |
| $T = 363.13 - 0.324d^2$ | Regression Value | 269.494 | 316.474 | 347.254 | 0.620 | 363.13 |
| | Error ($\Delta t_i$) | -0.394 | 0.996 | -0.624 | | |
| $T = 355.648 + 1.386d - 0.381d^2$ | Regression Value | 269.101 | 317.416 | 346.681 | 0.037 | 355.648 |
| | Error ($\Delta t_i$) | -0.001 | 0.054 | -0.051 | | |

Table 16: Regression analysis for temperature at the joint line with different models

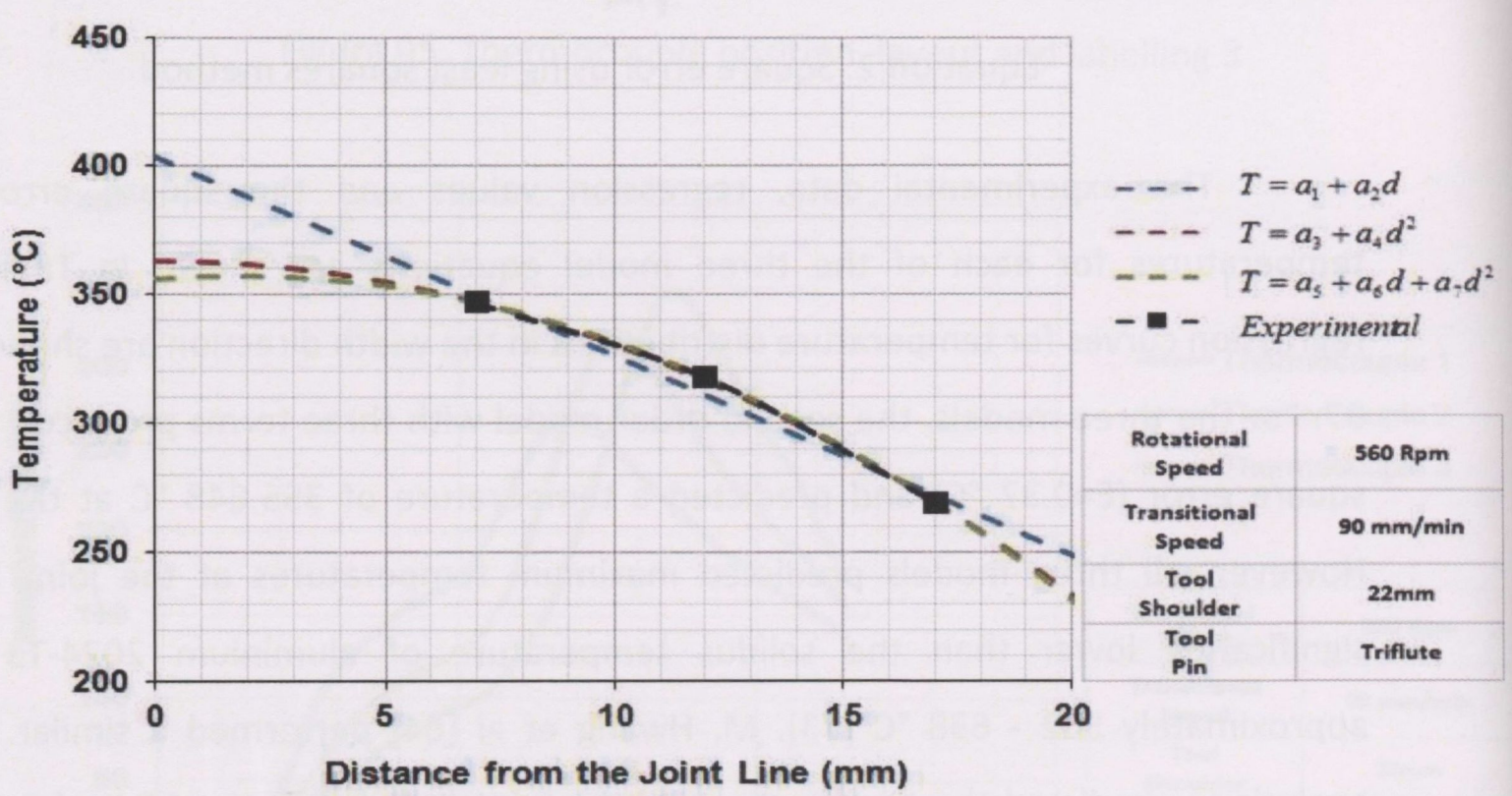


Figure 97: Regression curves for temperature distributions in the width direction

## 4.4 Forces Occurring in FSW :

The different forces occurring during friction stir welding are illustrated in Figure 98. The FSW machine must be powerful enough to deliver and support these forces, whereas the tooling and clamping arrangement must be robust enough to withstand the forces. The magnitude of the force depends on a number of factors:

- Workpiece material and thickness
- Operational Parameters
- Tooling material, shape and geometry
- Joint configuration and application

One of main disadvantages associated with FSW is the large forces generated as the process is purely mechanical. These large forces require expensive machinery that are capable of delivering and supporting these forces. A better understanding and characterisation of forces occurring during the FSW process can help:

- Reduce machine complexity, size, stiffness and power requirements
- Promote improved tooling designs
- Reduce tool wear and the risk of tool fracture
- Reduce operational cost and improve productivity

This project focused on the three main forces acting on the tool and machine during the FSW process:

1) $F_Z$ Vertical force (Z – direction)
2) $F_x$ Welding force (X - direction parallel to tool travel)
3) $M_Z$ Rotational Torque

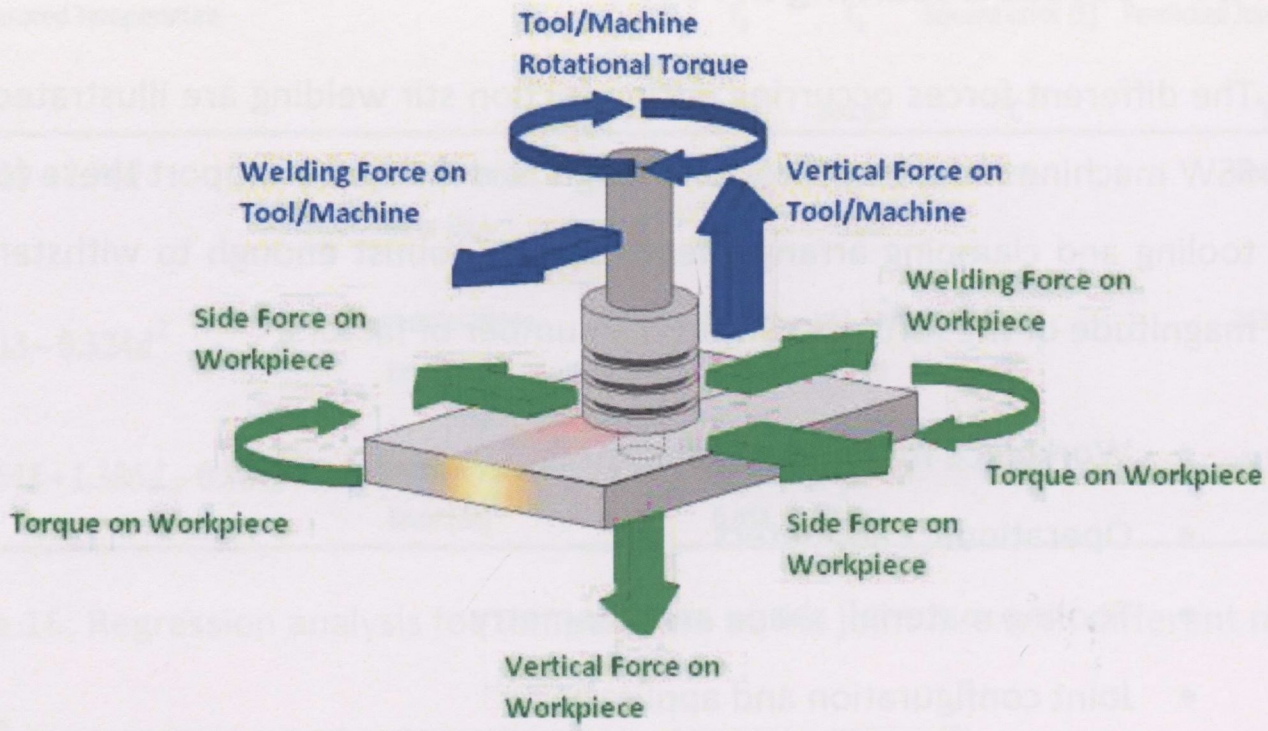


Figure 98: Forces occurring during FSW

To date only a limited number of papers have been published which indicate measurement of the forces generated during the actual FSW process as distinct from modelling. M. Melendez and W. Tang [88] used strain gages embedded into the workpiece to monitor both the vertical force and the welding force. They examined the effects of plunge depth, rotational speed and translational speed. Yu Yang et al [89] developed an algorithm to detect a gap occurring between the workpiece plates during the FSW of AA2024. These authors used a load cell to monitor the vertical force generated. A number of other authors [68, 69, 70, 71] also recorded the vertical force generated during the plunge stage when investigating *Friction Stir Spot Welding (FSSP). None of the authors referred above examined the forces over the range of operational parameters examined during in project. Also, these authors performed the FSW process using traditional FSW tooling which consisted of a concave tool shoulder (requires a tilt angle) and a screw threaded pin design. This project focused on more recent tooling developments such as a scrolled tool shoulder (no tool tilt angle required) and an Mx Triflute tool pin design.

*FSSP: A novel variant of the "linear" friction stir welding FSW process, FSSW creates a spot, lap-weld without melting. It involves only the plunge and dwell stages of FSW

### 4.4.1 Vertical Force (z-direction):

The vertical force was found to be the largest force generated during the FSW process and is therefore one of the main limiting factors in machine design because the machine must have adequate strength, power, stiffness and size to support the magnitude of this force. The existence of this vertical force also requires a backing bar or plate to be placed behind the workpiece to support the reaction force. Furthermore, this vertical force is one of the main causes of tool wear on the bottom surface of the tool pin and tool shoulder.

Figure 99 illustrates a typical measurement of the vertical force recorded during this project. Initial contact of the pin with the top surface of the workpiece causes the vertical force to rise. Its magnitude increases rapidly until it reaches an initial peak of 20.6 kN after approximately 16s. At this point the pin has penetrated into the workpiece to a depth of approximately 3.1mm but shoulder contact has not yet occurred. At this depth, the pin is capable of causing sufficient material deformation by means of a stirring/screwing effect provided by the three flute pin design. This effect also induces frictional heating and hence an increase in temperature is generated. The outcome is softening of the workpiece material which significantly reduces the yield strength of the workpiece and hence the vertical resistance acting against the tool is reduced. The vertical load continues to drop until it reaches 16 kN after 19s. At this point the tool pin has penetrated the workpiece to a depth of 4.1mm and the shoulder has now come into contact with the top surface of the workpiece. Due to the extra pressure transmitted by shoulder contact, the vertical force begins to rise again until the tool pin penetrates the workpiece to the target depth of 4.6mm. When the targeted plunge depth is achieved the vertical force reaches a maximum of 21.8 kN and the process then enters the dwell stage. During this stage the tool is held in a fixed vertical and longitudinal position whilst still rotating for approximately 8s. Because the tool is held in a fixed vertical position, one might expect the vertical force to reach a steady state. However, because the tool is not traversing longitudinally, increased heat generation occurs due to friction between the tool shoulder and the workpiece and hence the vertical force drops slightly during dwell stage due to material softening. Subsequent to the dwell stage the tool beings to traverse parallel along the joint line. The vertical force quickly reduces to a steady state value of approximately 14-15 kN until tool extraction. This steady state vertical force correlates

well with the steady state temperatures recorded during the project (see section 4.3.4 for further details). S. Mandal et [68] also reported two vertical force peaks during the plunge stage when researching the FSW of AA2024 plates 12.5mm thick. Yu Yang [89] reported similar steady state vertical forces during the FSW of AA2024 plates 3.175mm thick.

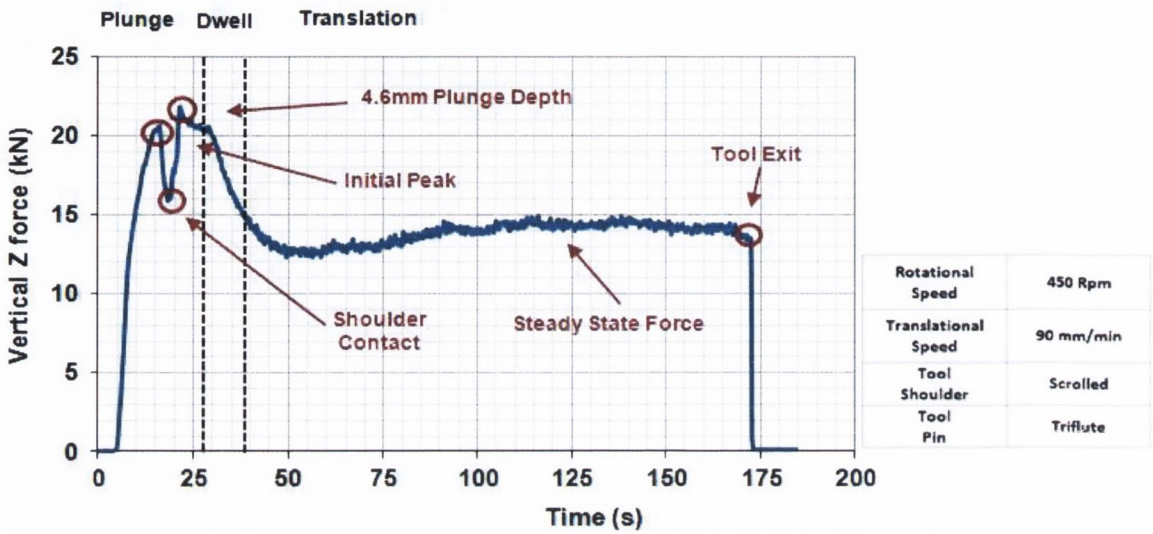


Figure 99: Typical vertical force measurement

#### 4.4.1.1 Maximum Plunge Force:

As illustrated in Figure 99, the vertical force reaches a maximum during the plunge stage as the tool penetrates into the workpiece surface. The controlling operational parameters during the plunge stage are the rotational speed and the plunge rate.

**Rotational Speed**

The effect of varying the rotational speed on the maximum vertical force is illustrated in Figure 100. It is clearly evident that the vertical load acting on the tool and machine decreases with increasing rotational speeds. When the tool is rotating at a higher speed, increased workpiece softening occurs due to a combinational of material deformation and friction heating. Similar results were recorded by S. Lathabai et al [69] who measured vertical forces during friction spot joining of an extruded Al-Mg-Si alloy. A reduction in vertical loading with increasing rotational speed was presented by these authors.

According to Figure 100, increasing the rotational speed from 280 Rpm to 900 Rpm reduces the required maximum force for tool penetration by 23% (6 kN). However, it must be stated that these particular test were performed at a plunge rate of 16mm/min.

It was found that the rotational speed had a dependant relationship with the plunge rate. Larger increases in the maximum vertical force were found as the plunge rate was decreased. This was expected, as a slower plunge rate permits more time for the rotational effect and consequently more time for thermal softening. The opposite argument was also found to be true; the rotational effect became less significant as the plunge rate was increased.

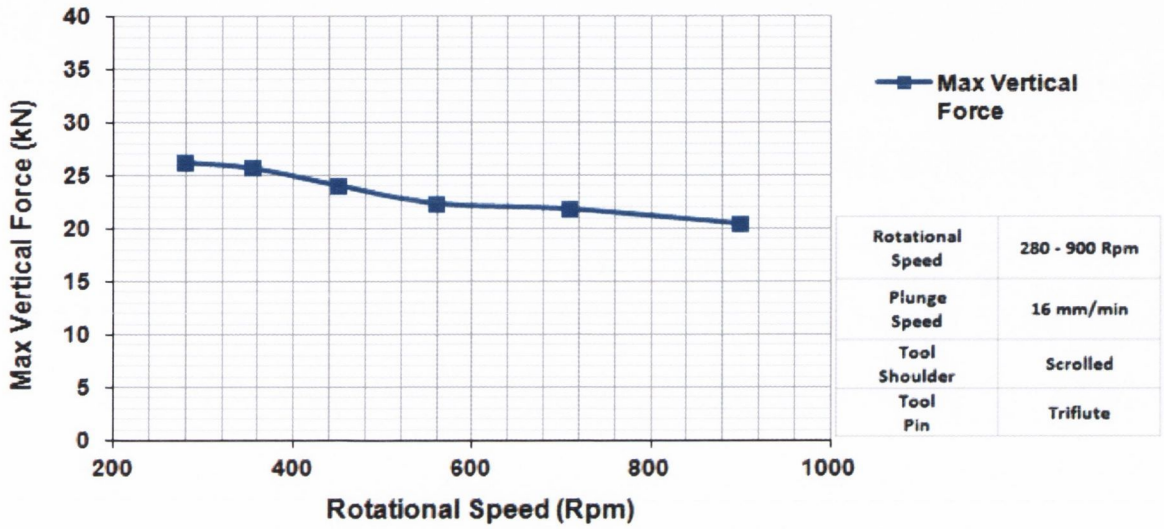


Figure 100: Effect of rotational speed on maximum vertical force

**Plunge Rate**

Further tests were carried out at different plunge rates to examine the effect this had on the maximum vertical force. During these tests, the rotational speed was fixed and only the plunge and dwell stages were performed as the maximum vertical force occurs during these stages. The results are shown in Figure 101. As mentioned previously, reducing the plunge rate permits more time for the rotational action to take place. Therefore, as expected, a reduction in both the initial peak and maximum vertical force was recorded with decreasing plunge rates. S. Lathabai [69] reported a similar increase in the maximum vertical force when the plunge rate was increased from 2mm/s to 7.5mm/s.

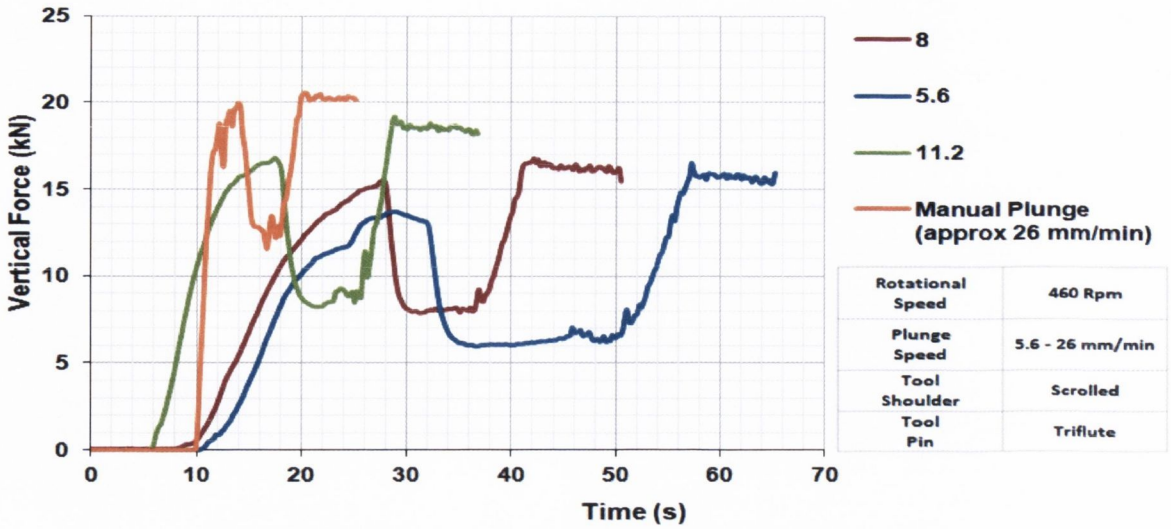


Figure 101: Effect of plunge rate on maximum vertical force

### Tooling Design and Geometry

The effect of varying the tool pin geometry on the maximum vertical force is illustrated in Figure 102. To ensure the comparability of each different pin design, the effective dynamic area of each pin when rotating was kept constant at 38.48mm$^2$.

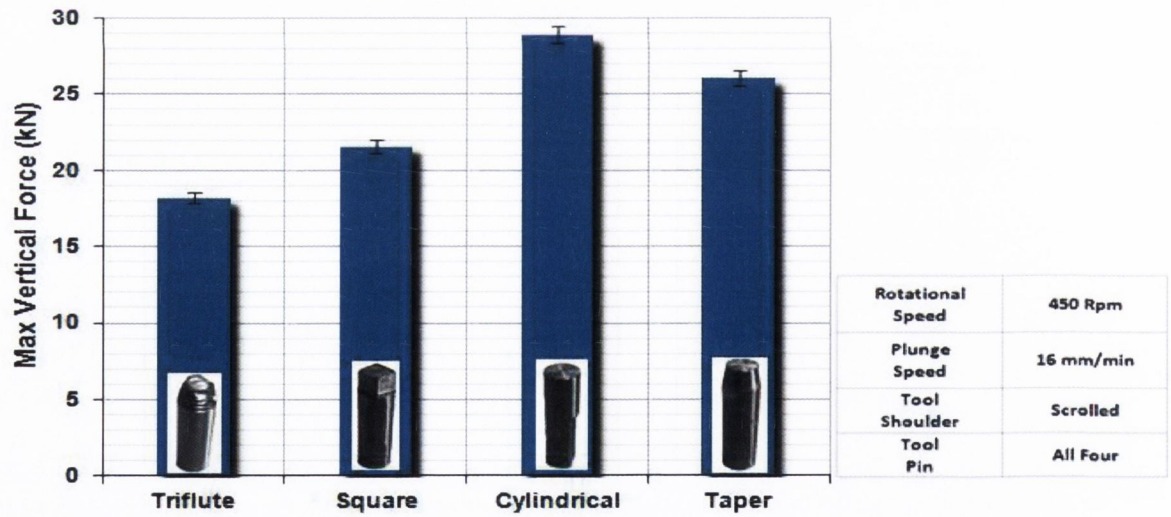


Figure 102: Effect of tool pin geometry on maximum vertical force

The Cylindrical and Tapered Cylindrical tool pins required somewhat greater forces than the Square and Triflute tool to fully penetrate the workpiece. This was seen for various operational parameters. The difference in maximum vertical force between the cylindrical (largest) and the triflute pin (lowest) was approximately 10 kN which equates to a 36% reduction. This can be attributed to the smooth pin surface area of

these tools which will produce less mixing and plastic softening of the workpiece material, thereby resulting in a higher load requirement. Although only a 10 deg taper was used on the Tapered tool pin, this resulted in a significant reduction in the maximum vertical force compared to the cylindrical pin. Due to the shape of the cylindrical pin, it can only compress the workpiece material directly beneath the pin. The workpiece material must then flow at a 90° angle around the edge of tool pin as it penetrates the workpiece. A schematic of the material flow is illustrated in Figure 103. However, if a taper is applied, this provides a smoother transition for the material to flow around the tool pin and provides more lateral flow and hence a reduction in the maximum vertical force was recorded.

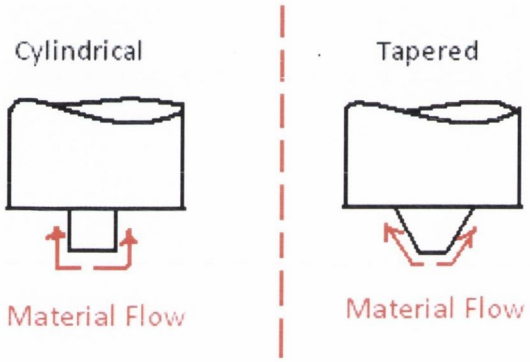


Figure 103: Material flow during the plunge stage for cylindrical and tapered pins

The low maximum vertical force recorded for the square pin can be attributed to its flat faces and corners. The corners of the pin have an effect of sweeping the material laterally rather than just simply displacing the space the pin occupies thereby reducing the maximum vertical force acting on the tool and machine.

The lowest maximum vertical force was recorded when the triflute pin was used. This can be attributed to the flutes and helical ridge features (Figure 104) machined onto the Triflute pin which produce a screwing action as it is plunged into the workpiece. Rotation of the tool works to screw the tool inwards thereby reducing the load. The uneven surface area of the pin will also cause a stirring effect, increasing the amount of material deformation and hence softening of the workpiece material. Also, the flutes and helical ridge features reduce the overall volume of the triflute pin, therefore the pin has less area to occupy when penetrating the workpiece which also contributed to the reduction in max vertical force.

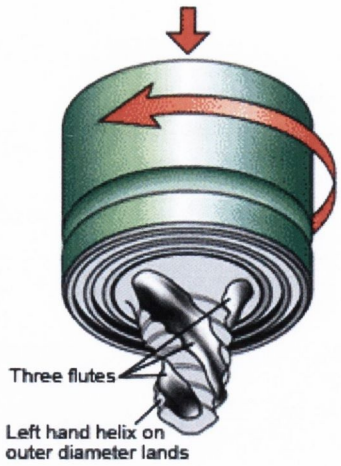


Figure 104: Flutes and helical ridge features machined onto the triflute pin [36]

Variation of the shoulder design (concave and scrolled) did not have a significant effect of the vertical force. However, significant increases in the vertical force (both maximum and steady state) were found when the plunge depth was increased and also when a larger shoulder diameter of 22mm was used compared to an 18mm shoulder diameter. This was expected because once the tool pin is completely immersed into the workpiece, the large vertical forces generated can be attributed to shoulder contact with the workpiece. Therefore, a larger shoulder diameter will required more force to plunge into the workpiece and increasing the plunge depth will increase the stresses/loads acting on the tool. Figure 105 shows the increase in the overall vertical force when the plunge depth is increased from 0.5mm to 1mm. Therefore, as mentioned previously, ensuring an optimal plunge depth (0.5mm in this project) not only minimises the occurrence of flash but also a reduction in the vertical force.

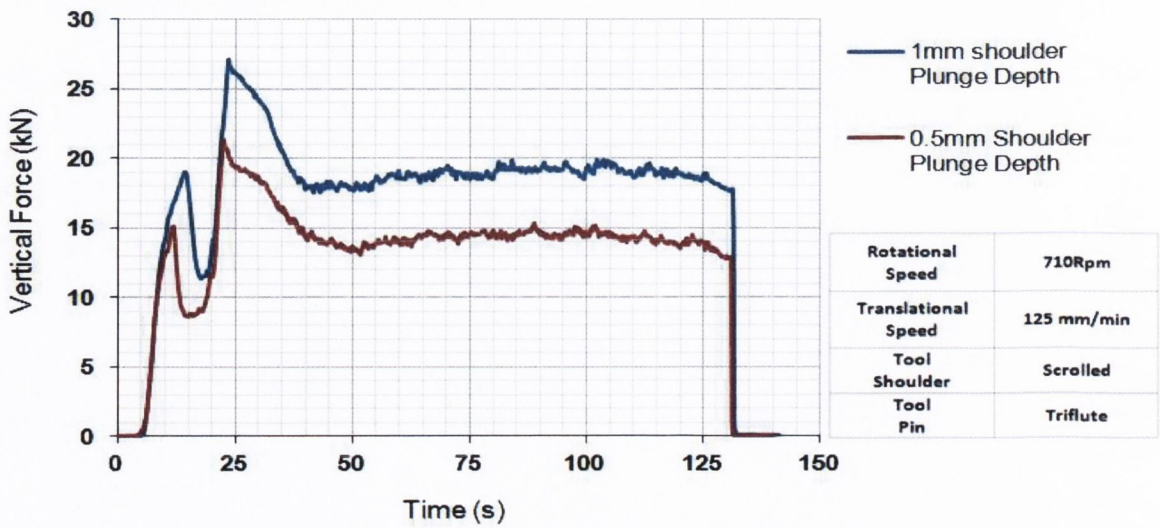


Figure 105: Effect of the plunge depth on the vertical force

#### 4.4.1.2 Steady State Vertical Force:

As illustrated in Figure 99 the vertical force reaches a steady state during the translational stage of the FSW process as the tool traverses along the joint line of the two abutted workpiece plates. The controlling operational parameters during this stage are the rotational speed and translational speed.

**Rotational Speed**

Although varying the rotational speed has a significant effect on the magnitude of the required maximum vertical force, this was not the case when considering the steady state vertical force. This is illustrated in Figure 106 for two different rotational speeds (280 rpm and 900 rpm) at a fixed translational speed (180 mm/min). A large difference in the maximum vertical force is recorded for the two different rotational speeds; however the steady state vertical forces recorded are equivalent. During the plunge and dwell stages the tool is held in a fixed horizontal position (x-direction). Therefore the rotary action of the tool which produces frictional heat and softens the workpiece material acts on one particular location of the workpiece (point of tool insertion) and hence has a greater effect on the vertical force during the plunge and dwell stages of the process. However, during the translational stage the tool is moving along the joint line and hence the heating and soften effect of the workpiece is reduced as the tool is not held in a fixed position. Hence variation of the rotational speed has less of an impact on the steady state vertical force, which occurs during the translational stage. Furthermore, small increases in temperature where recorded with increasing rotational speed as shown in section 4.3.1.2. Therefore one would expect the steady state vertical force to decrease with increasing rotational speed due to softening of the workpiece material. However, this additional heat generation was not sufficient to soften the workpiece material and provide a reduction of the steady state vertical force. This was attributed to the relative small shoulder diameter (18mm) used. Even when the translational speed was decreased to 63 mm/min to increase the number of revolutions per millimetre, variation in the rotational speed did not have a significant effect on the steady state vertical force. This was the case for all parameters within the testing matrix.

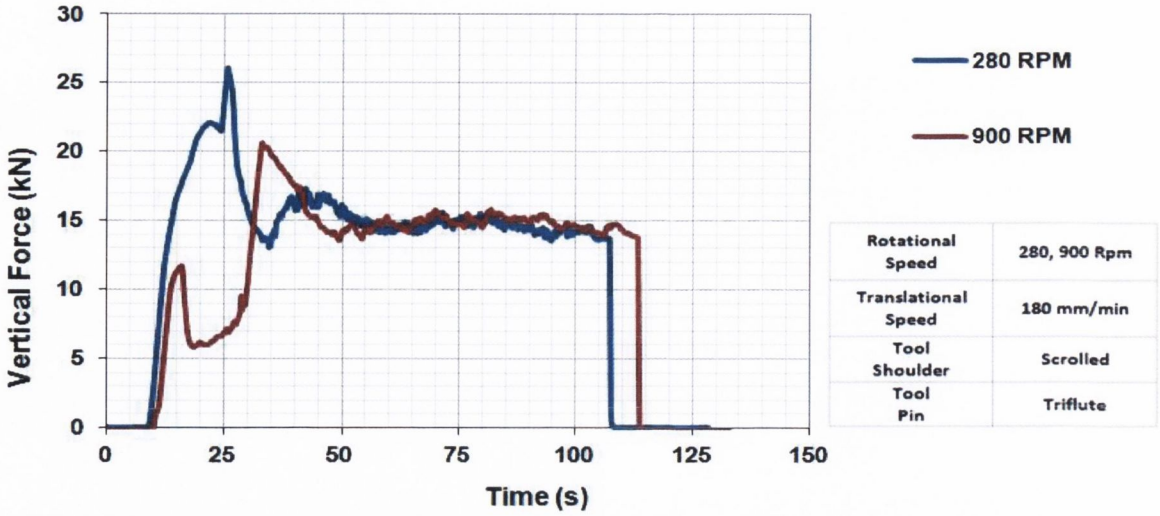


Figure 106: Effect of rotational speed on the steady state vertical force

**Translational Speed**

Changes to the translational speed had the most significant effect on the steady state vertical force. An example of this effect is shown in Figure 107. It is evident that the steady state vertical force decreases with decreasing translational speeds. For example reducing the translational speed from 355 mm/min to 63 mm/min results in a 5.5 kN reduction of the steady state vertical force which equates to a 31% reduction. The reduction in the vertical force with decreasing translational speeds can be attributed to enhance softening of the workpiece material when welding with a slower translational speed. As shown previously in section 4.3.1.1, significantly higher temperatures were recorded at slower translation speed compared to faster translational speeds. As the translational speed is increased, insufficient workpiece softening occurs and hence the tool exhibits greater vertical resistance as it traverses through the workpiece. This is illustrated in Figure 108 which shows the reduction in workpiece softening with increasing translational speed. This softening, or lack of softening, has implications for all forces acting on the tooling/machine and also on the weld strength as will be discussed later.

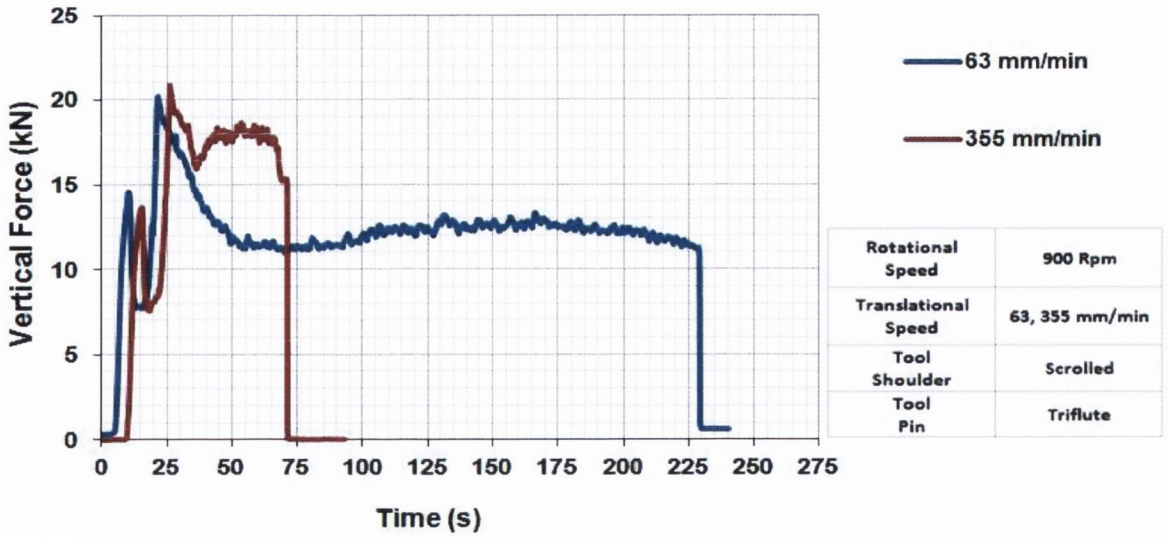


Figure 107: Effect of Translational speed on the steady state vertical force

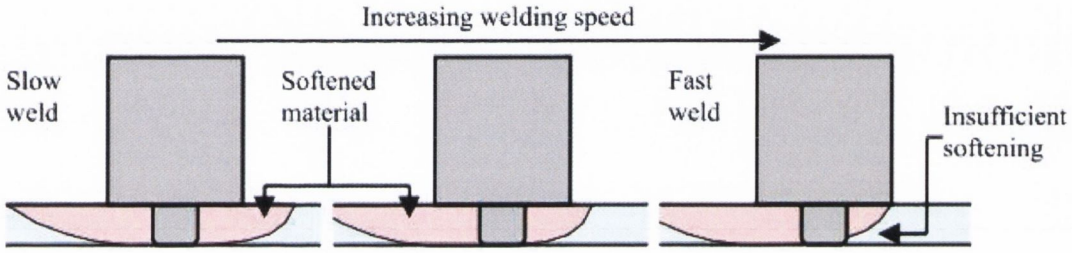


Figure 108: Softening of the workpiece material during FSW at increasing translational speed

Figure 109 shows the average steady state vertical force over 7 different translational speeds and clearly shows the large increase in the steady state vertical force as the translation speed is progressive increased from 63 mm/min to 500 mm/min. However, as the translational speed is increased beyond 355 mm/min, the rate of change of the steady state vertical force begins to decrease and stabilise to a common value of approximately 18 kN. Similar to the rotational speed, it was found that variation of the pin geometry did not have a significant effect on the steady state vertical force. Melendez and Tang [88] also report an increase in the steady state vertical force with an increase in translational speed during the FSW of AA2195. At a fixed rotational speed of 800 Rpm these authors reports a vertical force of 12.455 kN at a translational speed of 60 mm/min and a vertical force of 15.7 kN at a translational speed of 300 mm/min (increase of 3.25 kN).

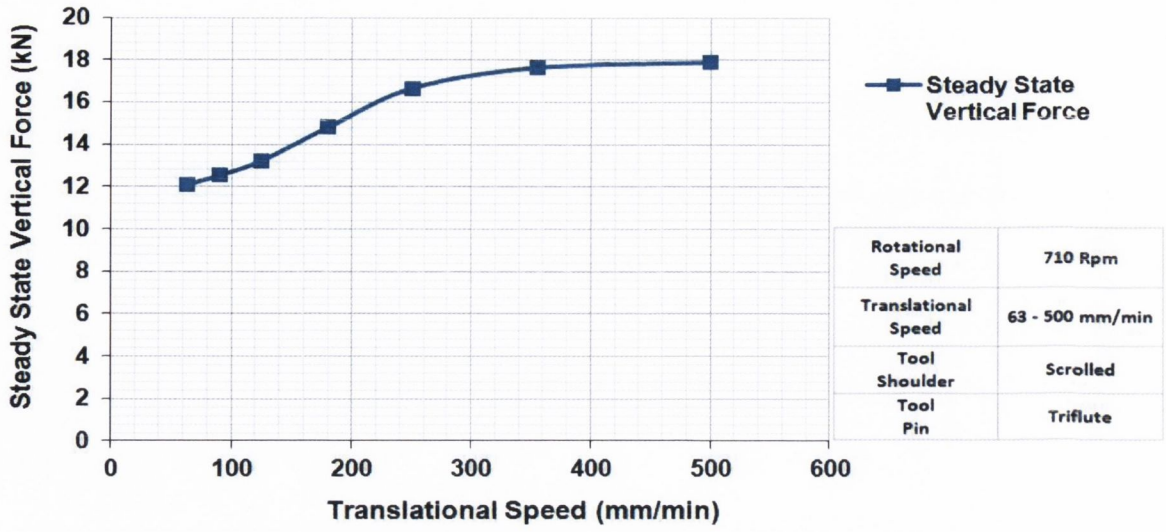


Figure 109: Steady state vertical force for a range of different translational speeds

### 4.4.2 The Welding Force:

The welding force is the force that the FSW machine must supply to drive the tool along the joint line. Both the tool pin and the clamping arrangement must be capable of withstanding this force. The welding force is the main cause of tool fracture and can therefore limit the translational speed, and hence production efficiency of the process. For industrial applications, it is desirable to maximise the translational speed to increase productivity. However this must not compromise weld strength or increase the risk of tool fracture.

Figure 110 illustrates an example of the welding forces recorded during FSW testing. The dynamometer measures the forces throughout each 360° revolution and therefore the output from the rotating component dynamometer is with respect to a rotating X – Y frame. Hence only maximum and minimum values of the welding force indicate the resistance acting against the tool as it traverses along the weld line. During the plunge and weld stages, only slight fluctuations of the welding force are recorded as the tool pin penetrates the workpiece. As expected, only when the tool begins to traverse along the joint line does the welding force start to increase significantly. In general, the welding force reaches a maximum value just as the translational stage is initiated and then reduces slightly to an almost steady state throughout the remaining tool translation. The average maximum welding force for the example shown in Figure 110 is approximately 1.22 kN. The magnitude of this force seems relatively low when compared to the vertical forces recorded under the same conditions, maximum vertical force = 21.8

kN and steady state vertical force = 13.83 kN. The welding force represents a mere 5.6 % and 8.9 % of these forces respectively. Therefore, the welding force should not have an influence on machine limitations considering its magnitude compared to the vertical force. However, the welding force may have an influence on tool wear and fracture, weld defects and weld strength.

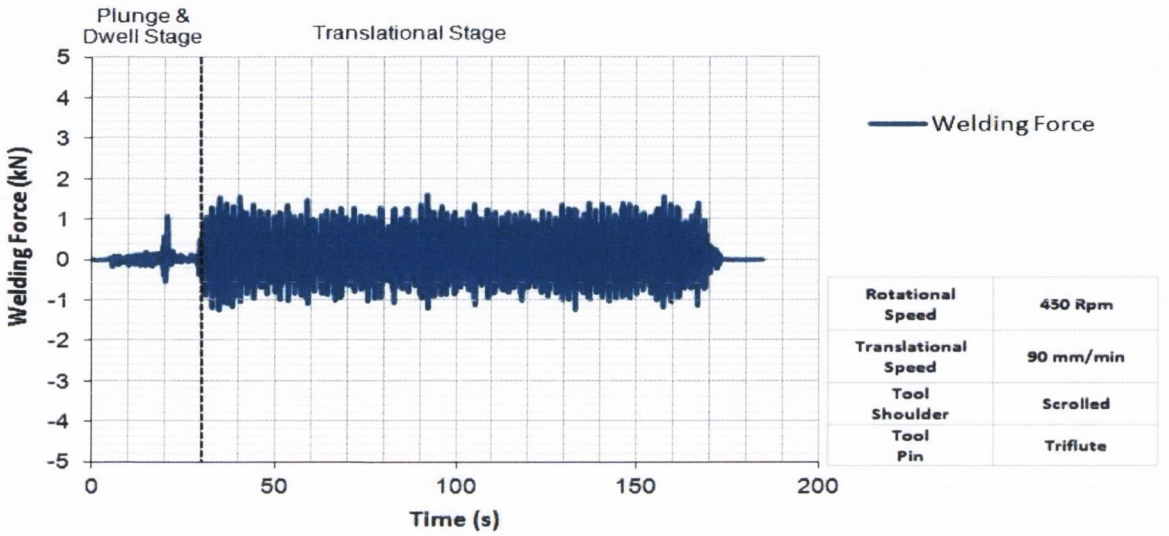


Figure 110: Typical Welding Force Measurement

#### 4.4.2.1 Effect of operating parameters:

Similar to the steady state vertical force, the rotational speed did not have a significant effect on the welding force for the range of rotational speeds tested during this project.

The effect of varying the translational speed on the welding force is shown in and Figure 111. Similar to the steady state vertical force, the welding force was found to decrease with decreasing translational speeds. Again, this can be attributed to an increase in the softening of the working material at lower translational speeds (see Figure 108) which will reduce the resistance acting on the tool as it traverses along the joint line. For example, decreasing the translational speed from 500 mm/min to 63 mm/min can reduce the welding force acting on the tool by approximately 4.1 kN (73%). Also, higher translational speeds results in fewer revolutions of the tool per mm travelled and hence the workpiece material is more likely to be squeezed around the pin in an extrusion like process rather than being rotated around the pin, again contributing to a larger welding

force. Similar results of increased welding forces with increasing translational speeds were reported by Melendez [88].

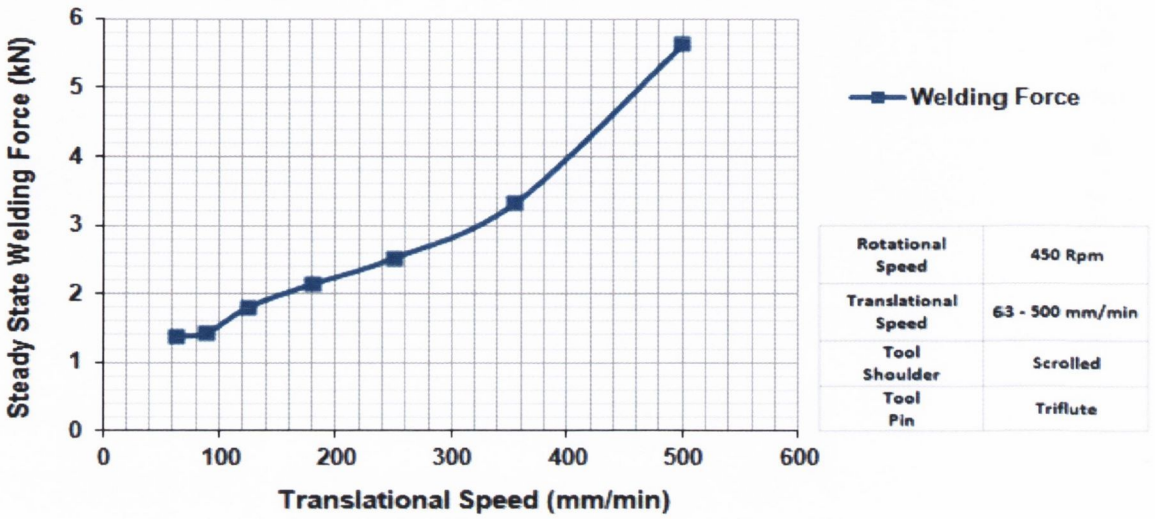


Figure 111: Average welding force for various translational speeds

As mentioned previously, large welding forces are the main cause of tool pin fracture. This can limit the translational speed and hence production efficiency of the process. Figure 112 shows a tool where the pin was intentionally fractured by not applying heat treatment to the pin and also FSW a brass workpiece. The pin became immersed in the workpiece material during this test. The welding force creates a moment load acting on the pin about the interface between the pin and the shoulder. If the pin cannot withstand this moment, fracture occurs about this interface. A tapered pin design with a thicker base can provide more strength to help withstand this moment and prevent fracture. A number of factors can increase the risk of tool fracture:

- High translational speeds
- Weak/soft tool pin material
- Large workpiece thickness
- Workpiece material of higher density
- Excessive heat generation

Figure 112: Tool pin fracture

During testing of all parameters and tooling designs throughout this project no pin fracture occurred, even at a maximum translational speed of 500mm/min. This can be attributed to the low density and relatively small thickness (4.82mm) of the AA2024-T3 workpiece and the high strength at elevated temperature of the material used to manufacture the tool pin (heat treated H13 tool steel). Therefore the limiting factor associated with increasing the translational speed and hence productivity of the FSW process was not pin failure due to large welding forces. The limiting factor was found to be the formability of the workpiece material as surface voids developed at higher translational speeds; this is discussed further in section 4.5.1.

#### 4.4.2.2 Effect of Tool design and Geometry:

**Pin Design**

The effect of different pin geometries on the welding force is shown in Figure 113. It is clearly evident that tool pin shape has a significant effect on the magnitude of the welding force. The largest welding force was recorded when the cylindrical pin (3.97 kN) was used, whereas the lowest welding force was recorded using the square pin design (2.28 kN), this represents a 42% reduction. This difference can be explained by examining how each pin deforms/displaces the workpiece material ahead as it traverses along the joint line as shown Figure 115.

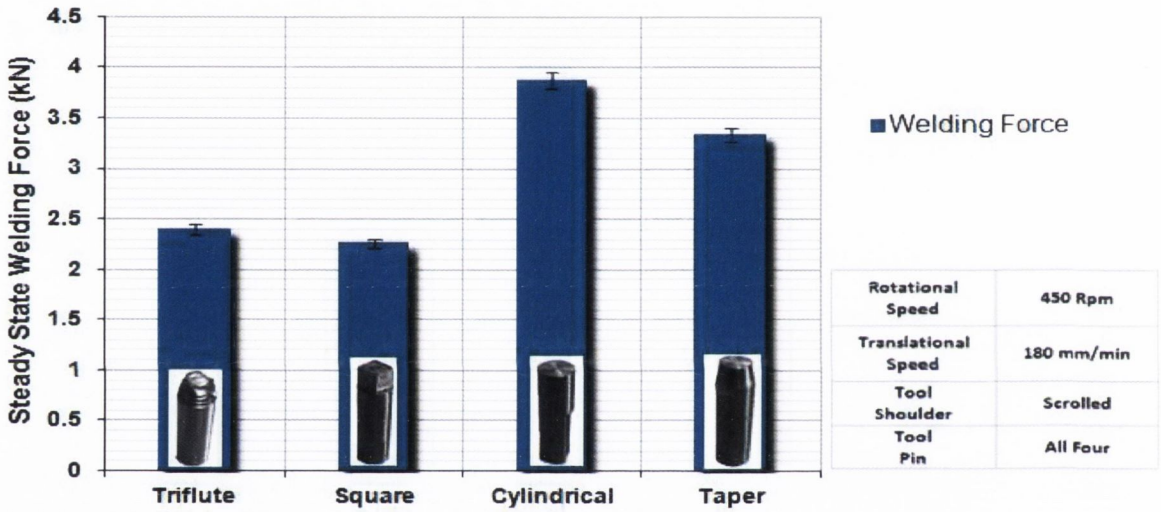


Figure 113: Welding force for different pin geometries

The flat faces on the square pin act like paddles which produce a pulsating stirring action (Figure 114). This softens the workpiece material through plastic deformation thereby reducing the workpiece resistance acting against the pin as it traverses through the workpiece. These paddles producing a churning action and displace the material ahead of the pin. Similar to a blender, the paddles sweep the material along the tool path thereby reducing the resistance acting against the traversing of the tool. The triflute pin has a similar material deformation effect due to its flutes producing an uneven surface. The smooth surface and circular shape of the cylindrical pin produces less material deformation ahead of the tool pin as it traverses. Alternatively, the cylindrical pin simply displaces the area along its paths causing a lot of workpiece material to flow around the sides of the pin similar to an extrusion process. This accounts for the higher welding force

recorded. However, it must be noted that some of the workpiece material will stick to the surface of the cylindrical pin and become engaged in the rotary action thereby producing some material deformation. The cylindrical tapered pin produces a similar effect. The 10° taper incorporated into its design reduces its cross sectional area compared to the basic cylindrical shaped pin and hence less force is required to push through the workpiece material. This accounts for the reduction in the welding force of the tapered pin compared to the cylindrical pin. Therefore although the magnitude of the welding force is relatively small compared to the vertical force, tool pin designs which enable material to be processed more efficiently can be identified by monitoring this force.

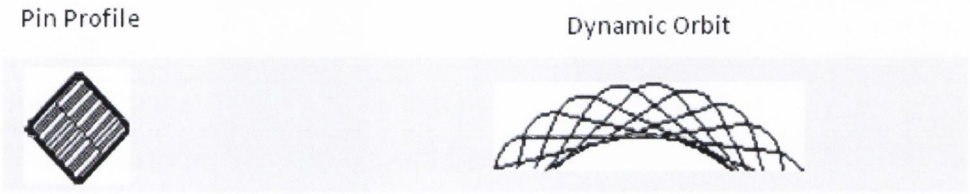


Figure 114: Pulsating action of square tool

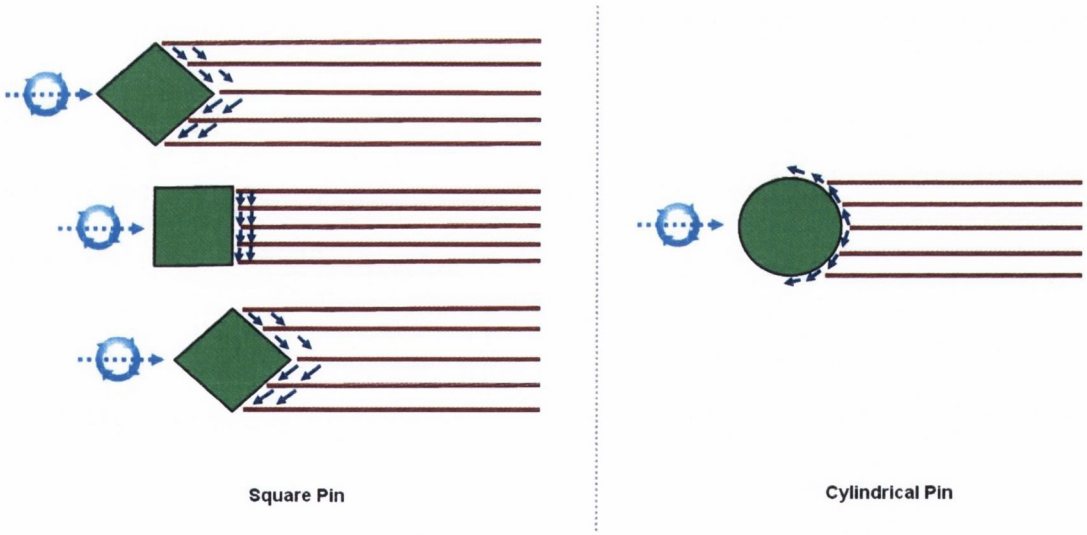


Figure 115: Material processing for different pin geometries

**Shoulder Geometry**

Similar to the vertical force, increasing the plunge depth resulted with an increase in the welding force. Increasing the plunge depth increases the volume of the tool that is immersed into the workpiece and hence the tool will encounter more resistance as it

traverses along the joint line. Figure 116 shows the effect of the plunge depth on the welding force. When the plunge depth is increased from 0.5mm to 1mm, the welding force is increased from 1.75 kN to 2.54 kN. This represents an increase of 0.79 kN or 45%. Also, slightly larger welding forces were recorded when a 22mm diameter shoulder was used compared to an 18mm shoulder due to the increase in surface area contact between the shoulder and the workpiece.

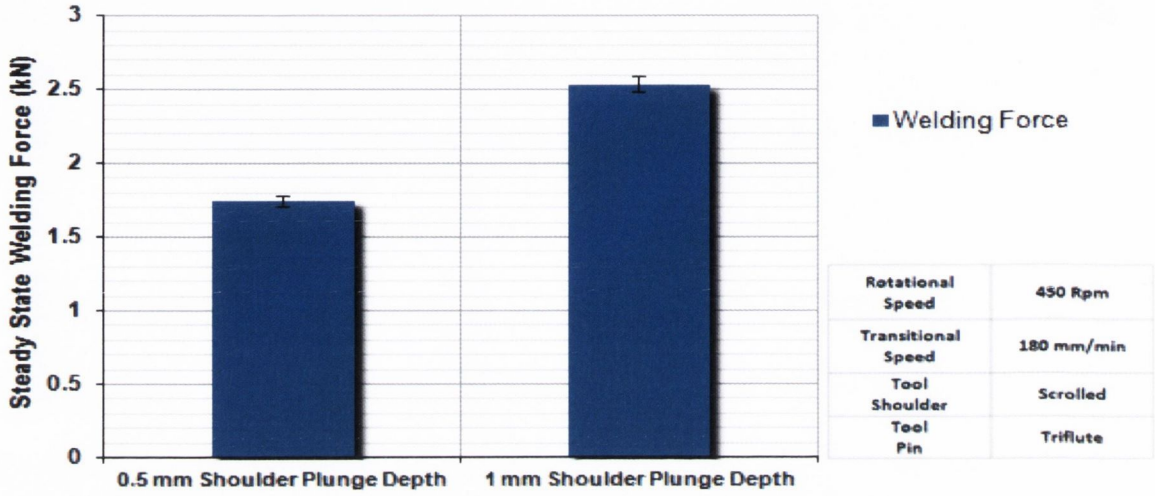


Figure 116: Effect of plunge depth on the welding force

### 4.4.3 Torque:

The torque is a measurement of the resistance encountered by the tool as it rotates through the workpiece during the FSW process. The torque also gives an indication of the power required. Although a wattmeter could be installed into the power supply to measure the machine power, this power input includes loses that occur within the motor and drive train. For this reason, calculating the power from the torque is a more accurate measurement of the actual power input into the weld. The weld power can be calculated using the following equation:

$$Weld\ Power\ (watts) = \frac{2\Pi \times \Omega \times T}{60}$$

Ω - Spindal rotational speed (rpm)

T - Torque (N.m)

Equation 3: Weld power

Figure 117 illustrates a typical torque measurement during the FSW process. The graph of torque against time is similar in shape to that of the vertical force and hence both are shown together. The torque rises gradually when the tool makes contact with the workpiece surface. However, after 16s when the pin has reached a depth of 3.1mm, the torque beings to rise more sharply. This change in torque corresponds to the point where the vertical force reaches its first peak. Unlike the vertical force which begins to decrease until shoulder contact occurs, the torque continues to rise after this point until it reaches a maximum of 58 N.m at shoulder contact. As the tool continues to penetrate the workpiece, more surface area of the tool pin is exposed to rotary resistance from the workpiece which explains the increase in torque. During the dwell stage, the tool is held in a constant vertical and horizontal position while still rotating. Therefore the shoulder generates additional heat due to friction between the workpiece which softens the workpiece material and hence a significant reduction in the torque is recorded during the dwell stage. As the tool beings to traverse along the weld line, the torque reduces to a steady state value of approximately 35 N.m until tool extraction.

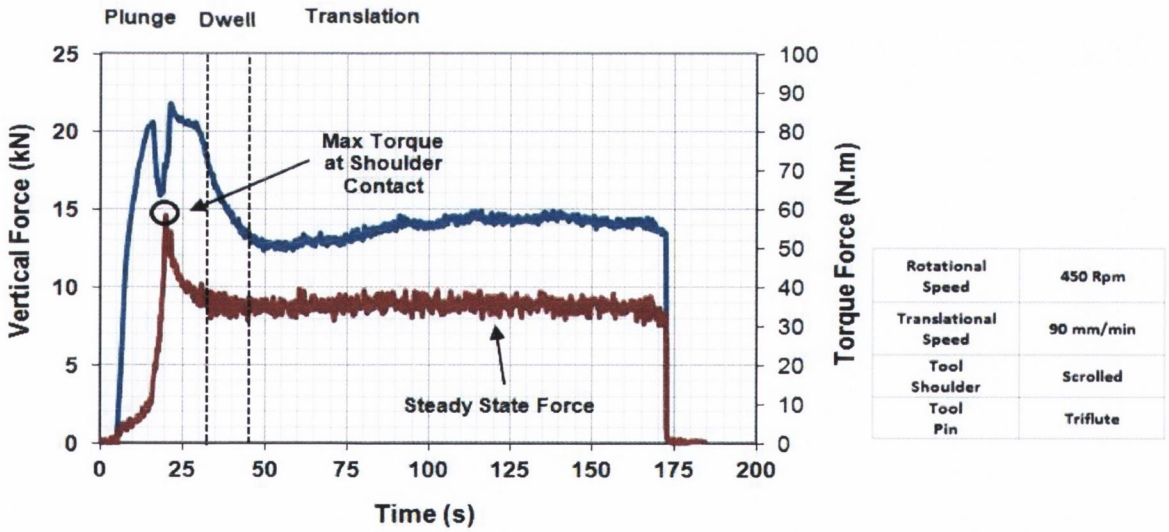


Figure 117: Typical torque measurement

#### 4.4.3.1 Maximum Torque:

Similar to the vertical force the torque reaches it maximum value during the plunge stage when the tool shoulder contacts the workpiece surface. Therefore, the controlling operational parameters associated with the maximum torque are the rotational speed and the plunge rate.

**Rotational Speed**

Changes to the rotational speed were found to have the largest effect on the torque compared to all other operational parameters. This was expected as torque is a rotary force measurement. The maximum torque recorded using various rotational speeds are shown in Figure 118. The maximum torque was found to decrease with increasing rotational speeds. This can be attributed to increased workpiece softening due to a combination of material deformation and friction heating associated with higher rotational speeds. This workpiece softening deceases the resistance encountered by the tool as it rotates within the workpiece material. As the rotational speed is increased beyond 710 rpm, the rate of change of torque with increasing rotational speed begins to decrease and level off to a value of 33 N.m.

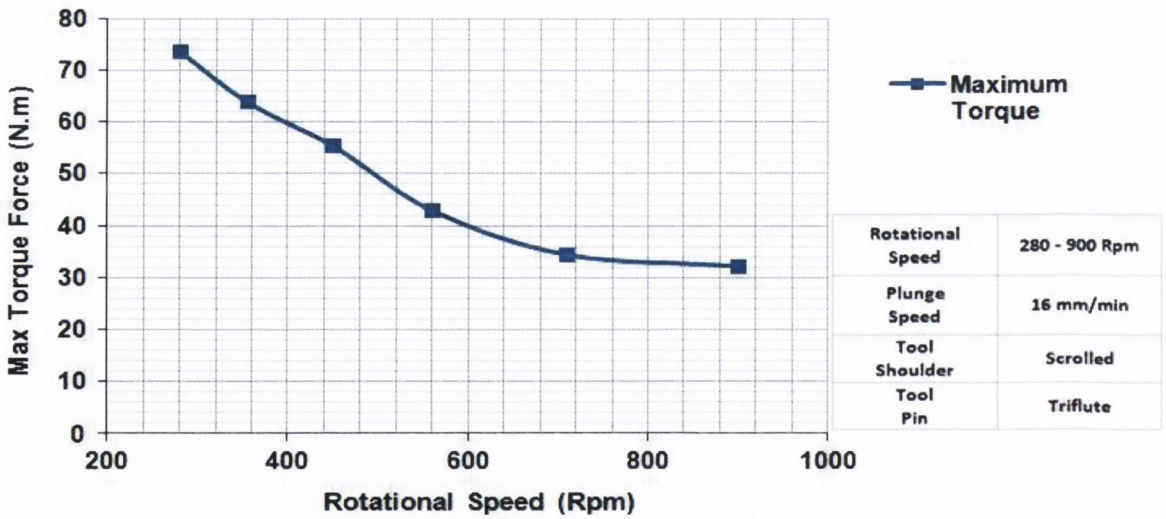


Figure 118: Maximum torque for various rotational speeds

**Plunge Speed**

The maximum torque recorded for various plunge speeds is shown in Figure 119. Again, similar to the vertical force, the maximum torque was found to decrease with decreasing plunge speeds. Reducing the plunge rate permits more time for the rotational action to take place and thereby increasing the amount of workpiece softening. Results also illustrate that the maximum toque begins to level off at plunge rates above 22 mm/min.

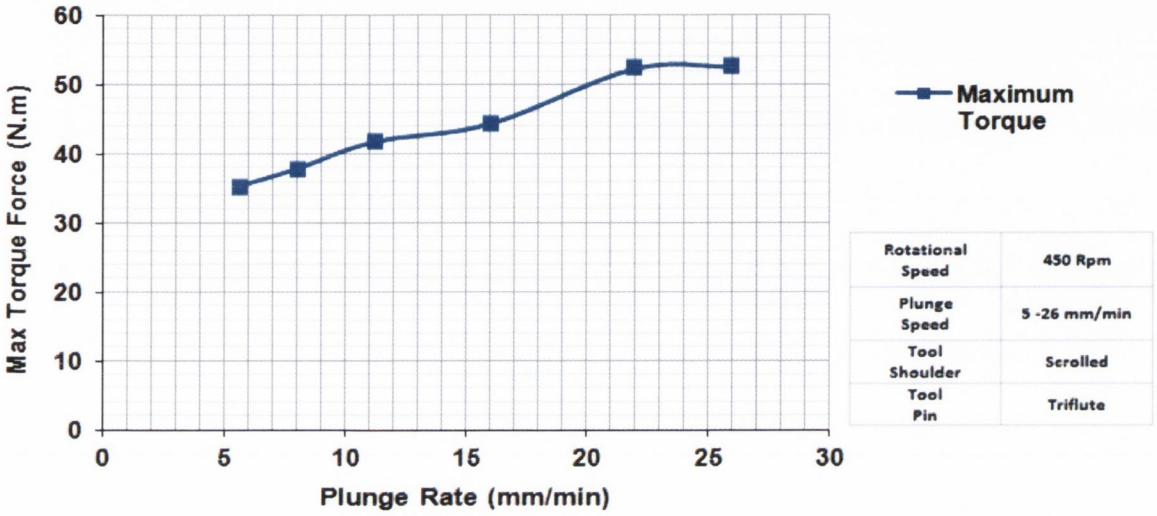


Figure 119: Maximum torque for various plunge speeds

#### 4.4.3.2 Steady State Torque:

As illustrated in Figure 117 the torque decreases to a steady value during the translational stage of the FSW process as the tool traverses along the joint line of the two abutted workpiece plates. The controlling operational parameters during this stage are the rotational speed and translational speed.

**Rotational Speed:**

Similar to the maximum torque, the steady state torque was found to decrease significantly as the rotational speed was increased as shown in Figure 120. Again, this can be attributed to softening of the workpiece at higher rotational speed due to additional material deformation. As the rotational speed is increased beyond 700 Rpm the rate of change to the steady state torque begins to decrease and level off to approximately 21 N.m.

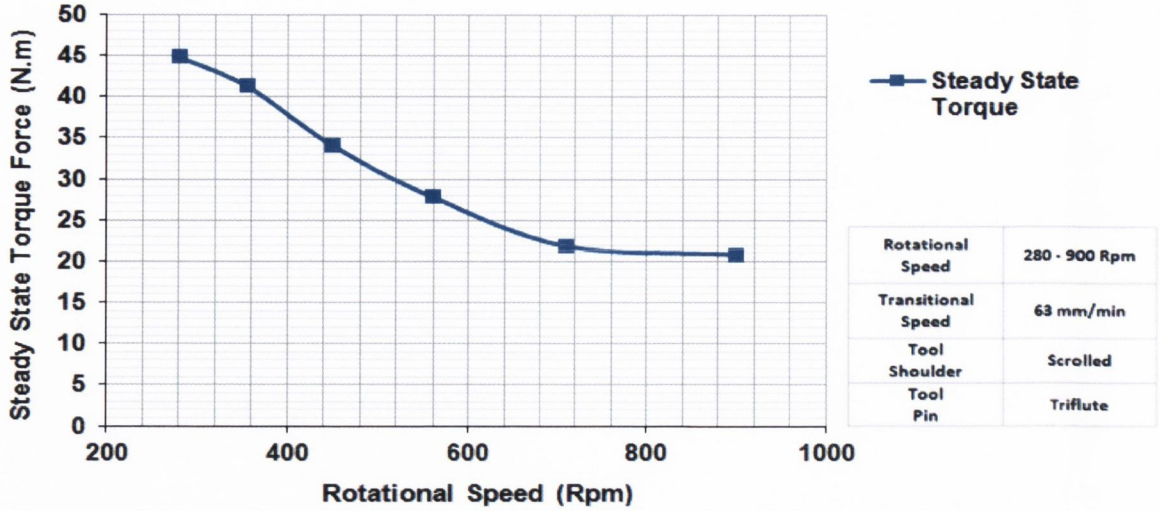


Figure 120: Steady state torque at various rotational speeds

### Translational Speed

The steady state torque for various translational speeds is shown in Figure 121. It is clearly evident that the torque increases slightly with increasing translational speeds. Slower translational speeds permit more time for the rotary action (revolutions per millimetre) to take place which leads to enhanced workpiece softening. As the translational speed is increased, insufficient workpiece softening occurs and hence the tool exhibits greater resistance as it rotates within the workpiece. As the translational speed is increased beyond 250 mm/min, the rate of change of torque is reduced and begins to level off to approximately 45 N.m.

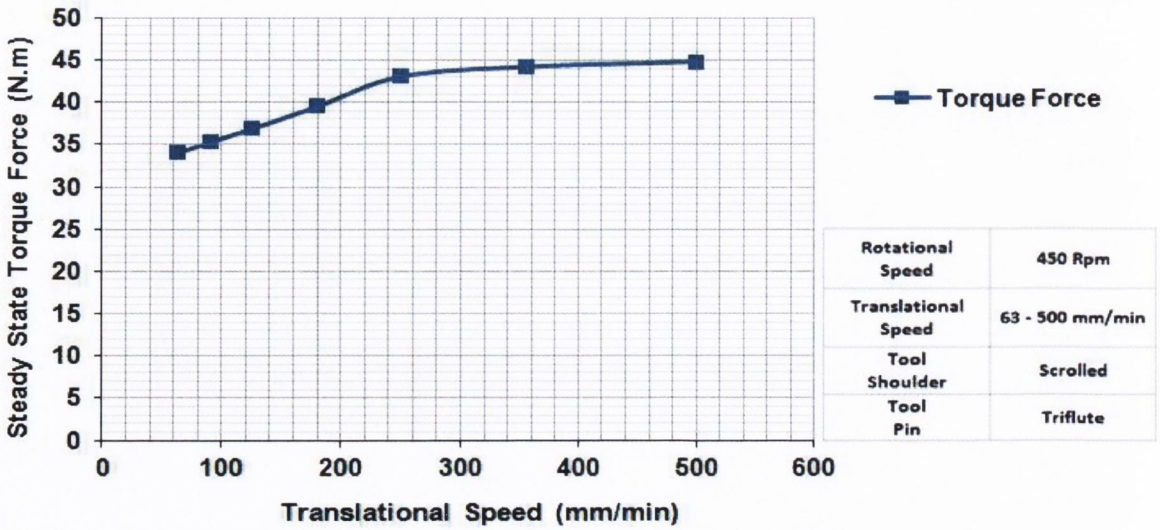


Figure 121: Steady state torque for various translational speeds

**Pin Geometry:**

Variation in the pin geometry was not found to have a significant effect on the toque (both maximum and steady state). This can be attributed to the size of the shoulder compared to the pin. The diameter of the tool shoulder is almost 3 times that of the tool pin, therefore once the shoulder is plunged to the required depth into the workpiece surface, it becomes the driving factor of torque generation.

**Shoulder Design and Geometry:**

Slightly higher torque were recorded using a concave shoulder design compared to using a scrolled shoulder design due the larger surface area contact between the shoulder and workpiece associated with the concave design. Similarly, increasing the plunge depth resulted in slightly larger torques. However, a more significant increase in the torque was seen when the shoulder diameter was increased from 18mm to 22mm which is shown in Figure 122. The steady state torque increases from 39.5 N.m to 47.7 N.m when the shoulder diameter is increased from 18mm to 22mm. Again this can be attributed to the increased surface area contact between the shoulder and the workpiece.

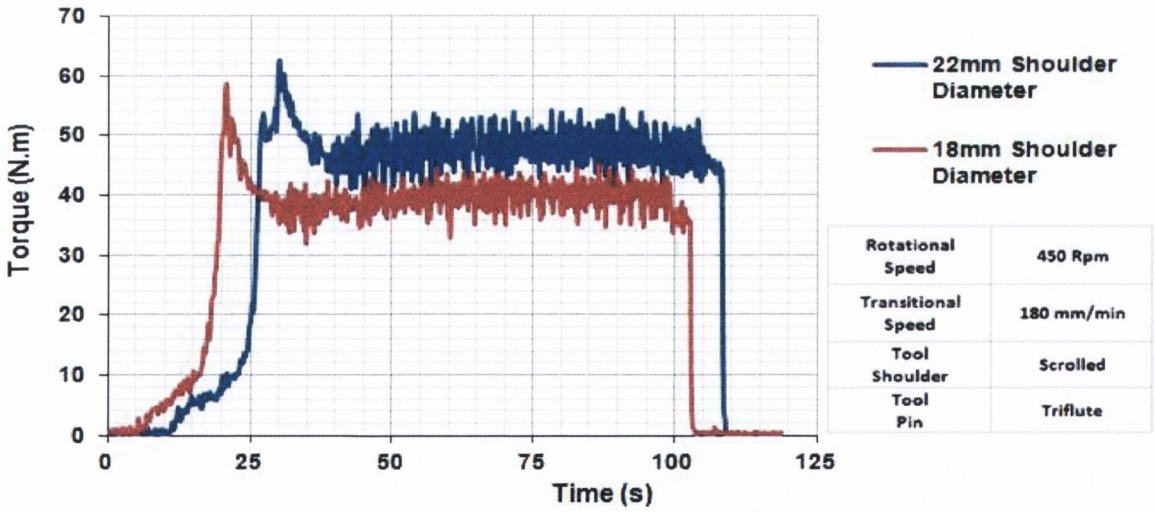


Figure 122: Effect of shoulder diameter on torque

## 4.5 Weld Strength Assessment:

### 4.5.1 Effect of Varying the Operational Parameters:

As mentioned in section 4.1 a test matrix was developed to vary the operational parameters of both rotational speed and translation speed in a systematic manner (see Table 13 pg84). 42 friction stir welds were fabricated using a scrolled shoulder and triflute pin design to establish a processing window for this grade of material in terms of weld strength and elongation. Each weld was sectioned to provide 4 tensile test samples, a sample for microhardness analysis and a sample for macrostructure/microstructure analysis. The sample pieces are illustrated in Figure 123.

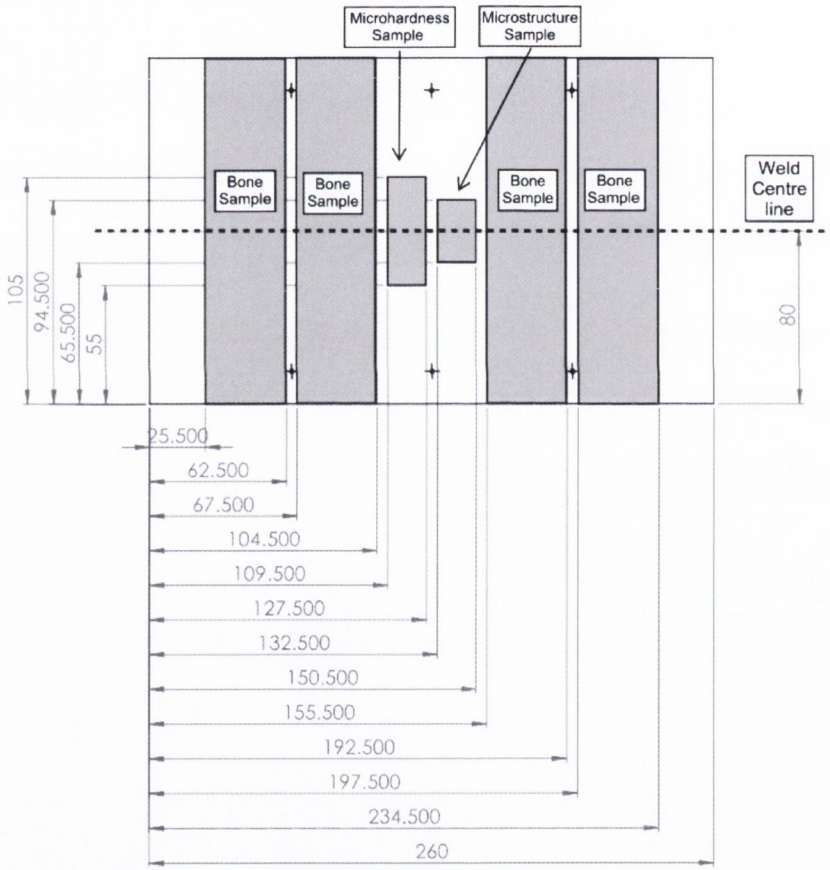

Figure 123: Weld sectioning

To measure the weld strength, tensile tests were conducted to failure on each of the 4 samples. Further information on tensile test procedure and test piece dimensions are given in section 3.6.1. The stress against elongation curve for a typical tensile test on a friction stir welded test piece is shown in Figure 124. It is evident that there is no major significant difference between the maximum stress (ultimate tensile stress) and the stress at fracture. The ultimate tensile stress (Equation 4) recorded is 419.5 MPa and the stress at fracture is 416.9 MPa. For convenience purposes the ultimate tensile stress (UTS) was used to compare the weld strength to the parent material and also when comparing the strength of the different welds.

$$\text{Ultimate Tensile Stress (UTS)} = \frac{\text{Max Stress}}{\text{Original Cross Sectional Area}}$$

Equation 4: Ultimate tensile strength

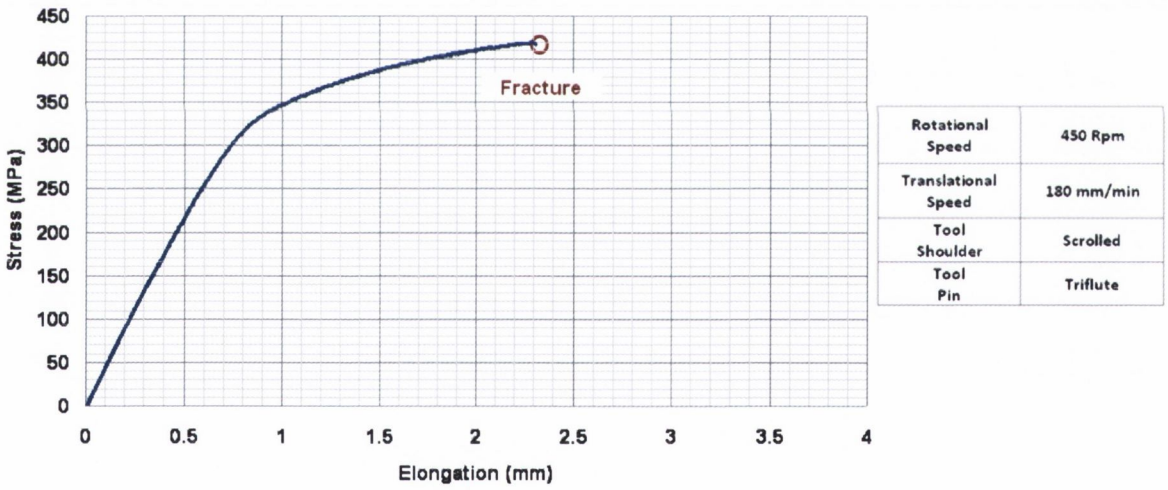


Figure 124: Typical FSW tensile test

The average UTS for the four tensile test specimens were recorded for each weld. Tensile tests were also conducted on un-welded parent material samples. An average UTS 454 MPa and elongation of approximately 15mm was recorded for the parent material. Hence the weld strength efficiency was calculated using the following formula:

$$\text{Weld Strength Efficiency} = \frac{UTS_{weld}}{UTS_{parent\ material}} \times 100$$

Equation 5: Weld strength efficiency

Table 17 displays the weld strength as a percentage of the base material for all 42 friction stir welds. An initial and important observation is that a processing window does exist and that variation of the operational parameters leads to a progressive change in the weld strength rather than random erratic results. For example, weld strength efficiencies above 80% and 90% are highlighted. These results are grouped together rather than randomly placed at different operational parameters. Table 18 shows the elongation at fracture as a percentage of the parent material and is an indication of the ductility of each weld. As expected, welds which displayed good strength also displayed good ductility. However, none of the welds retained similar ductility to that of the parent material which fractured after 15mm elongation. Similar results of low ductility were reported by a number of authors [91, 56, 93, 97]. The most ductile weld only retained approximately 30% of the parent material. This can be attributed to the heterogeneous complex grain structure and hardness distribution produced during the FSW process. Further information can be seen in sections 4.6 and 4.7.

It is also worth noting that the order in which the welds were fabricated was randomized to satisfy the statistical requirement of independence of observations. This acts as an insurance against the effects of lurking time-related variables such as the warm-up of tools and equipment. Welds fabricated at operational parameters labelled N/A did not undergo tensile testing due to the occurrence of severe defects during welding.

**Percentage Strength Efficiency (%)**

| Rotational Speed [RPM] | 63 | 90 | 125 | 180 | 250 | 355 | 500 |
|---|---|---|---|---|---|---|---|
| 900 | 69.39 | 68.25 | 71.59 | 62.24 | 51.09 | 38.78 | 39.46 |
| 700 | 60.54 | 74.97 | 76.98 | 59.39 | 66.90 | 42.43 | 26.90 |
| 560 | 69.92 | 73.59 | 76.93 | 75.04 | 85.80 | 70.70 | 63.23 |
| 450 | 70.71 | 77.22 | 88.23 | 88.78 | 89.68 | 77.16 | 47.28 |
| 355 | 79.45 | 81.36 | 85.83 | 93.61 | 94.06 | 67.68 | N/A |
| 280 | 81.47 | 84.28 | 86.22 | N/A | N/A | N/A | N/A |

Table 17: Strength efficiency results (%)

**Percentage Elongation Efficiency (%)**

| Rotational Speed [RPM] | 63 | 90 | 125 | 180 | 250 | 355 | 500 |
|---|---|---|---|---|---|---|---|
| 900 | 9.52 | 7.63 | 10.82 | 5.30 | 4.37 | 3.03 | 3.11 |
| 700 | 5.74 | 10.13 | 11.90 | 5.29 | 7.17 | 3.37 | 2.80 |
| 560 | 8.28 | 8.44 | 10.30 | 8.04 | 15.75 | 8.58 | 6.41 |
| 450 | 9.18 | 11.09 | 18.40 | 20.59 | 20.94 | 8.88 | 3.67 |
| 355 | 15.86 | 16.16 | 17.08 | 26.39 | 31.07 | 6.21 | N/A |
| 280 | 18.20 | 18.06 | 19.92 | N/A | N/A | N/A | N/A |

Table 18: Elongation efficiency (mm)

It is evident both the translational speed and rotational speed do not have an independent impact on weld strength and ductility. For example, a low rotational speed of 280 rpm works well at low translational speeds from 63 – 125 mm/min as the slow rotary action of the tool has sufficient time to produce a consolidated weld. However, increasing the translation speed beyond 125 mm/min at 280 rpm does not produce a consolidated weld because the low rotational speed does not have sufficient time to process and mix the two workpiece material together to form a consolidated weld and hence a void is form directly behind the tool as it traverses.

It can be seen that optimal weld strength above 85 - 95% of the parent material was recorded at translational speeds between 125 – 250 mm/min in conjunction with rotational speeds between 355 – 560 rpm. These operational parameters should be implemented during FSW of AA2024-T3 to achieve optimal results.

As mentioned in section 4.3.1.3, the method of rev/mm used by some authors [33, 54, 56] to characterise the two operational parameters together when analysing results does not give a true representation. For example, the following two sets of parameters both result in 3.94 revolutions per millimetre but produce two weld of different strength:

1) 355 rpm, 180 mm/min, Joint efficiency = 93.61%
2) 710 rpm, 90 mm/min, Joint Efficiency = 74.97%

**Impact of Translational Speed**

In general, it was found that both the weld strength and elongation increases with increasing translational speed until optimal values are reached at translational speeds between 125 – 250 mm/min. Further increases in the translational speed beyond 250 mm/min results in a large reduction of both weld strength and elongation. Figure 125 illustrates this effect for a fixed rotational speed of 450 rpm. The reduction in weld strength and elongation experienced at lower translational speeds (63 -90 mm/min) can be attributed to thermal damage caused by a high heat input with a slower cooling rate which can cause grain growth, partial reversal of the heat treatment the alloy initially underwent and severe clustering of CuAl precipitates[95, 96]. All of which lead to inferior weld properties. A higher heat input will also increase grain growth and softening within the welded zone which may also explain the reduction in strength. Optimal weld strength was achieved at translational speeds of 125, 180 and 250 mm/min.

Too high a translational speed will not allow sufficient time for the rotary/stirring action of the tool to produce a consolidated weld and hence a reduction in strength and elongation was recorded for all translational speeds above 250 mm/min. For example, surface defects were recorded for all welds fabricated at 500 mm/min and the majority of welds fabricated at 355 mm/min. As expected, surface defects act as a focal point for crack propagation and hence result in lower weld strength and elongation. Figure 126 displays a surface defect which occurred due to a high translational speed of 500 mm/min. Similar results were recorded by G. Biallas et al [72] who preformed tensile tests on 4mm thick AA2024 FSW joints. These authors reported an increase in weld strength with increases in translational speeds between the range of 80 -125 mm/min. Kristensen

et al [56] examined the effects of translational speed on the ultimate tensile strength of friction stir welded aluminium 2024-T3 plates of 6mm thickness and reported a decrease in weld strength with increasing the translational speeds between 270 - 550 mm/min.

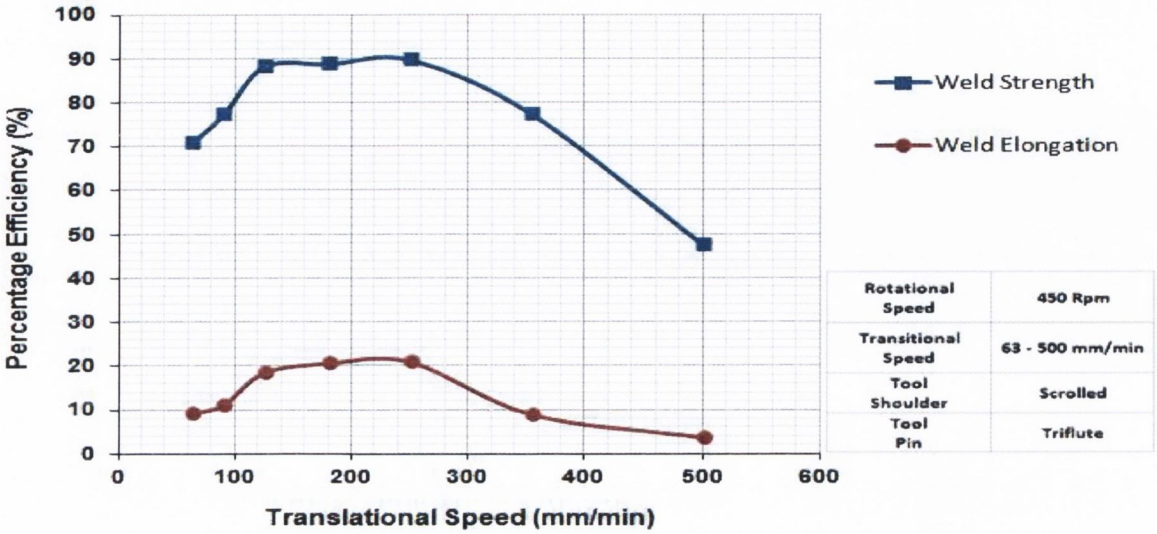


Figure 125: Effect of translational speed on weld strength and elongation

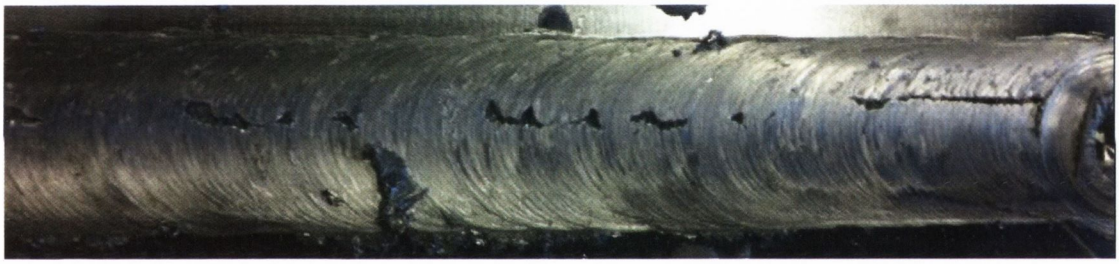

Figure 126: Surface defects due to a high translational speed

Producing good quality friction stir welds at maximum translational speeds is desirable in industrial and manufacturing application of the FSW process to reduce production time and increase process efficiency. However, the welding force which acts against the tool pin as it traverses along the joint line can cause fracture of the tool pin and its magnitude increases significantly with increasing translational speed (section 4.4.2). Nevertheless, pin fracture did not occur during the testing of all operational parameters and tooling designs, even at maximum translational speeds of 500mm/min as seen in section 4.4.2. Therefore the limiting factor associated maximizing translational speed is formability of the workpiece and not pin failure due to large welding forces. Hence the development of new tooling designs which can process and stir the workpiece materials more efficiently may enable higher translational speeds.

**Impact of Rotational Speed**

In general it was found that lower rotational speeds ranging from 280 – 450 rpm produced stronger and more ductile welds compared to those produced at higher rotational speeds ranging from 560 – 900 rpm. Figure 127 shows this effect for a fixed translational speed of 180 mm/min. Optimal weld strength was achieved at rotational speeds between 280 – 450 rpm. The large reduction in strength and elongation for rotational speeds greater than 450 rpm can again be attributed to higher heat input and also excessive material deformation. As shown in section 4.3.1.2, heat generation increases with rotational speed therefore thermal damage caused by a high heat input can lead to inferior weld properties. Higher rotational speeds also caused excessive release of stirred materials to the upper surface, which resulted in voids within the nugget zone and a poor surface finish with irregularities and voids. Both of which act as areas of crack propagation and result in decreased weld strength and elongation. However this could also be attributed to the vibration of the FSW machine with increasing rotational speeds. Therefore further testing would be required on the FSW machine with greater stiffness and stability.

M.A. Sutton et al [49] reported similar results in their investigation of the effect of rotational speed on ultimate tensile strength of Aluminium 2524-T3. Using a fixed translational speed of 2.11 mm/s and varying the rotational speed (100 to 800 rpm), Sutton reported an increase in weld strength with increasing rotational speeds up to a peak of 480 rpm. Further increases in rotational speeds above 480 rpm were accompanied with a decrease in weld strength. Sutton attributed this decrease to overheating (see section 2.2.1 for further details). J. Adamowski et al [75] investigated the effects of varying process parameters when FSW AW6082-T6 aluminium alloy plates. While maintaining a constant translational speed of 115 mm/min, Adamowski found that increasing the rotational speed from 330 to 880 Rpm resulted in a reduction in weld strength of approximately 30 MPa.

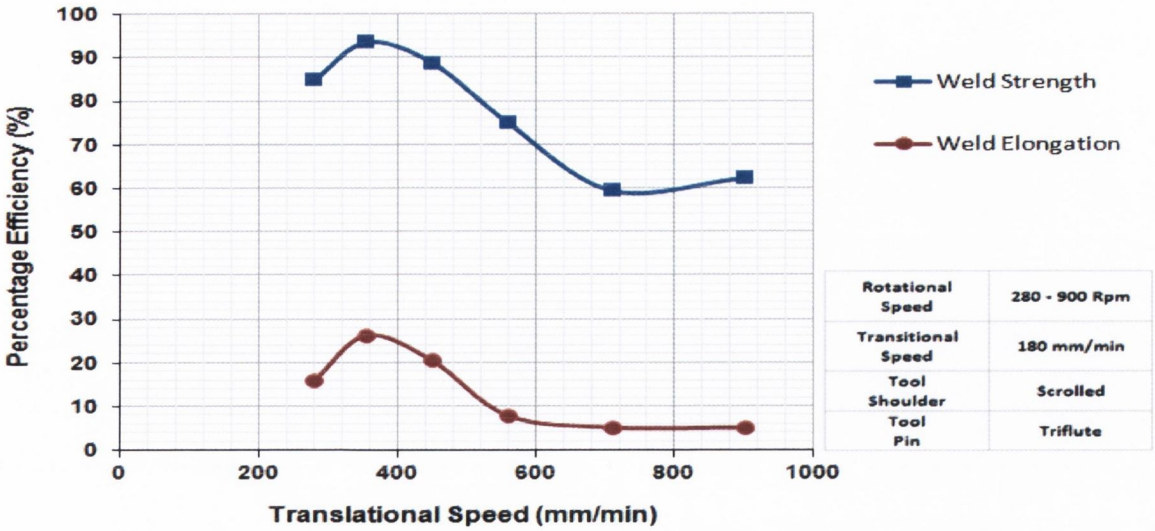


Figure 127: Effect of rotational speed on weld strength and elongation

As mentioned previously, surface defects can occur due to a high translational speeds and inadequate mixing of the workpiece materials as shown in Figure 126. However, this cannot be offset by simply increasing the rotational speed and increasing the number of revolutions per millimetre of tool travel. To examine this, a weld was fabricated at 1400 rpm with a translational speed of 500 mm/min which is shown in Figure 128. Weld strength of 29% of that of the parent material was recorded for this welded joint. This was attributed to the low heat input due to the high translational speed used and excessive deformation due the high rotational speed which produced a coarse and irregular surface finish with the occurrence of internal voids.

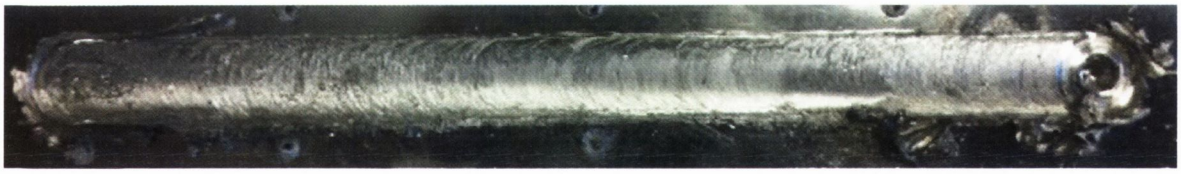

Figure 128: Weld fabricated at 500 mm/min and 1400 Rpm

### 4.5.2 Effect of Different Pin Design:

As mentioned in section 3.3.2, four different pin designs (Triflute, Square, Cylindrical and Tapered) were designed and manufactured to determine their effects on the FSW process. The primary function of the non-consumable rotating tool pin is to stir the plasticized metal and move the material from the front to the back of the pin to close the gap left behind in the tool wake to produce a consolidated joint. Pin geometry plays a crucial role in material flow which can determine the mechanical properties of the welded joint. Figure 129 illustrates the effect of different pin designs on weld strength and elongation as a percentage of the parent material.

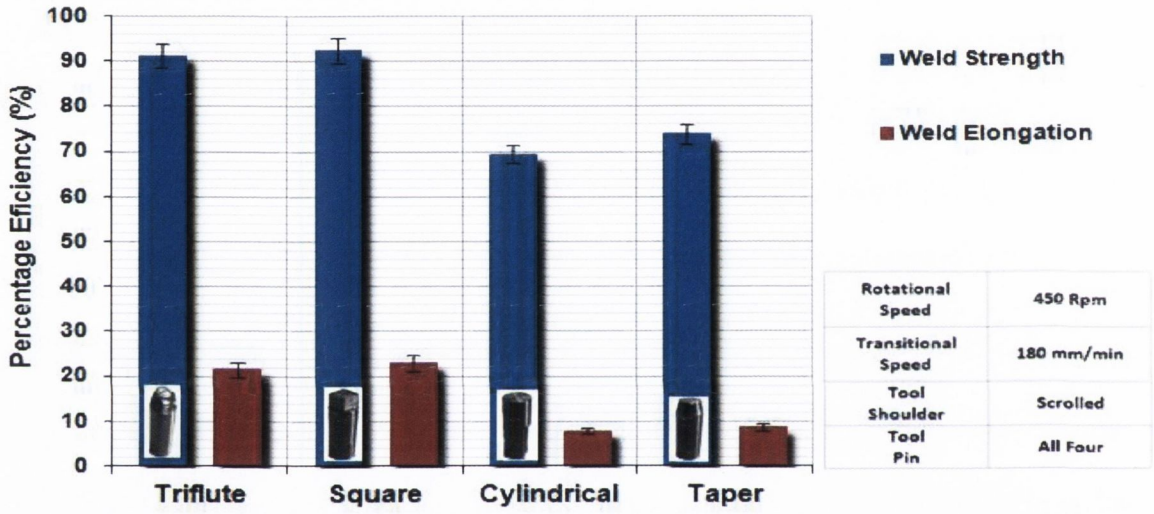


Figure 129: Weld strength and elongation efficiency for different pin designs

It is clearly evident that the four pin geometries can be separated into two different categories. The triflute and square pins, which are associated with increased material deformation capabilities, produced greater weld strength and elongation (91%, 20.6% and 92%, 22.1% respectively). Whereas the cylindrical and tapered pins, due to their smooth pin designs, produced lower weld strength and elongation (70%, 6.9 and 73%, 8% respectively). Note Similar results were also seen for different operational parameters.

Pin profiles with flat faces like the square pin are associated with eccentricity. This eccentricity allows compressible material to pass smoothly around the pin profile. Also, the flat faces and corners of the pin produce a pulsating stirring action, as illustrated in Figure 114 pg119. Both of which create a smoother flow and mixing of the workpiece

material to produce a strong consolidated weld. The flutes and helical ridge features machined onto the triflute tool result in the pin having an uneven surface area which causes an increased stirring effect that will increase material deformation and allow a smoother integration of the workpiece material from each plate to produce a strong weld. Both the Square and Triflute pins produce more turbulence due to their shape which increases material mixing.

The Cylindrical and Tapered pins do not have any flutes or flat faces to produce any enhanced stirring effect. Although some of the workpiece material will stick to the surface of the pin and become immersed in the rotary/stirring action, a lot of the plasticized material will simply extrude on the sides of the pin. Consequently tools having a smooth pin surface area will produce less mixing of the workpiece material, thereby resulting in a weaker weld.

Another observation that can be made is the fact that a simple square shape can produce equal, and in some case better, weld properties that a complex triflute shape. The complex shape of the triflute tool is also more expensive and difficult to machine than a simple square shape. The three flute design of the triflute pin reduces the volume of tool pin material and can influence the risk of pin failure when welding thicker or denser material. Therefore when pin failure becomes a limiting factor in FSW the triflute pin design may not be appropriate.

A recommend pin design from the results produced during this project is a pin which has flats, threads and a taper machined onto it. The flats and threaded features which produce a stirring action similar to the square and triflute pin. The taper and flats (instead of flute) will provide greater strength and stability when welding thick or more dense work pieces.

### 4.5.3 Effect of Different Shoulder Geometries:

**Concave versus Scrolled Shoulder**

To examine the effect of shoulder design, two welds were fabricated with a concave shoulder design using a required 2° tool tilt angle and compared with welds fabricated using a scrolled shoulder design (note both shoulders had a diameter of 18mm). The results are shown in Figure 130 and indicate that although the scrolled shoulder preformed slightly better there is no major significant difference in weld strength between the two different shoulder designs. Similar results were obtained when comparing elongation. However, these results only represent two sets operational parameter and therefore further test would be required to examine this over a larger range of operating parameters.

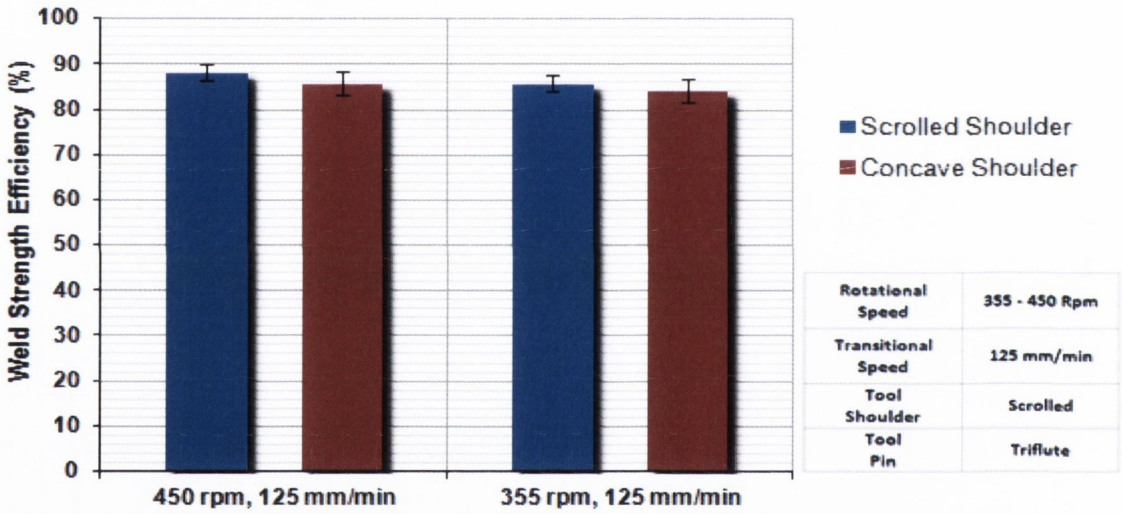


Figure 130: Effect of shoulder design on joint efficiency

The Above information shows no significant different in weld strength when using a scrolled shoulder compared to a concave shoulder. However the scrolled shoulder was found to enable higher translational speeds due to a reduction in tool lift. At high translational speeds, the tilt angle can cause the tool to partially come out of the workpiece, therefore taking away the necessary feed of material to the upper reaches of the tool pin which can initiate the formation of voids. Using a concave shoulder, translational speeds greater than 125mm/min were not possible due to this tool lift which resulted in a poor surface finish with the occurrence of voids and irregularities. Evidence for this can be seen in Figure 131. However the most significant advantage of using a

scrolled shoulder is its ability to weld with a zero tool tilt angle. This is an advantage if performing a friction stir weld around a corner or welding in a circular or oval shape (i.e. non-linear) where sophisticated machinery and a lot of precision would be required to maintain the appropriate tool tilt angle while using a concave tool shoulder. Figure 132 illustrates welds preformed during a training course at The Welding Institute (TWI) using a scrolled shoulder with a zero tilt angle.

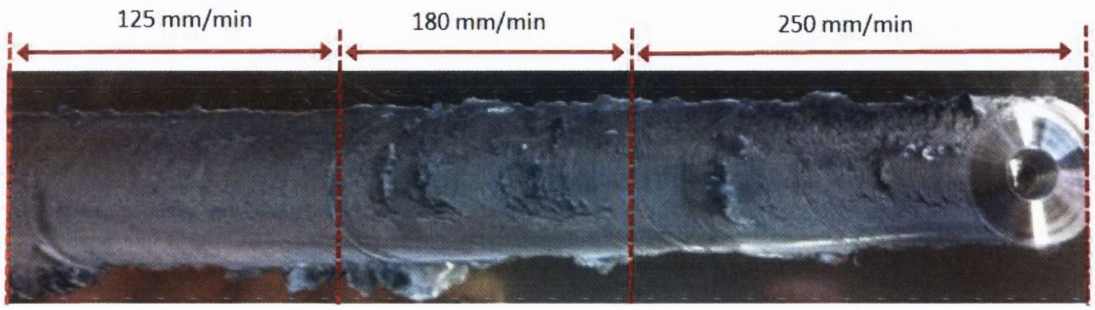


Figure 131: Tool lift using a concave shoulder

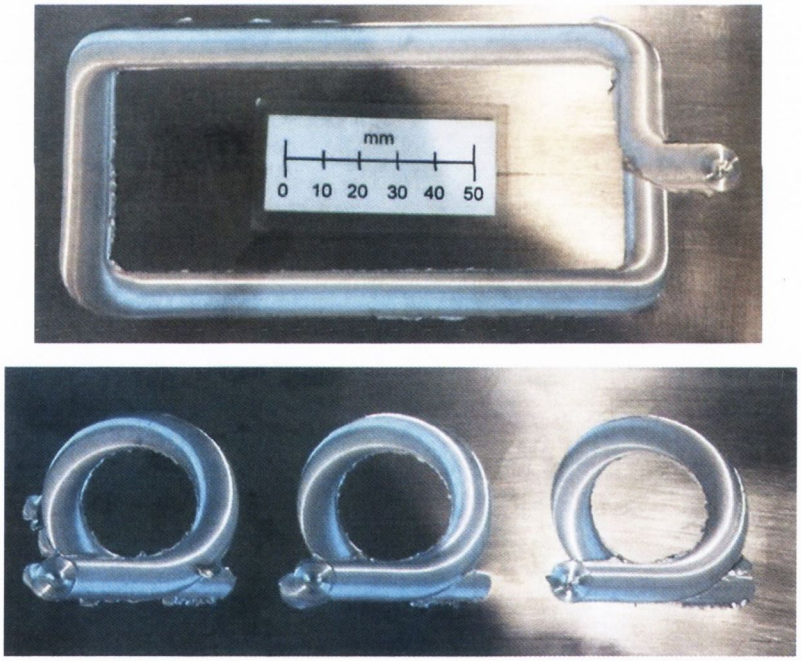


Figure 132: Non linear weld with a scrolled shoulder

**Shoulder Dimensions**

As mentioned previously initial testing at the beginning of this project focused on a larger shoulder diameter of 22mm. This diameter was based on the work of previous authors who preformed FSW on similar aluminium 2024-T3 plates [42, 43, 47, 49]. Results produced using the 22 mm shoulder was compared to those produced using a smaller shoulder diameter of 18mm. In all cases, the 18 mm shoulder diameter produced stronger more ductile welds. An example of this can be seen in Figure 133. Using an 18 mm shoulder diameter, a 20 % increase weld strength and 50% increase in elongation was recorded. This can be attributed to thermal damage associated with the larger 22mm shoulder diameter. A larger diameter will generate more heat due to increased surface area contact with the workpiece and higher peripheral velocities at the shoulder edge. A higher heat input can cause thermal damage to the workpiece and produce welds with inferior mechanical properties as mentioned in section 4.5.1.

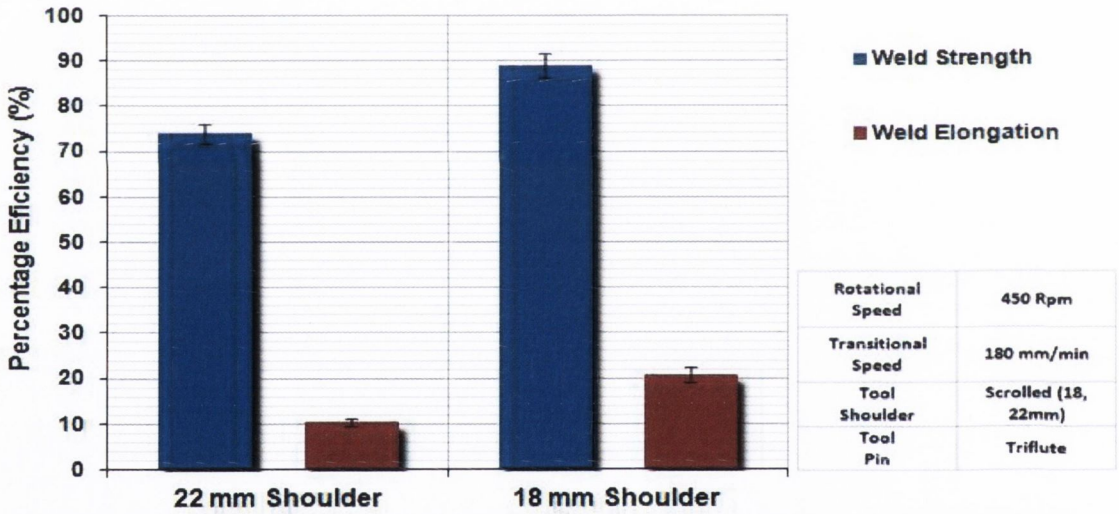


Figure 133: Joint efficiency and elongation using different shoulder dimensions

### 4.5.4 Repeatability:

A number of tests within the testing matrix were repeated to investigate the consistency of the friction stir welding process. All repeat testing, in terms of weld strength and elongation were found to be relative consistent with a standard deviation of approximately 7%. Figure 134 illustrates the consistency of two particular welds that performed particularly well during the initial testing. All four tests produced welds with strength approximately 90% of that of the parent material.

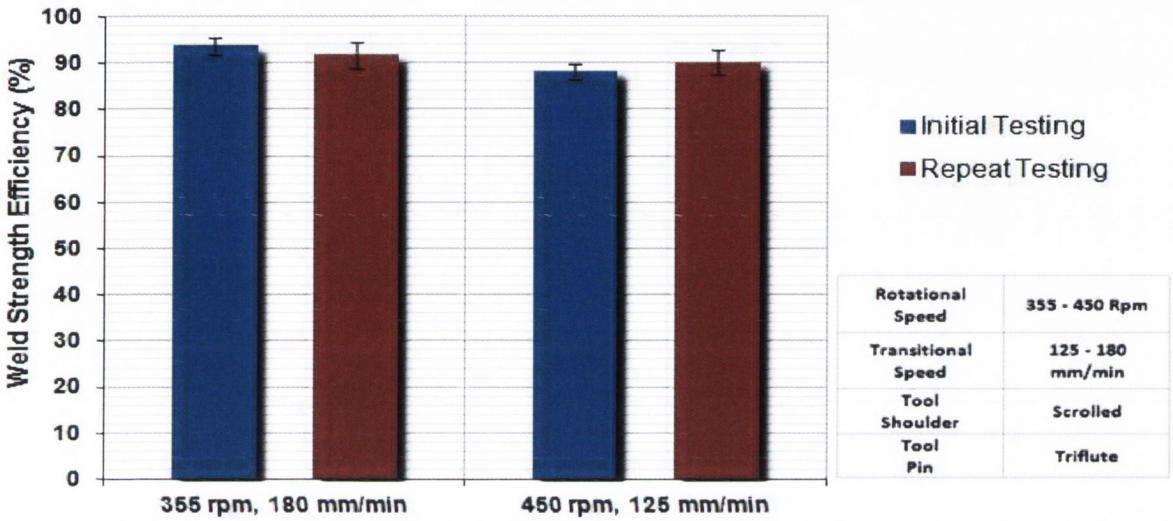


Figure 134: Joint efficiency repeat testing

## 4.6 Macrostructure and Microstructure:

### 4.6.1 Introduction:

To examine the macrostructure and micro structure of the friction stir welding process, cross sections from welds were mounted on resin, polished and etched using Keller's reagent to reveal the different weld zones. Figure 135 shows an example of a weld fabricated during this project with the different weld zones revealed. Further information on the procedure can be seen in section 3.6.3.

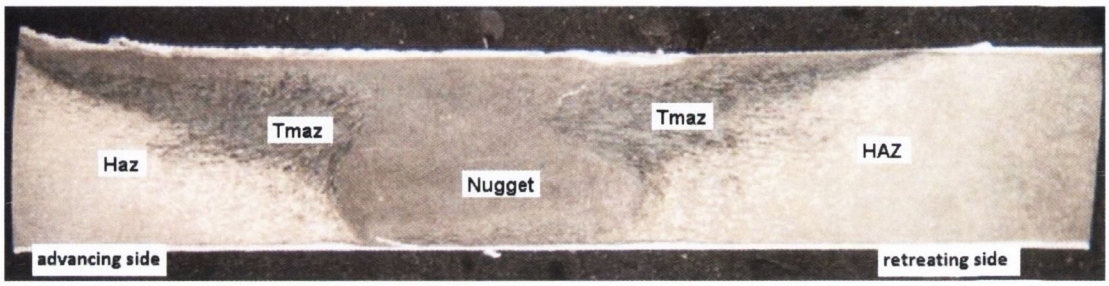


Figure 135: Macrostructure of the different weld zones

**Thermo-Mechanically Affected Zone (TMAZ):**

This is the part of the weld that is affected by both heat and deformation. In aluminium, only the hottest part will recrystallized to form the nugget. The Nugget Zone is the region of the weld that the pin occupies as it traverses along the joint line. This region undergoes intense material deformation at elevated temperatures. The original grains within this zone are completely demolished by the tool pin and replaced with fine, equiaxed grains. This process is called continuous dynamic recrystallization and an example is shown in Figure 136.

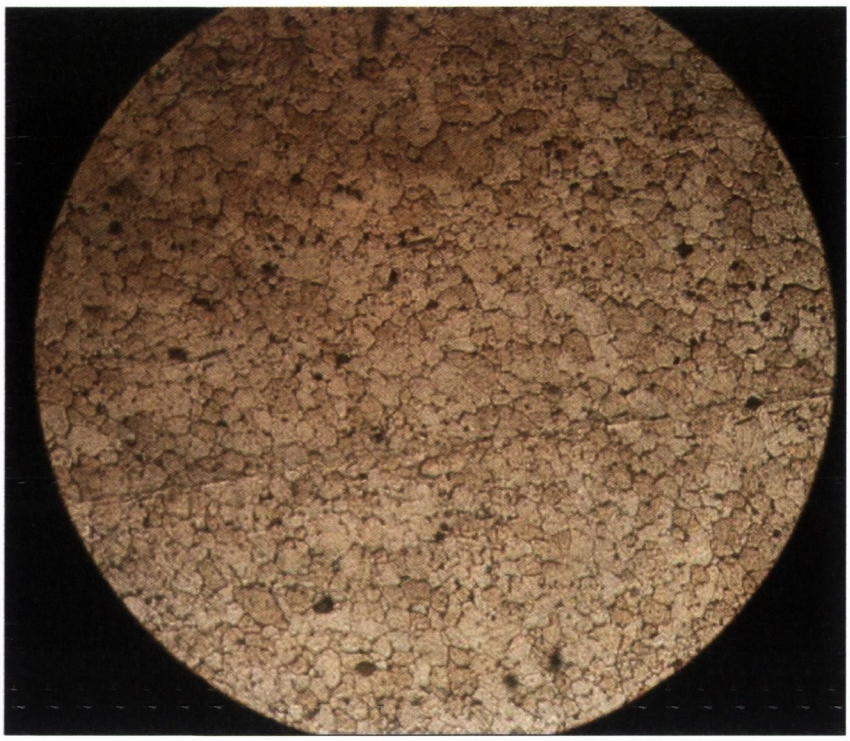

Figure 136: Dynamic recrystallization within the nugget zone at 1000x magnification

The TMAZ at either side of the nugget is a zone that has not undergone recrystallization. While this zone has not been directly subjected to the deformational action of the pin, however due to internal shear stresses it has experienced severe thermo-mechanical alteration. Consequently the microstructure of the TMAZ is recognisably that of the base material but severely deformed. The grains appear to have undergone a rolling/ straining deformation process which results in elongated grains, as shown in Figure 137. The temperatures in this zone although not great enough to cause dynamic recrystallization, will cause a slight tempering effect of the material. Therefore the material properties in this region tend to be lower than those found in the base material. The overall TMAZ also appears to have a V-Shape appearance, as shown in Figure 135. This is due to the heating and material deformation effect produced by the tool shoulder. Shoulder contact occurs at the workpiece surface and the effects of the shoulder decreases with depth away from the workpiece surface, therefore resulting in a V-Shape appearance. Also the size of the TMAZ is directly related to the tool shoulder diameter and it can be seen that there is a clear distinct boundary between the TMAZ and the nugget weld zone as illustrated in Figure 138.

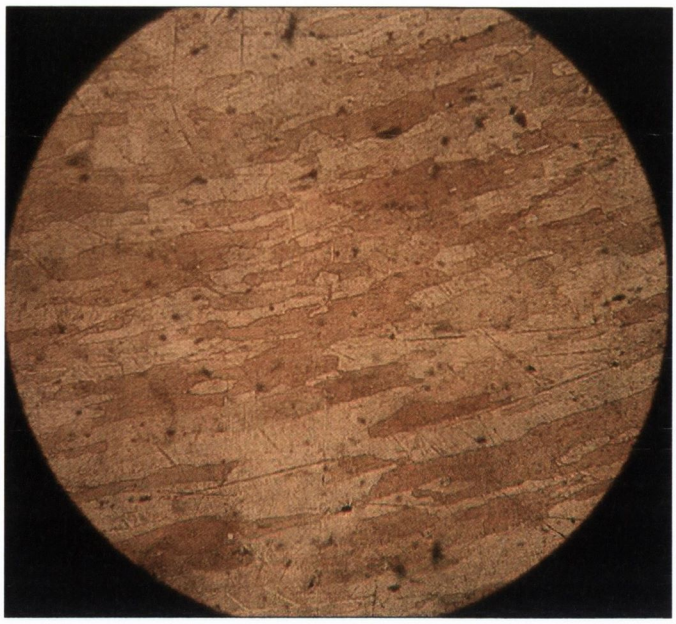

Figure 137: TMAZ zone at 200x magnification

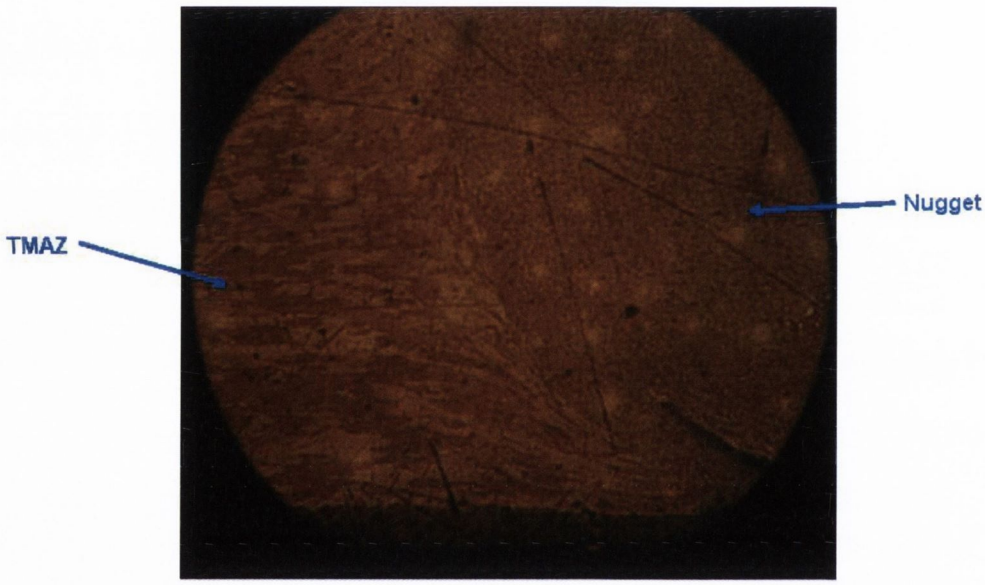


Figure 138: Boundary between TMAZ and Nugget zones at 100x magnification

**Heat Affected Zone HAZ:**

The Heat Affected Zone is located either side of the TMAZ. It is the part of the weld that is not mechanically affected but does undergo a considerable thermal cycle which leads to grain growth and softening in this region. Figure 139 shows the grains within the HAZ. Similar to the TMAZ region, the HAZ takes up a V-Shape appearance due to the shoulder action. The Transition from the TMAZ to HAZ is more gradual one with the grains becoming increasingly less deformed closer to the HAZ zone. This can be seen in Figure 140.

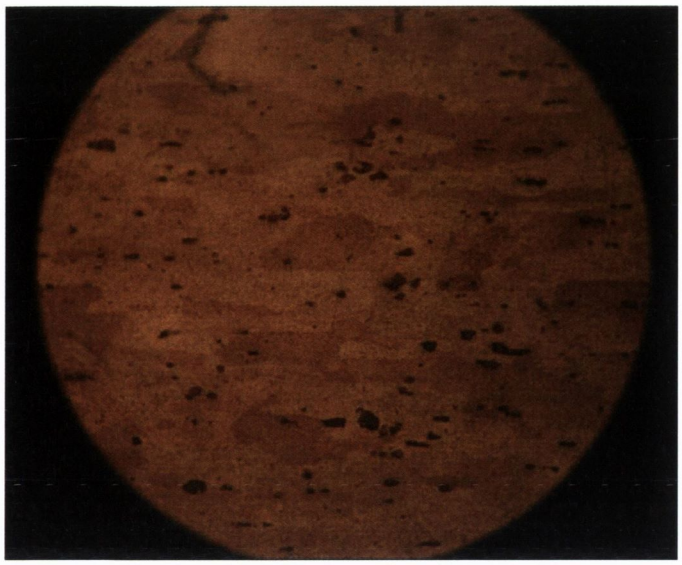

Figure 139: HAZ zone x200

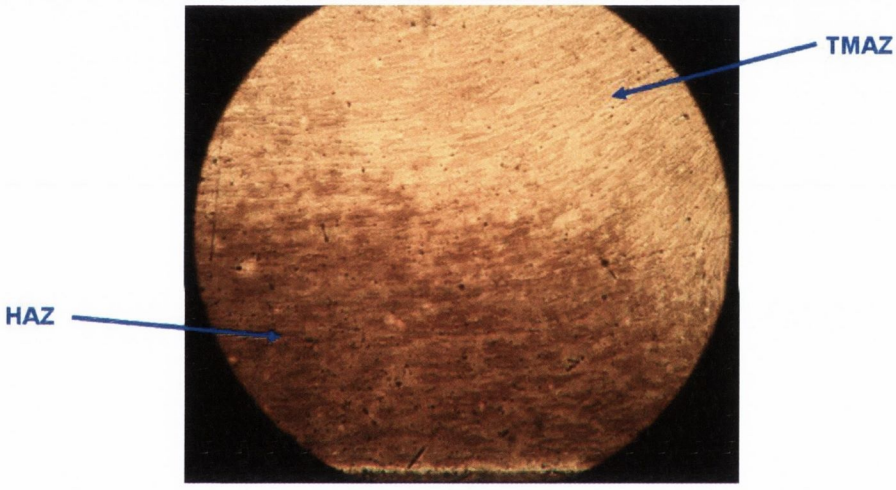


Figure 140: Transition from HAZ to TMAZ at 50x magnification

### 4.6.2 Effect of different Shoulder Dimensions:

As mentioned in section 4.5.3, welds were produced with tools having two different shoulder diameters (18mm and 22mm). The macrostructure of the two welds is illustrated in Figure 141. The nugget zone when using the 18 mm shoulder is less clearly defined and distinguished from the un-recrystallized TMAZ. This can be attributed to the reduction in heat input into the weld for the smaller 18mm shoulder diameter as recrystallization requires intense heat combined with deformation. Reducing the heat input will reduce the recrystallization process and hence the difference between the nugget zone and outer TMAZ will be less visible. Also, the size of the TMAZ and HAZ are smaller when a smaller tool shoulder is used. These are regions of low strength and hardness which will be discussed in section 4.7.3. This correlates well with the greater weld strength recorded for an 18mm shoulder diameter compared to a 22mm diameter as discussed in section 4.5.3. Also, it is worth noting that no distinctive difference was apparent when examining the microstructure of welds fabricated using a scrolled shoulder as opposed to a concave shoulder of the same diameter.

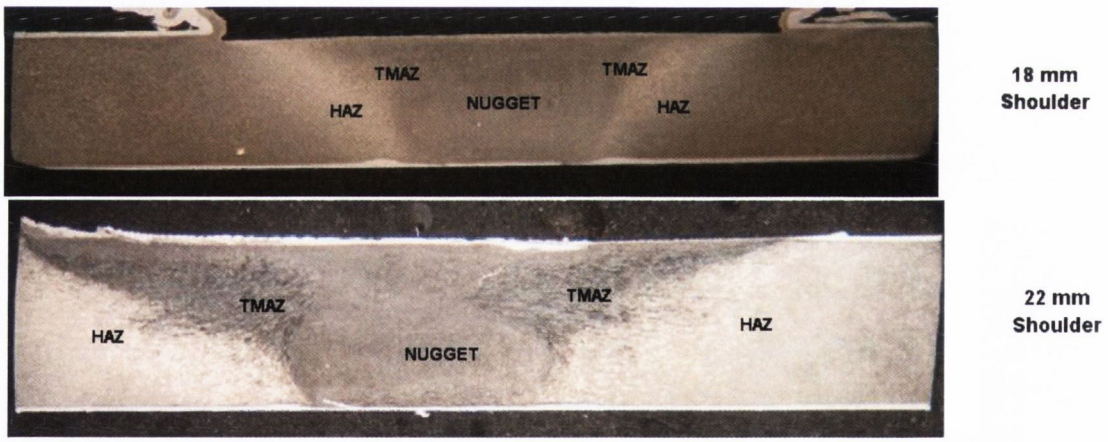


Figure 141: Macrostructure for different shoulder diameters

### 4.6.3 Effect of Different Pin Geometries:

In section 4.5.2, the increase in weld strength when welding with both the Square and Triflute pin geometries compared to the Cylindrical and Tapered pins was attributed to increased material deformation and mixing. Evidence for this can be seen in Figure 142 which compares the grains within the nugget zone and TMAZ for the triflute and cylindrical pins. Recrystallization occurs in the nugget zone regardless of the pin profile.

However the triflute pin produced a more finer, compact and equiaxed grain structure within the nugget zone compared to the cylindrical pin. Also, closer examination of the TMAZ reveals a greater amount of grain elongation produced using the triflute pin compared to the cylindrical pin. Both of which indicate greater amount of plastic material deformation. Note, the square pin produced similar grains to those produced by the triflute pin, and the tapered pin produced grains similar to those produced by the cylindrical pin

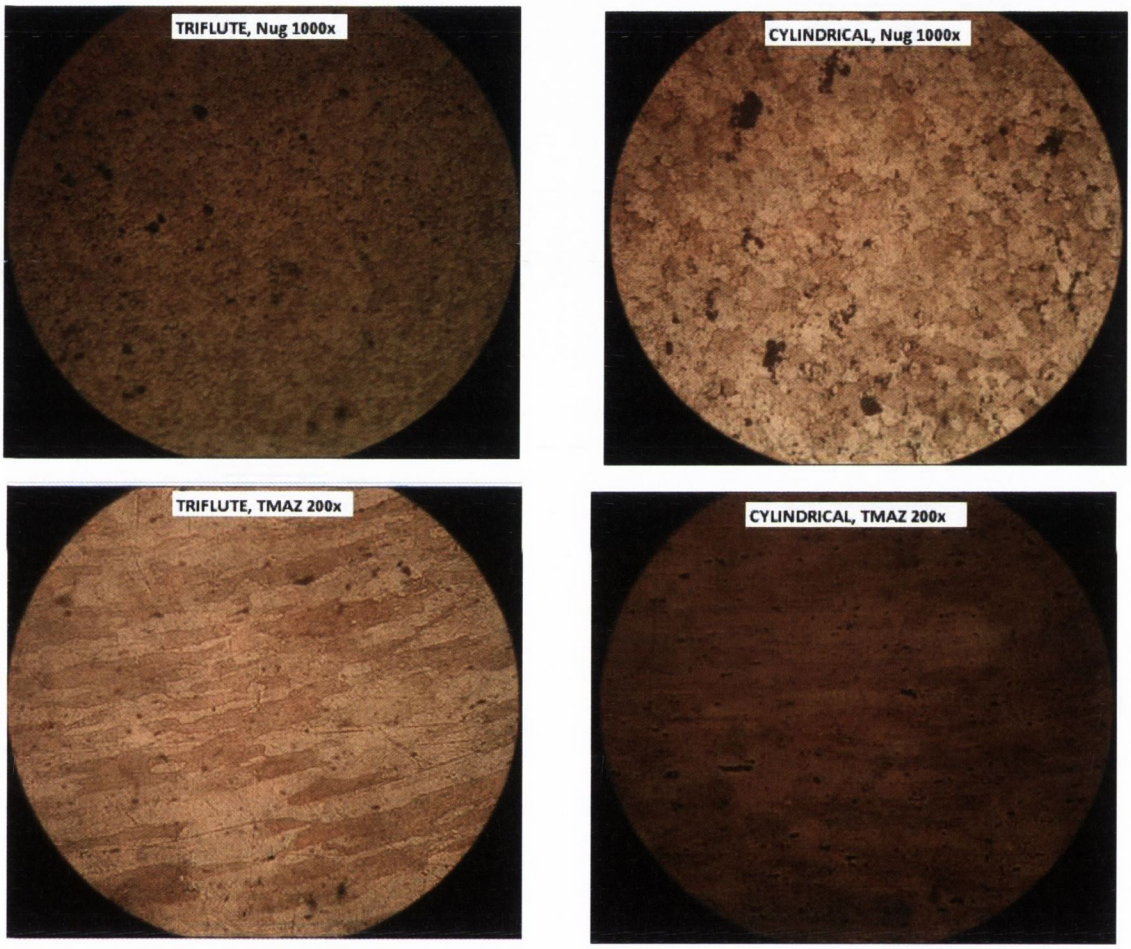


Figure 142: Nugget and TMAZ comparison for Triflute and Cylindrical tool pins

Further evidence of increased plastic material deformation is shown in Figure 143 which compares the macrostructure of welds produced using the square and cylindrical pins. The square pin produced a slightly larger overall TMAZ which suggests greater material mixing and deformation. Also, the square pin produced a consolidated weld throughout the entire thickness of the weld. However, results indicate that although both pins had the same height, the cylindrical pin did not produce adequate mixing and integration of the two workpiece material near the bottom surface of the joint and hence

a root flaw is formed. Therefore the bottom surface of the joint is an area of weakness which may have lead to the lower weld strength recorded for the cylindrical and tapered pins.

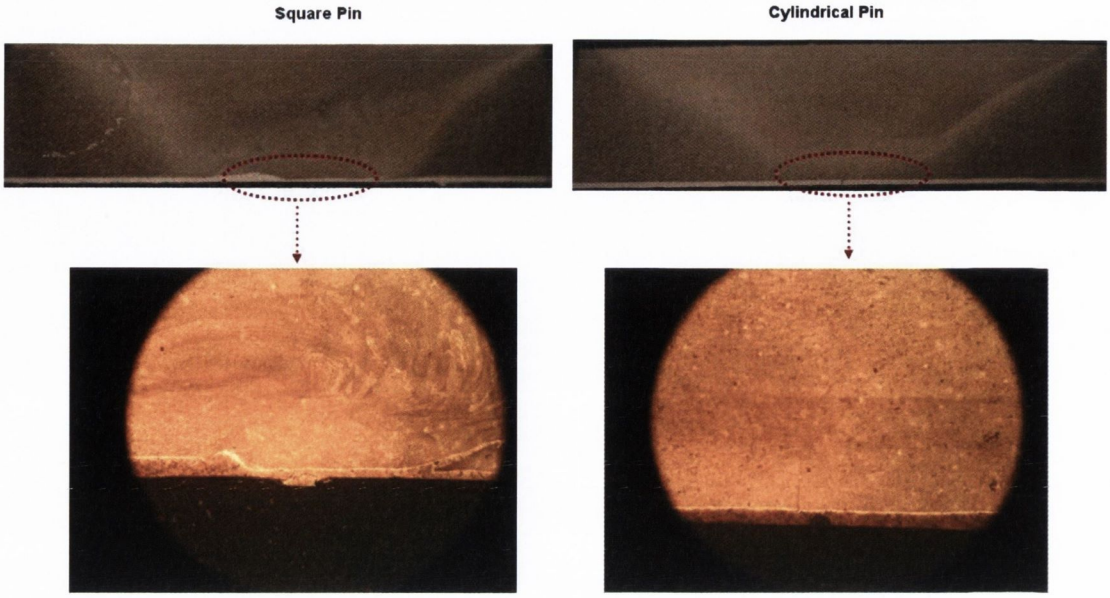


Figure 143: Macrostructure and microstructure of welds with different pin geometries

In some cases tunnel defects were found in welds produced by both the Cylindrical and Tapered pins. These tunnel defects appeared along the entire length of the weld on the advancing side at the interface between the Nugget and TMAZ near the bottom surface of the weld and can be seen in Figure 144. The location of these flaws refers to the edge of the tool pin and suggests that as the pin traverses through the workpiece, material is being forced around the sides of the pin (extruded) rather than being rotated around the front of the pin from the advancing side to the retreating side. Therefore, these defects can be attributed to inadequate mixing and material deformation due the smooth surface area of these pins. The presence of these tunnel defects can also account for the lower weld strength recorded for the tapered and cylindrical pins.

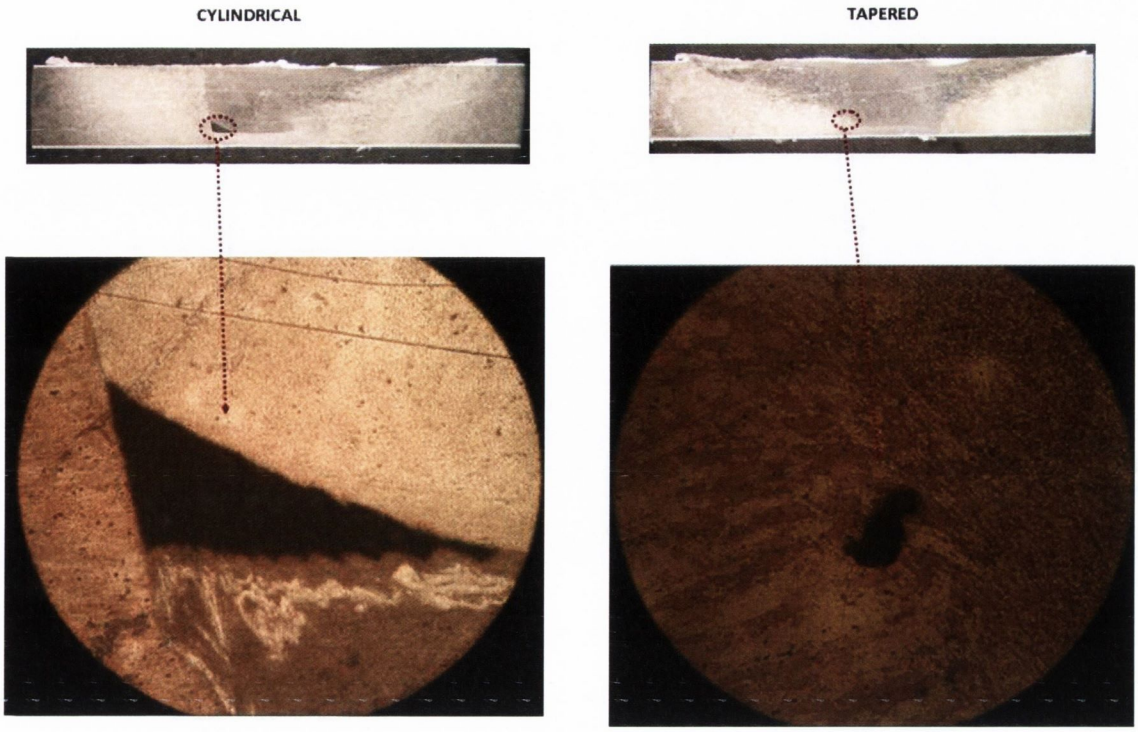


Figure 144: Tunnel defects at x100 magnification

## 4.7 Microhardness and Fracture Location:

### 4.7.1 Introduction:

Vickers Microhardness test were conducted on the cross sectional areas of the welded joint. Indentations measurements were taking at 1mm intervals either side of the weld centre line at mid-thickness depth of 2.41 mm from the workpiece surface as shown in Figure 145. The test involves the user measuring the diagonals of the diamond shape indentation mark. Therefore, human error can reduce the accuracy of the measurement. The minimise this, the hardness of each indentation mark was measured three times and the average hardness was recorded.

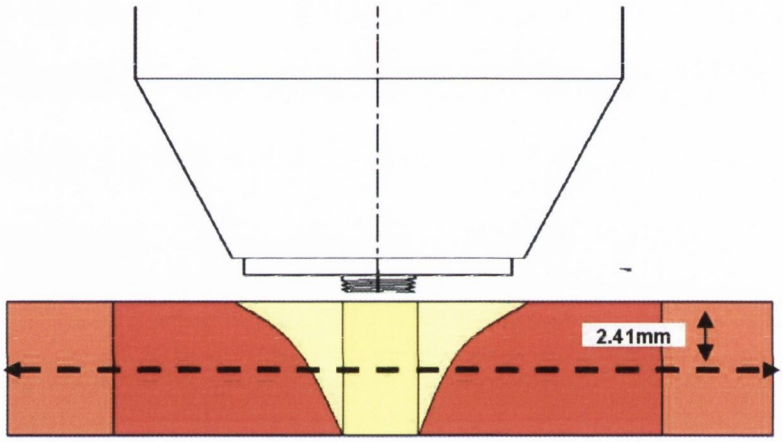


Figure 145: Schematic of Microhardness test

Figure 146 shows a typical microhardness graph for a Friction Stir Weld. Negative numbers represent the retreating side of the weld and positive numbers the advancing side. Points 1 to 2 represent the transition from the joint line to the edge of the area occupied by the tool pin i.e. the nugget zone. A high almost constant hardness of 132 - 135 HV is achieved in this region due to the high strain rates, elevated temperatures and dynamic recrystallization occurring. As mentioned previously, recrystallization produces fine equiaxed grains which produce a uniform resistance to deformation and hence a relatively larger hardness is recorded. This hardness is below that of the parent material hardness of approximately 147 HV which was measured from an un-welded sample. Points 2 to 3 represent transition from the un-recrystallized TMAZ to the HMAZ with low hardness values of approximately 118 - 119 HV recorded at point 3 approximately 5mm away from the joint line. The low hardness recorded within the transition from the TMAZ

to the HAZ can be attributed to dissolution, coarsening and overaging of the strengthening precipitates due to the thermal cycle without recrystallization occurring in this region [93, 97]. This region therefore experiences a reduction in strength and general softening which magnifies with increasing heat generation. Points 3 to 4 represent transition from the HAZ to parent material properties. The heating effects of the tool shoulder decreases with distance away from its periphery until the hardness begins to resemble that of the parent material.

It is evident that all weld zones experience a hardness value below that of the parent material. This may explain why none of the welds exhibited greater strength than the parent material. Kristensen [56] and Jariyaboon [57] performed Vickers microhardness tests on Aluminium 2024-T3 friction Stir Welds of 6mm and 6.35mm thickness respectively for a range of different operational parameters. Similar hardness values to those in Figure 146 were reported by these authors.

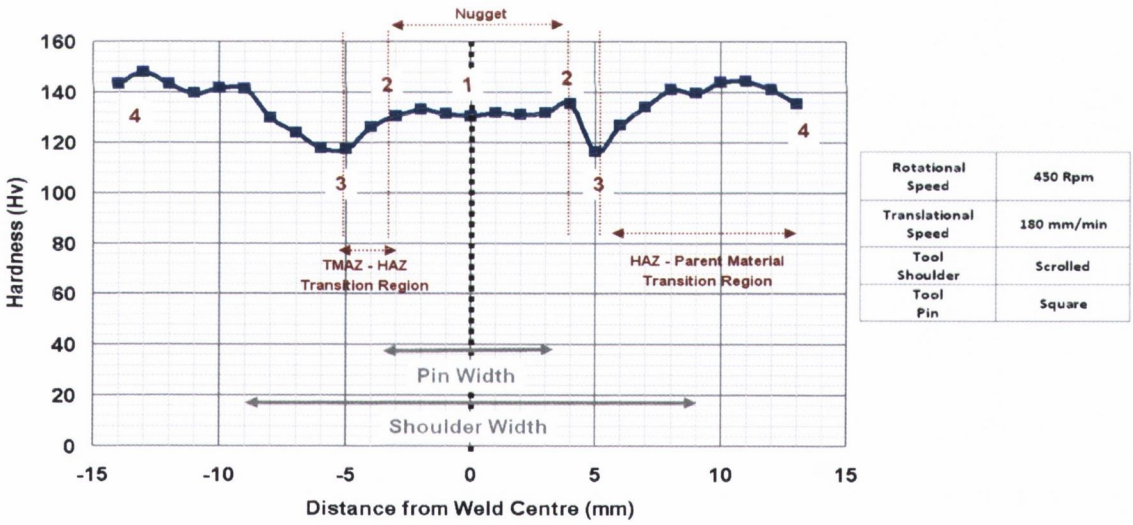


Figure 146: Typical microhardness curve

Figure 146 shows the large variation of hardness across the weld zone at a mid thickness depth and indicates a complex grain structure. There is also a variation in hardness along the thickness of the workpiece which further complicates the structure. Figure 147 shows the recorded hardness at 1.75 mm above the mid thickness depth and 1.75 mm below the mid thickness depth.

A larger nugget region with higher hardness was recorded at 1.75mm above the mid thickness level due to its close proximity to the shoulder. The action of the shoulder is to generate heat but also some material deformation. Recrystallization occurs due to grain deformation at an elevated temperature and hence a stronger/harder grain structure is experienced closer to the shoulder. The transition to the HAZ is also larger in size at 1.75 mm above the mid thickness and reaches it minimal value close to periphery of the tool shoulder at approximately 8-9 mm away from the weld centre line. Again this can be attributed to the influence of the shoulder.

A general decrease in size and hardness of the nugget zone, and also a reduction in size of the HAZ is experience at -1.75 mm below mid thickness depth. The influence of the shoulder is limited in depth as it only contacts the top surface of the workpiece. The effects of the shoulder become increasing less significant with increasing depth below the top surface.

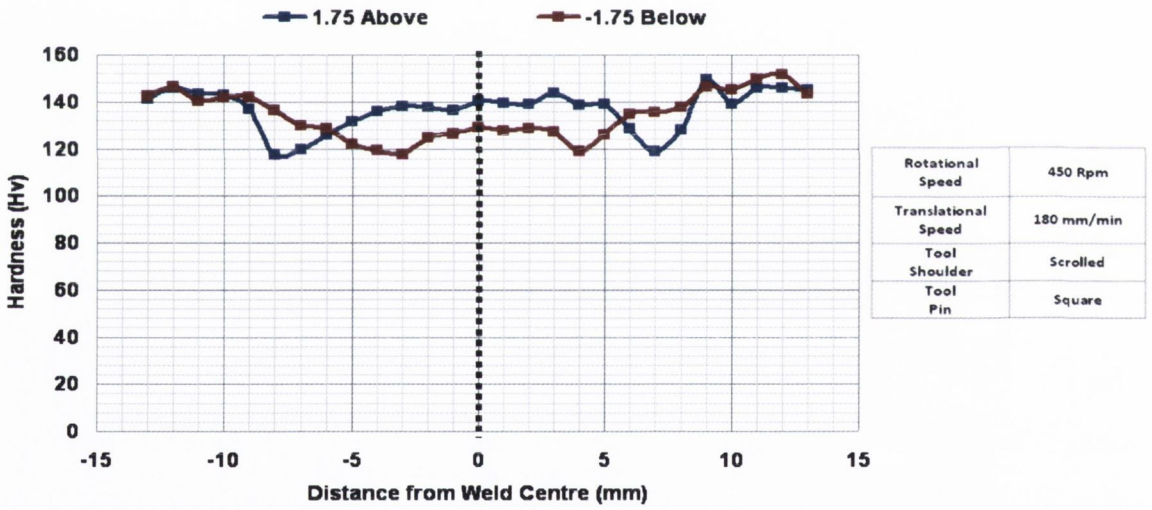


Figure 147: Microhardness at different thickness depths

### 4.7.2 Low Ductility of Welds:

As outlined in section 4.5, all welds exhibited a significantly lower ductility to that of the parent material. Evidence from the complex grain structure within the different weld zones (section 4.6.1) and the microhardness distribution along the width and thickness of the weld (section 4.7.1) suggest the FSW process produces a complex heterogeneous weld structure. Grains of different shapes and sizes possess different mechanical properties. Evidence for this can be seen in the variation of grain harness recorded which

is directly related to the tensile strength. The low ductility can be attributed to the grains having different mechanical properties which will vary the yield strength capabilities across the joint. A higher ductility is expected if a more uniform grain structure is produced throughout the weld zones similar to the parent material.

### 4.7.3 Identifying fracture location:

Although the FSW process produces a complex heterogeneous grain structure and hardness distribution. The relationship between hardness and tensile strength can help identify where fracture location is most likely to occur. Hardness is the measure of how resistant solid matter is to various kinds of permanent shape change when a force is applied. Therefore both hardness and tensile strength are indicators of a materials resistance to plastic deformation. When a joint is free of defects, the tensile properties of the joint are dependent on the microhardness distribution of the joint. When a tensile load is applied to a joint, the stress and strain concentration takes place in the region of lowest hardness/strength (commonly transition from TMAZ to HAZ) and consequently, the joint fails in this region. For example, in Figure 146 the lowest hardness value recorded is 119 Hv and its location was approximately 5mm from the weld centre (transition from TMAZ to HAZ). This indicates where failure is most likely to occur. Evidence for this can be seen in Figure 148 which shows the tensile specimen with failure occurring at approximately 5mm from the centre line. In all other welds, the location of lowest hardness gave a good indication of where fracture is most likely to occur provided no surface defects, internal defects and root flaws were present. Therefore a non-destructive micro hardness test can provide a good indication of the location of where fracture is mostly likely to occur.

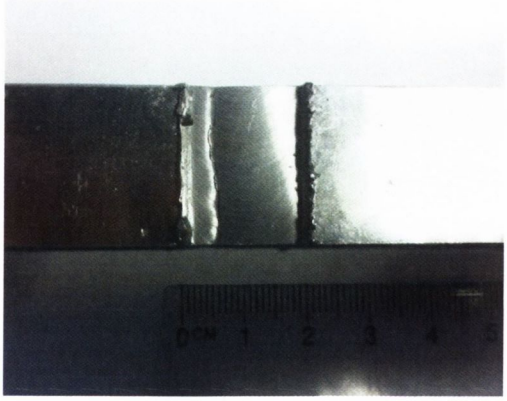

Figure 148: Fracture Location

### 4.7.4 Effects of Operational Parameters on Microhardness:

**Impact of Translational Speed**

The effect of increasing the translational speed on the microhardness can be seen in Figure 149. The nugget hardness of the test pieces is approximately equal with no major significant differences. However, it can be seen that the values of minimum hardness (TMAZ/HAZ region) increases with increasing translational speeds. Also, the distance from the weld centre at which this minimal value occurs, decreases with increasing translational. Both these effects can be attributed to the reduction in heat generation with increasing translational speeds as mentioned in section 4.3.1.1. Where the grains in the HAZ zone are not mechanically affected they do undergo a considerable thermal cycle which leads to grain growth and softening of the grain. Also grains within the TMAZ are also subjected to a tempering effect which will also cause grain softening. Hence a reduction in hardness occurs within these zones. Consequently an increase in heat generation at lower translational speeds will enhance this effect significantly as illustrated in Figure 149. Also, increased heat generation will also increase the width of the HAZ which explains the location of minimum values.

Furthermore, variation in hardness and transition towards the parent material hardness is less apparent for higher translational speed. This produces a more uniform microstructure and hardness distribution which may increase ductility. Therefore, higher translational speeds may produce stronger and more ductile welds in addition to reducing production time provided the tooling design can process the material efficiency and prevent the occurs of voids as seen in section 4.5.1. Kristen et al [56] recorded a similar increase in hardness in the HAZ when increasing the translational speed from 272 mm/min to 476 mm/min at a fixed rotational speed of 340 Rpm during the FSW of 6mm thickness aluminium 2024-T3 plates.

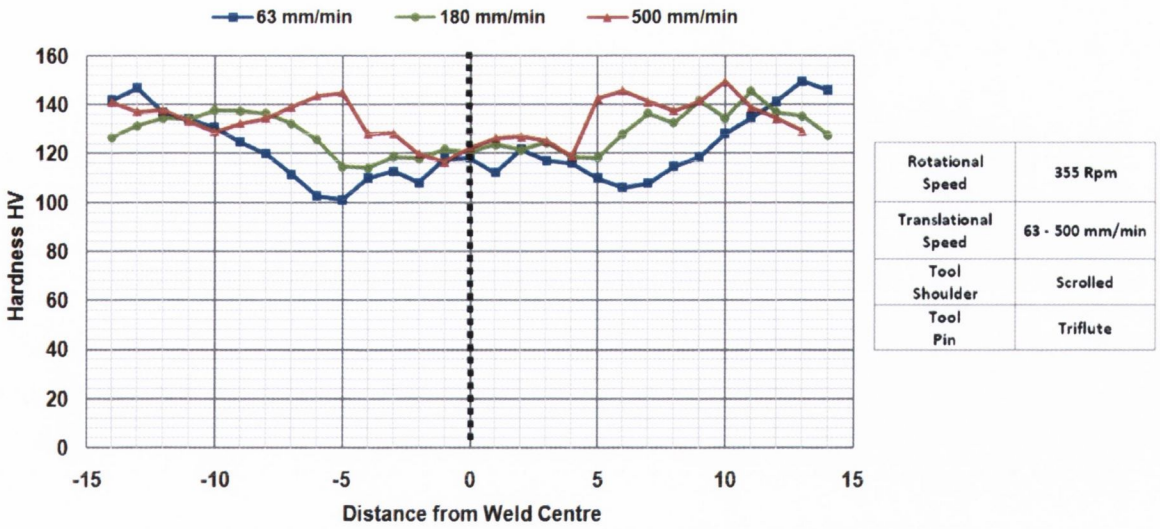


Figure 149: Effect of translational speed on microhardness

Comparing the results in Figure 149 to those in Table 17 (weld strength results pg 129) we can again see that hardness measurement gives an indication of the welds will most likely perform best. The weld fabricated at 500 mm/min recorded the highest hardness in the HAZ and therefore should have the greater strength. Unfortunately this was not the case due to the occurrence of surface defects produced at high translational speeds. However, no defects where detected in the welds produced at 63 and 180 mm/min. The 63 mm/min weld produced a lower hardness and weld strength, 79 % of that of the parent material. Whereas the 180 mm/min weld produced a higher hardness value in the HAZ zone and hence produced superior weld strength, 93 % of that of the parent material.

**Impact of Rotational Speed**

The effect of varying the rotational speed from 280 - 900 Rpm on the hardness is shown in Figure 150. The hardness in the nugget region was found to increase with increasing rotational speed. This was expected as increased rotational speed produces greater material deformation and heat generation (see section 4.3.1.2), both of which are required for recrystallization to occur. However, higher rotational speeds also resulted in lower minimal hardness values in the TMAZ-HAZ region. Again this reduction in hardness can attributed to an increase in heat generation.

Lower rotational speeds resulted in a faster transition from the HAZ to the parent material hardness and the difference in hardness between in the nugget region and the HAZ becomes less apparent with decreasing rotational speed. In some cases, for example the weld fabricated at 280 Rpm, the minimum hardness value was found in the nugget region. Again, this can be attributed to the reduction in heat generated. Jariyaboon et al [57] reported similar results during FSW of 6.35mm thick AA2024-T351 plates. These authors reported a low hardness in the nugget region of welds produced with a low rotational speed of 215 Rpm and found a higher hardness in the nugget region for welds produced with a higher rotational of 468 Rpm.

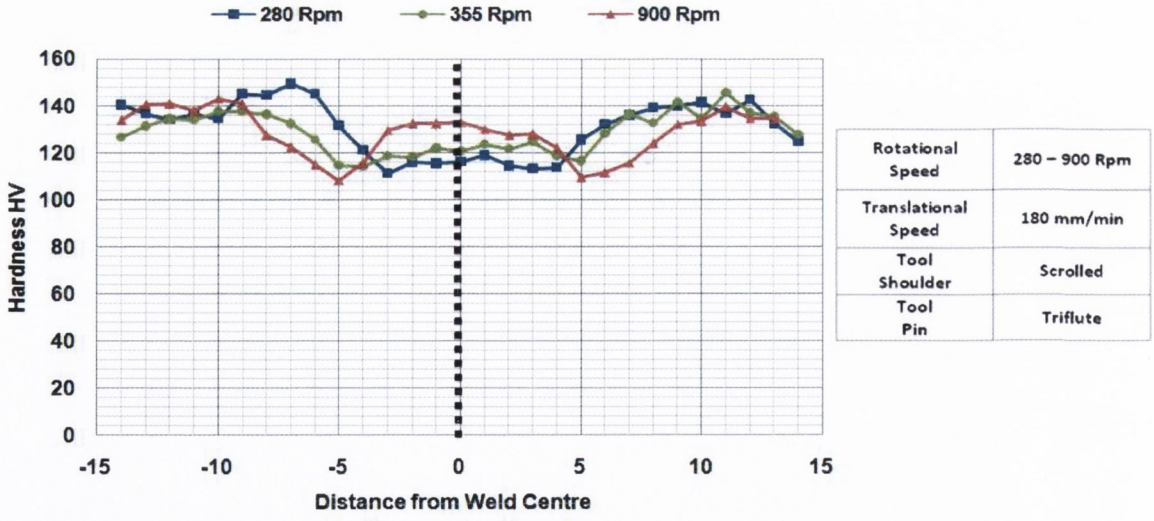


Figure 150: Effect of rotational speed on microhardness

### 4.7.5 Effect of Tool Design:

#### Pin Design

Due to increased material deformation, the triflute and square tool pins produced finer grains within the nugget zone and TMAZ compared to the cylindrical and tapered pin (section 4.6.3) which resulted in great weld strength (section 4.5.2). Further evidence for this can be seen in Figure 151 which shows the average nugget hardness for the four different pin designs. As expected, higher hardness is recorded for the triflute and square pin designs.

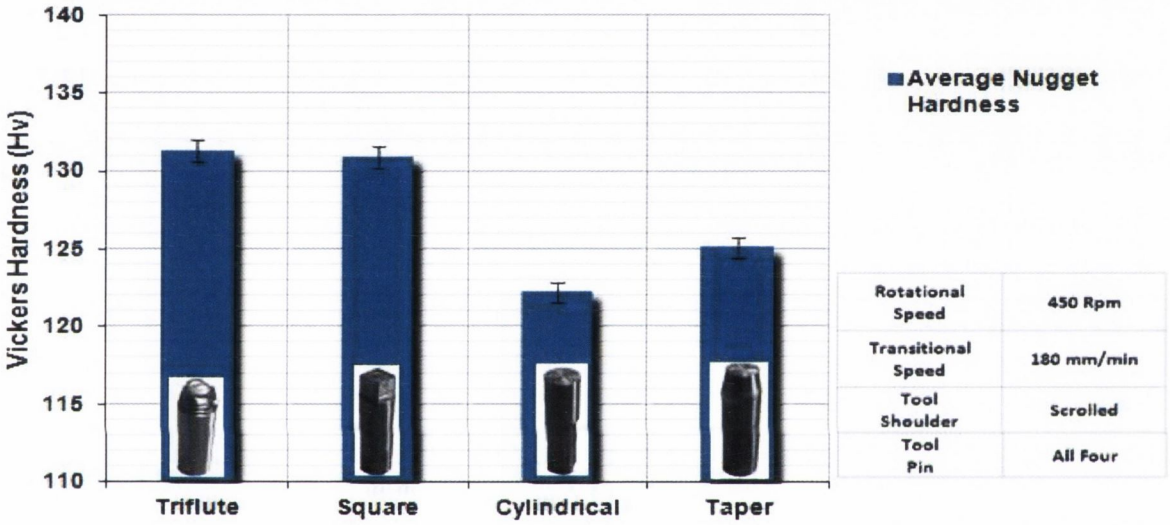


Figure 151: Average Vickers hardness within the nugget zone for different pin designs

#### Shoulder Design

The effect of shoulder geometry (concave and scrolled) on the hardness is illustrated in Figure 152. It can be seen that there is no significant different in the hardness value recorded for the two different shoulder designs. This was expected as welds fabricated using both shoulders produced similar weld strength as presented in section 4.5.3.


Figure 152: Effect of shoulder geometry on microhardness

## 4.8 Comparison of Post weld Results to Previous Research:

From the literature review it is evident there has been previously research focused on the FSW of 2xxx aluminium alloys, especially AA2024 due to its high strength to weight ratio and its many applications within the aerospace industry. In particular, Shanmuga et al, Balasubramanian et al, Elangovan et al, and Aydin et al have published papers focusing on examining the effects of operational parameters (rotational and translational speeds) to maximise weld strength. However, these authors along with many others which are illustrated in Table 7 pg32 all tend to implement higher rotational speeds and lower translational speeds compared to parameters used during this project. For example the four authors mentioned above recommended rotational speeds between 1200 – 2140 rpm and translational speeds between 40 – 75 mm/min, perhaps with the idea that lower translational speeds and higher rotational speeds will produce more mixing of the workpiece material and hence produce stronger joints. These authors achieved weld strength efficiencies between 60 – 76% of the parent material.

However, during this project, weld strength efficiencies between 85 – 95% of the parent material were achieved by implementing lower rotational speeds (355 – 450 rpm) and faster translational speeds (125 – 250 mm/min). These parameters also have productions befits such as lower energy input and a reduction in process time. From these results it is clearly evident that the amount of mechanical energy required to thermally soften and mix the workpiece material together has been over estimated by previous researchers.

High rotational speeds and low translational speeds produce a greater heat input into the weld. Microhardness testing demonstrated that an increase in heat input will reduce the hardness in the weakest part of the weld zones (TMAZ – HAZ interface) due to grain growth and softening. This reduces the strength of the weld leading to a reduction in the mechanical properties such as tensile strength. Similar to previous research [91, 56, 93, 97], welds recorded low ductility compared to the parent material. This was attributed to the large variation in microhardness distribution recorded in the different weld zone which indicated a complex heterogeneous weld structure.

Microhardness testing revealed that increasing the translational speed reduces the variation of harness within the different weld zones with respect to the parent material. This outcome is desirable as the closer the weld zones resemble that of the parent material, the greater strength and elongation achievable. Higher rotational speeds where found to produce a strong nugget zone of high hardness with fine equiaxed grains due to dynamic recrystallization. However, this was offset by the increase in heat input produced by the rotating shoulder which was found to be the primary source of heat generation.

Therefore, this project has identified tool designs and operational parameters to achieve greater weld strength with reduced energy input and faster production times compared to previous research. This was achieved by reducing the heat input into the weld (by implementing lower rotational speeds and faster translational speeds) and also finding the appropriate combinational of parameters to provide sufficient mechanical energy.

Further improvement to weld strength and in particular the ductility can only be achieved by reducing the heat input and producing a more uniform grain structure throughout the different weld zone. This can be achieved by reducing rotational speeds, increasing translational speeds and reducing the size of the shoulder. However maximising the translational speed is limited due to the occurrence of surface voids as the tool is travelling too fast to enable the rotation of the tool to join the 2 materials together. Off-setting this by increasing the rotational speed will only increase heat generation again. Therefore this research has identified two options:

1 Develop new tool designs which can process and stir the materials more efficiently to enable higher translation speeds, lower rotational speeds and a reduction of heat input.

2 The tool shoulder was identified as the main source of heat generation. Therefore developing a non-rotating shoulder will reduce the heat input, allow higher rotational speeds of the pin to increase mixing which in turn will enable higher translational speeds.

## 4.9 Finite Element Modeling:

The finite element package DEFORM 3D V5.1 was used to produce a finite element model of the friction stir welding process. The aluminium sheets were modelled as one continuous block rather than two separate objects to avoid numerical contact instabilities that resulted from the discontinuities present at the edge of the two sheets and caused the simulations to fail. The rotating tool moves forward and welds a crack left behind the pin as it advances along the welding line. A similar approach was taken by G. Buffa et al and also L. Fratini et al [85, 86, 87].

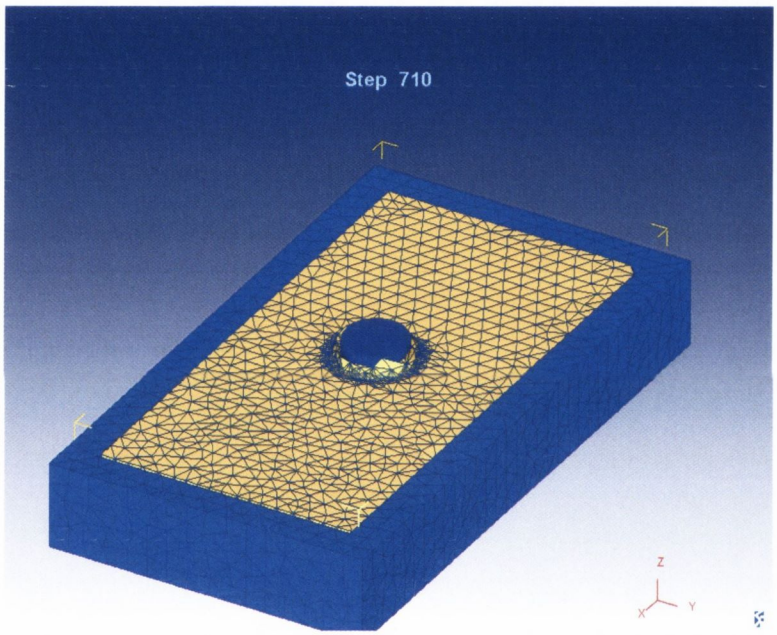


Figure 153: Finite element model of the FSW process using Deform 3D

The selection of the flow stress equation describing the workpiece was a critical feature of the model as the temperatures, stresses, strains and strain rates are all determined from the chosen flow stress equation. Initially three different flow stress equations were investigated and these are shown in Figure 154. They include the Sellers-Tegart law [98], Johnson Cook material law [99] and an empirical equation adopted by Fratini [87]. It was found that the equation developed by the Johnson Cook law gave the best representation of the FSW process and validation of the model is discussed in section 4.9.1.

Sellars-Tegart Law

$$\dot{\bar{\varepsilon}} = A\left[\sinh\left(\alpha\bar{\sigma}\right)\right]^n \exp\left[\frac{-\Delta H}{RT_{abs}}\right]$$

$A = 0.016$

$\alpha = 0.085$

$\Delta H = 148880$

$n = 4.27$

$R = 8.314$

Johnson Cook Material Law

$$\sigma_y = \left(A + B\left[\bar{\varepsilon}\right]^n\right)\left(1 + \ln\frac{\dot{\bar{\varepsilon}}}{\dot{\bar{\varepsilon}}_0}\right)\left(1 - \left(\frac{T - T_{ref}}{T_{melt} - T_{ref}}\right)^m\right)$$

$A = 369$

$B = 684$

$n = 0.73$

$C = 0.0083$

$m = 1.7$

$T_{melt} = 502$

$T_{ref} = 25$

Fratini

$$\sigma = KT^A\left(\dot{\bar{\varepsilon}}\right)^B\left(\bar{\varepsilon}\right)^C$$

$K = 2.69E10$

$A = -3.3155$

$B = 0.1324$

$C = 0.0192$

Figure 154: Different flow stress equation for AA2024-T3

However, there were many limitations associated with using DEFORM 3D when modelling the FSW process. Fine mesh windows with tetrahedral elements 1mm in length were used to concentrate the mesh density around the vicinity of tool pin and the shoulder contact area. This was necessary to consolidate the hole left by the tool pin as it advances along the weld line. Frequent remeshing (every 5 step) was also required to maintain mesh integrity. Both of these factor increased computational times significantly. For example, a typical model could take over 120 hours (5days) to run completely. Modelling the scrolled shoulder and the square pin was not possible due to contact instabilities and severe mesh distortion which constantly caused the simulation to fail. Therefore a concave shoulder with a 2° tilt angle with either a treaded or cylindrical tool pin were used in the FE model. However, a more up-to-date version of DEFORM 3D may reduce computational times and enable modelling of the scrolled shoulder and square pin design.

### 4.9.1 Validation of FSW Model:

The first step after the completion of each FSW simulation was to validate the model to ensure a good correlation with the experimental results before post processing model analysis. This was achieved by comparing the forces and temperatures predicted by the DEFORM 3D model to those recorded during the experimental testing.

**Temperature Validation:**

Figure 155 shows the FEM temperatures predicted at three different locations (T1, T2 and T3) during the translational stage of the FSW process. These measurements were taken at identical locations that the thermocouples were positioned during experimental testing. Each FE temperature measurement was taken 32.5mm away from one another; all were parallel and 15mm from the joint line as shown in Figure 92 pg 97.

Similar to experimental temperature measurement (Figure 83 and Figure 93), FEM temperatures reached steady state values during tool translation. Figure 156 shows the direct comparison between the experimental temperature and the FEM predicted temperatures. The maximum FEM temperature was 245°C, whereas the maximum experimental temperature was 262°C. This equates to a temperature difference of approximately 20°C and demonstrates a reasonable good correlation between the experimental and FEM predicted maximum temperatures.

However, the thermal flow ahead of the tool and behind the tool after it passes the thermocouple location seems to be greater for the experimental results. The FEM temperature does not increase significantly until the tool is -20mm from the thermocouple location, whereas the experimental temperature increases gradually at -40mm from the thermocouple location. Also, the FEM temperature decreases at a greater rate compared to the experimental temperature after the tool has passed the thermocouple location. This can be attributed to the flow stress equation implemented into the model describing the workpiece material which is critical as the temperatures, stresses, strains and strain rates are all determined from the chosen flow stress equation. Although the chosen flow stress equation correlated best with experimental results, additional refinement of the equation constants may further improve the model.

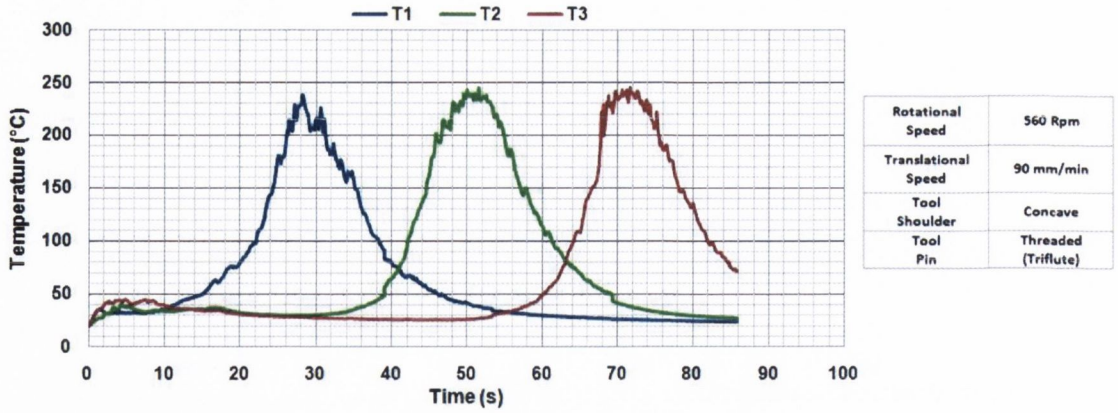


Figure 155: FEM temperature prediction

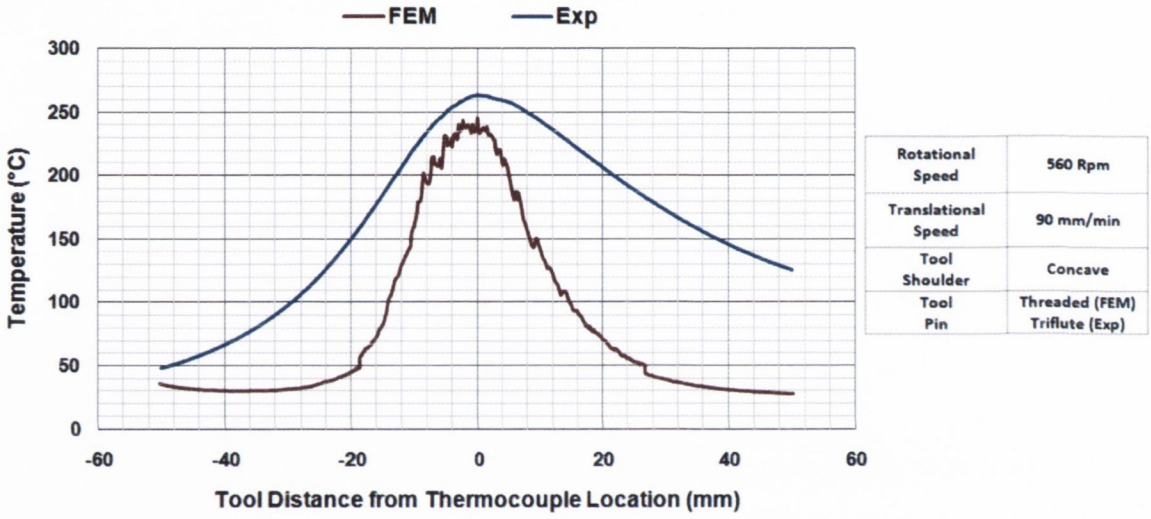


Figure 156: Comparison of experimental temperatures to those predicted by Deform.

### Force Validation

Comparison of the experimental and FEM vertical force, welding force and torque measurements are shown in Figure 157, Figure 158 and Figure 159 respectively. Similar to the experimental results, both the vertical force and torque reach maximum values during the plunge and dwell stages at shoulder contact. Also, all FEM forces reached steady state values during tool translation. The large number of peaks and troughs present in all the predicted forces are due to the intermittent contact between the tool and the workpiece nodes coupled with the large amount of remeshing required to maintain mesh integrity.

Of all the FEM predicted parameters, the torque correlated best with experimental results. Slightly larger vertical and welding forces were predicted by the model compared to the experimental results. This could be attributed to the lower temperatures predicted by the model which may reduce the softening of the workpiece and result in larger forces. However, a more reasonable explanation is that the flow stress equation does not exactly represent the behaviour of the aluminium workpiece exactly during the welding.

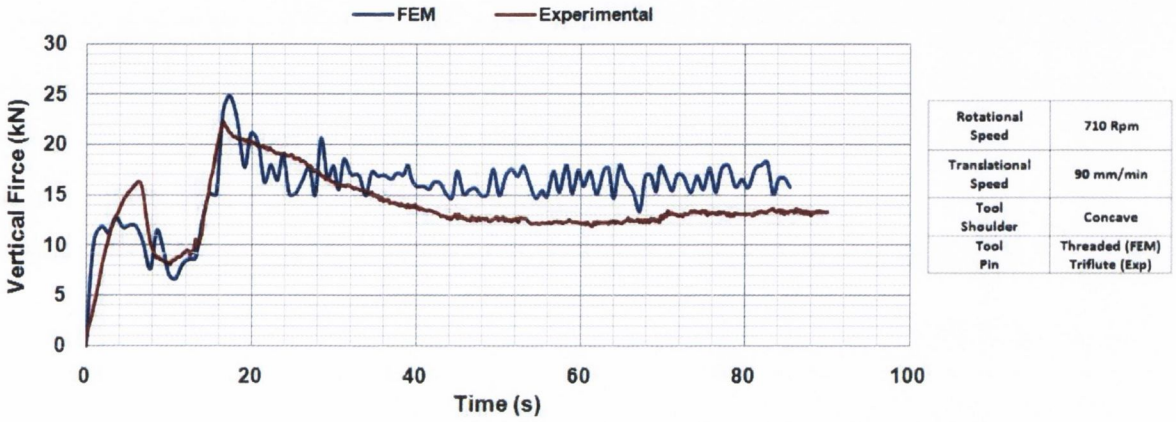


Figure 157: Comparisons of experimental and FEM vertical force

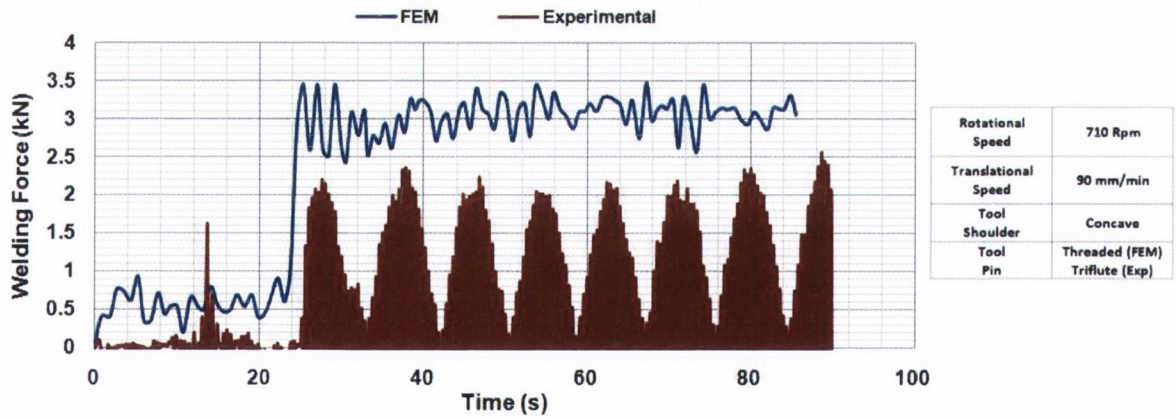


Figure 158: Comparison of experimental and FEM welding force

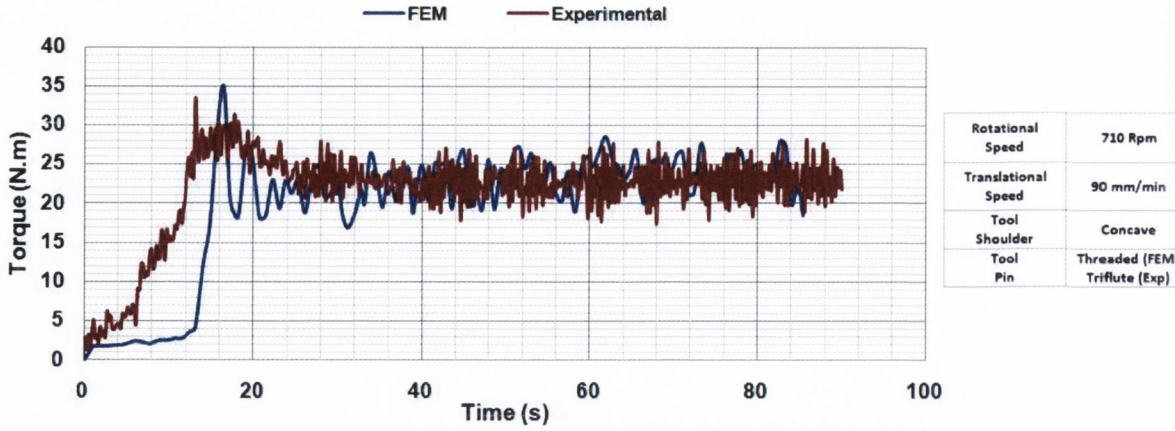


Figure 159: Comparison of experimental and FEM torque

Overall, the results from the DEFORM 3D model correlated well with experimental results and gave a good representation of the FSW process. Variation of the operational parameters (rotational and translational) within the model accurately represented the changes in the temperatures and loads recorded during experimental testing. As a result, it is proposed that the model can be used with some confidence to predict, with reasonable accuracy the temperatures and forces for different workpiece thickness, tooling designs, operational parameters and provide information on machine requirements. Furthermore, post processing analysis can predict material flow pattern, stresses, strains and thermal distribution, all of which would not be possible or difficult to measure experimentally.

### 4.9.2 FEM Thermal Analysis:

The FE model enabled prediction of the temperatures within the weld zone and also throughout the tool and backing plate. All of which could not be measured accurately by experimental techniques. Figure 160 illustrates the thermal flow through the workpiece and the tooling. As expected, the tool shoulder is subjected to higher temperatures (500+ °C) than the tool pin (380°C) because it is the primary source of heat generation (section 4.3.3). Temperatures within the workpiece reach maximum values of approximately 400°C along surfaces in contact with the tool shoulder, but are significantly lower than corresponding temperatures recorded along the tool shoulder. Therefore, it is critical that the tool shoulder material has excellent strength at elevated temperatures to prevent damage to the tool.

Another observation is that the tool acts as a local heat source generating little thermal flow throughout the workpiece outside the vicinity of the tool. Experimental results also highlighted this lack of thermal flow throughout the workpiece and this may be attributed to the large quantities of heat being conducted through the tooling and backing plate. Evidence for this can be seen in Figure 160 and Figure 161 which illustrate thermal flow throughout the tool and backing plate respectively.

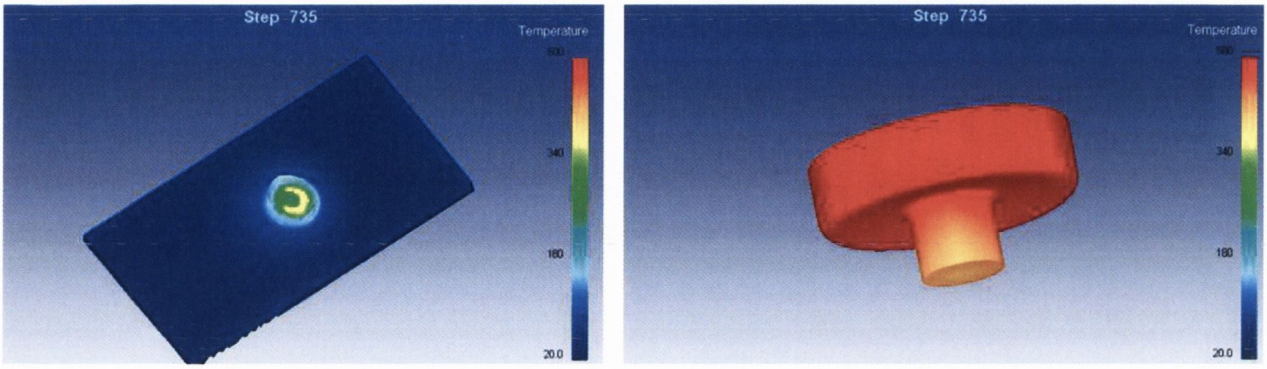


Figure 160: Thermal flow through workpiece and tool

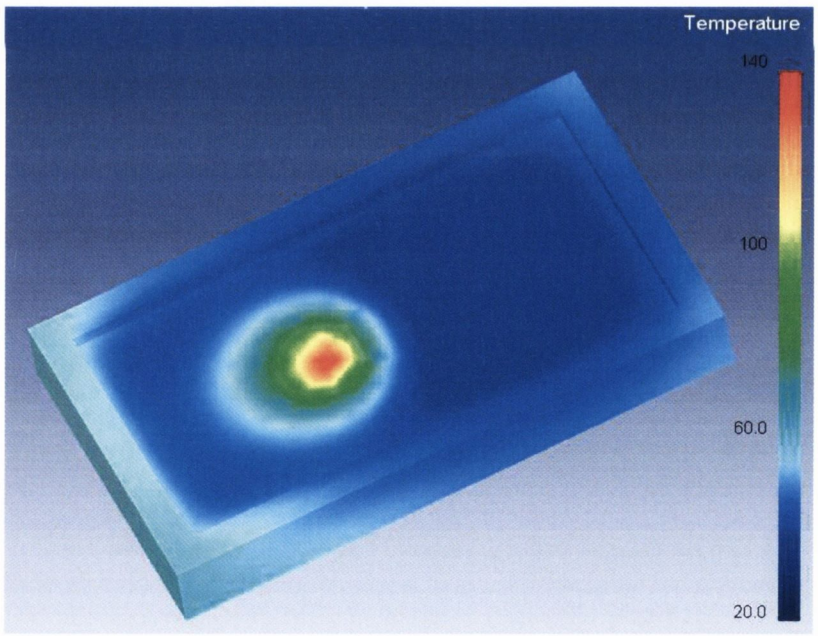


Figure 161: Thermal flow through the backing plate

The temperature across the cross sectional area of the workpiece just after the tool has past is shown in Figure 162. As expected, temperatures within the nugget are greatest along the cross sectional area. This high heat generation is necessary, along with plastic deformation, to form the recrystallized nugget zone with the TMAZ region. The heating effect of the shoulder decreases with increasing distance from the top surface and results in a V-shape thermal distribution region. A similar in shape was observed during macrostructure analysis in section 4.6.

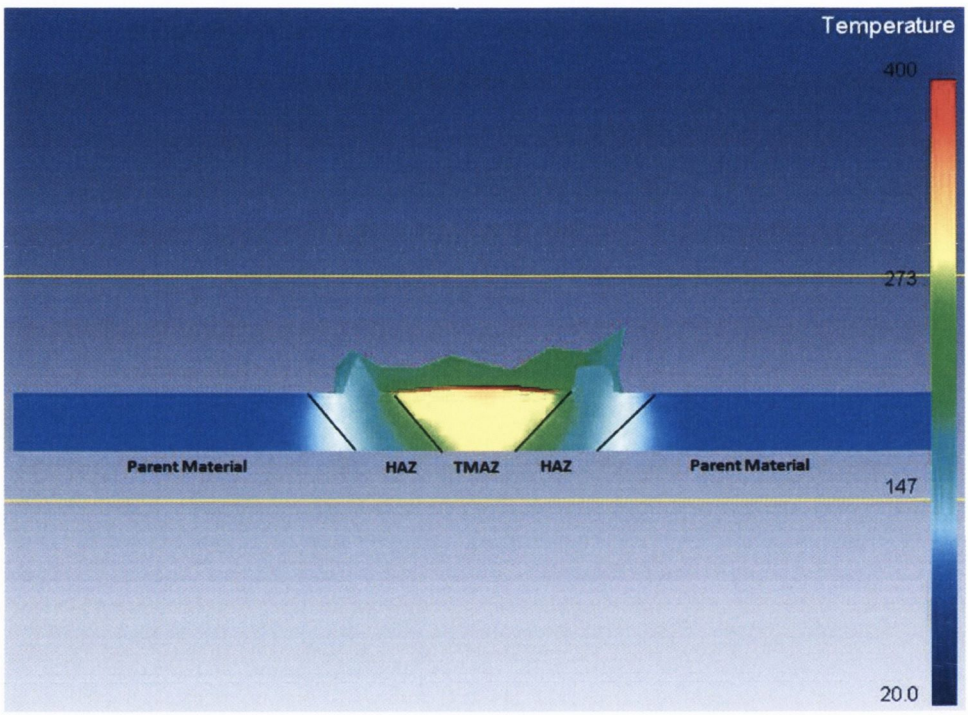


Figure 162: Thermal flow along workpiece cross sectional area

### 4.9.3 FEM Material Flow:

Using DEFORM 3D it was possible to monitor the flow of material during the FSW process. This could be achieved experimentally by embedding metal tracer particles into the workpiece at various positions and then using X-ray radiography to examine the position of the particles after the weld is completed. However, this process is expensive, time consuming and only reveals the final position of the particles compared to the DEFORM model which can monitor the position of each particle through each revolution of the tool.

The material flow along the top surface of the workpiece is illustrated in Figure 163. As expected, the tool shoulder dominates the flow of material over this region. Focusing on stage (a), points 6 – 11 and points 23-25 are initially in contact with the shoulder surface. Following these particular points through each stage it is evident that the thermal softened material is transported by the shoulder in the direction of rotation and deposited in the cavity of the concave shoulder as seen in stages (e) and (f). The material within this cavity acts as a reservoir to supply sufficient material to close/plug the hole formed by the tool pin. The forging action of the tilt angle and rotation of the pin compresses the material downward to fill the hole. Other points within the outer vicinity of the tool shoulder accumulate along the periphery of the shoulder sides and represent material flash as shown in stages (e) and (f).

A plan view of the material flow along mid thickness depth of the workpiece is illustrated in Figure 164. The material flow within this region is dominated by the tool pin. As the pin traverses, points which are close to the peripheral edges of the pin are swept in the direction of rotation and deposited behind the tool. Points tend to accumulate near the joint centreline behind the pin in chaotic arrangement. This indicates the mixing and consolidation of the two workpiece materials.

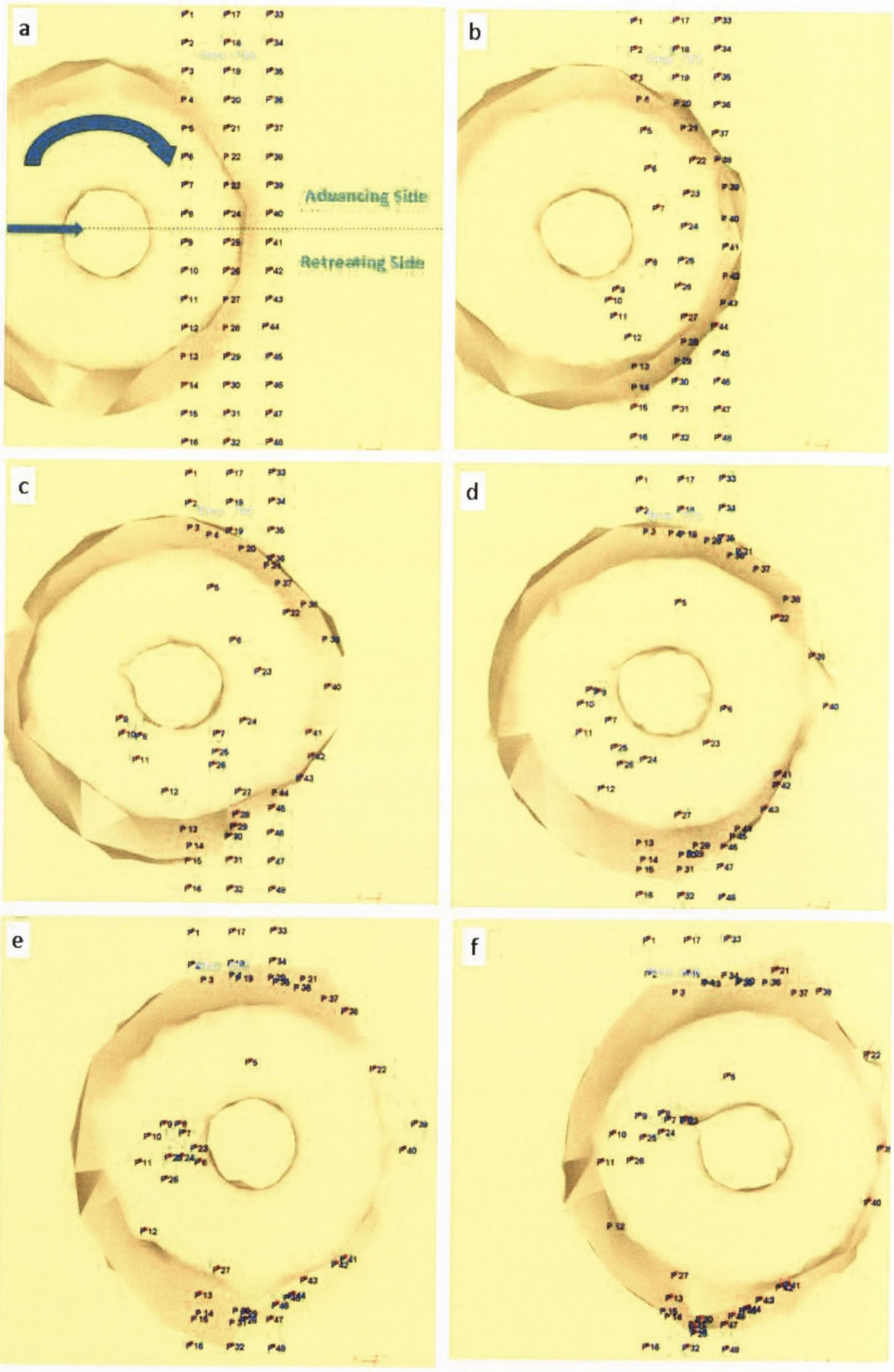


Figure 163: Material Flow along top surface

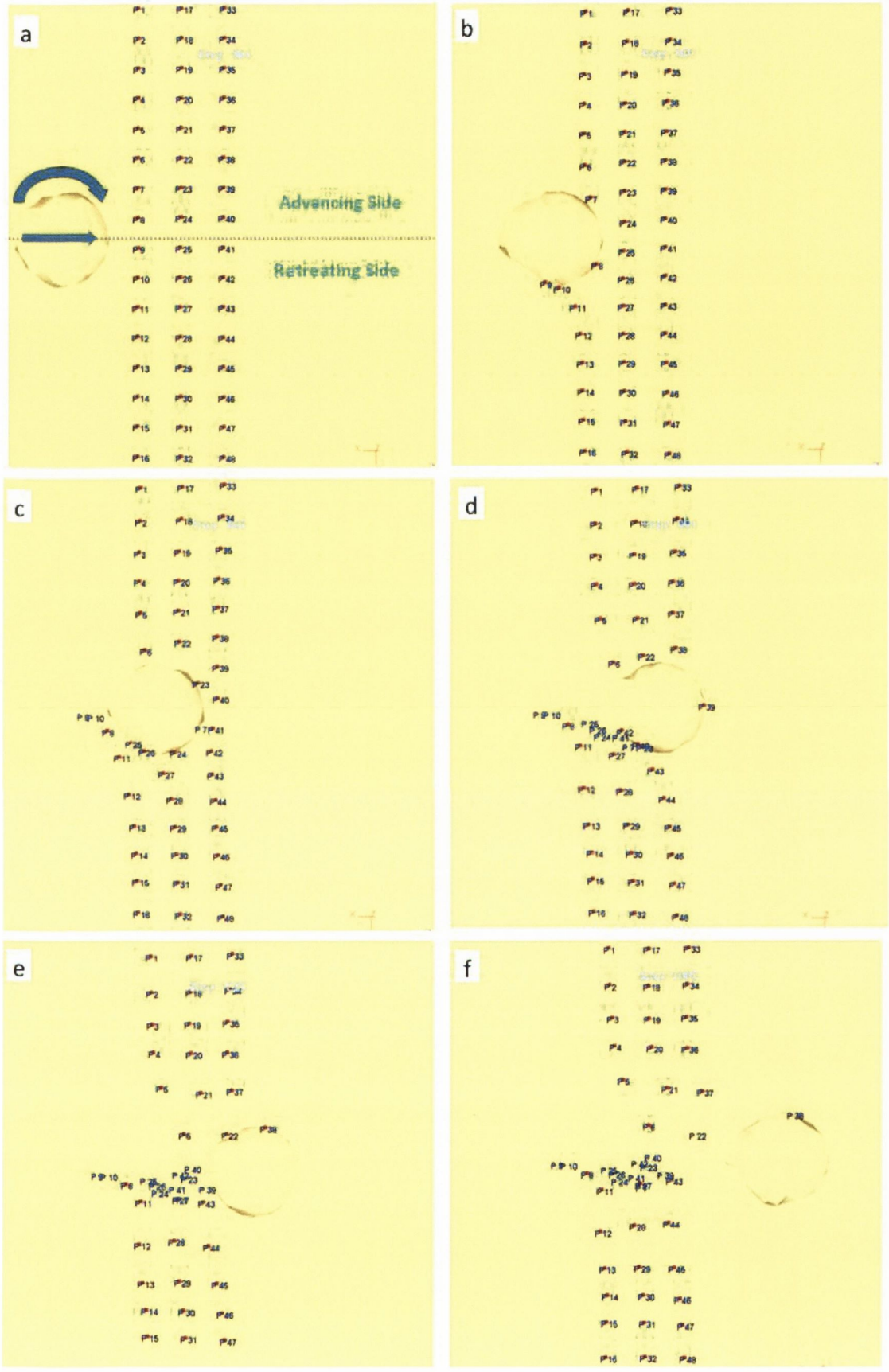


Figure 164: Material flow at mid thickness

A longitudinal view of the predicted material flow vertically through the workpiece thickness is illustrated in Figure 165. Results clearly indicate that there is vertical flow of the workpiece material during the FSW process. As the tool traverses forward, material along the leading edge of the pin is drawn slightly up towards the tool shoulder and then forced downwards along the trailing edge of the pin plugging the hole left in the tool wake.

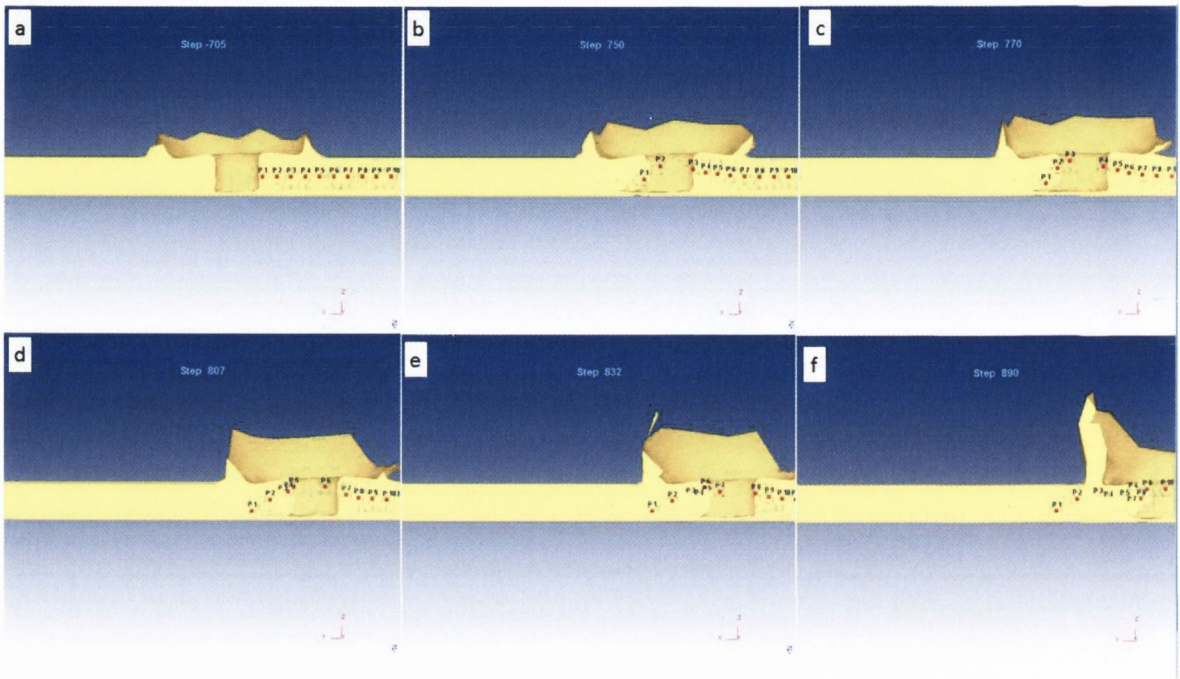


Figure 165: Material flow vertically

In section 4.5.2, it was shown that greater weld strength was recorded for the square and triflute pin designs compared to the cylindrical and tapered pins. This was attributed to the features on these pins which increased the amount of material deformation and stirring of the workpiece plates together. Evidence for this can be seen in the FE model. The material flow along mid thickness depth of the workpiece for the threaded and cylindrical pins is illustrated in Figure 166. It is evident that the threaded pin produces a more turbulent flow in the tool wake, which increases the mixing and integration of the workpiece materials. Further evidence for this can also be seen by examining the displaced contours left in the tool wake for both pins. The cylindrical pin produces considerably less displacement (plastic deformation) of the workpiece material.

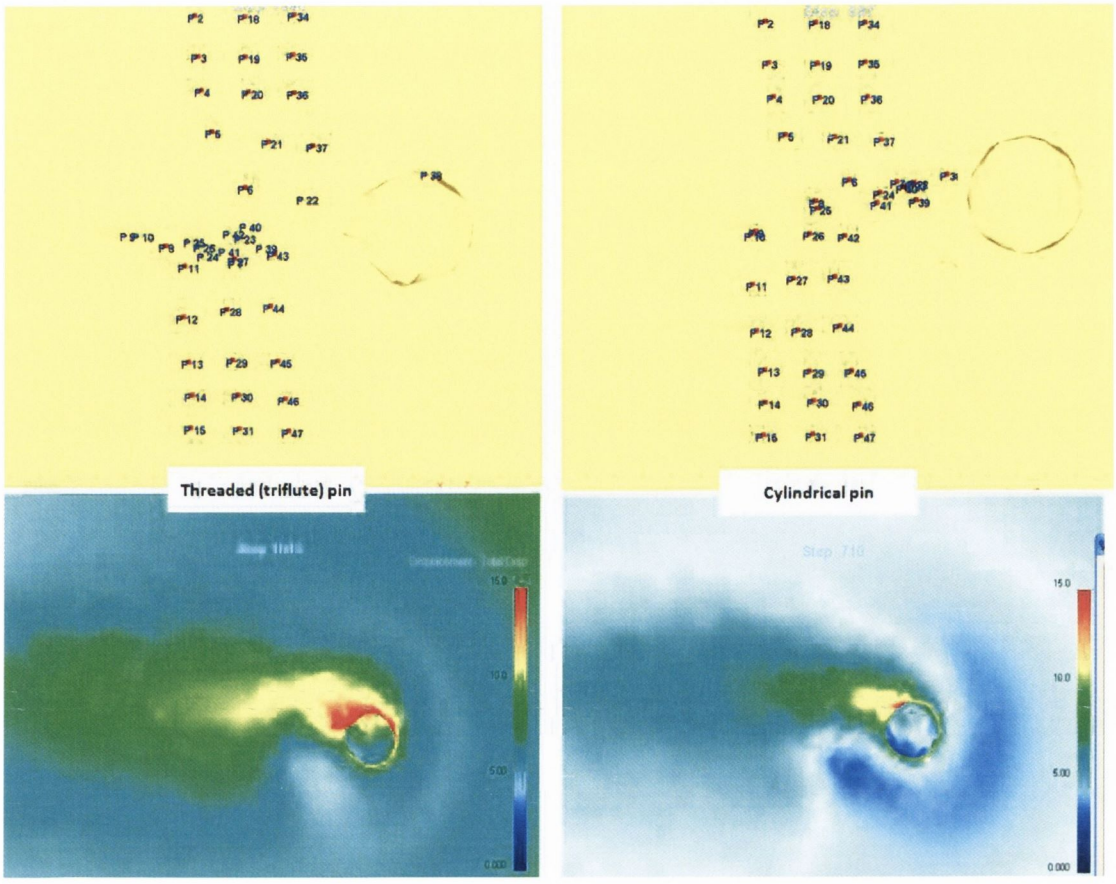


Figure 166: Material flow and displacement for different pin designs

### 4.9.4 FEM Stress and Strain Predictions:

Measuring the stresses and strains that occur during the FSW process is difficult, but the development of an accurate finite element model of the process enables relatively accurate predictions of both the magnitude and location of the most predominant stress and strains occurring during the process. However, the DEFORM 3D version used during this project (version 5.1) only enabled the prediction of stresses and strain occurring throughout the workpiece and not the tooling or the surrounding clamping. However, this may be possible using a more recent version of DEFORM 3D.

Figure 167 illustrates the strain occurring along the cross sectional area of a friction stir weld just after the tool have passed and consolidated the workpiece material together. Analysis of the strain value can help predict the location and size of the different weld zones formed by the FSW process. As expected strains are largest within the TMAZ as grains within this region are directly subjected to mechanical deformation. Significantly larger strains are generated along the central region of the TMAZ (shown in red) and represent the recrystallized nugget region. Minimal strains are predicted in the

HAZ and these can be attributed to grain growth due to the elevated temperatures within this region. The resulting V-shape of the strain contour is remarkably similar to the different weld zones that were revealed during macrostructural analysis in section 4.6.

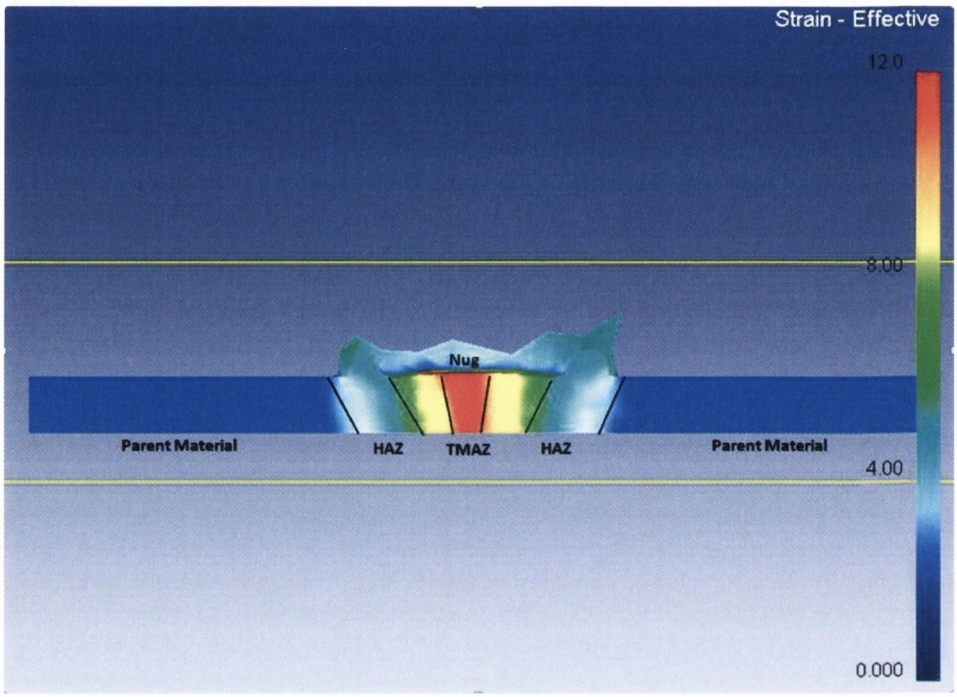


Figure 167: Cross sectional view of the strain in the weld zone

Similar to the predicted displacement of the workpiece material, larger strain values along the cross sectional area of the weld just after the tool has passed were predicted for the threaded pin compared to the cylindrical pin. This is illustrated in Figure 168. Again this highlights the increased workpiece material deformation and mixing produced by the threaded pin compared to the cylindrical pin as mentioned in section 4.9.3.

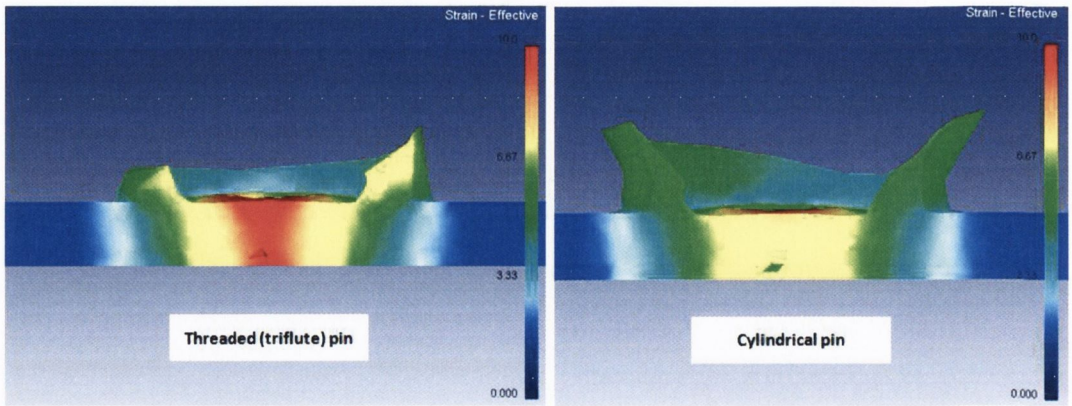


Figure 168: Effective strain for different pin designs

A longitudinal view of the effective stress acting within the workpiece is illustrated in Figure 169. Large stresses are predicted near the trailing edge of the tool, specifically where the shoulder is plunged into the workpiece surface. This can be attributed to the large vertical force (section 4.4.1) required to produce the forging action on the workpiece necessary to produce a consolidated weld. Large stresses were also predicted around the pin, these can be attributed to the welding force (section 4.4.2) acting against the tool pin as it traverses along the joint line. Although DEFORM was not capable of predicting the stresses acting on the tool, an examination of the location of stresses acting on the workpiece can give a good indication of where the tool is most likely to fail due to fracture or wear. The FE model indicates that the tool shoulder is most like to fail before the tool pin due to the larger stresses and temperatures generated in these regions. Experimental results also indicate that the welding force was not significant enough to cause pin failure, even at high translational speeds of 500mm/min. Therefore, during FSW of AA2024-T3 plates of 4.82mm thickness, wear of the tool shoulder is mostly likely to occur before either pin wear or fracture.

In section 4.3.5, reduction of the forces acting on the FSW tool was partly attributed to increased softening of the workpiece material due to increased heat generation. Evidence of this can be seen in Figure 170 which illustrates the temperature and stress within the workpiece during plunging of the tool. It is clearly evident that as the tool is plunged deeper into the workpiece and the temperature increases, the stress decreases significantly.

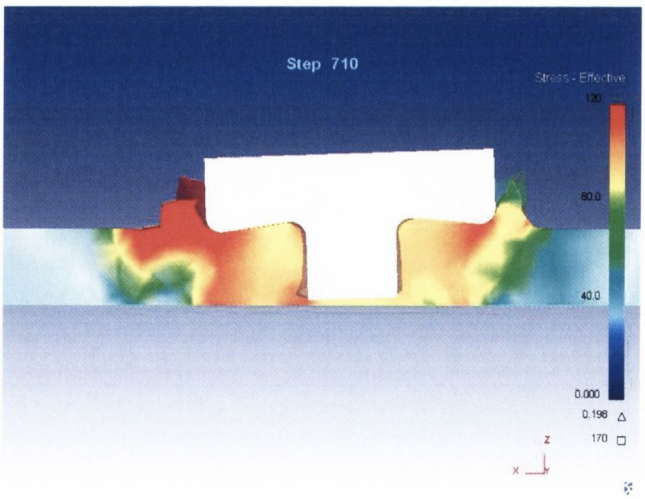


Figure 169: Longitudinal view of effective stress

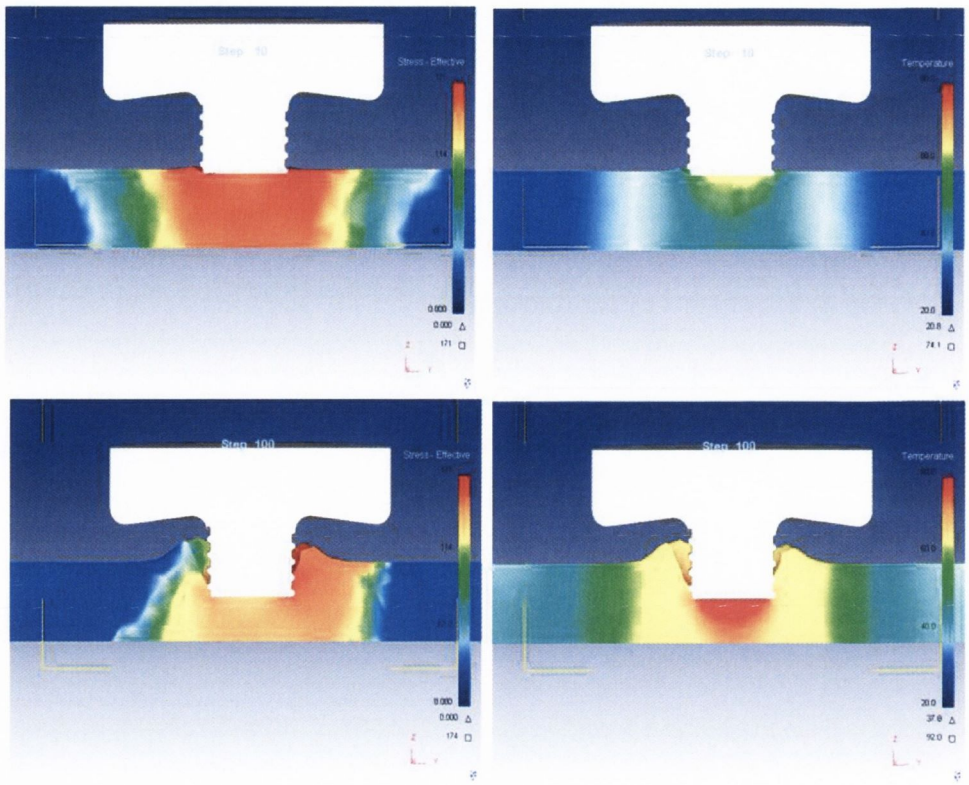


Figure 170: Effective stress at different temperatures

## 4.10 Summary of Results and Discussion:

### Process Specification on Plunge Depth and Pin length

When using the scrolled shoulder the optimal plunge depth was reached when the shoulder was plunged 0.3 – 0.5 mm into the workpiece surface. However, when a concave shoulder was used the optimal plunge was reached when 70 – 80% of the shoulder was in contact with the workpiece surface. An insufficient plunge depth produced welds with visible cracking and/or surface voids along the top surface. Whereas an excessive plunge depth produced excess flash and higher tool/machine forces. The optimal pin length was achieved when the clearance distance between the tip of the pin and the root of the weld during FSW was maintained at 0.1 – 0.2 mm. An Insufficient pin length resulted in the formation of root flaws and an excessive pin length increased the risk of the tip of the pin striking the backing plate and damaging the tool.

### Tooling Design and Performance

Four different pin designs (Triflute, Square, Cylindrical and Tapered Cylindrical), all having an effective dynamic area of 38.48 $mm^2$ when rotating, were used during FSW testing. The features on the triflute pin (flutes and threads) and the flat faces of the square pin increased the amount plastic deformation and mixing of the two plates and as a result produced stronger welds compared to welds produced using the cylindrical and tapered pin designs. The cylindrical and tapered pins did not have any flutes or flat faces to produce any enhanced stirring effect and consequently a lot of the plasticized material is simply allowed to extrude around the smooth sides of the pin. As a result tools having a smooth pin surface area will produce less mixing of the workpiece material, thereby resulting in a weaker weld. Further evidence of inadequate mixing of the workpiece material was found during subsequent microstructural analysis (evidence of tunnel flaws, root flaws, smaller nugget zones and TMAZ) for the cylindrical and tapered pins. The simple square shape produced equal, and in some case better, weld properties than the more expensive complex triflute shape.

The three flute design of the triflute pin reduces the volume of tool pin material and can increase the risk of pin failure when welding thicker or denser materials. Therefore, when pin failure becomes a limiting factor in FSW the triflute pin design may not be appropriate. A recommended pin design from the results produced during this project is one which has flats, threads and a tapered machined onto it. The flats and threaded features which promote a stirring action similar to the square and triflute pin. The taper and flats (instead of flutes) will provide greater strength and stability when welding thicker or more dense workpiece plates together.

Two different shoulder designs (Concave and Scrolled) and two different shoulder diameters (18mm and 22mm) were also investigated. Although no significant difference in weld strength was recorded for the Concave and Scrolled designs, higher translational speeds were recorded when using the scrolled shoulder due to a reduction in tool lift. Also, welding with a zero tilt angle was possible when using a Scrolled shoulder. Due to these advantages the scrolled shoulder is more preferable. Increased weld strength and elongation were recorded using the 18mm shoulder diameter compared to the 22mm diameter. This was attributed to the thermal damage caused by the 22mm shoulder which resulted in a higher heat input with a slower cooling rate which can cause partial reversal of the heat treatment the alloy initially underwent, tempering and softening of grains and severe clustering of CuAl precipitates.

Overall a combination of an 18mm scrolled shoulder design with either a triflute or square Pin is recommended because of increased strength and ductility, increased translational speeds and increased flexibility during non-linear welding of 4.82mm thick AA2024-T3 plates.

**Heat Generation and Temperature Measurement**

A combination of Type K thermocouples and a thermal imaging camera was used to monitor the heat generation occurring during FSW testing. During the translational stage of the process, thermocouples placed at identical distances from the joint line indicated steady state temperature measurements. The translational speed was found to have a greater effect on heat generation than the rotational speed. However, this was attributed to the relatively small 18mm shoulder diameter which reduced the heat generated due to

rotation. However, higher temperatures were recorded when the 22mm shoulder diameter was used due to increased surface area contact with the workpiece surface and greater peripheral velocities. In general, larger temperatures were recorded for low translational speeds and high rotational speeds.

The tool shoulder was found to be the primary source of heat generation and the tool pin the secondary source generating approximately 93 % and 7% respectively of the total heat. As a result, the tool pin design did not have a significant effect on the temperature recorded. Results on the thermal flow indicated that the tool acts as a local heat source generating little thermal flow throughout the workpiece. This was attributed to large thermal conduction through the backing bar and tool which act as major heat sinks. Therefore, in future work methods of temperature control could focus on a cooling system incorporated into the design of the backing bar, to focus on the path followed by tool. Or even a cooling system within the tool itself.

**Force Monitoring**

A Kistler Rotating 4-Component Dynamometer was used to measure the forces acting on the tooling/machine during welding. Both the vertical force and the torque reached peak values during plunging of the tool when the shoulder makes contact with the workpiece surface. Therefore developing new techniques of tool entry and tooling design may help reduce these peak values. Similar to the temperature measurement all the forces (vertical force, welding force and torque) were found to reach steady state values during the translation of the tool.

The vertical force was the largest force encountered and is therefore the limiting factor in FSW machine design. A reduction of the peak vertical force was achieved through increased rotational speeds and a reduction in plunge rates. However, low plunge rates increase production time which is not desirable for industrial applications. Nevertheless, it is possible to use a large rotational speed during the plunge and dwell stages to reduce the maximum vertical force and then switch to a lower optimal rotational speed (promote optimal weld strength) during the translational stage. Also, a reduction in the peak vertical force was achieved using a triflute pin design. This was due

to the increased material deformation produced by its threaded and flute design, and also due to its smaller volume compared to the other pin geometries. The translational speed was found to have the most significant effect on the steady state vertical force. A reduction in the vertical force was recorded for low translational speeds due an increase in heat generation. However, again this reduced speed will increase the production time of the process. Larger vertical force values were also recorded when the shoulder diameter was increased from 18mm to 22mm and also when the plunge depth was increased. An overview of the parameters influencing the vertical force is given in Figure 171.

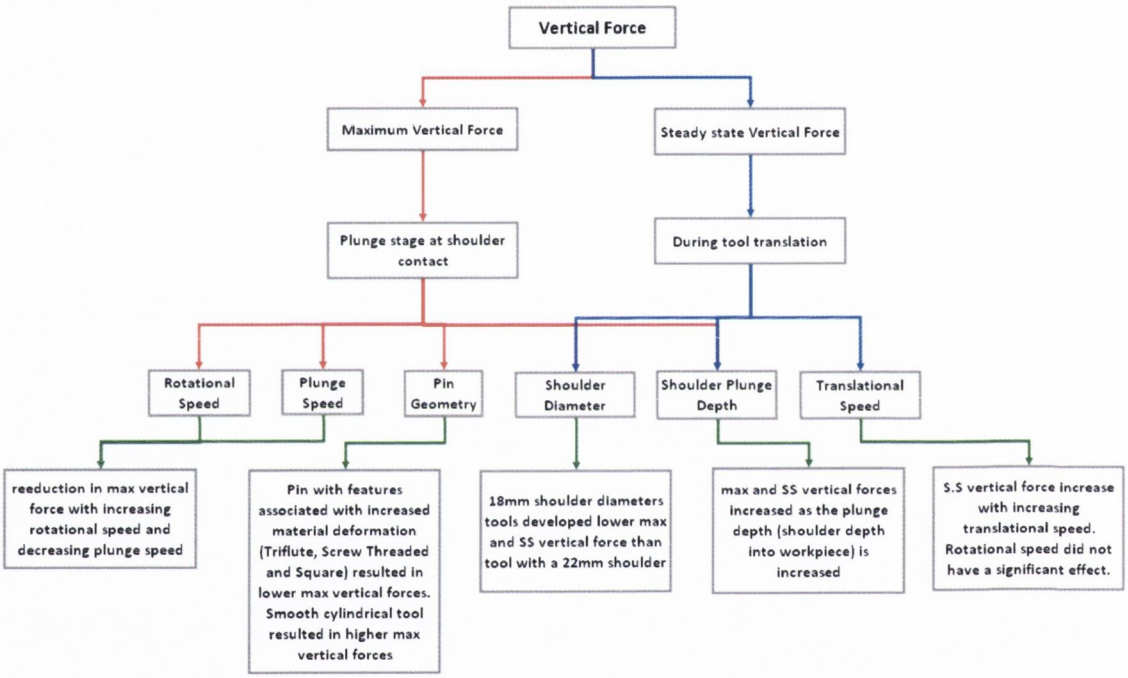


Figure 171: Overview of parameters influencing the vertical force

The magnitude of the welding force was significantly lower than the vertical force and is therefore not a limiting factor in terms of FSW machine design. Also, tool fracture did not occurring during this project even at a high translational speed of 500mm/min and hence the translational speed was not limited by tool fracture. However, it is expected that the risk of tool fracture will be more significant for larger workpiece thicknesses as the tool will encounter greater resistance. The translational speed was found to have the most significant effect on the welding force, large increases in the welding force was recorded with increasing translational speeds. A reduction in the welding force was also recorded when using the triflute and square pins compared to the

cylindrical and tapered pins. Therefore tool pin designs which enable the workpiece material to be processed more efficiently can be identified by monitoring this force. Slightly larger welding force was also recorded when the plunge depth and shoulder diameter were increased. An overview of the parameters influencing the welding force is given in Figure 172.

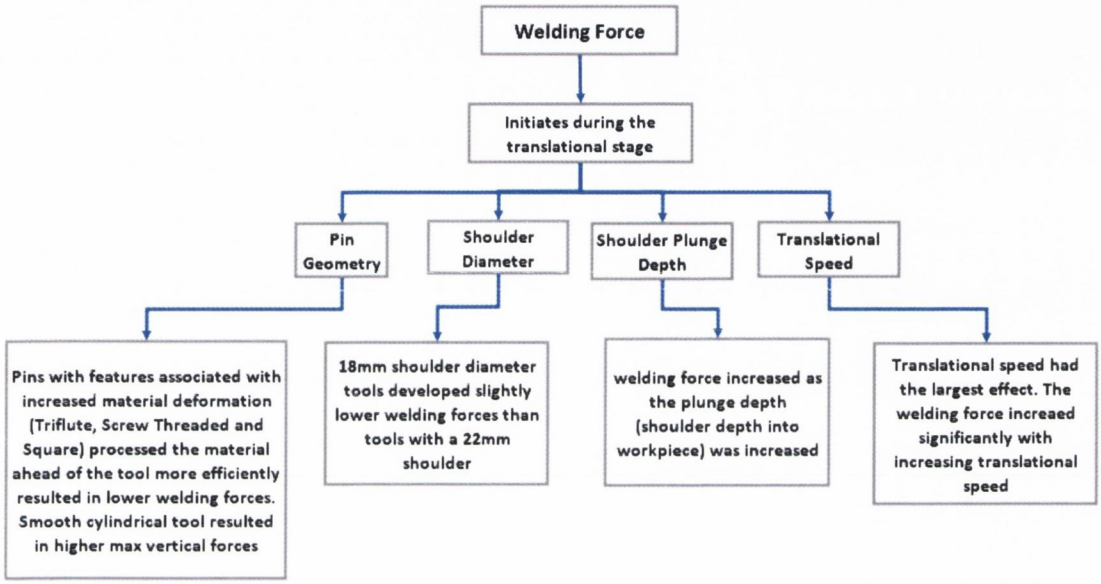


Figure 172: Overview of the parameters influencing the welding force

Changes to the rotational speed were found to have the greatest effect on the tool torque compared to the other operational parameters. This was expected as torque is a rotary force measurement. Large reductions in both the maximum and steady state torque values were recorded when the rotational speed was increased. Lower plunge rate and translational speeds also resulted in a reduction in torque. However, this resulted in increased production times which are not desirable for industrial applications. Variation in the pin design did not have a significant effect on the torque, however, increasing the shoulder diameter and plunge depth did result in larger torque values. An overview of the parameters influencing the torque is given in Figure 173.

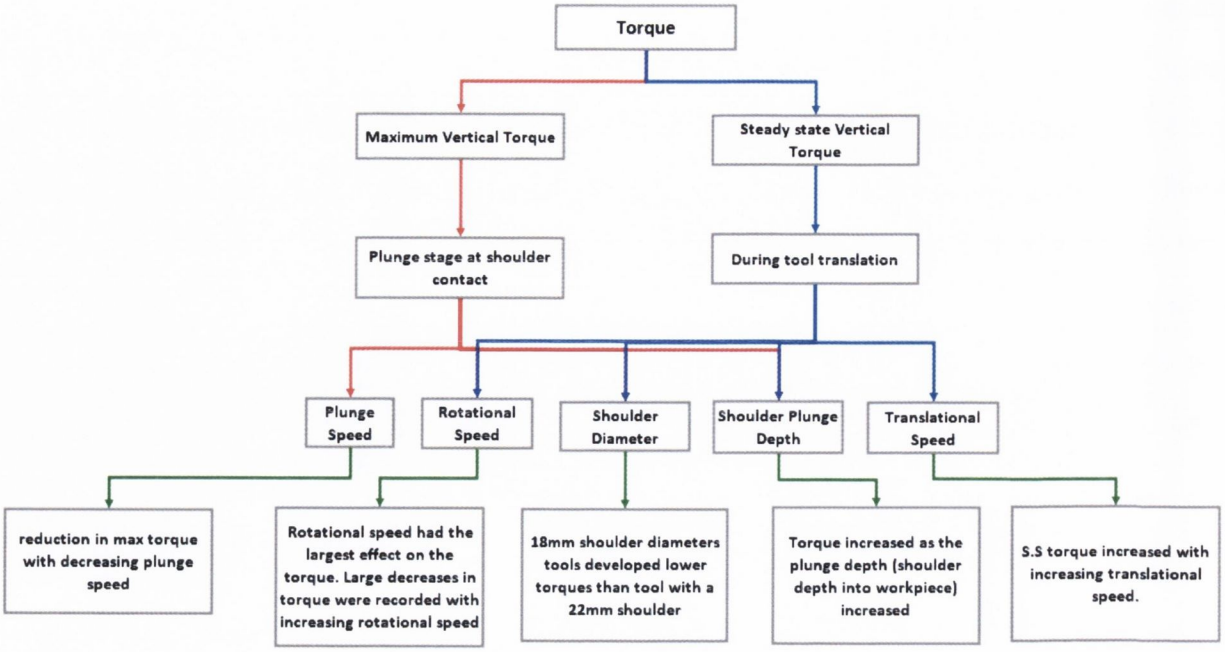


Figure 173; Overview of the parameters influencing the torque

**Post Weld Analysis**

Post weld analysis consisted of tensile tests, microstructural analysis and microhardness testing for a range of welds fabricated using different operational parameters in order to establish a processing window for the appropriate operational parameters to achieve optimal results. The results confirmed that a processing window does exist and that variation of the operational parameters leads to a progressive change in the weld strength rather than random erratic results. Optimal weld strength (above 85% - 95% of that of the parent material) was achieved using a translational speed in the range 125 – 250 mm/min combined with a rotational speed in the range of 355 – 560 rpm. Operational parameters outside this range resulted in thermal damage due to overheating, tunnels voids and surface defect due to either excessive or inadequate material deformation, all of which resulted in a reduction in weld strength.

These optimal parameters disagree with previous researcher who generally implements higher rotational speed between 1200 – 2140 rpm and translational speeds between 40 – 75 mm/min, perhaps with the idea that lower translational speeds and higher rotational speeds will produce more mixing of the workpiece material and hence produce stronger joints. However, the weld achieved joint efficiencies of only 60 – 76% of the parent material. The parameters identified during this research not only produce

greater weld strength but also reduce the energy input and the process time. From these results it is clearly evident that the amount of mechanical energy required to thermally soften and mix the workpiece material together has been over estimated by previous researchers.

Repeat testing was found to be relatively consistent with a maximum standard deviation of approximately 7%. However, none of the welds retained similar ductility to that of the parent material. This can be attributed to the complex grain structure and thermal damage produced during the friction stir welding process leading to a heterogeneous composite structure which posses different mechanical properties throughout the weld zone. Translational speeds above 250mm/min did not allow sufficient time for the rotary action of the tool to produce a consolidated weld and hence large tunnel voids were visible along the surface of the workpiece. Therefore, high translational speeds are limited by the formability of the workpiece and hence tooling designs which can process the workpiece material more efficiently may be capable of welding at higher translational speeds.

Microhardness testing and microstructural analysis revealed a complex weld region that varied along the width of the cross sectional area (due to the difference in size of the shoulder and pin) and also through the thickness of the workpiece (due to the action of the shoulder decreasing with workpiece depth). Using the results from microhardness tests it was possible to predict the approximate weld strength and the fracture location. Provided no defects were present, fracture occurred in the region of lowest harness which was most commonly found in the transition from the TMAZ to the HAZ. This weakness was attributed to dissolution, coarsening and overaging of the strengthening precipitates due to the thermal cycle without recrystallization occurring in this region. Variation of the rotational and translational speeds had the most significant effect on the microhardness. A reduction in the size of the TMAZ - HAZ region with an increase in hardness was found for high translational speeds due to a reduction in heat input. However, as mentioned previously tunnel defects occurred at high translational speeds. Therefore it is expected that improved tooling designs that will enable the workpiece material to be processed more efficiently will not only increase production times but will also improve the weld strength. High rotational speeds increased the

hardness in the nugget region due to increased material deformation but this also reduced the hardness and increased the size of the TMAZ – HAZ region due to increased heat input. A weld with a more uniform microstructure (similar to the parent material) would be ideal. Transition towards this could be achieved by reducing the amount of softening occurring in the TMAZ – HAZ through a reduction in shoulder diameter and hence heat input. Another alternative would be to investigate the possibility of welding with a non-rotating tool shoulder.

**Finite Element Model**

A full 3D finite element model of the FSW process was created using DEFORM 3D. The flow stress equation developed from the Johnson Cook material law gave the best representation of the process. The model was validated by comparing experimental loads and temperatures to those predicted by the model. The Deform 3D model correlated well with experimental results and gave a good representation of the FSW process. Similar to experimental results, both the torque and vertical forces reached peak value during the plunge stage, and all forces and temperatures reached steady state value during the translational stage. However, temperatures predicted by the model were slightly lower than experimental temperature and the loads were slightly greater. Additional refinement of the constants in the flow stress equation may further improve the model.

The model was capable of predicting the thermal flow throughout the entire workpiece, the tooling and the backing plate. The model could also predict the stresses, strains and material displacement within the workpiece. Maximum temperature and stress were predicted through or around the vicinity of the tool shoulder. This indicates that the tool shoulder is more like to fail due to wear before the tool pin. Therefore, it is critical that the tool shoulder material has excellent strength at elevated temperatures to prevent damage to the tool.

Thermal flow and strain contours along the cross sectional area of the workpiece gave an indication of the location and size of the different weld zones. Large strains and temperatures were predicted within the Nugget zone and TMAZ due to dynamic recrystallization and plastic material deformation within these zones. The shape of the

contours was remarkably similar to the different weld zones that were revealed during macrostructural analysis.

The model also proved useful in predicting the effect of tool shape on the material flow during the FSW process. Pin designs with features such as a threaded pin produced a more turbulent flow in the tool wake, which increases the mixing and integration of the workpiece materials compared to a smooth cylindrical pin design. Greater straining and displacement of the workpiece material was also predicted by the threaded pin. This correlated well with experimental tensile tests, where greater weld strengths were achieved by welds produced by pin with features such as the triflute and square pins compared to smooth pins such as the cylindrical and tapered pin design.

# Chapter 5

# Conclusions and Future Work

## 5.1 Conclusions:

When this project was initially undertaken the primary objectives were as follows:

1. Development of a FSW rig that can accommodate a range of different research instrumentation to monitor the FSW process.

2. Develop specific guidelines on how the FSW process should be implemented with respect to the chosen workpiece material.

3. Design, manufacture and test a number of complex tooling designs to determine which tooling arrangement produces optimal results.

4. Monitor the temperatures occurring during the process to get a better understanding of heat generation and thermal flow.

5. Characterize the forces and temperatures occurring during the process to get a better understanding on tooling/machine design and requirements

6. Develop a processing window for a range of different operational parameters to determine their effect on the resultant welded joint.

7. Develop a fully couple thermo mechanical FE model capable of modelling the FSW process.

The conclusions taken from this project are outlined below:

1. **FSW Rig:** A Correa vertical milling machine was modified to perform the FSW process during this project. A Kistler rotating 4-component dynamometer was incorporated on the welding rig to record the forces acting on the tool and machine, and a combination of type K thermocouples and infrared camera were used to record the temperature.

2. **Optimal Plunge Depth and Pin Length:** Process specifications on the optimal plunge depth and pin length were established. When using the scrolled shoulder an optimal plunge depth was reached when the shoulder was plunged 0.3 – 0.5 mm into the workpiece surface. However, when a concave shoulder was used an optimal plunge was reached when 70 – 80% of the shoulder is in contact with the workpiece surface. An optimal pin length was found when a clearance distance of between 0.1 – 0.2 mm was maintained between the tip of the pin and the root of the weld during FSW.

3. **Optimal Tooling Design:** A number of different tool pin and shoulder designs were tested. A tool consisting of an 18mm scrolled shoulder with a triflute or square pin design is recommended in terms of: increased strength and ductility due to increased plastic deformation, increased material processing and a reduction of the HAZ, increased translational speeds due to a reduction in tool lift and increased flexibility during non-linear welding.

4. **Temperature Monitoring:** Steady state temperatures were measured during the translational stage. The translational speed was found to have a greater effect on heat generation than the rotational speed when an 18mm shoulder was used. However, higher temperatures were recorded when the 22mm shoulder diameter was used due to its increased surface area contact and greater peripheral velocities. The tool shoulder was identified as the primary source of heat generation and the pin a secondary source. Results on the thermal flow indicated that the tool acts as a local heat source with significant thermal conduction through the backing plate and tooling.

5. **Force Monitoring:** All the forces acting on the FSW tooling/machine were measured and the magnitude of their impact on the process was established. The effect of varying the operation parameters and tooling design on the tool forces was also determined to help identify methods of reducing these forces and enhancing tooling designs. Both the vertical force and the torque reached peak values during the plunging of the tool. All forces (vertical force, welding force and torque) were found to reach steady state values during the translation of the tool. The largest force encountered was the vertical force and is therefore the limiting factor in FSW machine design. The main factors influencing the vertical force were the translational speed, shoulder diameter and plunge depth. The magnitude of the welding force was significantly lower than the vertical force and was not large enough to cause pin fracture. Therefore the welding force is not the limiting factor in machine design or increasing the translational speed. The main factors influencing the welding force were the pin design and translational speed. Also, tool pin designs that enable material to be processed more efficiently can be identified by monitoring the welding force. Measurement of the torque gave an indication of the weld power input. Changes to the rotational speed were found to have the greatest effect on the torque compared to the other operational parameters.

6. **Processing Window and Post Weld Analysis:** A processing window was developed to determine which operational parameters should be implemented to achieve optimal results. Optimal weld strength (85 – 95% of that of the parent material) was achieved using a translational speed in the range 125 – 250 mm/min combined with a rotational speed in the range of 355 – 560 rpm. These parameters not only produce greater weld strength but also reduce the energy input and the process time compared to previous research which recommends higher rotational speeds and lower translational speeds. From these results it is clearly evident that the amount of mechanical energy required to thermally soften and mix the workpiece material together has been over estimated by previous researchers. Repeat testing was found to be relatively consistent with a maximum standard deviation of approximately 7%. However, welds did not retained similar ductility to that of the parent material due to the complex heterogeneous weld

structure produced with grains of different shapes and sizes within the different weld zones. Further improvement to weld strength and in particular the ductility can only be achieved by reducing the heat input and producing a more uniform grain structure throughout the different weld zone.

7. **Finite Element Analysis:** A 3D model of the FSW process was successfully modelled using the finite element package Deform 3D. The model correlated well with experimental results and gave a good representation of the FSW process. As a result, the model could be used to accurately predict the temperatures and forces for different workpiece thickness, tooling designs, operational parameters and provide information on machine requirement. The model was capable of predicting the thermal flow throughout the workpiece, tooling and backing plate. The model could also predict the stresses, strains and material displacement within the workpiece. The FE model predicted that tool failure is most likely to occur by wearing of the tool shoulder due to the large stresses and strain predicted along the tool shoulder. The shape, location and size of the different weld zones were predicted by examining the strain and temperature contours along the cross sectional area of the weld. The model also proved useful in predicting the effect of tool shape on the material flow during the FSW process. Greater straining and displacement of the workpiece material was predicted for tool pin with features compared to smooth pin designs. This correlated well with experimental results.

## 5.2 Recommended Future Work:

**Joining Aircraft Stringers to Skin Panels**

The work presented throughout this project focused on the FSW of AA2024-T3 plates in a butt joint configuration. The main aerospace application of this type of process would be in the joining of aircraft skin panels together along the wingspan and fuselage. However another area of particular interest within the aerospace industry is the joining of aircraft stringers to skin panels. AA7075 is typically used for the aircraft stringer due to its greater strength compared to other series of aluminium alloys and as shown within this project, AA2024 is commonly used for aircraft skin panels. At present, these components are joined using rivets in a lap joint configuration. Future work could focus on the feasibility of friction stir lap welding of AA7075 stringers onto AA2024 skin panels (Figure 174). This research would present greater challenges than the present project as it would involve the FSW of dissimilar materials and also the welding of lap joints which are more prone to defects such as hooking, root flaws, top plate thinning and voids compared to butt joints.

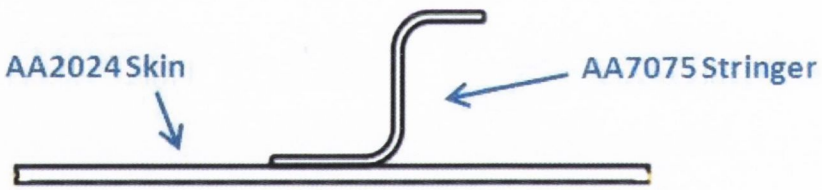


Figure 174: Lap joint of AA7075 stringer onto AA2024 Skin

**Controlling Large Vertical Forces**

One of the key limitations highlighted during this project concerned the large vertical forces required to produce a good quality weld. The vertical force is the limiting factor in machine design as adequate strength, power, stability and size is required to deliver and support these forces. Furthermore, a backing plate is required to support the reaction force and this adds to the complexity of the welding rig and reduces the flexibility of the process. A recent tool development by TWI is the Bobbin Tool (Figure 175) which has two shoulders acting on both the top and bottom surfaces. The two shoulders are joined by the tool pin from which rotation and torque is transmitted from the upper shoulder to the lower shoulder. The tool enters the workpiece from a horizontal position rather than a vertical position which was employed during this project. The shoulders react against one another, thereby reducing the vertical force to approximately zero and removing the need for a backing plate enabling more flexible applications and smaller machinery. The two shoulders also supply a uniform heat input which helps reduce distortion and also prevents the occurrence of root flaws. Similar to the triflute pin and scrolled shoulder design, there is only a limited amount of research and information on the performance of the Bobbin tool as TWI tends to keep their most recent/advanced tooling designs and results confidential to companies holding one of their FSW licences. Even papers that do report on the use of the Bobbin tool do not give any great detail of the design, operational parameters, results and process specifications. Therefore future work could also focus on the design and testing on a Bobbin tool design.

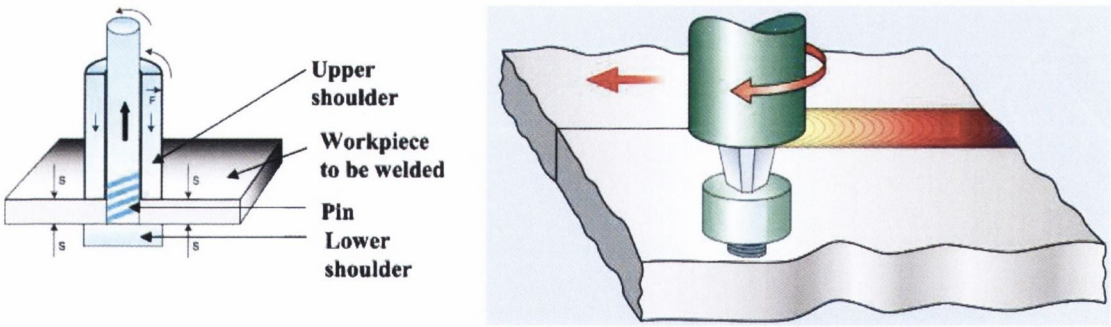


Figure 175: Schematics of FSW Bobbin tool

**Finite Element Modelling**

Future work could also focus on improving the 3D FE model through further refinement of the material constants within the flow stress equations and using a more recent version of the package such as DEFORM 3D version 10.1. This may reduce computational time and the ability to simulate more complex tooling. DEFORM could also be used to model the lap joining of dissimilar materials and the Bobbin tool as mentioned in the previous two sections.

# Chapter 9

# References


1. W.M. Thomas, Friction-stir butt welding. GB Patent No. 9125978.8, International patent application No. PCT/GB92/02203, 1991.

2. Friction Stir Link, description of the friction stir welding process, accessed on 07/06/2011, http://www.frictionstirlink.com/desc.html.

3. L.E. Murr, Y. Li, R.D. Flores, E.A. Trillo, Mater. Res. Innovat. 2 (1998) 150.

4. Y. Li, E.A. Trillo, L.E. Murr, J. Mater. Sci. Lett. 19 (2000) 1047.

5. Y. Li, L.E. Murr, J.C. McClure, Mater. Sci. Eng. A 271 (1999) 213.

6. R.S. Mishra and Z.Y. Ma, Mater. Sci. Eng. R, 50 (2005) 1

7. Aluminium and Aluminium Alloys ASM international: ASM speciality handbook

8. The Welding Institute UK, principle of the friction stir welding process invented at TWI, accessed on 07/06/2010, http://www.twi.co.uk/content/spjgpmar07.html.

9. W. Plot, A little friction at Boeing, Boeing Frontiers Online, Vol. 03 (2004) 5, accessed on 14/08/2011, http://www.boeing.com/news/frontiers/archive/2004/september/i_tt.html

10. Brent Christner, Eclipse Aviation Corporation, FSW System Development for Thin-Gauge Aerospace Structures, Fourth International Conference on FSW, May 2003.

11. Marine Aluminium, Friction Stir Welding Capabilities, 2011, accessed 16/08/2011, http://www.marine-aluminium.com/frictionstirwelding1.cfm

12. University of Wisconsin-Madison, News archive 2010, Friction stir welding fuses engineering research and Wisconsin industry, accessed on 17/08/2011, http://www.engr.wisc.edu/news/archive/2010/Nov05.html

13. Mazda the first to use friction stir welding for aluminium body assembly, Aluminium Now Online, Vol 5, May 2003, The Aluminium Association, accessed 02/06/2011, http://www.aluminium.org/ANTam

14. Fontaine Trailers, accessed on 05/08/2010, http://www.fontainetrailer.com/pdfs/Revolution%20Aluminum.pdf

15. Hitachi Rail, Products and Services, FSW, accessed on 08/08/2011, http://www.hitachi-rail.com/products/rv/a_train/features/index_2.html

16. C.Schilling, RIFTEC GmbH, Germany, FSW Serial Production of Aluminium Drying-Trays from the Food Industry, 5th International Conference on FSW, Sept 2004.

17. C.G. Anderson, R.E. Andrews, Fabrication of Containment Canisters for Nuclear Waste by FSW, First International Conference on FSW, June 1999

18. Application of FSW machinery used in Boeing Co., Delta II programme of space rockets, accessed on 18/06/2011, http://www.fswelding.com/application-of-friction-stir-welding-in-aircraft-structures/examples-of-machinery-used-by-industrial-producers

19. TWI course, An Introduction to FSW, Rotherham, United Kingdom, 19/04/2010 – 22/04/2010.

20. T.J. Lienert, W.L. Stellwag, Friction Stir Welding Studies on Mild Steel, Weld. J. (2003) 1-9.

21. MatWeb, Material property data, AISI H13 Hot Work Tool Steel, accessed on 12/04/2010, http://www.matweb.com/search/datasheettext.aspx?matguid=8cb4b6c4b61040d7be8563dcacab0440

22. Engineer's Handbook, 2011, Coefficient of Friction, accessed on 10/09/2010, http://www.engineershandbook.com/Tables/frictioncoefficients.htm

23. C.J. Dawes, W.M. Thomas, Development of improved tool designs for friction stir welding of aluminium, First International Conference on FSW, June 1999.

24. K. Elangovan, V. Balasubramanian, Influences of tool pin profile and tool shoulder diameter on the formation of friction stir processing zone in AA6061 aluminium alloy, J. Mater. Des. 29 (2008) 362-373.

25. W.M. Thomas, Friction Stir Welding, U.K. Patent Application 2,306,366, October 1996

26. N. Shanmuga Sundaram, N. Murugan, Tensile behaviour of dissimilar friction stir welded joints of aluminium alloys, J. Mater. Des. (2010) 4184-4193.

27. A. Scialpi, L.A.C. De Filippis, Influence of Shoulder Geometry on Microstructure and Mechanical Properties of FSW 6082 Aluminium Alloy, J. Mater. Des. 28 (2007) 1124-1129

28. R.M. Leal, C. Leitao, Material flow in heterogeneous friction stir welding of thin aluminium sheets: effect of shoulder geometry, J. Mater. Sci. Eng. A 498 (2008) 384-391

29. The Welding Institute, Tool Technology, accessed on 20/03/2010, http://www.twi.co.uk/content/c1073a.html

30. R.W. Fonda, J.F. Bingert, Texture and grain evolutions in a 2195 friction stir weld, 5th International Conference on FSW, Sept 2004.

31. C.D. Sterling, T.W. Nelson, Friction Stir welding of Quenched and Tampered C-Mn Steel, Friction Stir Welding and Processing II, 2003, p 165-171

32. K.J. Colligan, J. Xu, and J.R. Pickens, Welding Tools and Process Parameter Effects in FSW of Aluminium Alloys, Friction Stir Welding and Processing II, 2003, p 181-190.

33. H. Fujii, I. Cui, Effect of tool shape on mechanical properties and microstructure of friction stir welded aluminium alloys, J. Mater. Sci. Eng. A 419 (2006) 25-31.

34. K. Elangovan, V. Balasubramanian, Influences of pin profile and rotational speed of the tool on the formation of friction stir processing zone in AA2219 aluminium alloy, J. Mater. Sci. Eng. A 459 (2007) 7-18

35. K. Elangovan, V. Balasubramanian, Influences of tool pin profile and welding speed on the formation of friction stir processing zone in AA2219 aluminium alloy, J. Mater. Process. Technol. 200 (2008) 163-175

36. W.M. Thomas, E.D. Nicholas, S.D. Smith, Friction Stir Welding-Tool Developments, Aluminium 2001, Proceedings of the TMS 2001 Aluminium Automotive and Joining Sessions, p213

37. W.M. Thomas, D.G. Staines, I.M. Norris, R. de Frias, Friction Stir Welding-Tool Developments, FSW Seminar, Dec 3, 2002 (Porto, Portugal), Instituto de Soldadura e Qualidade.

38. M. Strangwood, C. Davis. Microstructural Development and Thermal Fields Modelling in FSW of Strain-Hardened Al-Alloys, 5th International Conference on FSW, Sept 2004.

39. L. Cederqvist, A Weld That Lasts for 100,000 Years: FSW of Copper Canisters, 4th International Conference on FSW, September 2004.

40. C.J. Dawes. P.L. Threadgill, Development of the New Friction Stir Technique for Welding Aluminium-Phase II, TWI member report 5651/35/95, Nov 1995

41. S. Brinckmann, A. Von Strombeck, Mechanical and Toughness Properties of Robotic-FSW Repair Welds in 6061-T6 Aluminium alloys, 2nd International Conference on FSW, June 2000

42. A.P. Reynolds, W. Tang, Alloy, Tool geometry and Process Parameter Effects of FSW Energies and Resultant FSW Joint Properties, Friction Stir Welding and Processing, K.V. Jata, M.W. Mahony, R.s. Mishra, S.L. Semiatin, 2001, P 15-23

43. M.A. Sutton, B. Yang, Mixed Mode Fracture of 2024-T3 Friction Stir Welds, *Eng. Fract. Mech*. 70 (2003) 2215-2234.

44. Z.W. Chen,R. Maginness, Formation of weld zones during FSW of aluminium alloys, 5th International Conference on FSW, September 2004.

45. H. Fujii, Y. Takada, Friction Stir Welding of Ultrafine Grained Materials, 5th International Conference on FSW, September 2004.

46. J.H. Record, J.L. Covington, C.D. Sorensen, Fundamental Characterization of Friction Stir Welding, 5th International Conference on FSW, September 2004

47. M.A. Sutton, A.P. Reynolds, Microstructure and Fracture of AA2524-T351 Base Material and Friction Stir Welds, *Eng. Fract. Mech.* 73 (2006) 391-407.

48. T. Yasui, T. Ishii, Y. Shimoda, Friction Stir Welding between Aluminium and Steel with High Welding Speed, 5th International Conference on FSW, September 2004

49. M.A. Sutton, R. Taylor, Mode I Fracture and Microstructure for 2024-T3 Friction Stir Welds, *Mater. Sci. Eng. A*, 354 (2003) 6-16.

50. M. Attallah, H.G. Salem, Effect of FSW process parameters on the mechanical properties of as-weld and post-weld heat treatment AA2095, 5th International Conference on FSW, September 2004

51. M.J. Brooker, A.J.M van Deudekom, P.D. Sketchley, Applying Friction Stir Welding to Arian 5 Main Motor Trust Frame, 2nd International Conference on FSW, June 2000

52. A. K. Lakshminarayanan, V. Balasubramanian, process parameters optimization for friction stir weld of RDE-40 aluminium alloy using Taguchi technique, trans. Nonferrous Met. Soc. China 18 (2008) 548-554

53. M. Attallah, H. Salem, Friction stir welding parameters: a tool for controlling abnormal grain growth during subsequent heat treatment, Mater. Sci. Eng. A 391 (2005) 51-59

54. V. Balasubramanian, Relationship between base metal properties and friction stir welding process parameters, Mater. Sci. Eng. A 480 (2008) 397–403

55. J. Yan, M.A. Sutton, A.P. Reynolds, Process–structure–property relationships for nugget and heat affected zone regions of AA2524–T351 friction stir welds. Sci. Technol. Weld. Joining, 10 (2005) 725-736.

56. j. Kristensen, C. Dalle Donne, T. Ghidini, J. Mononen, Properties of Friction Stir Welded Joints in the Aluminium Alloys of 2024, 5083, 6082/6060 and 7075, 5th International Conference on FSW, September 2004

57. M. Jariyaboon, A.J. Davenport, R. Ambat, B.J. Connolly, S.W. Williams, D.A. Price, The effect of welding parameters on the corrosion behaviour of friction stir welded AA2024-T351, Corros. Sci. 49 (2007) 877-909

58. A.P. Reynolds, J. Pohlman, proceeding of the seventh international conference on trends in welding research, May 2005, (Calloway Gardens, GA), AWS/ASM International.

59. H.B. Chen, K. Yan, The investigation of typical welding defects for 5456 aluminium alloy friction stir welds, J. Mater. Sci. Eng. A 433 (2006) 64-69

60. B. Heinz, B. Skrotzki, characterization of a friction-stir-welded aluminium 6013, Metall. Mater. Trans. B, 33 (2002) 489-498.

61. A. Squillace, A comparison between FSW and TIG welding techniques: modifications of microstructure and pitting corrosion resistance in AA 2024-T3 butt joints, J. Mater. Process. Technol. 152 (2004) 98-99.

62. K.Elangovan, V.Balasubramanian, Influences of post-weld heat treatment on tensile properties of friction stir-welded AA6061 aluminum alloy joints, Mater. Charact. 59 ( 2008 ) 1168 – 1177.

63. W. Tang, X. Guo, J.C. McClure, L.E. Murr, and A. Nunes, Heat input and Temperature Distribution in Friction Stir Welding, J. Mater. Process. Manuf. Sci. 7 (1998) 163-172.

64. Y.M. Hwang, Z.W. Kang, Y.C. Chiou, Experimental study on temperature distributions within the workpiece during friction stir welding of aluminium alloys, Int. J. Mach. Tools Manuf. 48 (2008) 778-787.

65. M.J. Russell, H.R. Shercliff, Analytical Modelling of Microstructure Development in Friction Stir Welding, 1st International Conference on FSW, June 1999.

66. P. colegrove, M. Painter, T. Miller, 3-Dimensional Flow and Thermal Modelling of the Friction Stir Welding Process, 2nd International Conference on Friction Stir Welding, June 2000.

67. T. Dickerson, J. Przydatek, The significance of root flaws in friction stir welds in aluminium alloys, TWI Members Report 714/200, September 2000.

68. S. Mandal, J. Rice. Experimental and numerical investigation of the plunge stage in friction stir welding, J. Mater. Process. Technol. 203 (2008) 411-419

69. S. Lathabai, M.J. Painter, G.M.D. Cantin, V.K. Tyagi. Friction spot joining of an extruded Al-Mg-Si alloy, Scr. Mater. 55 (2006) 899-902

70. A. Gerlich, P.Su, T.H. North, Tool penetration during Friction Spot Welding of Al and Mg Alloys, J. Mater. Sci. 40 (2005) 6473-6481.

71. H. Badarinarayan, Y. Shi, X. Li, K. Okamoto, Effect of tool geometry on hook formation and static strength of friction stir spot welded aluminium 5754-0 sheets. Int. J. Mach. Tools Manuf. 49 (2009) 814 – 823.

72. G. Biallas, R. Braun, C. D. Donne, Mechanical Properties and Corrosion Behaviour of Friction Stir Welded 2024-T3, 1st International Conference on Friction Stir Welding, June 1999.

73. Mechanical Properties of Aluminium Alloy 2024 Sheet and Plate for different Tempered States, ALCOA, accessed on 12/04/2010, http://www.alcoa.com/global/en/products/product.asp?prod_id=595&Product=Aerospace%7CSheet%20and%20Plate&Category=26%7C346&Query=aluminium 2024&page=0,

74. Chao YJ, Qi X, Tang W. heat transfer in friction stir welding experimental and numerical studies. J. Manuf. Sci. Eng. 2003, 138-45

75. J. Adamowski, M. Szkodo. Friction Stir Welds of aluminium alloy AW6082-T6. J. Achievements Mater. Manuf. Eng. 20, (2007).

76. A. J. Leonard, S. A. Lockyer, Flaws in Friction Stir Welds, 4th International Conference on Friction Stir Welding, May 2003.

77. Aerospace Specification Metals Inc, Material data sheet Aluminium 2024-T351, accessed on 12/04/2010, http://asm.matweb.com/search/SpecificMaterial.asp?bassnum=MA2024T4

78. J.E. Gould, Z. Feng, Heat Flow Model for Friction Stir Welding of Aluminium Alloys, J. Mater. Process. Manuf. Sci. 7 (1998) 185-194

79. Nastran Finite Element Analysis and Simulation Software, accessed on 07/06/2010, http://www.nenastran.com/fea/automotive.

80. American Infrared, FLIR P20, FLIR P25, FLIR B20, accessed on 05/06/2010, http://www.americaninfrared.com/ProductDetail.asp?ID=59

81. S. Xu, X. Deng, Proceeding of the 21st Southeastern Conference on Theoretical and Applied Mechanics (SECTAM XXI), Orlando, Florida, May 19–21, 2002, pp. 699–704.

82. C.M. Chen, R. Kovacevic, Mach. Tool. Manu. 43 (2003) 1319–1326.

83. P.A. Colegrove, H.R. Shercliff, Sci. Technol. Weld. Joining. 9 (2004) 483–492.

84. P.A. Colegrove, H.R. Shercliff, Proceedings of the 4th International conference on FSW, 2003.

85. G. Buffa, J. Hua, R. Shivpuri, L. Fratini, A continuum based fem model for friction stir welding, Mater. Sci. Eng. A 419 (2006) 389-396

86. G. Buffa, J. Hua, R. Shivpuri, L. Fratini, Design of the friction stir welding tool using the continuum based FEM model, Mater. Sci. Eng. A 419 (2006) 381-388

87. L. Fratini, G. Mandolfo, S. Pasta, Residual stresses and FCP prediction in FSW through a continuous FE model. J. Mater. Process. Technol. 209 (2009) 5465-5474.

88. M. Melendez, W. Tang, Tool Forces Developed during Friction Stir Welding, internal paper, NASA Technical Reports Server, accessed on 02/04/2010, http://ntrs.nasa.gov/archive/nasa/casi.ntrs.nasa.gov/20030071631_2003069405.pdf.

89. Y. Yang, P. Kalya, R.G. Landers, K. Krishnamurthy, Automatic gap detection in friction stir butt welding operations, Int. J. Mach. Tools. Manuf. 48 (2008) 1161 – 1169.

90. P. Ulysse, Three-dimensional modelling of the friction stir welding process, Int. J. Mach. Tools. Manuf. 42 (2002) 1549-1557.

91. C. Genevois, A. Deschamps, Comparative study on local and global mechanical properties of 2024 T351, 2024 T6 and 5251 O friction stir weld, Mater. Sci. Eng. A 415 (2006) 162-170.

92. S.T. Amancio-Filho, S. Sheikhi, Preliminary study on the microstructure and mechanical properties of dissimilar friction stir welds in aircraft aluminium alloy 2024-T351 and 6065-T4, J. Mater. Process. Technol. 206 (2008) 132-142.

93. H. Aydin, A. Bayram, A. Uguz, Tensile properties of friction stir welded joints of 2024 aluminium alloy in different heat-treated-state, Mater. Des. 30 (2009) 211-2221.

94. E. Bousquet, A. Poulon-Quintin, M. Puiggali, Relationship between microstructure, microhardness and corrosion sensitivity of an AA 2024-T3 friction stir welded joint, Corros. Sci. 53 (2011) 3026-3034.

95. C. Genevois, A Deschamps, A. Denquin, Quantitative investigation of precipitation and mechanical behaviour for AA2024 friction stir welds, Acta Mater. 53 (2005) 2447-2458.

96. B.L. Won, Y.M. Yeon, S.B. Jung, Evaluation of the microstructure and mechanical properties of friction stir welded 6065 aluminium alloys, Mater. Sci. Technol. 19 (2003) 1513-1518.

97. T.S. Srivatsan, S. Vasudevan, L. Park, The tensile deformation and fracture behaviour of friction stir welded aluminium alloy 2024, J. Mater. Sci. Eng. A 466 (2007) 235-245.

98. C.M. Sellars, W.J. Tegart. International metallurgical Rev. 17 (1972) 1-24.

99. H. Schmidt, J. Hattel, A local model for the thermomechanical conditions in friction stir welding, Modelling Simul. Mater. Sci. Eng. 13 (2005) 77-93.

100. A.A. Giordano, F.M. Hsu, Least Square Estimation with Applications to Digital Signal Processing, Wiley, New York, 1985.

# Chapter 7

# Appendices

## 7.1 FSW Rig Detailed Drawing:

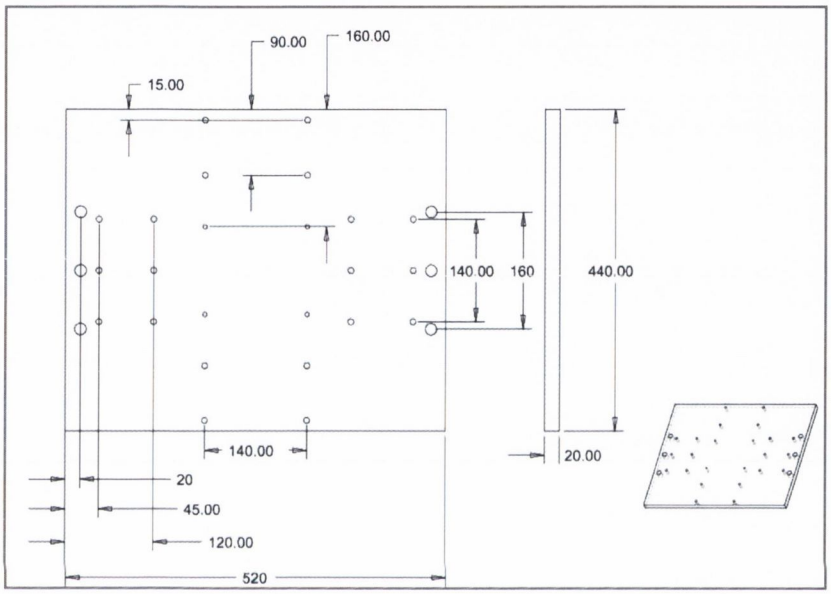


Figure 176: Base Plate

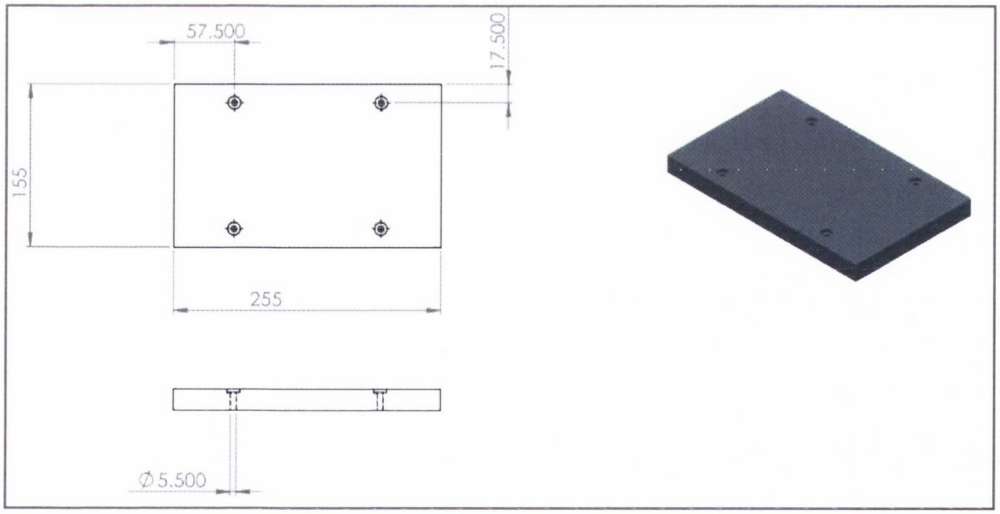


Figure 177: Backing Plate

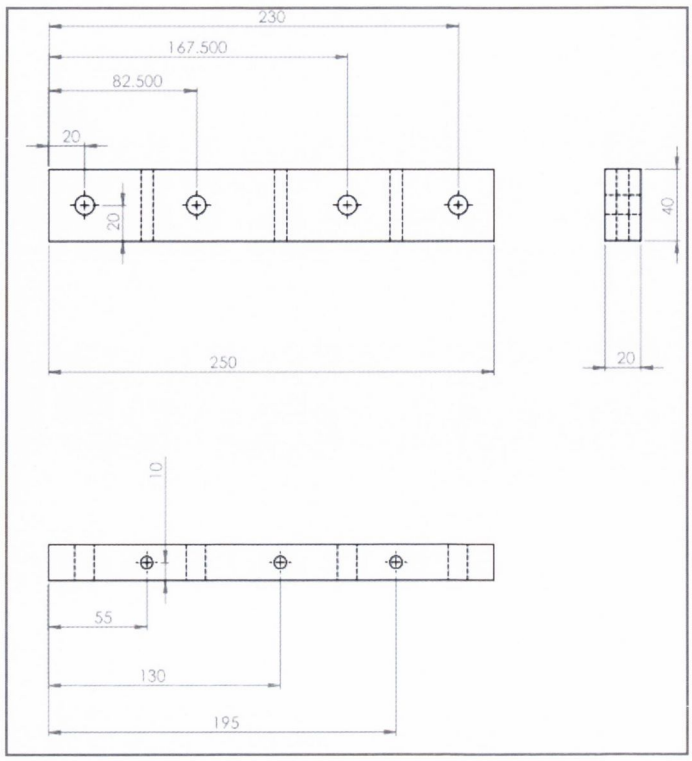


Figure 178: Thrust Clamps

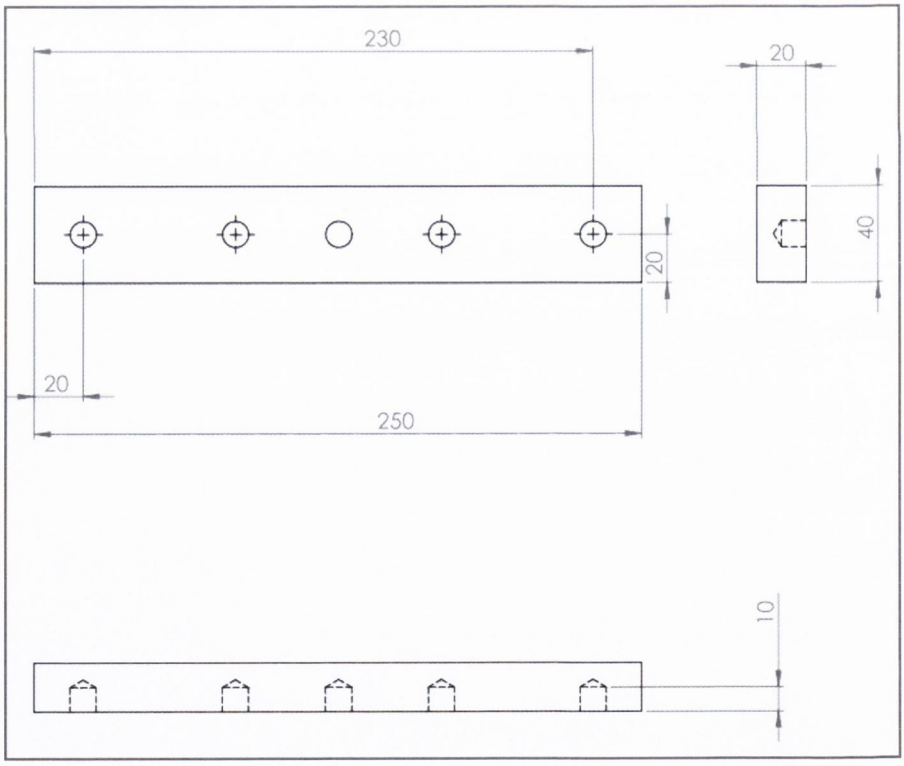


Figure 179: Side Clamps

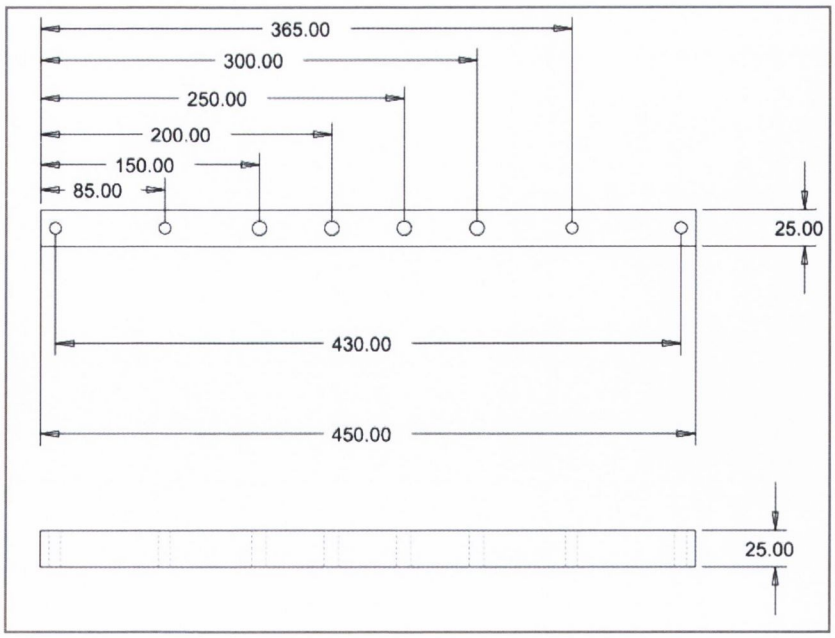


Figure 180: Vertical Clamps

## 7.2 Detailed Drawing of Tooling:

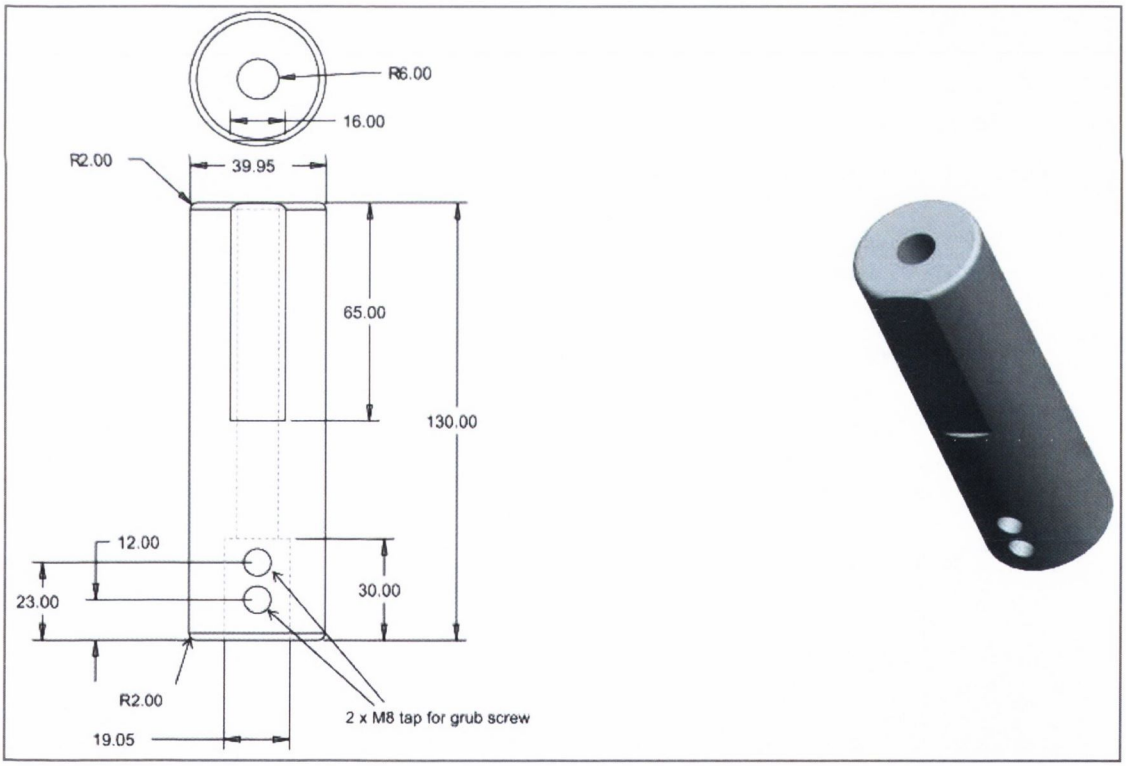


Figure 181: Parent Holder

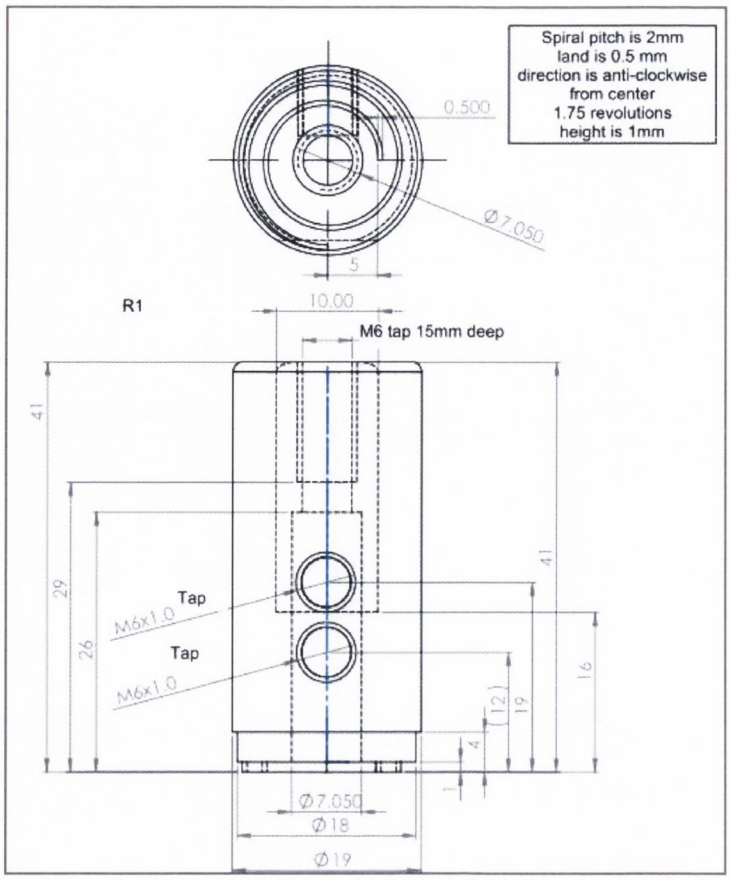


Figure 182: 18mm Scrolled Shoulder, also Manufactured a 22mm Shoulder

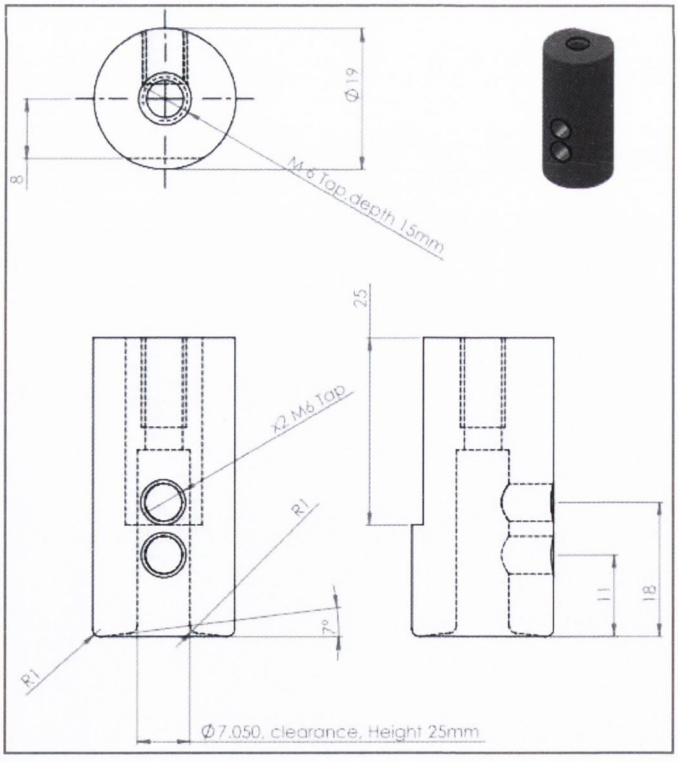


Figure 183: 18mm Concave Shoulder, also Manufactured a 22mm Shoulder

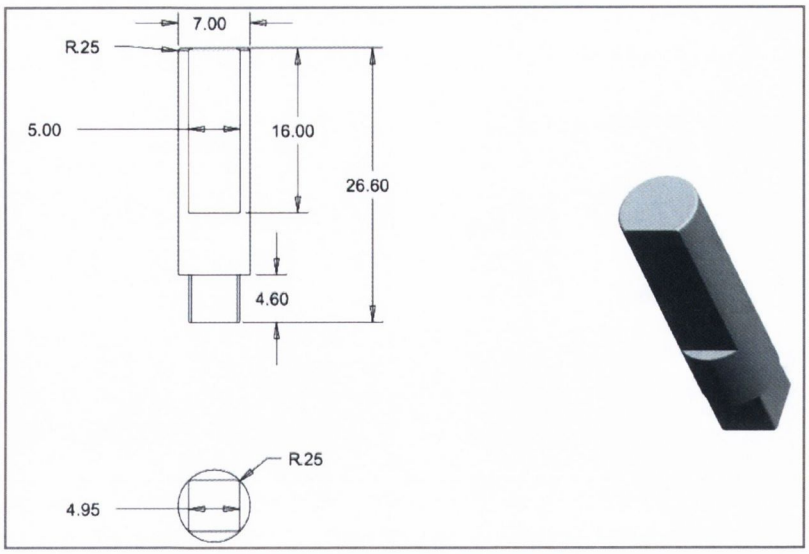


Figure 184: Square Pin

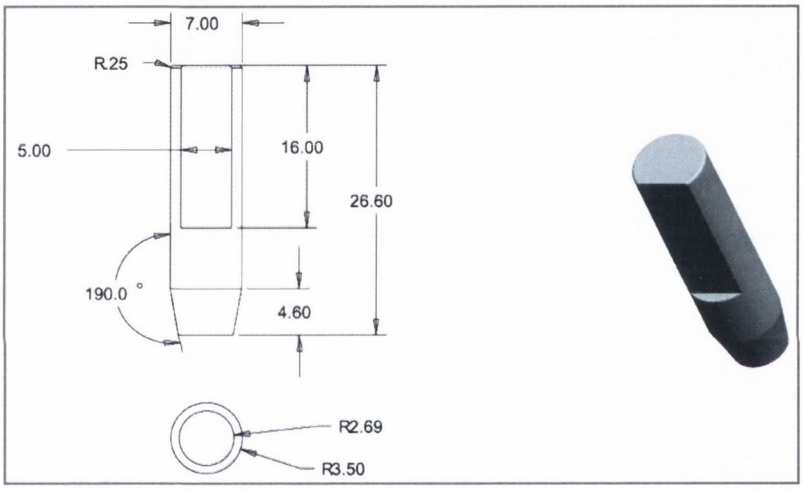


Figure 185: Tapered Cylindrical Pin

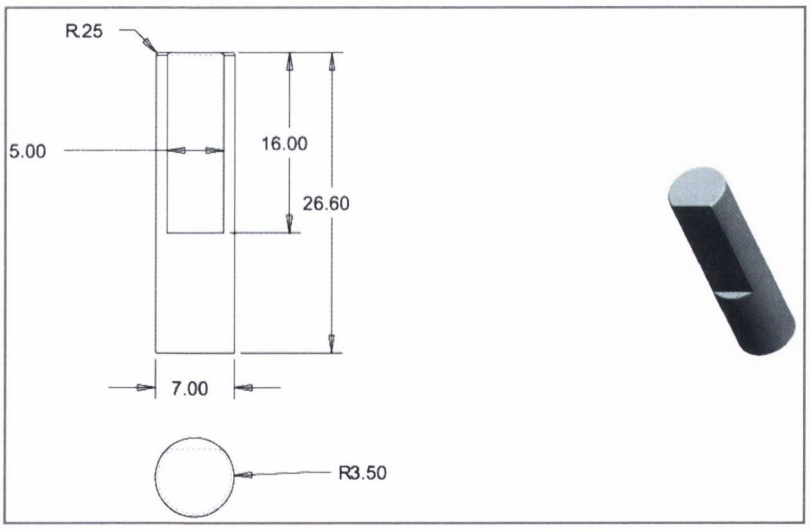


Figure 186: Cylindrical Pin

10.1 CIRP Annals 2012

# Force Generation during Friction Stir Welding of AA2024-T3

D. Trimble, J. Monaghan, G. E. O'Donnell

Department of Mechanical and Manufacturing Engineering, Trinity College, Dublin, Ireland

**Abstract:**
Force measurement in Friction Stir Welding (FSW) provides a significant insight into the process in terms of machine and tool limitations and design. In the present research the tool forces were investigated experimentally using a rotating component dynamometer and through the development of a finite element model. The model correlated well with experimental temperatures and tool forces were capable of predicting tool forces for different welding parameters, predicting regions were tool failure is likely to occur and identifying tool pin designs which can process the workpiece more efficiently.

**Keywords:**
Friction Stir Welding (FSW), Force, Finite Element Modelling

## 1. Introduction

Friction stir welding (FSW) was experimentally proven at The Welding Institute (TWI) in 1991 and has become a relevant technology aimed at joining materials that are so called difficult to weld or even unweldable [1-2]. The process involves the joining of two metal pieces without melting by joining their molecules together. The tool traverses along the joint causing sufficient frictional heat to soften the material and rotation of the tool then stirs the molecules together leaving behind a fully consolidated joint.

Due to its solid state nature FSW has many benefits over fusion welding techniques. However, its main advantage is its ability to weld all series of aluminium alloys, in particular the 2xxx series alloys. These alloys are used extensively within the aerospace industry for applications such as fuselage and wing skins panels due to their high strength to weight ratio. However, these alloys are mostly non-weldable using fusion welding methods due to problems with oxidization, solidification, shrinkage, sensitivity to cracking, hydrogen solubility and the resultant porosity problem [3]. Therefore, the majority of aircraft structural parts all tend to be mechanically joined using rivets. FSW offers a solution to welding these alloys and an alternative to riveting. FSW has many advantages over riveting which include: greater fatigue strength, increased structural rigidity and weight reduction.

The friction stir welding process can be described by three stages: plunge, dwell and translational stage. During the plunge stage a non-consumable rotating tool is slowly plunged into the joint line between the two materials to be welded. Once the tool reaches the required depth it is held in position for 5-20 seconds while still rotating,

this is called the dwell stage. The purpose of this stage is to soften the workpiece material ahead of the tool before welding. During the translational stage the tool traverses along the joint line of the two workpiece plates leaving behind a fully consolidated weld.

Process monitoring is an important application during the machining of aerospace components for detecting tool wear and failure [4]. FSW is similar in nature to milling operations but considerably larger forces are generated. The different tool and workpiece forces generated during the FSW process are illustrated in Figure 187. It is important to characterize the tool forces as a better understanding can promote the development of improved tooling designs and clamping arrangements to help reduce machine complexity, size and power, and reduce operational costs and improve productivity.

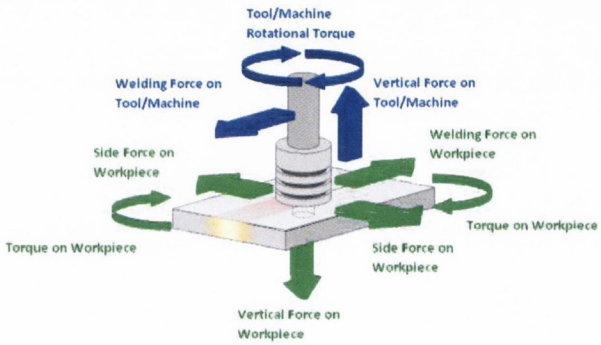


Figure 187: Forces acting on the Tool and Workpiece during FSW

To date there has been little quantitative data published quantifying these forces. Melendez et al [5] used strain gages embedded into the workpiece to monitor both the vertical and welding force. However their analysis did not measure the forces acting directly on the tool but rather the forces experienced by the workpiece. Yu Yang et al [6] developed an algorithm to detect a gap occurring between the workpiece plates during the FSW of AA2024 using a load cell. However, these authors only measured the vertical force generated. A number of other authors [7-8] also recorded the vertical force occurring during the plunge stage when investigating Friction Stir Spot Welding (FSSP).

Furthermore, very few publications report on accurate numerical modeling of the forces generated during the process but rather report on the development of models validated by temperature comparison to experimental results to numerically predict the forces generated. Ulysse [9] presented a 3D FEM visco-plastic model for FSW of thick aluminium plates using FIDAP. This author validated the model by achieving a reasonable agreement between the predicted and the measured temperatures, and used the model to predict the forces acting on the tool pin. Colegrove and Shercliff [10] used a CFD commercial software for a 2D and 3D numerical investigation of the influences of pin geometry during FSW. However, these authors reported poor prediction of the welding forces. Buffa et al [11-12] are one of the few authors reporting successful modeling of the FSW process using DEFORM-3D. However, these authors only modeled a cylindrical smooth tool pin and also validated the model through comparison between the experimental and predicted temperatures.

The aim of this present work is to measure and fully characterise the different forces acting on the tool during the FSW of AA2024-T3 plates and to establish the magnitude of their impact on the FSW process. This is achieved by experimentally measuring the tool forces using a rotating component dynamometer and developing a 3D model of

the process capable of predicting the tool forces and temperatures with a reasonable degree of accuracy.

## 2. Experimental procedure

Aluminium 2024-T3 plates (260mm x 80mm x 4.8mm) were friction stir welded using a butt joint configuration. All tools and clamping were manufactured from hardened AISI H-13 tool steel. The tool shoulder was concave, 18mm diameter and had a 7° recess angle. Two different pin designs were examined, a threaded cylindrical and smooth cylindrical each with a diameter of 6.5mm and a height of 4.6mm. The welding parameters were as follows: rotational speed 450rpm, plunge speed 16mm/min, translational speed 90, 180mm/min and a 2° tool tilt angle. During welding, a distance of 0.2mm was maintained between the tip of the tool pin and the bottom surface of the aluminium plates to ensure a consolidated weld. The concave shoulder was plunged until approximately 80% of the shoulder was in contact with the workpiece surface.

A rotating component dynamometer was incorporated onto the welding rig to record the tool forces, the rig setup is illustrated is Figure 188. The dynamometer was capable of measuring the torque and forces in the X, Y, and Z directions. The forces were measured using piezo-electric crystals, the signals from which are continuously sampled at a rate of 7.8 kHz for each channel, and are processed through the Kistler 9124B multi-channel signal conditioner. Ten type K thermocouples, 1.5mm diameter, were used to recorded temperatures during testing. Holes 1.6mm diameter to a depth of 4mm were drilled 12mm away from the joint line and a high conductive thermal glue was used to endure the ends of the thermocouple probes remained in contact with the workpiece. Thermocouples were positioned 32.5mm away from one another and were placed 50mm from tool entry and exit points.

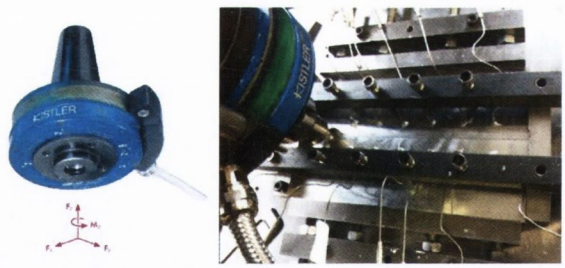


Figure 188: Kistler Dynamometer and FSW rig with thermocouples

## 3. Finite element model

The finite element package DEFORM 3D was used to model the FSW process. The two aluminium sheets were modelled as a continuous block rather than two spate objects to avoid numerical contact instabilities that resulted from the discontinuities present at the edge of the two sheets. As the The rotating tool moves forward it welds a crack left behind the pin as it advances along the welding line. The model was broken down into the three experimental stages, plunge dwell and translational. The material properties for the workpiece, tooling and clamping were selected or inserted into the model. An absolute mesh density was chosen with tetrahedral elements approximately 5mm in length to mesh the workpiece and the Johnson-Cook material law was used as the flow stress equation. Mesh windows with elements 0.5mm in length were used to concentrate mesh density around the vicinity of tool pin and shoulder contact. Mesh windows were set to follow the tool path during thereby

ensuring they remain active throughout the welding process. No boundary conditions or constrains were placed on the nodes of the workpiece so as not to impede any material flow. Therefore a box die meshed with tetrahedral elements 5mm in length was used shown to house the workpiece and simulate the experimental clamps. The two pin designs with a concave shoulder were meshed with tetrahedral elements 0.4mm in length. The finite element model and different tool designs are shown in Figure 189.

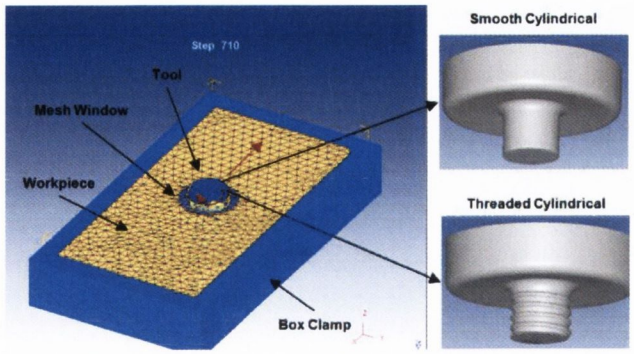


Figure 189: Finite element model and different tool designs

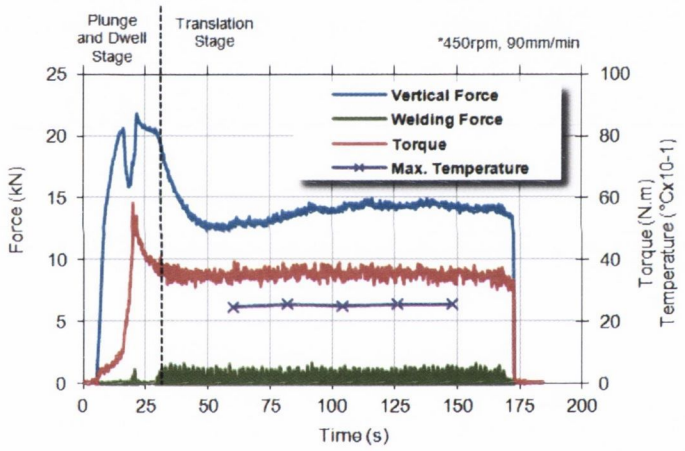


Figure 190: Experimental force and temperate generation.

## 4. Experimental results

The three tool forces and the maximum temperatures that were recorded during testing are shown in **Figure 190**. Both the vertical force and torque reach peak values during the plunging of the tool into the workpiece when the shoulder reaches the target depth. However, both forces reduced significantly (approx. 35%) during the translational stage. Hence the tool can be susceptible to failure during the plunge stage. Therefore developing new techniques of tool entry and new tooling designs may reduce these peak values. Two peaks were recorded for the vertical force. The first peak represents the force acting on the pin to achieve penetration into the workpiece and the second peak is attributed to shoulder contact with the workpiece. All three forces (vertical, welding and torque) reach relative steady state values during the translational stage, this correlated well with steady state temperatures that were also recorded during this stage. The vertical force is significantly larger than the other two forces and is therefore the limiting factor in machine design, and the main force influencing tool wear or fracture particularly during the plunge stage.

The dynamometer measures the forces throughout each 360° revolution and therefore records forces in every direction during each revolution. Hence only maximum values of the welding force indicate the resistance acting against the tool as it traverses along the weld line.

## 5. Model validation

The model was validated by comparing forces and temperatures predicted by the model to those recorded experimentally. Figure 191 shows a comparison of the predicted FEM forces and to those recorded experimentally. The high fluctuations of the predicted forces are due to the intermittent contact between the tool and the workpiece nodes coupled with the large amount of remeshing required to maintain mesh integrity. Although the predicted forces did not map exactly onto the experimental, they behaved similar to the experimental with peak vertical and torque forces occurring during the plunge stage, and all forces reaching almost steady state values during the translational stage. However, the model predicted slightly greater forces compared to experimental results, 14.1%, 13.6% and 18.7% greater for the vertical, torque and welding force respectively.

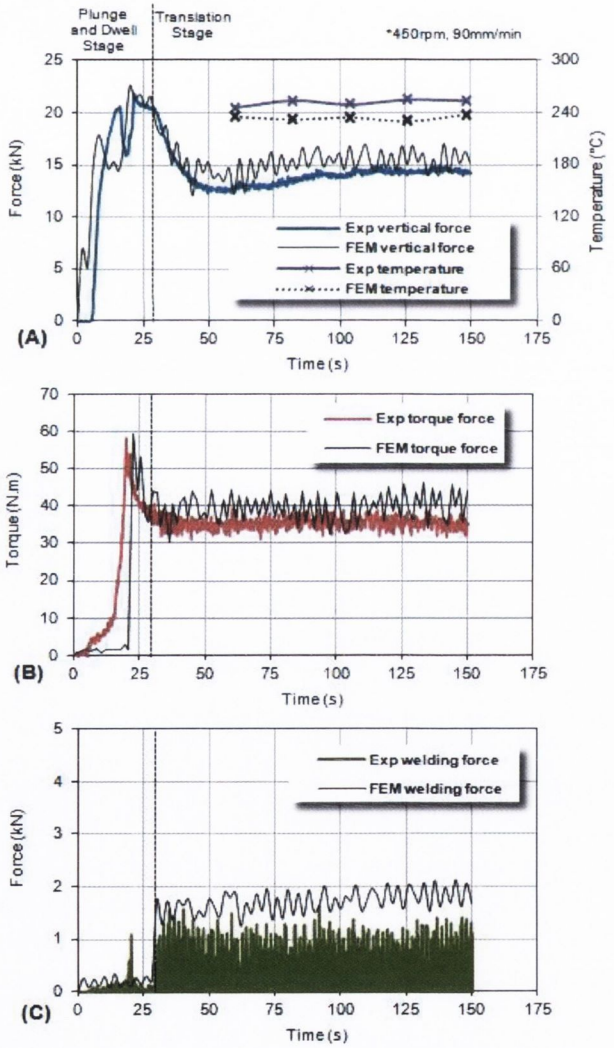


Figure 191: Comparison of experimental and FEM values, (A) vertical force and temperature, (B) torque and (C) welding force.

The model was also used to predict the temperature within the workpiece at the corresponding experimental thermocouple locations. A comparison of the

experimental and FEM temperatures is shown in Figure 191 (A). Similar to experimental results, maximum FEM temperature remain constant during the translational stage. However, the model predicted lower temperatures than those recorded experimental with an average reduction of approximately 17.5 °C. This may account for the higher forces recorded due to a reduction in thermal softening of the workpiece. Results suggest that the flow stress equation does not accurately represent the workpiece exactly. Further refinement of the material constants may improve the model. However, overall the model correlated well with experimental results and gave a good representation of the FSW process.

## 6. FEM results

The model was capable of predicting tool forces generated at various operating parameters. Figure 192 shows the FEM predicted forces for various translational speeds. All forces were found to increase significantly with increasing translational speeds. This is attributed to a reduction in thermal softening of the workpiece due to reduced heat generation which increases the resistance acting on the tool as it traverses along the joint line. Increasing the rotational speed had the opposite effect due to an increase in heat generation.

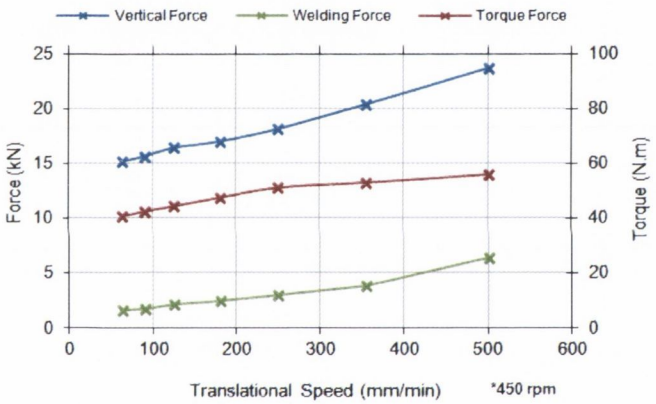


Figure 192: FEM predicted forces for various translational speeds

The predicted FEM temperatures and stresses acting on the FSW tool are illustrated in Figure 193. During the translational stage, significantly larger stresses and temperatures were found to occur on the tool shoulder rather than the tool pin. However, during the plunge stage, the pin is subjected to larger stresses during tool penetration of the workpiece. Therefore, the model predicted that during the initial plunge stage of the process damage to the tool pin is most likely to occur, whereas during the translational stage damage to the tool shoulder is most likely to occur.

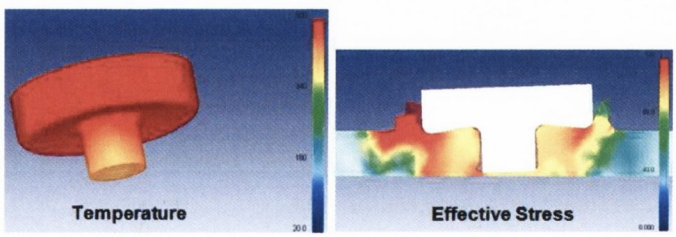


Figure 193: FEM temperatures and stresses on the FSW tool

Variation of the pin design only had an effect on certain forces during particular stages of the process. Variation of the pin design only had a significant effect on the

maximum vertical force during the plunge stage because during the translational stage the forging pressure exerted by the shoulder generates the vertical force. Variation of the pin design did not have a significant effect on the torque. Torque is a rotary measurement and the diameter of the shoulder is 2.7 times that of the pin hence rotation of the shoulder is the main driving factor of torque generation. However, variation of the pin design did have an effect on the welding force which directly opposes translation of the tool. The cross section area of the pin in contact with the workpiece is greater than that of the shoulder. Hence the tool pin is the main driving factor of the welding force. Figure 194 shows the predicted FEM force for both the threaded and smooth pin designs. Lower maximum vertical and welding forces were predicted for the threaded pin. This is attributed to the threads producing a screwing action and increased material deformation which sweeps the material away along the tool path rather than simply displacing the area occupied by the pin as is the case with the smooth cylindrical pin.

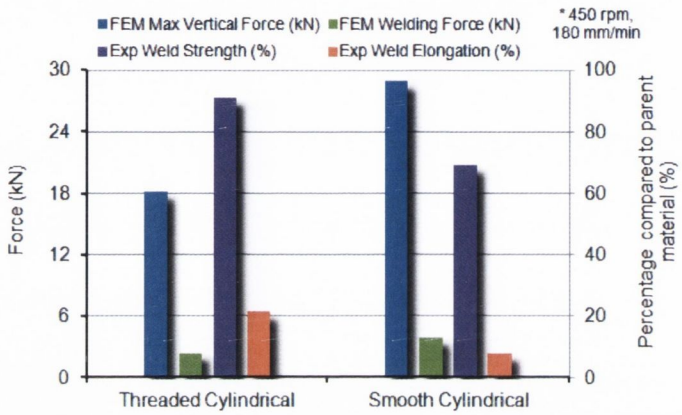


Figure 194: FEM forces and tensile results for different pin designs

Evidence of increased material deformation and stirring of the workpiece material by the threaded pin can be seen in Figure 195 which shows the material displacement for the two pin designs. Furthermore, tensile test were conducted to British Standard (BSEN 10002-1:2001) on welds producing using the two pin designs. Four test samples were taken from each weld and the average Ultimate Tensile Strength was calculated. The percentage weld strength and elongation compared to the parent material is shown in Figure 194. Greater weld strength and elongation were recorded using the threaded pin due to increased material deformation and mixing of the workpiece material. Therefore, the model can also help identify tooling designs which can process the workpiece material more efficiently.

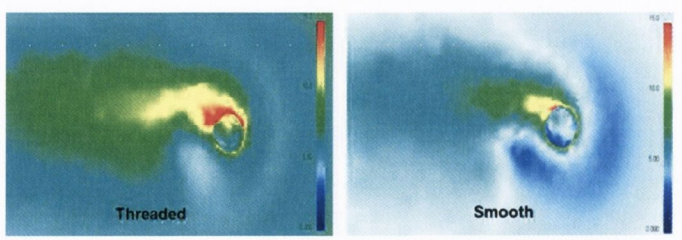


Figure 195: Material displacement for threaded and smooth cylindrical pins

## 7. Conclusions

In the present paper the tool forces generated during the FSW of AA2024-T3 plates has been investigated. This was achieved by experimentally measuring the tool

forces using a rotating component dynamometer and developing a 3D model of the process capable of predicting the tool forces. The model predicted slightly larger forces and lower temperatures compared to experimental results but overall gave a good representation of the process. Results indicate the maximum forces occur during the plunge stage and these reduce significantly (35%) during the translational stage. During the initial plunge stage of the process damage to the tool pin is most likely to occur, whereas during the translational stage damage to the tool shoulder is most likely to occur. The model was capable of identifying tooling designs which can process the workpiece material more efficiently. A pin with a threaded designs produced increased material deformation and mixing of the workpiece material compared to a smooth pin design. As a result lower maximum vertical and welding forces, and higher weld strength and elongation were recorded for the threaded pin.

**References**


[1] Mishra, R.S., Ma, Z.Y., 2005, Friction Stir Welding and Processing, J. Mater. Sci. Eng. R, 50: 1–78.

[2] Fratini, L., Buffa, G., Hua, J., Shivpuri, R., 2006, Friction Stir Welding of Tailored Blanks: Investigation on Process Feasibility, Annals of CIRP, 55/1: 279–282.

[3] Flores, O.V., Kennedy, C., Murr, L.E., Brown, D., Pappu, S., 1998, Microstructural issues in a Friction-Stir-Welded Aluminum Alloy, Scripta Materialia 38: 703–708.

[4] Byrne, G., O'Donnell, G.E., 2007, An Integrated Force Sensor Solution for Process Monitoring of Drilling Operations, Annals of CIRP, 56/1: 89–92.

[5] Melendez, M., Tang, W., Schmidt, C., McClure, J. C., Nunes, A. C., Murr, L. E., 2003, Tool Forces Developed during Friction Stir Welding, Nasa Technical Reports Server, Document ID: 20030071631.

[6] Yang, Y., Kalya, P., Landers, R, Krishnamurthy, K., 2008, Automatic Gap Detection in Friction Stir Butt Welding Operations, Int. j. Mach. Tool. Manu. 48: 1161–1169.

[7] Mandal, S., Rice, J., 2008, Experimental and Numerical Investigation of the Plunge Stage in Friction Stir Welding, J. Mater. Process. Tech. 203: 411-419.

[8] Badarinarayan, H., Shi, Y., Li, X., Okamoto, K., 2009, Effect of Tool Geometry on Hook Formation and Static Strength of Friction Stir Spot Welded Aluminium 5754-0 sheets, Int. J. Mach. Tool. Manu. 49: 814-823.

[9] Ulysse, P., 2002, Three-dimensional modelling of the friction stir welding process, Int. J. Mach. Tools. Manu. 42: 1549–1557.

[10] Colegrove, P.A., Shercliff, H.R., 2004, 2-Dimensional CFD modelling of flow round profiled FSW tooling, Sci. Technol. Weld. Join. 9: 483-492.

[11] Buffa, G., Hua, J., Shivpuri, R., Fratini, L., 2006, A continuum based fem model for friction stir welding-model development, Mater. Sci. Eng. A. 419: 389-396.

[12] Buffa, G., Fratini, L., Hua, J., Shivpuri, R., 2006, Friction Stir Welding of Tailored Blanks: Investigateion on Process Feasibility, Annals of CIRP, 55/1: 279-282.

## 10.2 Journal of Materials Processing Technology 2012:

# Effect of Operational Parameters and Tooling on Force Generation during Friction Stir Welding of AA2024-T3

D. Trimble, J. Monaghan, G. O'Donnell

Department of Mechanical & Manufacturing Engineering

Trinity College Dublin, Ireland

## Abstract:

A better understanding of the tool forces occurring during friction stir welding (FSW) provides a significant insight into the process in terms the development of improved tooling designs and clamping arrangements to help reduce machine complexity, size and power, reduce operational costs, improve productivity and reduce tool wear. In the present work, all the forces acting on the FSW tooling/machine were measured and the magnitude of their impact on the FSW process was established during the welding of aluminium 2024-T3 plates. The effect of varying the operation parameters and tooling design on the tool forces was also determined to help identify methods of reducing these forces and enhancing tooling designs. Core testing was performed using an Mx Triflute pin and Scrolled shoulder designed tool over seven different translational speeds and six different rotational speeds. Welds were also fabricated using a Square and Cylindrical pin, and also a larger shoulder diameter to compare different tool pin and shoulder designs.

*Keywords:* Friction Stir Welding; Forces, AA2024-T3; Tool design; Operational Parameters; Temperature

## 1. Introduction

The fusion welding of aluminium and its alloys presents a great difficulty for designers and technologists. Martukanitz (1993) highlighted that the difficulties associated with these kinds of joints are mainly related to the presence of a tenacious oxide layer, high thermal conductivity, high coefficient of thermal expansion, solidification shrinkage, and high solubility of hydrogen and other gases in molten state. Fusion welding of aluminium alloys leads to the formation of brittle inter-dendritic structure and eutectic phases due to melting and re-solidification of the fusion zone. Su et al (2003) reported that the formation of brittle structure in the weld zone leads to a drastic decrease in the mechanical properties such as hardness, strength and ductility.

Starke and Staley (1996) highlighted the applications of modern aluminium alloys to aircraft. Due to its excellent high strength to weight ratio and ductility, AA2024 is used extensively within the aircraft industries for applications such as fuselage skins, fuselage frames and wings. However, this alloy like all 2xxx series aluminium alloys have poor weldability due to the copper content which causes hot cracking, poor solidification and porosity in the fusion zone.

Friction stir welding (FSW) was invented and experimentally proven at The Welding Institute (TWI) by Thomas (1991). One of the major advantages of this process is its ability to weld all series of aluminium alloys, particular those classified as unweldable using fusion techniques. The process involves the joining of two metal pieces without melting by joining their molecules together. The tool traverses along the joint causing sufficient frictional heat to soften the material, but without melting. The rotation of the tool then stirs the molecules together leaving behind a fully consolidated joint. What sets FSW apart from other fusion welding techniques is that it is a solid-state process. The melting

temperature of the workpiece is never achieved and remains as a solid throughout the process. Because melting does not occur and joining takes place below the melting temperature of the material, a high-quality weld is produced. This characteristic greatly reduces the ill effects of high heat input, including distortion, and eliminates solidification defects which are usually associated with fusion welding. The basic principle of the process is illustrated in **Figure 196**.

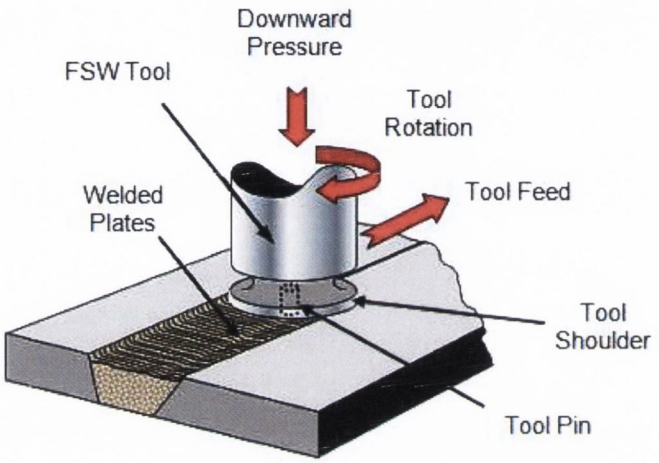


Figure 196: A schematic of the friction stir welding process.

The friction stir welding process can be described by three stages: plunge, dwell and translation stage. During the plunge stage a non-consumable rotating tool is slowly plunged into the joint line between the two materials to be welded. Once the tool reaches the required depth it is held in position for 5-10 seconds while still rotating, this is called the dwell stage. The purpose of this stage is to soften the workpiece material ahead of the tool before welding. During the translational stage the tool traverses along the joint line of the two workpiece plates leaving behind a fully consolidated weld.

One of the major limitations of FSW is the large forces generated as the process is purely mechanical. Hence, FSW of sensitive components can be restricted due to the large

downward forces and heavy duty clamping required to fix the workpiece into position. This is especially the case in the aerospace industries as rigidly clamping structural components can sometimes be geometrically difficult. This is not a problem with riveting which is much more flexible than FSW. In FSW it is also necessary to have a backing plate underneath the workpiece to support the high vertical forces, again highlighting the low flexibility of the process. Due to the large forces generated, equipment can be expensive as most commercially made equipment is individually designed for a given application and hence is more expensive than mass produced machines. Also, the large forces acting on the tool can cause tool wear and fracture. Mandal et al (2008) reported that tool wear is most likely to occur during the plunge stage due to the large forces generated during an experimental and numerical investigation of the plunge stage in FSW.

A number of different forces act on both the tooling/machine and the workpiece component during the FSW process; these forces are illustrated in **Figure 197**. It is important to characterize the forces acting on the tool/machine as a better understanding of these forces can promote the development of improved tooling designs and clamping arrangements to help reduce machine complexity, size and power, reduce operational costs, improve productivity and reduce tool wear.

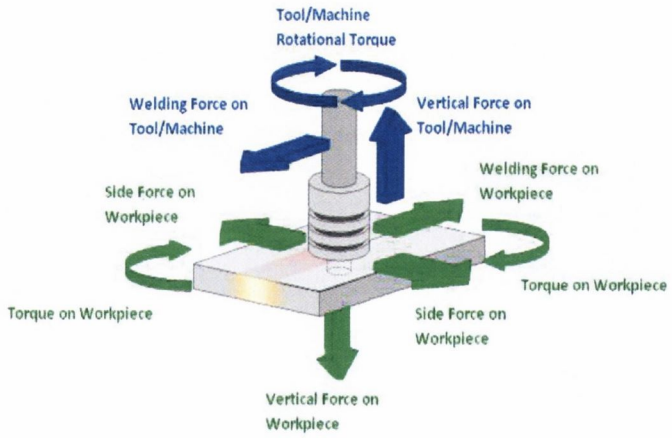


**Figure 197:** Forces generated during FSW.

To date there has been little quantitative data published by other researchers quantifying the tool forces for different tooling designs and operational parameters during the FSW of AA2024. Furthermore, there is a lack force monitoring on the Mx Triflute pin and Scrolled shoulder tools developed by TWI. Melendez and Tang (2005) measured both the vertical force and the welding force during the FSW of two different aluminium alloys, AA6061-T6 and AA2195-T6. They examined the effects of plunge depth, rotational speed and translational speed. However, these authors used strain gages embedded into the workpiece to measure the forces experienced by the workpiece. Yang et al (2008) used a load cell to monitor the vertical force during the development of an algorithm to detect a gap occurring between the workpiece plates during the FSW of AA2024 plates. Yan et al (2004) measured the torque and the welding force for different translational and rotational speeds during the FSW of AA2524-T351 plates. However these authors only examined one particular tooling design which consisted of a cylindrical threaded pin and a concave shoulder. Lathabai et al (2006) and Gerlich et al (2005) measured the vertical force generated during friction stir spot welding (FSSW) of aluminium and magnesium alloys. A number of authors have attempted to predict the forces by developing a 3 dimensional model of the FSW process. Colegrove and Shercliff (2003) used computational fluid dynamics (CFD) software to model the flow around a threaded friction stir welding tool pin but reported poor predictions of the welding forces. Ulysse (2002) modeled the friction stir welding process using three dimensional visco-plastic modeling. The model was used to predict the force acting on the tool for various translational and welding speeds, and also determine if tool failure is likely to occur. However, no experimental measurements were used to validate the predicted tool forces.

The aim of this present work is to measure and fully characterise the different forces acting on the tool during the FSW of AA2024-T3 plates and to establish the magnitude of their impact on the FSW process. In particular, examining the effects of varying operational parameters (translational and rotational speeds) and tooling designs (pin and shoulder) to help identify methods of reducing these forces and enhancing tooling designs.

## 2. Experimental Procedure

All FSW tests were conducted on a Correa F3UE milling machine which was modified for use as a FSW rig. The workpiece material was aluminium 2024-T3 plates (260mm x 80mm) with a thickness of 4.82mm which were welded using a butt joint configuration. A 3-piece tooling system was developed to enable interchangeable shoulder and pin components for different designs and also if tool failure occurs due to fracture or wear. All tools were manufactured from hardened AISI H-13 tool steel. A scrolled shoulder design with two different diameters (18mm and 22mm) and three pin designs (Mx Triflute, Square and Cylindrical) were tested and are shown in **Figure 198**. The welding parameters and tooling designs/dimensions are presented in **Table 19**. Core testing consisted of 42 welds over the range of operating parameters while recording the forces and temperatures generated. These welds were produced using the 18mm scrolled shoulder and Triflute pin. Additional welding was performed using the different tooling arrangements at specific operational parameters to compare results. During welding, a distance of 0.2mm was maintained between the tip of the tool pin and the bottom surface of the aluminium plates to ensure a consolidated weld was produced. The height of the scrolled feature was 1mm and this was plunged 0.5mm into the workpiece surface during welding. Using a scrolled shoulder design it was possible to weld with a zero tool tilt angle.


**Figure 198:** FSW tooling, shoulder and pin designs.

Table 19: **Welding operational parameters and tooling dimensions.**

| Parameters | Units | Values |
|---|---|---|
| Rotational Speed | rpm | 280, 355, 450, 560, 710, 900 |
| Translational Speed | mm/min | 63, 90, 125, 180, 250, 355, 500 |
| Plunge Rate | mm/min | 16 |
| Dwell Time | s | 8 |
| Pin Length | mm | 4.6 |
| Pin Diameter | mm | 6.5 |
| Shoulder Diameter | mm | 18, 22 |
| Tool Tilt Angle | ° | 0 |

A rotating 4-component dynamometer from Kistler was incorporated onto the welding rid to record the forces acting on both the FSW tool and welding machine. The dynamometer connected directly into the spindle of the milling machine and is shown in Figure 199. The dynamometer was capable of measuring the torque and forces in the X, Y, and Z directions. The forces were measured using piezo-electric crystals, the signals from which are continuously sampled at a rate of 7.8 kHz from each channel, and are processed through the Kistler 9124B multi-channel signal conditioner. Ten type K thermocouples, 1.5mm diameter, were used to recorded temperatures during testing. Holes 1.6mm

diameter to a depth of 4mm were drilled 15mm away from the joint line and a high conductive thermal glue was used to ensure the ends of the thermocouple probes remained in contact with the workpiece. Welds fabricated using the different pin designs and shoulder dimensions were sectioned to provide four tensile test sample which were conducted to British Standard (BSEN 10002-1:2001). The experimental rig, dynamometer and thermocouple set up is illustrated in **Figure 199**.

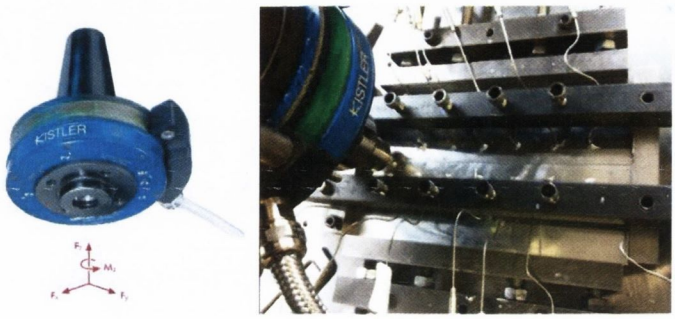


Figure 199: **Experimental rig, dynamometer and thermocouple setup.**

## 3. Results and Discussion

### 3.1 Introduction

The dynamometer was used to measure the three forces, welding, vertical and torque, which act directly on the FSW tool. **Figure 200** displays a sample of the forces that were recorded during testing. Both the vertical and torque forces reach peak values during the plunging of the tool into the workpiece at shoulder contact and hence the tool can be susceptible to failure during this stage. Therefore developing new techniques of tool entry and new tooling designs may reduce these peak values. All three forces (vertical, welding and torque) reach steady state values during the translational stage, this correlates well with steady state temperatures that were also recorded during the translational stage. **Figure 201** shows the average maximum temperature between adjacent thermocouples separated from the joint.

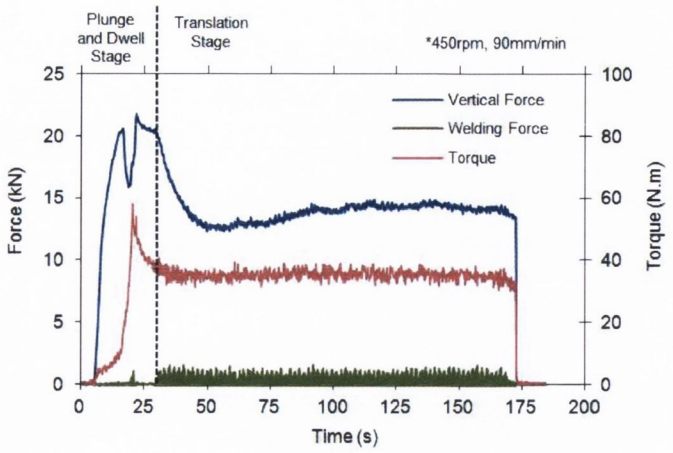


Figure 200: Vertical force, welding force and torque generated during FSW.

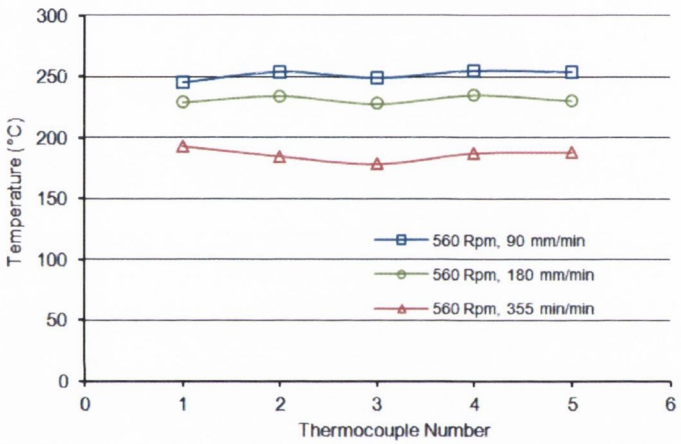


Figure 201: Average maximum temperature between adjacent thermocouples separated from the joint.

The vertical force generated the largest force during testing and is therefore the limiting factor in respect of the machine design. It rises rapidly once the tip of the tool pin contacts the workpiece surface and reaches a first peak. At this point the pin is immersed to a sufficient depth within the workpiece to cause heat generation through friction and plastic material deformation that softens the workpiece, and hence the force decreases slightly. The force begins to rise again at shoulder contact and reaches a second maximum peak when the desired plunge depth is reached. A slight drop in the force occurs during the 8s dwell stage and the force decreases to a steady state during the translational stage. The

reduction in the vertical force from the plunge/dwell stage to the translational stage is significant, approximately 35%.

Similar to the vertical force, the torque reaches its peak value during the plunge stage and decreases to a steady state value during tool translation. It rises gradually when the tool makes contact with the workpiece. However, during plunging the rate of increase changes and becomes sharper. This change in torque corresponds to the point where the vertical force reaches its first peak. The torque reaches a maximum value at the end of the plunge stage when the shoulder is immersed into the workpiece to the required depth. Its magnitude decreases significantly during the dwell stage and reaches a steady state value during the translational stage. The reduction in magnitude between the maximum and steady state torque is surprising similar to the reduction in the vertical force, approximately 34%.

The dynamometer measures the forces throughout each 360° revolution and therefore records forces in every direction during each revolution. Hence only maximum and minimum values of the welding force indicate the resistance acting against the tool as it traverses along the weld line. During the plunge stage, only slight fluctuations of the welding force are recorded as the tool pin penetrates the workpiece. As expected, the weld force only starts to increase when the tool begins to traverse along the joint line. In general, the weld force reaches a maximum value when the translational stage is initiated and then reduces slightly to an almost steady state throughout the remaining tool translation. Its magnitude is significantly lower than the vertical force and hence the welding force should not have an influence on machine limitations.

### 3.2 Effect of Translational Speed

**Figure 202** shows the average steady state forces and the average maximum temperature values recorded across all 10 thermocouples during the translational stage for a range of different translational speeds and a fixed rotational speed of 450 rpm. All three forces were found to increase with increasing translational speeds. The variation in force can be attributed to the amount of workpiece softening occurring at different translational speeds. During FSW, heat is generated through friction between the tool and workpiece, and also by plastic deformation of the workpiece material. As expected, higher temperatures are recorded for slower translational speeds as more time is available for heat generation to occur; this increases the amount of workpiece softening and hence reduces the resistance/loading acting on the tool during welding.

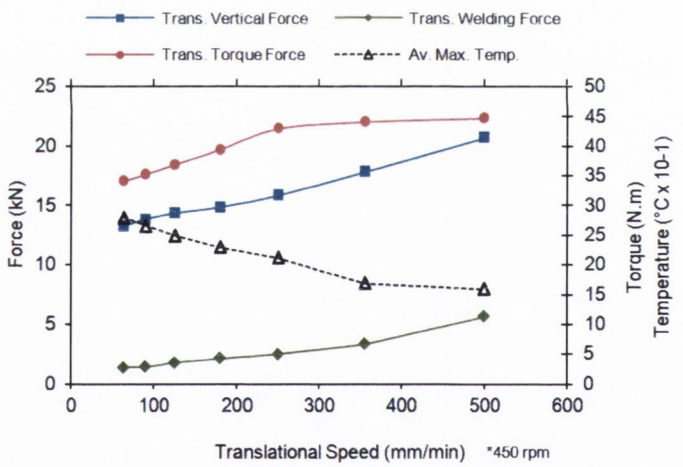


Figure 202: Effect of translational speed on the average steady state forces and average maximum temperature during the translational stage.

Of all the operational parameters, the translational speed had the most significant effect on the welding force. This was expected, as the welding force is generated from the resistance of workpiece acting against tool as it traverses along the joint line. The welding force creates a moment load acting on the pin about the interface between the pin and the shoulder. If the pin cannot withstand this moment, fracture occurs about this interface.

However, pin fracture did not occur during testing, even at maximum translational speeds of 500mm/min. Therefore the limiting factor associated with increasing the translational speed and hence the productivity of the process is not pin failure due to large welding forces. The limiting factor is the formability of the workpiece as surface defects, which are illustrated in **Figure 203,** were detected at high translational speed above 355mm/min.

Figure 203: Surface defects at 500mm/min translational speed.

### 3.3 Effect of Rotational Speed

**Figure 204** shows the average steady state forces and the average maximum temperature values recorded across all 10 thermocouples during the translational stage for a range of different rotational speeds and a fixed translational speed of 180mm/min. Variation of the rotational speed was found to have less of an impact on the three forces compared to variation of the translational speed. Higher temperatures are normally associated with increasing rotational speeds due to increased friction between the workpiece and the tool, and plastic deformation of the workpiece. Jariyaboon et al (2007) reported an increased in temperature of approximately 60°C when the rotational speed was increased from 215 rpm to 468 rpm during the FSW of AA2024-T351 plates. These authors used concave shoulder with a 20mm diameter. A reduction of the tool forces generated is expected with increasing rotational speeds due to workpiece softening. However, relative small increases in temperature were recorded with increasing rotational speeds as illustrated in **Figure 204**. This can be attributed to the scrolled shoulder design which has less shoulder surface area

contact with the workpiece compared to a concave shoulder design and also the relative small shoulder diameter of 18mm.

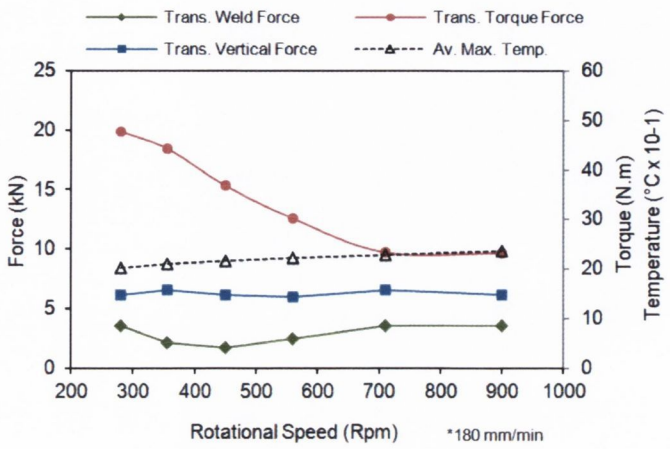


Figure 204: Effect of rotational speed on average steady state forces and average maximum temperature during the translational stage.

As a result, variation of the rotational speed did not have a significant impact on both the vertical and welding force. This behavior was recorded even at low translational speeds of 63mm/min to increase the rotational effect. The translational vertical force remained almost constant with increasing rotational speeds. The translational welding force decreased slightly with increasing rotational speed until 450 rpm after which an increase in the welding force was recorded. The initial decrease of the welding force can be attributed to an increase in material deformation which softens the workpiece material. However, the increase above 450 rpm maybe caused by the larger volume of material in the dynamically recrystallized zone that the pin has to create while advancing. Another explanation maybe the reduction in pressure generated behind the pin while the pressure in front of the pin remains constant. Unsurprisingly, variation of the rotational speed had a significant impact on the torque force. This was expected as torque is a rotary force measurement. The torque reduced significantly with increasing rotational speed even though only small increases in temperature where recorded. The diameter of the shoulder is 2.6 times that of the pin

diameter, hence the shoulder is the main driving factor in torque generation. Therefore the torque reduction can be attributed to an increase in material deformation at the top surface of the workpiece caused by the channels on the scrolled shoulder. This results in workpiece softening at the top surface and a reduction of the resistance encountered by the shoulder as it rotates within the workpiece.

The effect of rotational speed on the maximum vertical and torque forces during the plunge and dwell stages is shown in **Figure 205**. Although variation of the rotational speed did not have a significant effect on the translation vertical force, the maximum vertical was found to decrease with increasing rotation speeds. During the plunge and dwell stages, the tool remains in a stationary horizontal position whilst rotating. Hence the heat produced through friction between the tool shoulder and the workpiece is more intense and localized as the tool is not traversing, as a result, the workpiece softens and the force decreases. Similar to the translation torque, the maximum torque decreases significantly with rotational speed. Again this can be attributed to workpiece softening through friction and plastic workpiece deformation.

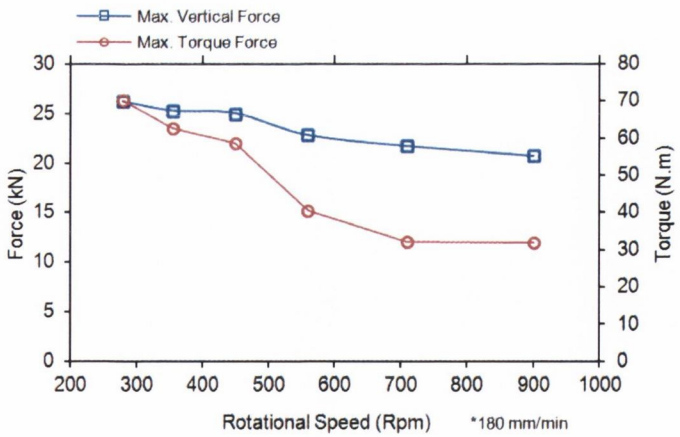


Figure 205: Effect of rotational speed on maximum forces during the plunge and dwell stages.

### 3.4 Effect of Pin Design

Many authors report that the majority of heat generation is contributed by the tool shoulder through friction with the workpiece and amount of heat input from deformational heating around the pin has been estimated to range from 2% to 5%. Through numerical studies on heat generation during the FSW process, Tang et al (1998) and Russell and Shercliff (1999) estimated that the percentage of heat generated by the tool pin to be 5% and 1% respectively of the total heat generated. To examine this further experimentally, temperature measurements were recorded during welding with no tool pin present and compared to temperatures recorded with a tool pin present. Results indicated that the shoulder accounts for approximately 93% of the total heat generated and the pin accounts for 7%. In general, the amount of workpiece softening due to heat generation is an important factor in force reduction. Therefore, variation in the tool pin design did not have a significant effect on all the forces generated. For example, only slight variation of the steady state vertical force was recorded for the different tool pin design during tool translation. Therefore downward forging action produced by the shoulder generates the majority of the vertical force. This suggested that wear of the shoulder due to the large forces and heat it generates is more likely to occur before pin wear or pin fracture. Similarly, variation of the pin design did not have a significant effect on the torque. This can be attributed to the shoulder having a much larger diameter compared to the pin and hence is the main driving factor in torque generation. However, variation of the pin design did have an impact on the welding force and the maximum vertical force.

During the plunge stage, vertical forces arises from the tool pin penetrating the workpiece whereas during the translational stage the vertical force is generated from the forging pressure the shoulder imparts to the workpiece to achieve a consolidated weld. Hence, pin design has a larger impact on the maximum vertical force which occurs during the plunge

stage compared to the steady state vertical force during the translational stage. **Figure 206** shows the effect of pin design on the maximum vertical force. The lowest force was recorded when welding with the Triflute pin. This can be attributed to the flutes on the Triflute pin producing a screwing action as it is plunged into the workpiece. Rotation of the tool works to screw the tool inwards thereby reducing the load. The uneven surface area of the pin due to the flutes will also cause a stirring effect, which will sweep the material beneath the pin away laterally rather than simply displacing the area occupied by the pin. Also, the unique flute design decreases the volume of the pin compared to a Cylindrical pin and hence less force is required to penetrate the workpiece. The largest vertical force was recorded when welding with the Cylindrical pin. This can be attributed to the smooth surface area of the pin which generates less material mixing and simply compress the workpiece material beneath the pin resulting in larger forces. The flat faces of the Square pin also create a sweeping effect similar to the flutes on the triflute pin and hence a reduction in force is recorded compared to the Cylindrical pin.

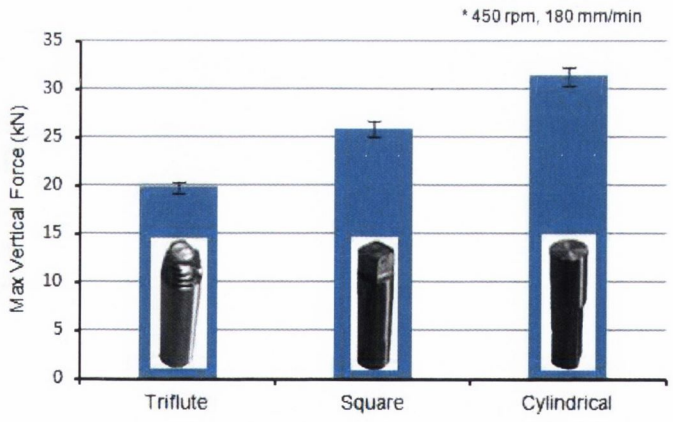


Figure 206: Effect of pin design on the max vertical force.

The effect of different pin designs on the welding force is shown in **Figure 207**. Similar to the maximum vertical force, larger forces were recorded for the Cylindrical pin compared to the Triflute and Square pins. This difference can be explained by examining how each

pin deforms/displaces the workpiece material ahead as it traverses along the joint line, as shown in **Figure 208**. The flat faces on the Square pin act like paddles producing a churning action which displaces the material ahead of the pin. Similar to a blender, the paddles sweep the material along the tool path thereby reducing the resistance acting against the traversing tool. The Triflute pin has a similar material deformation effect due to its flutes and threads producing an uneven surface. The smooth surface and circular shape of the Cylindrical pin produces less material deformation ahead of the tool pin as it traverses. Alternatively, the Cylindrical pin simply displaces the area along it paths causing a lot of workpiece material to flow around the sides of the pin similar to an extrusion process which accounts for the higher welding force recorded. Therefore although the welding force is significantly lower than the vertical force, tool pin designs which enable material to be processed more efficiently can be identified by monitoring the welding force.

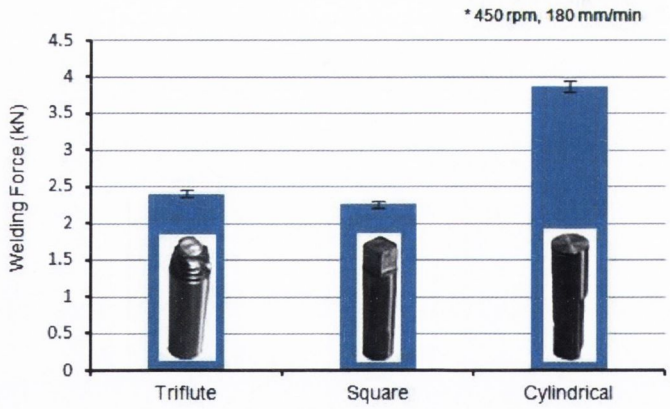


Figure 207: Effect of pin design on the welding force.

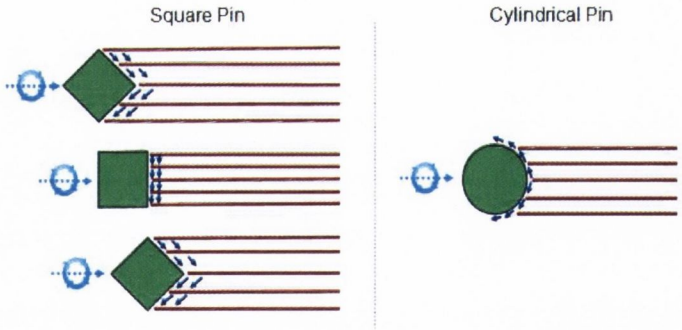


Figure 208: Material processing for different pin designs.

Evidence of increased material deformation and processing produced by the Triflute and Square pins compared to the Cylindrical pin can be seen in Figure 209 which shows the weld strength and elongation as a percentage of the parent material for the different pin designs. As expected, higher weld strength and ductility were recorded for the Triflute and Square pins due to increased material deformation and mixing of the workpiece material. Therefore tool pin designs with features which enhance the amount of material deformation will not only reduce the forces acting on the tool but will also increase the weld strength.

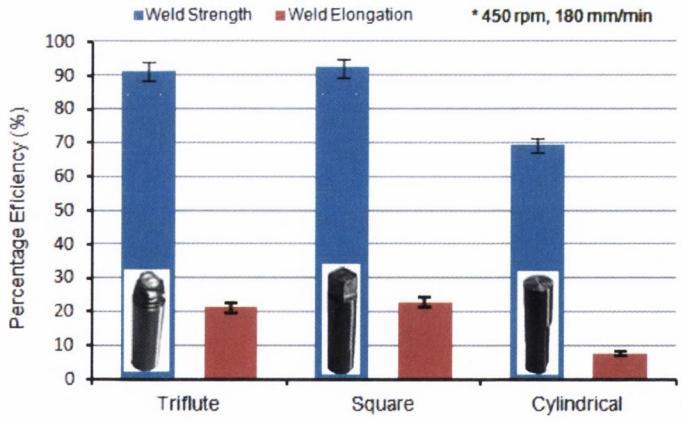


Figure 209: Effect of tool pin design on weld strength and weld elongation.

### 3.5 Effect of Shoulder Diameter and Plunge Depth

Larger vertical forces, torques and to a less extent welding forces were recorded when a larger 22mm shoulder diameter was used compared to an 18mm shoulder diameter. This can be attributed to the greater contact area between the tool shoulder and the workpiece causing a greater reaction force. Also, a larger shoulder diameter will require more material to be processed and directed by the channels on the spiral and may also result in larger forces. Larger forces were also recorded when the plunge depth of the shoulder was increased. This was expected because as the shoulder is plunged deeper into the workpiece, it must move a greater volume of material. Samples of these results are illustrated in **Figure 210**.

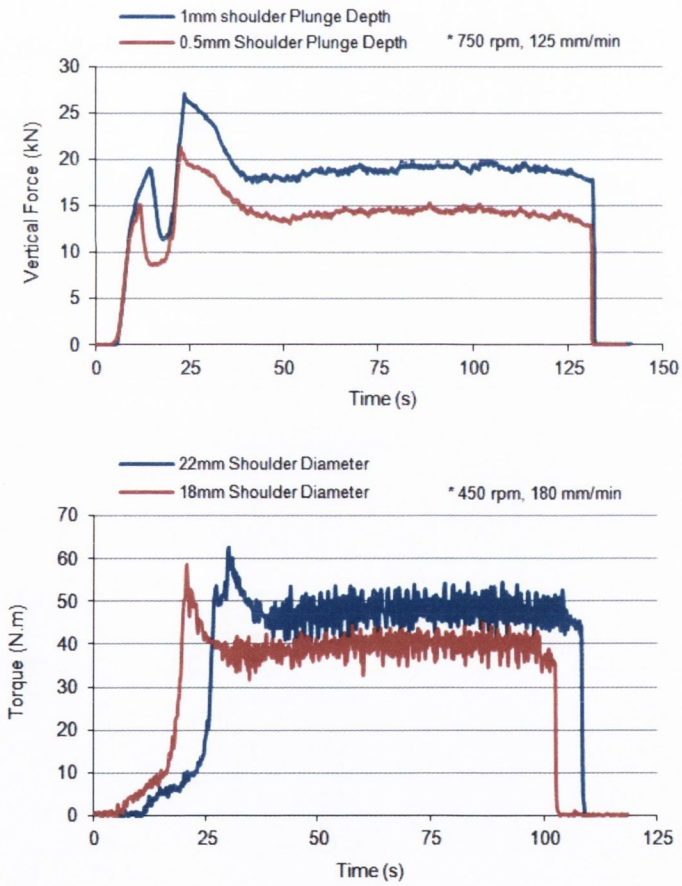


Figure 210: Effect of the plunge depth on the vertical force, and effect of shoulder diameter on the torque.

## 4. Conclusions

This work has demonstrated the effect of varying operational parameters and tooling designs on force and temperature generation during the FSW of aluminium 2024-T3 plates. Seven different translational speeds and six different rotational speeds were investigated. Three different tool pin design and two different shoulder diameters were used during welding.

The vertical and torque forces reach maximum peak values during the plunging of the tool into the workpiece. Hence the tool can be susceptible to tool failure during this stage. Developing new techniques of tool entry and new tooling designs may reduce these peak values. However, all three forces reduce to steady state values during the translational stages as the tool traverses along the joint line. This correlated well with steady state temperature also recorded during this stage. The reduction of the vertical and torque force from peak values to steady state values was significant, approximately 35% reduction.

Variation of the translational speed had greater effects on tool forces than variation of the rotational speed. All three forces were found to increase significantly with increasing translational speeds. This was attributed to a reduction in heat generation and hence softening of the workpiece material which was verified through thermocouple measurements. Although higher temperatures are normally associated with increasing rotational speeds, this was not recorded during this work as only relatively small increases in temperature were recorded with increasing rotational speeds. This was attributed to the relatively small shoulder diameter and scrolled shoulder design which has less shoulder surface area contact with the workpiece compared to a concave shoulder design. As a result, variation of the rotational speed only had an effect on the torque force. From this work it is clear that the amount of heat generation is directly related to the magnitude of

the tool force generated. Therefore localized preheating of the workpiece material will reduce the forces considerably rather than implementing operational parameter to maximize heat generation which may deteriorate weld properties. An example would be the use of a laser as a supporting technology to heat and soften the workpiece directly ahead of the tool path.

The shoulder was found to generate 93% of the total heat and the tool pin 7%. As a result pin design only had an effect on the welding force during the translational stage and the maximum vertical force during the plunge stage. Lower forces were recorded by the Mx Triflute and Square pins due to an increase in material processing and deformation ahead of the tool pin rather than simply displacing the area occupied by the pin as was the case for the smooth surface area design of the Cylindrical pin. Evidence of increased material deformation and processing was recorded through tensile tests. Greater weld strength and elongation was recorded using the Mx Triflute and Square pins compared to the Cylindrical pin.

The magnitude of the vertical force is significantly larger than the other forces. The downward forging action produced by the shoulder generates the majority of the vertical force. This suggested that wear of the shoulder due to the large forces and heat it generates is more likely to occur before pin wear or pin fracture. Although the welding force is significantly lower than the vertical force, tool pin designs which enable material to be processed more efficiently can be identified by monitoring the welding force. The limiting factor associated with increasing the translational speed and hence productivity of the process was the formability of the workpiece and not pin failure due to the occurrence of large welding forces.

Due to an increase in the amount of surface area contact between the tool shoulder and the workpiece, larger vertical forces and torques were recorded when the plunge depth was increased and also when a larger 22mm shoulder diameter was used compared to an 18mm diameter.

**References**

Colegrove, P.A., Shercliff, H.R., 2005. 3-Dimensional CFD modeling of flow round a threaded friction stir welding tool profile, J. Mater. Process. Technol. 169, 320-327.

Gerlich, A., Su, P., North, T.H., 2005. Tool penetration during friction spot welding of Al and Mg Alloys, J. Mater. Sci. 40, 6473-6481.

Jariyaboon, M., Davenport, A.J., Ambat, R., Connolly, B.J., Williams, S.W., Price, D.A., 2007. The effect of welding parameters on the corrosion behaviour of friction stir welded AA2024-T351, Corros. Sci. 49, 877-909.

Lathabai, S., Painter, M.J., Elmustafa, A.A., 2006. Friction spot joining of an extruded Al-Mg-Si alloy, Scripta Mater. 55, 899-902.

Mandal, S., Rice. J., 2008. Experimental and numerical investigation of the plunge stage in friction stir welding, J. Mater. Process. Tech. 203, 411-419.

Martukanitz, R.P., 1993. Selection and Weldability of heat-treatable aluminium alloys, in welding, brazing and soldering, ASM Handbook, vol.6, 528-536.

Melendez, M., Tang, W., 2005. Tool forces developed during friction stir Welding, internal paper, NASA Technical Reports Server, http://ntrs.nasa.gov/archive/nasa/casi.ntrs.nasa.gov/20030071631_2003069405.pdf, 8/11/2011.

Starke, E.A., Staley, J.T., 1996, Application of modern aluminium alloys to aircraft. Prog. Aero. Sci. 32, 131-72.

Su, J.Q., Nelson, T.W., Mishra, R., Mahoney, M., 2003. Microstructural investigation of friction stir welded 7050-T651 aluminium. Acta. Mater. 51, 713-729.

Thomas, W.M., 1991. Friction stir welding, International Patent Application No. PCT/GB92/02203 and GB patent Application No. 9125978.8, December 1991, U.S Patent No. 5,460,317.

Ulysse, P., 2002. Three-dimensional modeling of the friction stir welding process, Int. J. Mach. Tool. Manu. 42, 1549-1557.

Yan, J., Sutton, M.A., Reynolds, A.P., 2004. Process-structure-property relationship for nugget and HAZ regions of AA2524-T351 FSW joints. 5th Internationa; FSW Symposium, Metz, France.

Yang, Y., Kalya, P., Landers, R., Krishnamurthy, K., 2008. Automatic gap detection in friction stir butt welding operations, Int. j. Mach. Tool. Manu. 48, 1161 – 1169.

## 10.3 International Manufacturing Conference 2010:

# OPTIMISATION OF PROCESS PARAMETERS AND TOOLING DURING FRICTION STIR WELDING

Daniel Trimble, John Monaghan, Garret O'Donnell

Department of Mechanical & Manufacturing Engineering
Trinity College Dublin, Ireland

**ABSTRACT:**

FSW is considered as a green technology because of its energy efficiency, environmental friendliness and versatility. When compared with conventional welding methods, FSW consumes considerably less energy, no consumables such as a cover gas or flux are used, and no harmful emissions are produced during welding. It is also relatively quiet thereby making the process environmentally friendly and a sustainable manufacturing technology.

However, one of the obstacles preventing large implementation of the process within the manufacturing industry is the lack of specifications and design guidelines. The objective of the work presented in this research paper is to provide guidelines on which process parameters and tooling designs result in optimum weld properties during the FSW of aluminium 2024-T3. A tool having a scrolled shoulder, with either a square or triflute pin design, and using translational speeds between 125 – 250 and rotational speeds between 355 – 450 produced optimum joint strength and ductility.

**Keywords:** Friction Stir Welding, tooling designs, process parameters, weld strength.

## 1. INTRODUCTION:

Friction Stir Welding (FSW) is a solid state joining process invented and experimentally proven by Wayne Thomas and a team of his colleagues at The Welding Institute UK in December 1991 1. During the process, as illustrated in Figure 1, a rotating cylindrical shouldered tool with a profiled pin is slowly plunged into the joint line between the materials to be welded. Frictional heat is generated which causes the workpiece to soften without reaching its melting point and allows traversing of the tool along the weld line. The plasticised material is transferred from the leading edge of the tool to the trailing edge of the tool pin and is forged by the intimate contact of the tool shoulder and the pin profile. It leaves a permanent solid phase bond between the two pieces.

FSW is considered a green technology because of its energy efficiency, environmental friendliness and versatility. When compared with conventional welding methods, FSW consumes considerably less energy, no consumables such as a cover gas or flux are used, and no harmful emissions are produced during welding and it is relatively quiet thereby making the process environmentally friendly and a sustainable manufacturing technology. Another advantage FSW has over fusion welding is the ability to easily weld 2xxx and 7xxx series aluminium alloys which are considered unweldable using standard fusion techniques.

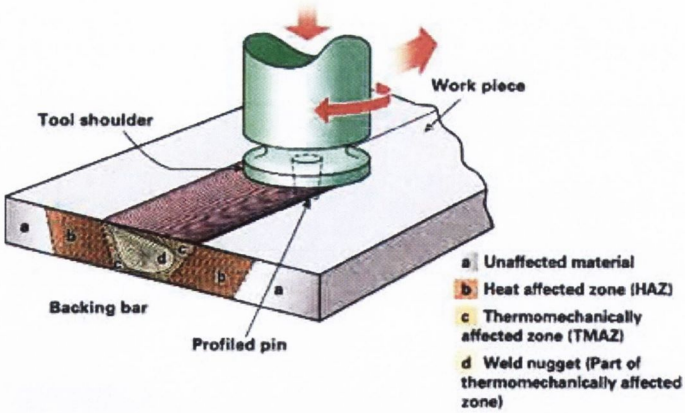


Figure 211: A schematic of the friction stir welding technique

Although FSW has many advantages over tradition fusion welding techniques, the process has not been implemented within the manufacturing industry to the extend that one would have anticipated. One of the reasons for this is a lack of process specifications and design guidelines and this presents a serious barrier for industry-wide technological implementation. The objective of work presented in this research paper is to investigate the mechanical properties of 4.82mm thick aluminium 2024-T3 butt welded samples for a range of process parameters (rotational and translational speeds) and tool designs. And to provide guidelines as to which process parameters and tooling designs give optimum weld properties.

## 2. EXPERMENTAL PROCEDURE:

All FSW tests were conducted on a Correa F3UE milling machine which was modified for use as a FSW rig. The workpiece material was rolled sheets of aluminium 2024-T3 alclad with a thickness of 4.82mm. The sheets were cut to the required size (260mm x 80mm) and were welded using a butt joint configuration. A 3-piece tooling design was developed to enable interchangeable shoulder and pin components for different designs and also if tool failure occurred. Two shoulder designs (scrolled and Concave) and four pin designs (Mx Triflute, Square, Cylindrical and Tapeered) were tested and are shown in Figure 212.

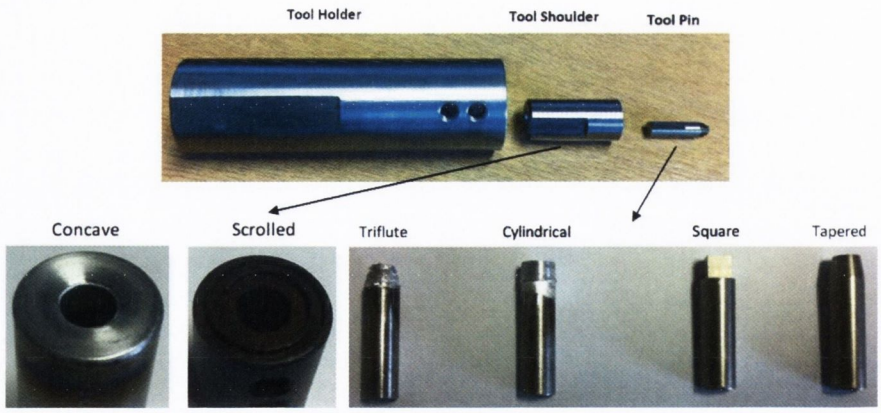


Figure 212: FSW Tooling

The welding parameters and tooling dimensions are presented in Table 20. Core testing consisted of 42 welds over the range of operating parameters while recording the forces and temperatures generated. These welds were produced using the scrolled shoulder and Triflute pin as these are more recent FSW tool developments. Additional welding was preformed using the different tooling arrangements at specific operational parameters to

compare results. During welding, a distance of 0.2mm was maintained between the tip of the tool pin and the bottom surface of the aluminium plates to ensure a consolidated weld was produced. The height of the scrolled feature was 1mm and this was plunged 0.5mm into the workpiece surface during welding. Using a scrolled shoulder design it was possible to weld with a zero tool tilt angle. When using the concave design, the shoulder was plunged until 80% of the shoulder was in contact with the workpiece.

Table 20: Welding parameters and tooling dimensions

| Process Parameters | Values |
|---|---|
| Rotational speed (rpm) | 260, 355, 450, 560, 710, 900 |
| Translational speed (mm/min) | 63, 90, 125, 180, 250, 355, 500 |
| Plunge rate (mm/min) | 16 |
| Dwell time (s) | 8 |
| Pin length (mm) | 4.6 |
| Pin diameter (mm) | 7 |
| Shoulder diameter | 18, 22 |
| Tool tilt angle (°) | 2 |

After welding, each plate was sectioned to provide four tensile test specimens. Tensile testing was conducted to British Standard (BSEN 10002-1:2001) at a rate of 1mm/min. The average Ultimate Tensile Stress (UTS) or maximum stress for the four tensile test specimens was recorded for each weld. Tensile tests were also conducted on un-welded base material samples (average UTS 454 MPa and elongation of approximately 15mm) and hence the joint efficiency was calculated using the following formula:

$$\frac{\text{Average UTS}_{weld}}{\text{Average UTS}_{Base Material}} \text{x} 100 = \text{Joint Efficiency} \qquad \text{Eq 1}$$

## 3. EXPERIMENTAL RESULTS:

Table 21 displays the joint efficiency as a percentage of the strength of base material for all 42 friction stir welds. The order in which the welds were fabricated was randomized in order to satisfy the statistical requirement of independence of the observations. This acts as an insurance against the effects of lurking time-related variables such as the warm-up of tools and equipment. Weld fabricated at operational parameters labelled N/A did not undergo tensile testing due to the occurrence of severe defects during welding. An initial and important observation is that a processing window does exist and that variation of the operational parameters leads to a progressive change in the weld strength rather than random erratic results. For example, joint efficiencies above 80% and 90% are highlighted. These results are grouped together rather than randomly occurring with different operational parameters. Table 18 shows the extension in millimetres at fracture and hence an indication of the ductility of each weld. As expected, welds that displayed good strength also displayed good ductility. However, none of the welds exhibited ductility as high as that of the parent material which fractured after 15mm elongation. The most ductile weld had a ductility that was approximately 30% of that of the parent material. This can be attributed to the complex grain structure and thermal damage produced during the friction stir process.

Table 21: Joint efficiency results (%) based on **Error! Reference source not found.**

Joint Efficiency %

| Rotational Speed [RPM] | 63 | 90 | 125 | 180 | 250 | 355 | 500 |
|---|---|---|---|---|---|---|---|
| 900 | 69.39 | 68.25 | 71.59 | 62.24 | 51.09 | 38.78 | 39.46 |
| 700 | 60.54 | 74.97 | 76.98 | 59.39 | 66.90 | 42.43 | 26.90 |
| 560 | 69.92 | 73.59 | 76.93 | 75.04 | 85.80 | 70.70 | 63.23 |
| 450 | 70.71 | 77.22 | 88.23 | 88.78 | 89.68 | 77.16 | 47.28 |
| 355 | 79.45 | 81.36 | 85.83 | 93.61 | 94.06 | 67.68 | N/A |
| 280 | 81.47 | 84.28 | 86.22 | 84.90 | N/A | N/A | N/A |

Translational Speed [mm/min]

Table 22: Elongation at fracture (mm)

Elongation at Fracture (mm)

| Rotational Speed [RPM] | 63 | 90 | 125 | 180 | 250 | 355 | 500 |
|---|---|---|---|---|---|---|---|
| 900 | 1.43 | 1.15 | 1.62 | 0.80 | 0.66 | 0.45 | 0.47 |
| 700 | 0.86 | 1.52 | 1.78 | 0.79 | 1.08 | 0.51 | 0.42 |
| 560 | 1.24 | 1.27 | 1.55 | 1.21 | 2.36 | 1.29 | 0.96 |
| 450 | 1.38 | 1.66 | 2.76 | 3.09 | 3.14 | 1.33 | 0.55 |
| 355 | 2.38 | 2.42 | 2.56 | 3.96 | 4.66 | 0.93 | N/A |
| 280 | 2.73 | 2.71 | 2.99 | N/A | N/A | N/A | N/A |

Translational Speed [mm/min]

It can be seen that optimal joint efficiency above 85% of the parent material, was recoded at translational speeds between 125 – 250 mm/min and at rotational speeds between 355 – 560 Rpm. These operational parameters should be implemented during FSW of AA2024-T3 to achieve optimal results. Also, a number of tests were repeated to investigate the consistency of the friction stir welding process. All repeat testing, in terms of joint efficiency/strength and displacement at fracture (ductility), was found to be relative consistent with a standard deviation of approximately 7%.

### 3.1 Impact of Translational Speed:

In general, it was found that both the joint strength and ductility increases with increasing translational speed until an optimal value is reached at which point the joint strength and ductility begins to decrease. Figure 213 illustrates this effect of translation speed on joint efficiency/strength for a fixed rotational speed of 450 Rpm.

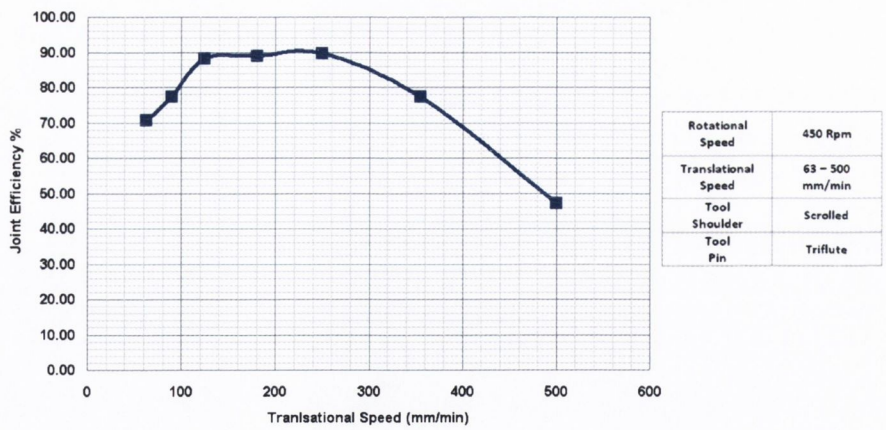


Figure 213: Effect of translational speed on joint efficiency

The reduction in joint efficieny experienced for lower translational speeds (63 -90 mm/min) can be attributed to a high heat input. A low translational speed will increase grain growth and softening within the welded zone which may explain the reduction in strength. Furthermore, the high heat input generated at low translational speeds may cause thermal damage thereby reversing the T3 heat treatment the alloy initially went through leading to inferior weld properties. Too high a translational speed will not allow sufficient

time for the rotary action of the tool to produce a consolidated weld and hence a reduction in strength was recorded for all translational speeds above 250 mm/min. For example, surface defects were recorded for all welds fabricated at 500 mm/min and the majority of welds fabricated at 355 mm/min. As expected, a surface defects will act as a focal point for crack propagation and hence result in a lower joint efficiency/strength. Figure 126 shows a surface defect which occurred due to a high translational speed of 500 mm/min. Similar results were recorded by G. Biallas et al 72 who performed tensile tests on 4mm thick AA2024 FSW joints. These authors reported an increase in weld strength with increases in translational speeds between the range of 80 -125 mm/min. Kristensen et al [3] examined the effects of translational speed on the ultimate tensile strength of friction stir welded aluminium 2024-T3 plates of 6mm thickness and reported a decrease in weld strength with increasing the translational speeds between 270 - 550 mm/min.

Figure 214: Surface defects due to a high translational speed 355mm/min

### 3.2 Impact of Rotational Speed

In general it was found that lower rotational speeds ranging from 280 – 450 Rpm produced stronger and more ductile welds compared to those produced at higher rotational speeds ranging from 560 – 900 Rpm. Figure 127 shows the effect of varying the rotational speed on the joint efficiency for a fixed translational speed of 125 mm/min. Higher joint efficiency associated with lower rotational speeds can also be attributed to reduced thermal damage as mentioned previously when comparing the translational speed effect. Also, high rotational speeds can lead to excessive deformation and a rough surface finish, which result in the occurrence of small internal and surface voids which reduce the strength of the weld. A rough surface finish cause by excessive rotational speeds can leave uneven surface indentation marks left in the shoulder wake as it traverses along the joint line. These marks can act as tiny stress raisers or cracks resulting in failure in these region and a reduction in strength.

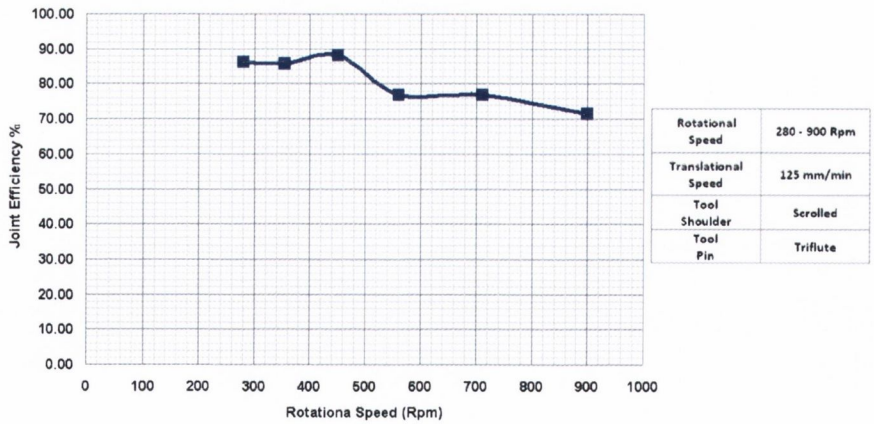


Figure 215: Effect of rotational speed on joint efficiency

M.A. Sutton et al 49 reported similar results in their investigation of the effect of rotational speed on ultimate tensile strength of Aluminium 2524-T3. Using a fixed translational speed of 2.11 mm/s and varying the rotational speed (100 to 800 rpm), Sutton reported an increase in weld strength with increasing rotational speeds up to a peak of 480

Rpm. Further increases in rotational speeds above 480 rpm were accompanied by a decrease in weld strength which Sutton attributed to overheating. J. Adamowski et al 75 investigated the effects of varying process parameters when FSW AW6082-T6 aluminium alloy. While maintaining a constant translational speed of 115 mm/min, Adamowski found that increasing the rotational speed from 330 to 880 Rpm resulted in a reduction in weld strength of approximately 30 MPa.

### 3.3 Effect of Different Pin Geometries:

As mentioned previously, four different pin geometries (Triflute, Square, Cylindrical and Tapered) were designed and manufactured to determine their effects on the FSW process. The primary function of the non-consumable rotating tool pin is to stir the plasticized metal and move the material behind it to produce a consolidated joint. Pin geometry plays a crucial role in material flow and in turn could possibly regulate the welding speed of the FSW process. Figure 129 and **Error! Reference source not found.** illustrate the effect of different pin geometries on joint efficiency and elongation (ductility) respectively.

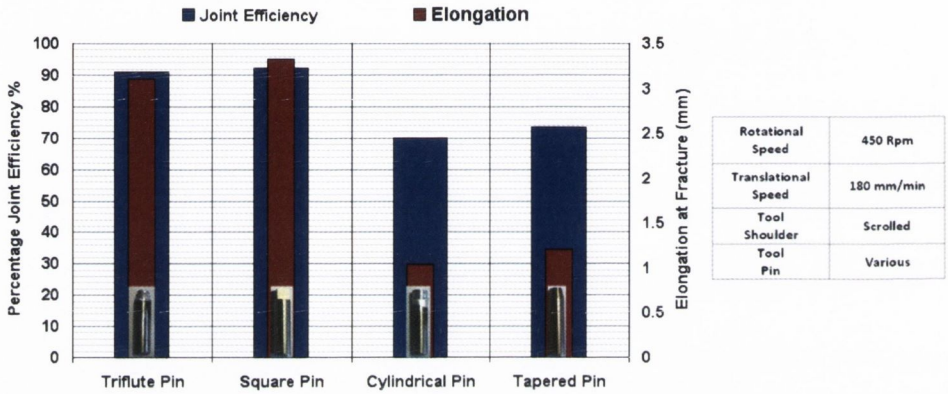


Figure 216: Percentage joint efficiency and elongation at fracture for different pin geometries

It is clearly evident that the four pin geometries can be separated into two different categories. The triflute and square pins, which are associated with increased material deformation capabilities, produced more desirable joint efficiencies and ductility (91%, 3.1mm and 92%, 3.2mm respectively). Whereas the cylindrical and tapered pins with smooth designs produced lower joint efficiencies and ductility (70%, 1.1mm and 73%, 1.21mm respectively). Note Similar results were also seen for different operational parameters.

Pin profiles with flat faces like the square pin are associated with eccentricity. This eccentricity allows compressible material to pass around the pin profile. Also, the flat faces and corners of the pin produce a pulsating stirring action. Both of which create a smoother flow of material and generate sufficient heat through friction to produce a strong consolidated weld. The flutes on the Triflute tool result in the pin having an uneven surface area and this causes an increased stirring effect that will increase material deformation and allow a smoother integration of the workpiece material from each plate to produce a strong weld. Both the Square and Triflute pins produce more turbulence due to their shape which increases material mixing. Another observation that can be made is the fact that a simple square shape can produce equal, and in some cases better, weld properties that a complex triflute shape. The complex shape of the triflute tool is also more expensive and difficult to machine compared to a simple square shape. The three flute design of the triflute pin reduces the volume of tool pin material and can influence the risk of pin failure when welding thicker or denser material. Therefore when pin failure becomes a limiting factor in FSW a pin with flats such as a square design may provide extra strength and stability.

The Cylindrical and Tapered pins do not have any flutes or flat faces to produce any stirring effect and the plasticized material is simply allowed to extrude on the sides of the pin. Consequently tools having a smooth pin surface area will produce less mixing of the workpiece material, thereby resulting in a weaker weld.

### 3.4 Effect of Different Shoulder Geometries:

To examine the effect of shoulder design, two welds were fabricated with a concave shoulder using a required 2° tool tilt angle and compared with welds fabricated using a scrolled shoulder design. The results are shown in Figure 130 and indicate that although the scrolled shoulder preformed slightly better there is no significant difference in joint efficiency/strength between the two different shoulder designs. Similar results were obtained when comparing ductility. However, these results only represent two sets operational parameter and therefore further test would be required to examine this over a larger range of operating parameters.

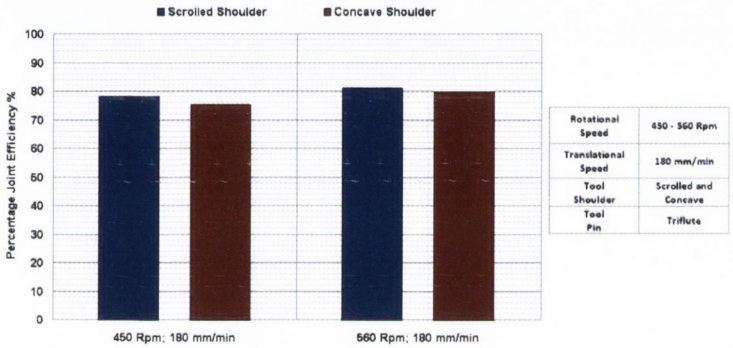


Figure 217: Effect of shoulder design on joint efficiency

Regardless of the above information, using a scrolled shoulder rather than a concave shoulder has the advantage that there is no need for a tool tilt angle. This is desirable if performing a friction stir weld around a corner or welding in a circular or oval shape (i.e. non-linear) where sophisticated machinery and a lot of precision would be required to maintain the appropriate tool tilt angle while using a concave tool shoulder. Figure 132 illustrates welds produced by the author during a training course at The Welding Institute (TWI) using a scrolled shoulder with a zero tilt angle. Also, the scrolled shoulder was found to enable higher translational speeds due to a reduction in tool lift. Using a concave shoulder, translational speeds greater than 125mm/min were not possible when welding with a concave shoulder due to tool lift which resulted in a poor surface finish with the occurrence of voids. Evidence for this can be seen in Figure 219.

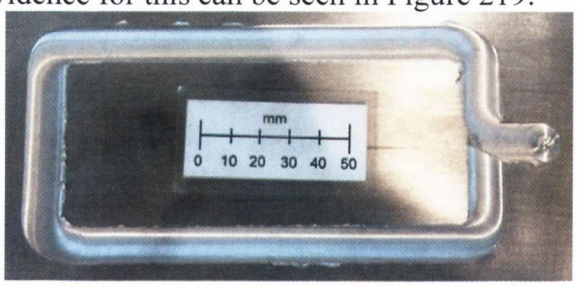


Figure 218: Non linear weld with a scrolled shoulder

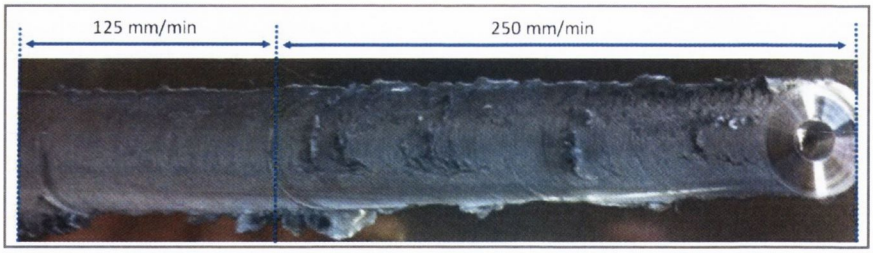

Figure 219: Tool lift using a concave shoulder

## 4. CONCLUSIONS:

A processing window was developed for the FSW of 4.82mm thick aluminium 2024-T3 plates to determine which operational parameters gave optimal joint strength and ductility. It was found that a rotational speed in the range of 355 – 450 rpm and a translational speed in the range of 125 – 250mm/min produced optimal joint properties. Repeat testing was also conducted and results showed a standard deviation of approximately 7%. The amount of heat input, material deformation and the occurrence of defects determined optimal joint efficiencies. The square and triflute pin geometries produce stronger more ductile welds than those produced using the cylindrical and tapered pin geometries. This was attributed to increased material mixing and integration of the workpiece plates due to flat features of the square pin and flutes of the triflute pin. No significant difference in joint strength or ductility was recorded when comparing a scrolled shoulder to a concave shoulder of equal diameter. However, there is no need for a tilt angle when using a scrolled shoulder. This is desirable when performing a non-linear friction stir weld.

## 5. REFERENCES

[1] W.M. Thomas, E.D. Nicholas, J.C. Needham, M.G. Murch, P. Temple-Smith, C.J. Dawes, Friction Welding, in: United States Patent, 5,460,317, The Welding Institute, Cambridge, GB, 1995.

[2] G. Biallas, R. Braun, C. Dalle Donne. "Mechanical Properties and Corrosion Behaviour of Friction Stir Welded 2024-T3," 1st International Conference on Friction Stir Welding, June 1999, Rockwell Science Center, Thousand Oaks, California.

[3] J. Kristensen, C. Dalle Donne, T. Ghidini, J. Mononen, Properties of Friction Stir Welded Joints in the Aluminium Alloys 2024, 5083, 6082/6060 and 7075, 5th International Conference on FSW, September 2004, Metz Congres, Metz, France.

[4] M.A. Sutton and R. Taylor, Mode I Fracture and Microstructure for 2024-T3 Friction Stir Welds, *Mater. Sci. Eng. A*, Vol 354, 2003, P 6-16

[5] J. Adamowski, M. Szkodo. Friction Stir Welds of aluminium alloy AW6082-T6. Journal of achievements in materials and manufacturing engineering. Vol 20, issues 1-2, 2007.

# Optimisation of Process Parameters and Tooling during Friction Stir Welding of AA2024-T3

Daniel Trimble

Dept. of Mechanical and Manufacturing Engineering, Trinity College Dublin Ireland

## ABSTRACT

Friction Stir Welding (FSW) is a relatively new joining technique that involves the joining of two metal pieces at the molecular level without melting. Because it is a solid state process and joining takes place below the melting temperature of the material, a high-quality weld is created and the problems associated with fusion welding techniques are avoided. Furthermore, all series of aluminium alloys can be welding using this process. In particular the 2xxx series which is used extensively within the aerospace industry for wing and fuselage skin panels due to their high strength to weight ratio and are deemed un-weldable using fusion techniques.

The overall aim of the project was to optimise the operational parameters and tooling design, and also to provide a comprehensive understanding of the FSW process during the welding of AA2024-T3 plates. This was achieved through the development of a processing window for various operational parameters; testing of new tooling designs and the comparison of their performance to traditional FSW tooling; characterisation of the forces and temperatures generated and the development of a FE model to simulate the process.

New tooling designs were developed which increased the amount of material deformation and mixing, and also enabled higher welding speeds. Operating parameters capable of achieving joint strengths efficiencies up to 95% of that of the parent material where identified. New techniques of process implementation and tooling designs were identified to reduce tool forces significantly enabling the process to be more flexibly. Using the FE model it was possible to predict thermal flow throughout the workpiece, tool and surrounding clamping; predict the forces for different operating parameters, workpiece thicknesses and tooling designs, Analyse material flow patterns; Analyse the stresses and strains acting throughout the workpiece and tooling; predict the mechanism of tool wear/failure and how to prevent it.